UNIVERSITÉ DU QUÉBEC

THÈSE PRÉSENTÉE À

L'UNIVERSITÉ DU QUÉBEC À CHICOUTIMI
COMME EXIGENCE PARTIELLE
DU DOCTORAT EN RESSOURCES MINÉRALES

PAR

Zhiwei Bao

Geochemistry of the Sediment-hosted Disseminated Gold Deposits in Southwestern Guizhou Province, China

August 5, 2001

Bibliothèque
Paul-Émile-Boulet

UQAC
Université du Québec
à Chicoutimi

Mise en garde/Advice

Afin de rendre accessible au plus grand nombre le résultat des travaux de recherche menés par ses étudiants gradués et dans l'esprit des règles qui régissent le dépôt et la diffusion des mémoires et thèses produits dans cette Institution, **l'Université du Québec à Chicoutimi (UQAC)** est fière de rendre accessible une version complète et gratuite de cette œuvre.

Motivated by a desire to make the results of its graduate students' research accessible to all, and in accordance with the rules governing the acceptation and diffusion of dissertations and theses in this Institution, the **Université du Québec à Chicoutimi (UQAC)** is proud to make a complete version of this work available at no cost to the reader.

L'auteur conserve néanmoins la propriété du droit d'auteur qui protège ce mémoire ou cette thèse. Ni le mémoire ou la thèse ni des extraits substantiels de ceux-ci ne peuvent être imprimés ou autrement reproduits sans son autorisation.

The author retains ownership of the copyright of this dissertation or thesis. Neither the dissertation or thesis, nor substantial extracts from it, may be printed or otherwise reproduced without the author's permission.

ABSTRACT

The sediment-hosted disseminated gold (SHDG) deposits in southwest Guizhou Province, China, are located near the buried edge of the Yangtse craton. Although some investigations have been carried out on their geological and geochemical characteristics, in general, most of the studies are based on limited database. The source of the gold in the deposits and the relationship between gold and the organic matter in the ores are still not clear. Hence, the role of organic matter and the source of Au in SHDG mineralization have been the major objectives of this study.

Three deposits, the Lannigou, Getang and Zimudang were chosen for this study. The deposits are hosted by rocks of distinct sedimentary environment and were formed at low temperatures (120~240 °C) from solutions of low salinity, weak to neutral acidity, and in a reducing environment. The analysis of the ores and host rocks of this study shows that high field strength elements, such as Nb, Ta, Zr and Hf, were immobile during the hydrothermal alteration. However, REE were mobile during the alteration, within which LREE were depleted while HREE were enriched. A differentiation of PGE concentrations was observed; the ores are relatively enriched in Pd and Pt, and this is consistent with the higher solubility of these two elements. But the Pd/Ir ratios of the ores are lower than those of the ultramafic rocks and the Emeishan basalts. The PGE plots of ores suggest that the ultramafic intrusives could not be the main source of the gold mineralization in the SHDG deposits. The gold in the deposits most likely derived from a mixed source that includes the host rocks, the underlying crustal formations and the widespread Au rich basaltic rocks.

In southwest Guizhou Province, the SHDG deposits are commonly hosted by the same fold crests, usually containing a remarkable amount of hydrocarbon material that is common to SHDG deposits. The organic fluid inclusions in the ores are made up of light hydrocarbons, crude oil and pyrobitumen. The total organic carbon contents of the ores and host rocks are usually less than 1%. The reflectance of vitrinite and pyrobitumen in the ores and the host rocks ranges from 1.5 to 4.5, often in the range of 2~3. The reflectance of vitrinite and pyrobitumen in the ores are usually somewhat higher than those within the host rocks in the Lannigou deposit. The estimated maximum paleo-temperature on the vitrinite reflectance of the Lannigou deposit is similar or somewhat lower than the homogenization temperature of the fluid inclusions, which is consistent with the observed hydrothermal impact on the organic matter in the altered host rocks. But estimated maximum paleo-temperatures on the vitrinite reflectance of the Getang and Zimudang deposit are higher than the homogenization temperatures of the fluid inclusions in the ores. These are consistent with regional high paleo-thermal gradient in the study area and signify that oil generation predate Au mineralization. This study confirmed that there is no correlation between the organic contents and Au concentrations in the ores. However, it is interesting to note that there is a positive correlation between the S_2 (a parameter of Rock-Eval analysis), Au and As contents of the ores in the Lannigou deposit. Organic matter maturation and migration is apparent from the TOC (total organic carbon) vs. HCI diagram.

From the crosscutting relationship of bitumen and quartz veins, the bitumen migration was likely to have taken place before the gold mineralization. However, the possibility that some of the hydrocarbons were brought in by the ore forming solution cannot be ruled out.

Furthermore, group analysis of the dichloromethane extractable organic component of the ores and host rocks shows that the degree of maturation of the ores is slightly higher than the host rocks. However, the compositions of their alkanes, steranes and terpenes, which serve as biomarkers, are quite similar; this suggests that the organic matter found in the ores and host rocks has a common source. Since hydrocarbon maturation took place prior to SHDG mineralization it is possible that the hydrocarbons in the anticline and their dissolution in the oilfield brines might have contributed to gold migrations. However, this could not be verified since it was beyond the scope of the present study. Results from this study as well as other studies show that within the co-existing systems of auriferous pyrite, lignite and crude oil the solubility of Au in crude oil can attain ppm levels. Au solubility at low temperatures (80°C) is quite high (710ppb), much higher than that in the inorganic solution (around 10ppb). This data suggests the hydrocarbons in the hydrothermal solution possibly contributed to Au migration but warrants further investigation.

Finally, organic matter most probably contributed significantly to the preconcentration of Au in the host rocks. However, its role in the primary and secondary generation of crude oil and its migration apparently predate mineralization in most SHDG deposits. Hence, crude oil was not a likely potential agent of Au transportation. Hydrocarbons in the system, on the other hand, clearly contributed to the emplacement of the gold mineralization through thermal sulfate reduction. The colloidal crude oil, hydrocarbons and organic acids in solutions could have greatly increased gold solubility as organic complexes, or protected the gold colloidal in solution. In addition to Au bisulfide complexes, gold colloidal solution likely played an important role in gold leaching and transportation, especially in the case of SHDG deposits where there is evidence showing the participation of hydrocarbons in the process. Mineral-water interfacial reactions, including absorption-reduction and surface complexation, of which Au oversaturation is not a prerequisite, are also likely important processes for gold deposition.

In conclusion, organic matter was an active component in the SHDG mineralization under study. It contributed to the thermal reduction of sulfate and thus pyritization. Hydrocarbons in the solution may have increased the potential of the hydrothermal solution to transport Au. The hydrocarbons were mainly derived from the host rocks while the gold might have been derived from a mixed source including host rocks, underlying crustal rocks, basaltic rocks and possibly ultramafic rocks. Our data suggests that the SHDG deposits in southwest Guizhou are most likely amagmatic in origin, which is supported by the complete lack of igneous intrusives in the vicinity of the deposits, the very weak metamorphic grade of the crustal rocks and lack of metamorphic event within the time range of the SHDG mineralization, and the coincidence of the time frame of mineralization with the regional extension.

RÉSUMÉ

Les gisements d'or disséminé encaissés dans des sédiments (GODES) au sud-ouest de la province de Ghizhou, en Chine, sont situés près de la limite enfouie du craton du Yangtsé. Bien que l'on ait effectué certaines recherches sur les caractéristiques géologiques et géochimiques de ces gisements, la plupart de ces recherches ne s'appuient que sur des bases de données limitées. La question de l'origine de l'or dans ces gisements, de même que celle du rapport entre l'or et la matière organique, n'ont pas de réponses claires. En conséquence, le rôle de la matière organique et l'origine de l'or dans les processus de minéralisation associés aux GODES sont les principaux objectifs de l'étude.

L'étude se limite aux gisements de Lannigou, de Getang et de Zimudang. Ces gisements sont encaissés dans des roches provenant de milieux sédimentaires distincts. Ils se sont formés à basse température (120-240 °C) à partir de solutions à salinité faible, avec un niveau d'acidité allant de faible à neutre, dans un environnement réducteur. Dans l'analyse des minerais et roches encaissantes, on trouve que les éléments à haute énergie (high field strength elements), tels que Nb, Ta, Zr et Hf, étaient immobiles durant l'altération hydrothermale. Toutefois, les éléments de terres rares, eux, étaient mobiles lors de cette altération, au cours de laquelle il y a eu appauvrissement des terres rares légères et enrichissement des terres rares lourdes. On a observé une différenciation dans la concentration des éléments du groupe des platinoïdes: les minerais sont relativement enrichis en Pd et Pt, ce qui est en harmonie avec la solubilité relativement plus élevée de ces deux éléments. Mais les ratios Pd/Ir dans les minerais sont plus bas que ceux des roches ultramafiques et des basaltes d'Emeishan. Les diagrammes des platinoïdes suggèrent que les intrusions ultramafiques ne sont pas la source principale de la minéralisation de l'or dans les GODES. Il est fort probable que l'or de ces gisements provienne de diverses sources, incluant les roches encaissantes, les formations sous-jacentes dans la croûte, et les roches basaltiques riches en or, très répandues.

Dans le sud-ouest de la province de Ghizhou, les GODES sont généralement encaissés dans les mêmes charnières de pli, contenant souvent une accumulation remarquable d'hydrocarbures, ce qui est courant dans les GODES. Les inclusions fluides organiques dans les minerais sont constituées d'hydrocarbures légers, de pétrole brut et de pyrobitume. Le contenu total de carbone organique dans les minerais et les roches encaissantes est généralement moins de 1%. La réflectance de la vitrinite et du pyrobitume dans les minerais et roches encaissantes varie de 1,5 à 4,5, se situant le plus souvent dans l'intervalle 2-3. La réflectance de la vitrinite et du pyrobitume dans les minerais est généralement supérieure à celle des roches encaissantes pour le gisement de Lannigou. La paléo-température maximale estimée par la réflectance de la vitrinite du gisement de Lannigou est équivalente ou légèrement inférieure à la température d'homogénéisation des inclusions fluides dans les minerais, ce qui est en accord avec l'impact hydrothermal observé sur la matière organique dans les roches encaissantes altérées. Par ailleurs, les paléo-températures maximales estimées par la réflectance de la vitrinite des gisements de Getang et de Zimudang sont supérieures aux températures d'homogénéisation des inclusions fluides dans les minerais. Ces résultats sont en accord avec le gradient paléo-thermal élevé de la région étudiée, et ils impliquent que la génération du pétrole est antérieure à la minéralisation de l'or. Cette étude a confirmé qu'il n'y a pas de corrélation entre les composantes organiques et la concentration en or dans les minerais. Cependant, il est intéressant de noter qu'il y a une corrélation positive entre les valeurs de S_2 (un paramètre de l'analyse Rock-Eval), de Au et de As dans les minerais du gisement de Lannigou. La maturation et la migration de la matière organique sont mises en évidence dans le diagramme

opposant TOC (carbone organique total) et HCI. À partir de la relation de recoupage du bitume et des veines de quartz, la migration du bitume devrait vraisemblablement avoir eu lieu avant la minéralisation de l'or. Toutefois, il n'est pas exclu que certains hydrocarbures aient été introduits par le biais du fluide minéralisateur.

De plus, l'analyse de groupe de la composante organique des minerais et roches encaissantes, extraite par dichlorométhane, montre que le degré de maturation des minerais est légèrement supérieur à celui des roches encaissantes. Toutefois, la composition des alcanes, "steranes" et terpènes de ces minerais qui sont utilisés comme biomarqueurs, est à peu près similaire entre les minerais, ce qui suggère une source commune de la matière organique dans les minerais d'une part, et celle dans les roches encaissantes d'autre part. Étant donné que la maturation des hydrocarbures s'est produite antérieurement à la minéralisation des GODES, il est possible que les hydrocarbures dans les parties anticlinales et leur dissolution dans les saumures de champs pétrolifères puissent avoir été un facteur favorisant la migration de l'or. Toutefois, ceci n'a pas pu être vérifié parce qu'en dehors de la portée de cette étude. Les résultats de la présente étude, de même que ceux d'autres études, montrent que, dans le cadre de systèmes où la pyrite aurifère, la lignite et le pétrole coexistent, la solubilité de l'or dans le pétrole brut peut atteindre le niveau des ppm. La solubilité de l'or à basses températures (80 °C) est assez élevée (710 ppb), en fait beaucoup plus élevée que pour les solutions inorganiques (10 ppb). Ces données suggèrent que les hydrocarbures dans des solutions hydrothermales ont probablement contribué à la migration de l'or, ce qui devrait faire l'objet de futures recherches.

Finalement, il est presque certain que la matière organique a contribué significativement à la préconcentration de l'or dans les roches encaissantes. Toutefois, son rôle dans la génération primaire et secondaire du pétrole brut, de même que sa migration, serait antérieur à la minéralisation dans la plupart des GODES. Donc, le pétrole brut ne fut vraisemblablement pas un facteur potentiel dans le transport de l'or. La présence d'hydrocarbures dans le système, par ailleurs, a clairement contribué à la minéralisation de l'or par le biais d'une réduction thermale des sulfates. Le pétrole brut colloïdal, de même que les hydrocarbures et acides organiques en solution, auraient grandement augmenté la solubilité de l'or sous forme de complexes organiques ou auraient protégé les colloïdes d'or en solution. En plus des complexes bisulfurés d'or, l'or sous forme colloïdale en solution a vraisemblablement joué un rôle important dans le lessivage et le transport de l'or, spécialement dans le cas des GODES qui présentent des signes de l'implication d'hydrocarbures dans le processus. Les réactions dans l'interface minéral-eau, incluant l'absorption par réduction et la complexation de surface, où la sursaturation en or n'est pas une condition préalable, sont également des processus importants contribuant à la création de dépôts d'or.

En conclusion, la matière organique a été une composante active dans les GODES sujets de cette étude. Ce facteur a contribué au processus de réduction thermale des sulfates, et ainsi, à la pyritisation. Les hydrocarbures en solution peuvent avoir augmenté le potentiel des solutions hydrothermales au transport de l'or. Les hydrocarbures ont été principalement dérivés des roches encaissantes, alors que l'or serait provenu de sources diverses, incluant des roches encaissantes, des roches sous-jacentes dans la croûte, des roches basaltiques et probablement des roches ultramafiques. Nos données suggèrent que les GODES au sud-ouest de Ghizhou sont probablement d'origine amagmatique, ce qui s'appuie sur l'absence totale de roches intrusives ignées dans le voisinage de ces gisements, sur le très faible grade métamorphique des roches de croûte et le l'absence d'événements métamorphiques dans l'intervalle de temps de la mineralisation des GODES, et sur la superposition d'époque de la minéralisation et de l'extension régionale.

摘要

黔西南微细浸染型金矿分布于扬子克拉通西南缘，主要产于二叠至三叠系粉砂岩和泥质灰岩中。自二十世纪八十年代以来，很多单位和个人对区内该类型矿床的地质地球化学特征，金的赋存状态和成因模式作过研究，但对微细浸染金矿与有机质成熟和演化的关系以及金成矿物质来源缺少系统研究。论文通过对典型矿床有机质存在状态、组成特征探讨其成熟和演化过程中对金成矿的贡献，通过对矿石、围岩、区内玄武岩和超基性侵入体微量元素(包括稀土、铂族元素)地球化学特征的研究对金成矿物质来源进行了论证。

选取烂泥沟、弋塘、紫木凼三个均形成于低温(120~240 °C) 、弱酸性至中性、还原环境，但产于不同地质背景下的微细浸染型金矿床作为考察对象。矿石及赋矿围岩的微量元素分析表明，高场强元素如 Nb、Ta、Zr、Hf 在成矿热蚀变过程为惰性元素。然而，稀土元素明显受蚀变作用的影响，其中轻稀土元素相对亏损而重稀土元素相对富集。铂族元素分异明显，由于 Pd 和 Pt 在溶液中的溶解度较大而在矿石中相对富集。矿石的 Pd/Ir 高于赋矿地层, 但显著低于峨嵋山玄武岩和超基性侵入体。矿石的铂族元素分布型式及铅同位素组成特征显示玄武岩和超基性侵入体不可能是主要的金成矿物质来源. 金来源可能包括赋矿围岩、下伏地壳岩石和区内广为分布的玄武岩类岩石。

黔西南微细浸染型金矿床常赋存于背斜或穹隆构造中，而这些构造中常含有一定量的烃类物质。矿石及赋矿围岩中常含有低于 1%的有机质，有机质如轻烃类、原油和热变沥清亦见于流体包裹体中。矿石及围岩中的镜质体和热变沥清的反射率变化范围为 1.5%至 4.5%, 但大多介于 2~3%。烂泥沟金矿矿石中的镜质体和热变沥清的反射率一般略高于赋矿围岩。由镜质体反射率推断的古地温近于或略低于流体包裹体的均一温度，受热液系统的影响相应的蚀变岩石及矿石中镜质体反射率略高。弋塘和紫木凼金矿矿石和围岩中镜质体的反射率较高，相应的古地温高于流体包裹体的均一温度。镜质体较高的反射率表明赋矿地层中有机成熟 (石油液态窗) 早于热液成矿作用。矿石有机质含量与金丰度间无相关关系，但有趣的是在烂泥沟金矿中矿石及蚀变围岩 S_2 (Rock-Eval 分析参数)与金和砷含量之间呈显著的正相关。TOC (有机碳总量)与 HCI (烃指数)的关系表明赋矿围岩及矿石中的有机质曾发生过迁移作用。矿石中沥清脉常为石英脉体穿截，显示出沥清质运移发生于金成矿之前。但目前没尚不能排除由成矿流体带入部分碳氢化合物的可能性。

矿石及赋矿地层中有机质的族组分析表明矿石中有机质的成熟度略高。有机质的气相质谱分析显示二者生物标记物组成非常相似，应具有相同的来源。鉴于有机

质的成油作用先于金成矿过程，储存于构造圈闭中的碳氢化合物及溶解于油田卤水中的有机质可能参与成矿流体对矿源层(岩)中金的淋滤和迁移作用。对含金黄铁矿、褐煤、原油及无机溶液实验体系中，金在石油中的溶解度可达 ppm 级。80°C 的温度条件下石油中金的溶解度达 710ppb,而相应条件下无机溶液中仅 10ppb 左右。在无石油的体系中，褐煤在粘土矿物催化作用下所产生的可溶有机物同样在很大程度上提高了金的溶解度。实验结果表明有机质很可能对热液成矿过程中金的迁移有某种程度的贡献，有必要做进一步的研究。

有机质对金成矿的贡献表现在如下几个方面。首先赋矿地层中的有机质在沉积、成岩过程中有利于金的预富集。有机质成油和迁移作用发生在成矿作用之前，石油不可能是微细浸染型金矿床成矿过程中金的运移媒介。然而，成矿热液体系中的碳氢化合物及有机酸的存在可以提高胶体金在溶液中的稳定性或形成金和的有机配合物有利于热液流体对矿源层(岩)中金的汲取和运移。有机质的存在有利于胶体金的稳定，使之成为金的硫氢配合物之外的重要运移形式。S_2 与金的相关性及含金黄铁矿硫同位素组成显示，碳氢化合物对硫酸盐类的还原作用对黄铁矿化和金的沉淀有重要贡献。矿物表面过程如吸附还原作用和表面配合作用可能是金沉淀的重要过程，这两种沉淀机理均不需要溶液中金达到过饱合状态。

总之，有机质在微细浸染型金矿成矿过程中应是一种活跃组分，对硫酸盐还原及黄铁矿化作用有重要影响。有机质可以提高成矿热液运移金的能力。体系中的有机质主要来源于赋矿地层，而金则可能来源于包括赋矿地层、下伏岩石、玄武岩类和超基性岩在内的混合来源。黔西南地区岩浆岩的缺如、极低的区域变质程度且缺少与成矿时代相呼应的变质事件，以及矿床的地质、地球化学特征表明区内微细浸染型金矿床应为非岩浆成因。成矿时代与区域性燕山晚期拉张作用一致，拉张作用产生的地热异常可能是区域成矿作用的热引擎。

ACKNOWLEDGEMENTS

This dissertation is part of the joint project of University of Quebec at Chicoutimi (Université du Québec à Chicoutimi, UQAC) and the Guangzhou Institute of Geochemistry, Chinese Academy of Sciences. I would like to thank the following individuals and organizations for their contributions to this work.

This work has been supported by AUCC-CIDA SULCP program supervised by professor Jayanta Guha. I would like to express my appreciation to professor Jayanta Guha (UQAC) and professor Zhenhua Zhao (Guangzhou Institute of Geochemistry, Chinese Academy of Sciences) for their constant encouragement, motivation, and considerate supervision throughout the whole doctoral program. Committee members, professor Huanzhang Lu (UQAC) and professor A. E. Williams-Jones (McGill University) are thanked for their helpful reviews and constructive comments.

I would like to thank Mr. Xunfeng Liu, the engineer-in-chief of Geological Bureau of Guizhou Province, for his helpful suggestions and information, and the Zimudang gold mine, Getang gold mine, and the Gold Industry Bureau of Zhenfeng County, for the access to the mining area and additional assistance during the field observation and sampling for this study.

Professor Lu Jialan, Professor Qian Zhixin, Ms. Yu Chiling, Ms. Hu Guangqina, Ms. Chai Pingxia of the Guangzhou Institute of Geochemistry, Mr. Qi Liang of the Institute of Geochemistry, Chinese Academy of Sciences are thanked for their assistance during the laboratory work. Dr. Li Jing of the Guangzhou Institute of Chemistry, Chinese Academy of Sciences is thanked for the access to the laboratory and supply of chemicals. Mr. Michel Tremblay, administrative adjunct of Centre d'Etudes sur les Ressources Minerales (CERM) is thanked for his kindly help during the whole program.

Ms. Diana Coonrod and Mr. Denis Masson are thanked for translating the abstract to French and editing the manuscript that greatly improved the readability.

TABLE of CONTENTS

List of tables:

List of figures:

1

INTRODUCTION

1.1 Distribution of sediment-hosted disseminated gold deposits

Sediment-hosted disseminated gold (SHDG) deposits, also referred to as Carlin-type gold deposits, have been recognized as a distinct type of ore mineralization only relatively recently. Although high-grade portions of these deposits, such as those at the Mercur deposit, Utah, U.S.A., have been mined since the last century (Jewell and Parry, 1987), they were not recognized as a distinct class until the discovery of disseminated gold mineralization in carbonate rocks in 1961, and the development of bulk-tonnage mining of Carlin deposits between 1962 and 1965 (Hausen and Kerr, 1968). The Carlin Trend, including past production and resources, forms the largest and most prolific accumulation of gold deposits in the North America. To date, over 25 million ounces of gold have been mined in the Carlin Trend from 26 separate past-producing or operating mines (Teal and Jackson, 1997). Besides the SHDG ore deposits found in the U.S.A., deposits have been reported elsewhere, and these include some so called Carlin-like gold deposits which are genetically associated with magmatic activity, i.e., in China, Hungary, Ukraine, Iran, Slovakia, Indonesia, Malaysia, Philippines, Greece, Spain, Mongolia, Peru, Italy, and

Canada (Turner et al., 1994; Shumlyanskiy and Ivantishina, 1998; Knesl and Kneslova, 1999; Korpas and Hofstra, 1999; Lattanzi, 1999; Asadi et al., 2000; Cluer et al., 2000). Nevertheless, most of the gold resources of this type are found in the U.S.A.; even though China ranks second as to available SHDG type gold reserves, its reserves are incomparable to U.S.A.

1.2 SHDG deposits in China

In China, the first SHDG deposit was recognized and explored in a former small mercury mine in Shixia, Hengdong, Hunan Province (Liu et al., 1994a). The deposit occurs in Devonian argillic limestone and was considered to be similar to Carlin gold deposits in the U.S.A. Since then, over 100 SHDG deposits have been discovered in Guizhou, Sichuan, Yunnan, Guangxi, Shanxi, and other provinces, and have become an important gold resource in China (Fig.1-1). Most of the deposits, however, are small (Liu and Geng, 1985; Cunningham et al., 1988. Table 1-1, 1-2), and their size and bulk tonnage are significantly smaller than those in the U.S.A. In addition, the total production is limited because mining activities are largely restricted to oxidized ores due to technical limitations.

1.3 Main controls on the distribution of SHDG deposits

Deposits, both in China and in the U.S.A,. are located near the buried edge of a Precambrian craton. More specifically in China, the SHDG deposits are mainly located along the edge of the Precambrian Yangtze Craton (Fig.1-2), and are hosted by the upper Permian to Triassic Sequences (Fig.1-3). In the U.S.A., the deposits found in the Carlin

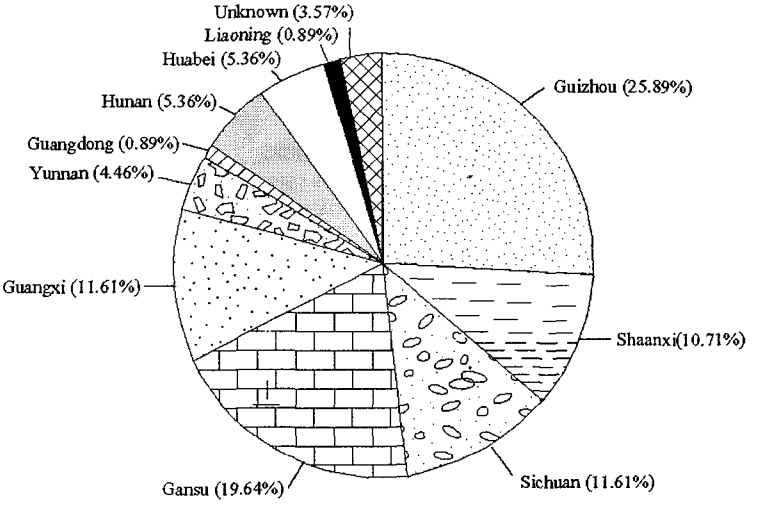

Fig.1-1. Distribution of Chinese SHDG deposits by Provinces (Li and Peters, 1998).

Table 1-1. Size* and location of Chinese SHDG Deposits

Location	Province	Large	Medium	Small	Unknown	Total
	Yunnan	1	1		3	5
Dian-Qian-Gui	Guizhou	3	2	8	16	29
	Guangxi	1	1	3	8	13
	Guangdong	1				1
	Shaanxi	4	1	3	4	12
Qinling	Sichuan	4	3		6	13
	Gansu	1	5	4	12	22
	Hunan	1		1	4	6
	Huabei	1	2	3		6
Other	Laoning	1				1
	unknown				4	4
	Total	18	15	22	57	112

* Large: >20 tons Au (include extra large >50 tons Au)
Medium: 5 to 20 tons Au
Small: <5 tons Au
Unknown: not yet identified resource

From: Li and Peters, 1998.

Table 1-2. Comparison of SHDG deposits in Nevada and China

Geological Feature	Nevada SHDG Deposits	Chinese SHDG Deposit
Tectonic setting	transform zone of miogeocline	rift area of cratonic margin
Host strata	carbonate rocks of Paleozoic, especially Silurian and Devonian age	carbonate and clastic rocks of mostly Devonian and Triassic age
Host rock types	impure carbonates, fine-grained clastic rock, breccia; high TOC content in some rocks	fine-grained clastic rock, Carbon + Silica argillite, breccia; high TOC content in some rocks
Metamorphic grade	slate - phyllite, dynamo-metamorphic	slate - phyllite
Igneous intrusions	igneous intrusion of Cretaceous - Jurassic age; Tertiary volcanic rarely present	dikes of Cretaceous,Tertiary age present in some deposits
Metallogenic epoch	late Cretaceous - Tertiary	Cretaceous-Tertiary
Paragenesis-metals	Hg, Sb, As, Tl	Hg, Sb, As, Tl
Ore control structure	structural window in low-angle faults, high- angle normal faults, breccia zone in strata	regional deep faults, faults parallel to axis of anticlines, breccia zone in strata, density squeezed fracture zones, and unconformities
Deposit morphology	stratiform, lensoidal, vein, irregular	stratiform lensoidal, vein
Alteration	decalcification, jasperoid silicification, argillization, pyritization, dolomitization	silicification, argillization, pyritization, dolomitization, (albitization)
Structure of ore	disseminated, stockworks, breccia	disseminated, stockworks, breccia
Size of gold grains	microscopic - submicroscopic grains native gold	microscopic - submicroscopic grains native gold, rare visible gold (in oxidized ore)
Mineral assemblage	native gold, pyrite, realgar, orpiment, cinnabar, stibnite, arsenopyrite, Tl minerals, quartz, clay minerals, carbonate barite, organic carbon	native gold, pyrite, realgar, orpiment, cinnabar, stibnite, arsenopyrite, lorandite, (pyrrhotite), quartz, clay minerals, carbonate, barite, organic carbon
Pathfinder elements	Au, As, Hg, Sb, Tl, W, Mo	Au, As, Hg, Sb, Tl (Ag)
Au / Ag	3 to 17	> 1 to 25
Zone of oxidation	common	common, but less important than primary ore

Modified after Liu et al., 1994a.

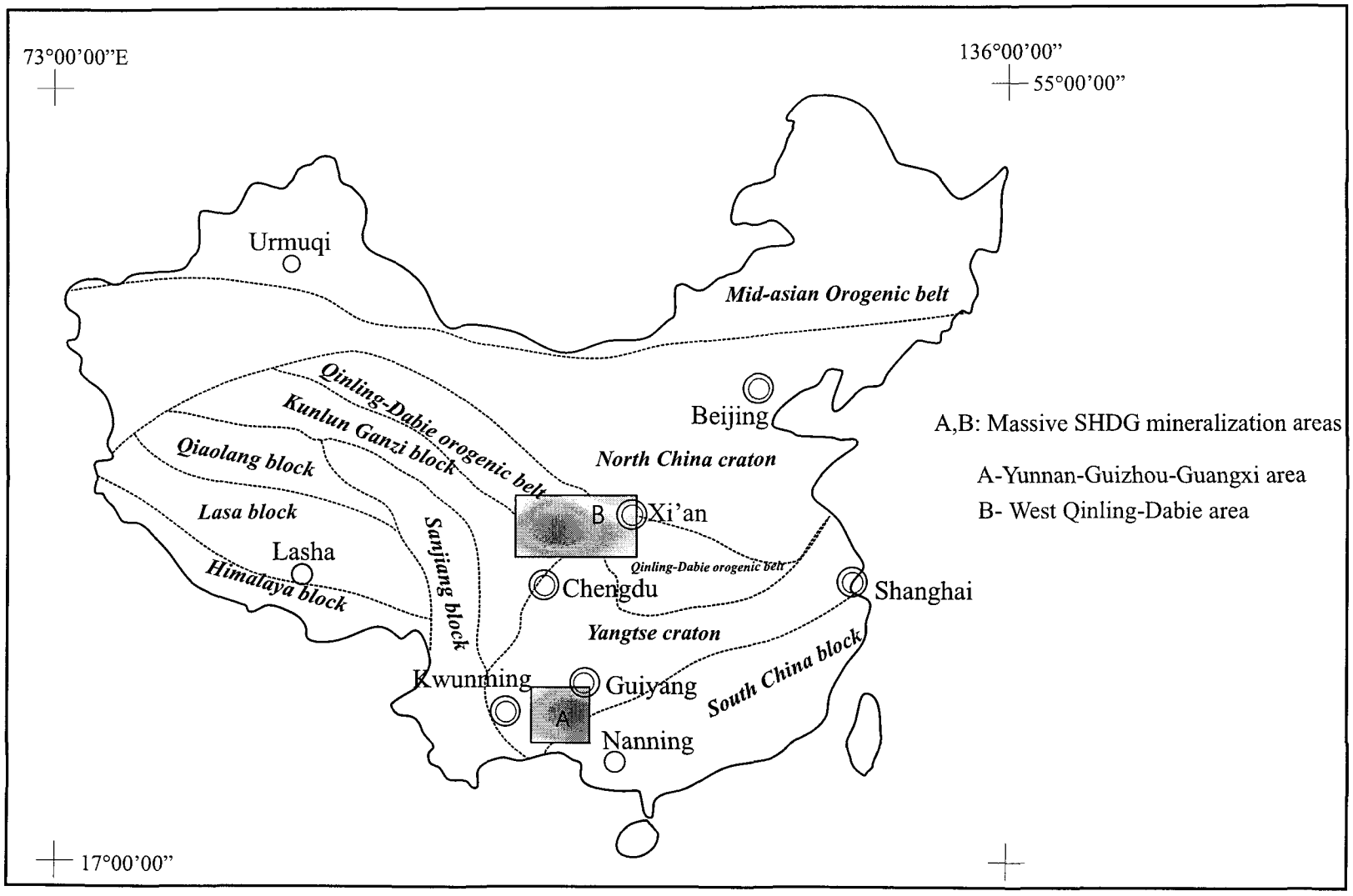

Fig. 1-2. Location of the main SHDG mineralization areas in China
The SHDG deposits are mainly distributed in the Yunnan-Guizhou-Guangxi area at the southwestern margin of the Yangtse craton and the Qinling-Dabie orogenic belt area on the northern margin of the Yangtse craton.
Modified from Liu et al., 1994a.

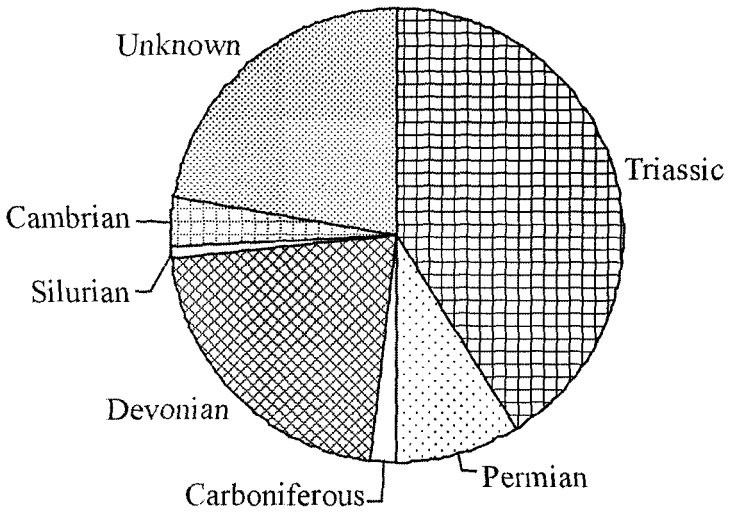

Fig.1-3. Distribution of Chinese SHDG deposits by age of host rocks.

trend are hosted by a variable stratigraphic package of Ordovician through Lower Devonian rocks, which are generally older than the host rocks of the SHDG deposits in China.

The host rocks of the known SHDG deposits, in southwest Guizhou Province, China, are generally turbidite or carbonate formations with detrital, siliceous and basic volcanic rock, and ash tuff. The age of the strata ranges from the Cambrian to the Triassic Period. Gold mineralization commonly occurs at the contact of the detrital and carbonate layers on the side of the detrital rocks. Generally speaking, there is no special affiliation of the SHDG deposits with particular strata, yet gold mineralization is usually limited to one or two horizons in certain area. The formations hosting the gold generally belong to open sea platforms to shallow sea facies. The ore-hosted formations are usually characterised by (1) enrichment in organic matter, (2) turbidites with volcanic rock and siliceous interlayers, and (3) a higher content of ferrous carbonate (ferrodolomite-siderite).

In the U.S.A., where most of the known SHDG deposits are found in the Great Basin, the host rocks are mainly Lower Paleozoic sedimentary rocks, namely Silurian and Devonian, but may range in age from Cambrian to Mississippian. A few deposits are located primarily in younger sedimentary rocks (e.g., the Standard deposit, Triassic), and a few other showings of minor mineralization occur in igneous rocks (e.g., the Post deposit, Getchell). Many of the large ore deposits (e.g., the Carlin, the Post/Betze deposit) occur in the Silurian-Devonian Roberts Mountains and in the Popovich Formations (Evans, 1980).

In China, the SHDG deposits are hosted by strata ranging from Palaeozoic to Mesozoic Era, from Cambrian to Triassic age, with most of the deposits occuring in Triassic formations. In the latter, the host rocks consist mainly of pelitic siltstone with carbonate interlayers. Since most SHDG deposits are mainly hosted by impure carbonate and detrital (turbidite) sedimentary formations, and since gold mineralization, in certain areas, is limited to one or two strata, it was taken for granted that SHDG deposits were strata-bound or even syn-sedimentary (Li et al., 1989b; Yang and Dong, 1994). However, the distribution of the ore bodies is largely controlled structurally.

Ore-controls may be considered at a number of different scales. In a regional sense, they are tectonically restricted to the boundary of terranes. In China, the SHDG deposits are mainly distributed in the Mesozoic and/or Palaeozoic depressions around the Yangtze Craton. The SHDG mineralization zones are controlled by deep faults, thus, are closely associated with rifts. For instance, the SHDG deposits in the Dian (Yunnan Province)-Qian (Guizhou Province)-Gui (Guangxi Province) are intimately related to the Youjiang-Nanpangjiang-Liupanshui rift that developed in the Caledonian and Indo-Chinese Epoch. Local control of individual ore-bodies is associated with faults and folds, especially where the faults cut folds containing favourable stratigraphic horizons.

1.4 Main geochemical characteristics of SHDG mineralization

The hydrothermal alteration associated with SHDG mineralization include sulfidation, silicification, decarbonatization, argillization and late stage carbonatization. SHDG

mineralization is also closely associated with As, Hg, Sb, and Tl anomalies, sometimes with As, Tl and Hg mineralization of economic significance. Au/Ag ratios are generally more than one, which means that silver is not of significant value in the ores. The ore minerals usually consist of the so-called low temperature mineral assemblage, such as arsenian pyrite and arsenopyrite, orpiment, realgar, cinnabar, stibnite. In some areas, native mercury, native As, separate thallium minerals like lorandite were also observed. In China, some of the SHDG deposits were found within or near former As and/or Hg mine areas (as in the Lannigou and Danzhai deposits). Most of the gold in the SHDG deposits is extremely fine-grained (Wells and Mullens, 1973; Arehart et al., 1993a; Arehart, 1996) and occurs in hydrothermal arsenian pyrite, and less commonly in quartz, carbonaceous matter and fine-grained phyllosilicates.

The general geological characteristics of a number of SHDG deposits in U.S.A. have been tabulated by Tooker (1985), Bagby and Berger (1985), and Ilchik and Barton (1997). The similarities and differences of the U.S. and Chinese SHDG deposits have been analyzed by Yang and Dong (1994). Even though subtle differences exist between them, the deposits of the two countries share sufficient general characteristics that the term "SHDG deposit" will be used herein to encompass all the deposits that share these characteristics. The general characteristics of the SHDG deposits in Nevada, U.S.A and those in China are listed in Table 1-2.

Until the past few years, the prevailing hypothesis regarding the formation of these deposits was that they are related to near-surface hydrothermal systems. Several

investigators have inferred a shallow epithermal origin, that is, formation at low temperature and near the contemporary ground surface (Radtke, 1985; Rye, 1985; Rota, 1988). Similarly, Joralemon (1951,1975) suggested that the SHDG deposit at the Getchell Mine was very young and that the outline of the ore-body could be related to the modern ground surface. Partly as a result of this genetic model, most exploration for SHDG deposits was restricted to shallow (<150m) depth and many shallow deposits were discovered through the late 1970s and early 1980s (Teal and Jackson, 1997). In contrast, Kuehn and Rose (1995) estimated that the Carlin deposit was formed at a depth of 3.8±1.9 km within a temperature range of 215±30 °C. The high-density CO_2 inclusions and the newly discovered deep ores suggest that a relatively shallow geological setting is not a prerequisite for SHDG mineralization.

1.5 Definition of SHDG mineralization

Although there is not a universally accepted terminology to describe this type of mineralization, the SHDG deposits can be characterised by:

1) Sedimentary host rocks mainly consisting of carbonate and fine clastic sequences;

2) Ore mineral assemblages consisting of submicron native gold, arsenian pyrite, pyrite, arsenopyrite, realgar, orpiment, cinnabar, stibnite, barite, calcite, fluorite and quartz. Native gold grains occur as submicron particles often ranging from 20Å to 200Å in diameter within the lattices of arsenian pyrite and pyrite, though most are near the lower figure (Arehart, et al., 1993b);

3) Ore-forming element assemblages consisting of Au, As, Hg, Tl, Sb, and a greater than 1 Au/Ag ratio in the ores;

4) Alteration including silicification, sulfidation, argillic alteration of primary silicate minerals, and decalcification (carbonate dissolution);

5) Amagmatic origin for most if not all of the deposits (Yang and Dong, 1994; Ilchik and Barton, 1997). Some of the deposits are associated with intrusive rocks spatially but not temporally and genetically. Since geological data indicates that igneous activity predated gold mineralization, there is, therefore, no evidence that links mineralization and igneous activity (Hofstra, et al., 1991) with the exception of a few so called Carlin-like deposits, such as the Lone Tree deposit (Doebrich and Theodore, 1996).

Deposits clearly associated with magmatic activity and/or metamorphism will not be included in the SHDG deposit type in this study. Even though disseminated gold is observed in some mesothermal gold mineralization associated with magmatic activity or metamorphism, these deposits are different from the SHDG deposits and, therefore, should not be included in this category. For example, the Maoling disseminated gold deposit, which occurs in Proterozoic sedimentary rocks in the North China Craton, clearly shows a genetic relationship with magmatic activity (Cheng et al, 1992). The deposit consists mainly of fine disseminated arsenopyrite and pyrrhotite. The host rocks have undergone green-schist- to amphibolite-facies metamorphism, and some ores occur within andalusite-grade contact metamorphic rocks of the intrusion. Other examples are the mesothermal gold deposits of the Meguma Terrace in Nova Scotia, Canada, where disseminated low-grade

gold has recently been recognised. These deposits were metamorphosed from green-schist to amphibole facies and were subsequently intruded by ca. 370Ma peraluminous granites and minor mafic intrusions. Isotopic investigations and dating of the vein minerals indicate that the mineralization was related to migration of metamorphic fluids from multiple reservoirs in the waning stages of the Acadian Orogeny (Ryan and Smith, 1998).

Finally, the SHDG deposit type in this study is confined to low to medium temperature hydrothermal gold mineralization occurences mainly in sedimentary unmetamorphosed and/or super-low grade metamorphosed sedimentary rocks; however, some volcanic rocks and magmatic rocks may also host some of the ores. The deposits consist of a series of low to medium temperature hydrothermal mineral assemblages, within which gold predominantly occurs as submicron to micron scales in arsenian pyrite.

1.6 Debate on the source of gold and the genetic association of SHDG gold mineralization with organic matter

The source or sources of the ore-forming material, including the gold and hydrothermal solution, for SHDG mineralization have been extensively debated and is still not quite clear. Different models regarding the gold source have been proposed: (1) The source bed hypothesis suggests that gold derived mainly from the gold-rich strata during deep circulation of meteoric water. The water was driven either by elevated geothermal gradients during regional extension and accompanying magmatism (Liu and Geng, 1985; Wang et al., 1992; Hofstra, 1995; Ilchik and Barton, 1997), or as a result of regional metamorphism and dehydration of these same metasedimentary rocks (Philips and Powell,

1993; Keuhn and Rose, 1995). Some researchers have proposed that the gold, heat and fluid (formation water) all come from the host rocks (He et al., 1993; He, 1996). (2) In models proposing a magmatic link, gold is derived from a stock or pluton (Sillitoe and Bonham, 1990; Zhu et al., 1998a; Liu et al., 1999). A variation on the magmatic model proposes that plutons simply provided the thermal energy necessary for focussing a hydrothermal system (Arehart et al., 1993c; Yang and Dong, 1994; Keuhn and Rose, 1995). In this case, gold was derived largely from sedimentary rocks with little or no contribution from the plutons. (3) The mixed source model suggests that gold and fluid derived from multiple sources, including host rocks, magmatic rocks, and even from lower or middle crustal rocks (Zhang et al., 1996; Tosdal et al., 1998).

The question of the source of gold for the SHDG deposits in southwest Guizhou has been discussed by many researchers and is still actively debated. Geologists of Guizhou Geological Bureau suggest that host rocks are the main source and claim that all the gold, fluid and heat were derived from the same source beds (e.g., Han and Sheng, 1996). That is, the gold in SHDG deposits and the petroleum in ancient oil traps originated from the same source beds ("double source bed"), from which they migrated together to the reservoir where the breakdown of hydrocarbons resulted in gold mineralization (e.g., Lin et al., 1993a,b). Recently, a few researchers have proposed that the gold of SHDG deposit was mainly derived from the mantle (e.g., Ni et al., 1997) or a mixture of mantle and crust (e.g., Zhu et al., 1998a). It is well known that SHDG deposits are closely associated with organic

matter since the host rocks and the ores typically contain variable amounts of organic matter.

Concerning the origin and role of the hydrocarbon materials, two theories have been debated. According to the first theory, the evolution of organic matter is a separate event and the oil and gold are apparently related only in so far as they accumulated in the same structural traps (Presnell, 1993). The second theory considers organic matter as the dominating factor controlling leaching, migration and deposition (Lin et al., 1993b; Liu et al., 1994b).

1.7 Objectives and methodolgy

Several research papers, mostly in Chinese, have been published on the SHDG deposits of southwest Guizhou Province but they are rather general and have contradicting conclusions, especially on the aspects of the role of organic matter and the contribution of the ultramafic intrusions. The principal objective of this study is to bring some new insights as to the role of organic matter in the formation of SHDG deposit. On a broad scale, it is hoped that this study will be able to throw some light on the role of organic matter in hydrothermal ore forming processes. The secondary objective is to contribute to the understanding of the source or sources of gold deposits in southwest Guizhou.

The first objective was attained through (1) observation of the occurrence of the organic matter in the host rocks and the ores; (2) determination of the total organic carbon content of the altered and unaltered host rocks and the ores; (3) establishing the degree of

maturation of the organic matter in the host rocks and the ores; and (4) analysis of the extractable hydrocarbons in the host rocks and the ores. The above results have enabled to infer the source of the organic matter in the ores (autochthonous versus allochthonous) and to evaluate the association between the gold mineralization and the maturation of the organic matter. Furthermore, a simulation experiment was carried out to examine the possible effect of organic matter on the gold solubility. The secondary objective was approached through trace element investigation of the host rocks, altered host rocks and the ores.

To fulfill these objectives geochemical investigations of three typical SHDG deposits in southwest Guizhou Province, China were undertaken. The Lannigou, the Getang, and the Zimudang gold deposits were selected for detailed field observation, sampling and laboratory investigation. The emphasis was on the Lannigou deposit since in the other two deposits access to the primary ore was limited. Observation of the occurrence of the organic matter in the host rocks and the ores both in the field and in the laboratory under microscope has been carried out. Conventional petroleum geological methods such as Rock-Eval analysis, extractable organic components grouping and gas chromatograph-mass spectrum (GC-MS) analysis of the host rocks and ores were utilized to determine the type, content, maturation, and the biomarkers of the organic matter in the samples. A simulation experiment on the influence of hydrocarbons (lignite and crude oil) on gold solubility were also carried out to study the possible contribution of organic matter to gold transportation. Samples of ultramafic rocks, host rocks, and ores from the surface and underground were

analyzed for trace elements including rare earth elements (REE) and platinum group elements (PGE). The ICP-MS method was adopted to analyse these elements and to determine (1) their mobility during hydrothermal alterations, (2) whether the mantle was a possible source of Au mineralization, and (3) geochemical prospecting possibilities. Au, As and Hg contents of the ores and host rocks were analysed on the purpose of examining the possible relationship of their enrichment and association with organic matter.

The type, content, maturation and biomarkers of the organic matter in the ores were compared with those in the host rocks to verify the significance of allochthonous organic matter and the genetic relationship between organic matter and gold mineralization. The trace element patterns of the ores were compared with the altered and unaltered host rocks, and nearby basaltic rocks and the ultramafic rocks to trace the possible sources of gold. The result of this study has been synthesized with the published data to present an overall idea of the geology, the geochemical characteristics, and the prevailing ideas on genesis of these deposits.

2

REGIONAL GEOLOGY

The SHDG deposits found in China, like those in the U.S.A., are located near the buried edge of a Precambrian craton. In China specifically, the SHDG deposits occur along the edge of the Precambrian Yangtse Craton. Most of the known SHDG deposits in China are distributed in two Palaeozoic to Mesozoic sedimentary basins tectonically surrounding the Yangtse Craton. The Dian (Yunnan)-Qian (Guizhou)-Gui (Guangxi) area is located on the southwestern margin of the Yangtse Craton and the Qinling area on the northwestern margin (Fig. 1-2; Fig. 2-1). The Dian-Qian-Gui "gold triangle" occurs on a large cryptic crustal discontinuity, which is host to many large-scale deposits as shown by the lead isotopic mapping in south China (Fig.2-2). The multiphased activities of the crustal discontinuity in the region may have contributed to a high ancient geothermal gradient, mantle-crustal interaction and, thus, to mineralization processes. Within the "triangle" area, southwest Guizhou Province hosts the major part of the SHDG mineral resources. In this study, "southwest Guizhou Province" designates the area comprising the counties

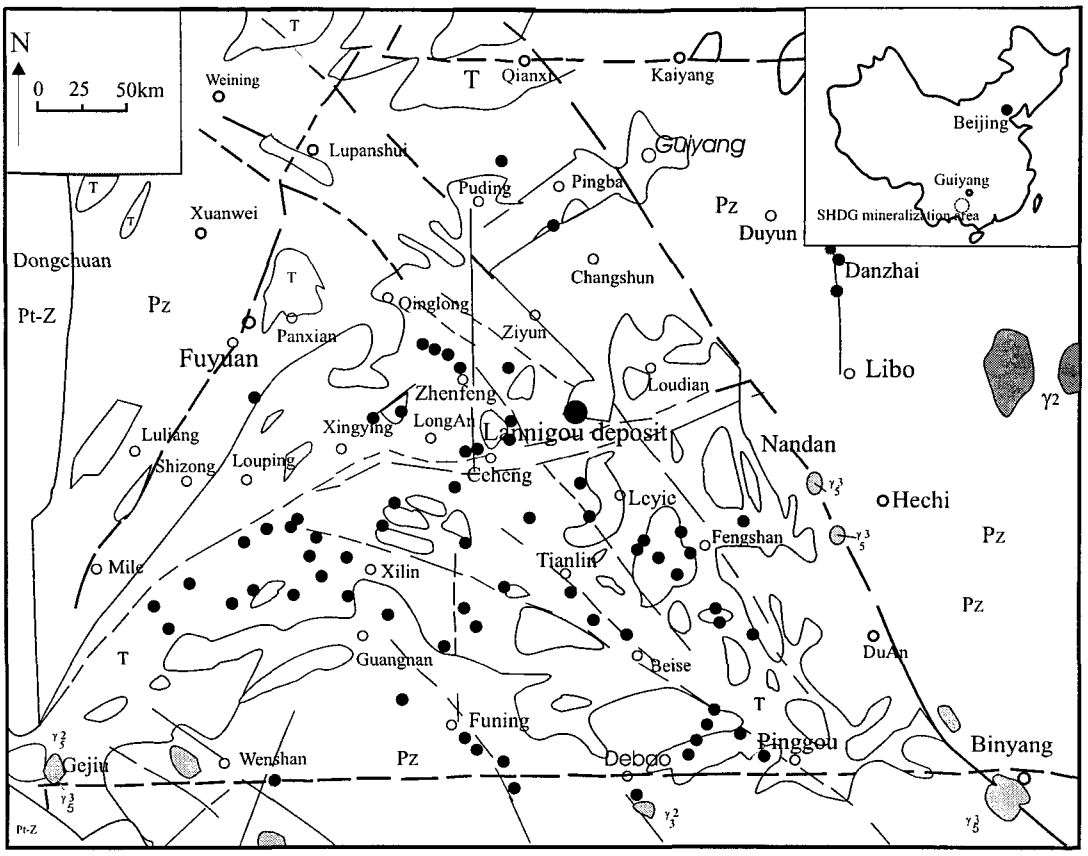

Fig.2-1. Simplified map showing SHDG deposit distribution in the Yunnan-Guizhou-Guangxi triangle district.

Pt-Z Precambrian strata	Pz Paleozoic strata
T Triassic strata	γ_2 Early Paleozoic granite
γ_3^2 Calidonian granite	γ_5^3 Late Yanshanian granite
Fault	SHDG deposit (mineralization)
γ_5^2 Early Yanshanian granite	

(After Yang and Dong, 1994)

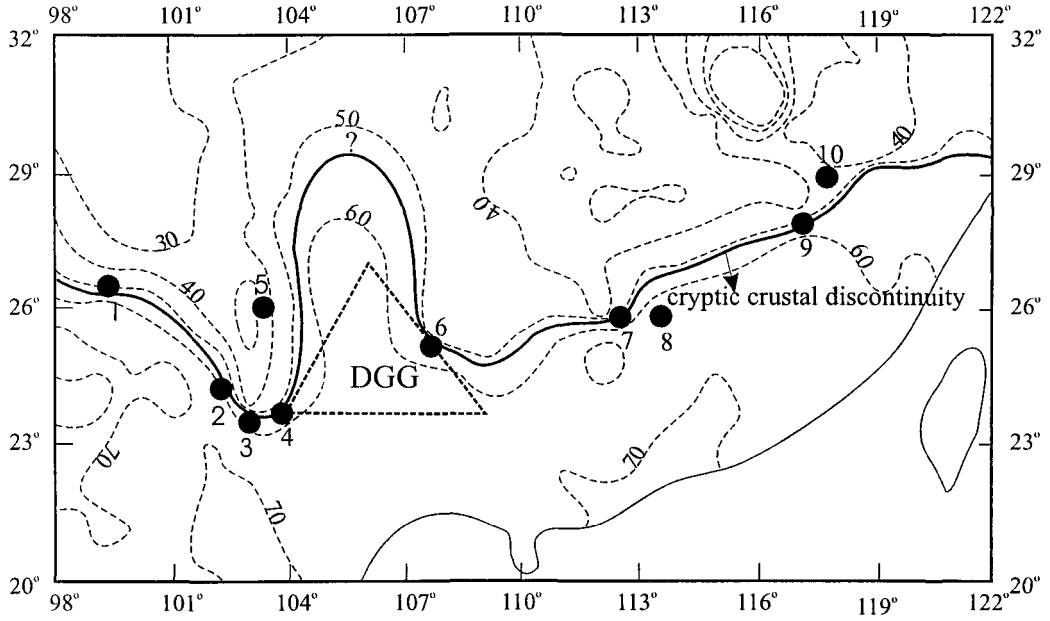

Fig.2-2. Lead isotopic (V1) isopleth of the south China showing the relation between a cryptical crustal discontinuity and large deposits (after Yang and Dong, 1994).
•-The known large deposit (1.Lanping Jinding; 2. Dahongshan; 3. Gejiu; 4.Mengzi Bainiuchang; 5.Dongchuan Tangdan; 6. Dachang; 7. Shizhuyuan; 8. Xihuashan; 9.Lengshuitan; 10. Dexing);
DGG - Main SHDG mineralization area in the Yunnan-Guizhou-Guangxi Province.
V_1parameter introduced to eliminate the age effect from the Pb isotope composition and to elucidate the actual differences in U/Pb and Th/U, for method of calculation see Zhu, 1995).

tectonically located on the southern fringe of the Yangtse Craton; the counties are Qinglong, Puanxian, Pa'an, Xingren, Anlong, Ceheng, Mowang and Ziyun (Liu, 1994).

Geological investigations in southwestern Guizhou Province began at the very beginning of the 20th century, and these include regional geological mapping, mineral resource reconnaissance, petroleum exploration, etc. The area is famous for its coal, limestone, antimony, mercury, and sulfur mineral reserves. Other mineral resources, such as copper, arsenic, manganese, aluminum, lead and zinc, have also been explored and mined in the area. The history of gold production in Guizhou Province can be traced back 1 000 years; however, it was not until 1978 that SHDG mineralization, often also referred to as Carlin-type, was discovered in the area. The first sediment-hosted disseminated gold (SHDG) deposit, the Banqi gold deposit, was discovered within a former antimony mining area in Ceheng County. Since then, more than twenty SHDG deposits of varied scale have been explored, most of them associated with Hg, As, Sb anomalies or mineralization.

2.1. Tectonic settings of the research area

In the last decade, two contradictory hypotheses regarding the tectonic evolution of southeast China have been proposed. One school suggests that after the two phases of orogenic movement during the Late Proterozoic and Early Paleozoic Era, the southeast China orogenic belt converted to a relatively stable platform in the Late Paleozoic Era (Ma et al., 1992; Xu et al., 1992). The other school advocates that southeast China consisted of two blocks, the Yangtse and South China block, with an active transient or oceanic crust in-

between the two. These two blocks collided and sutured along the Hunan-Jiangxi-Zhejiang belt during the Mesozoic Era (Xu et al., 1987; Li et al., 1989a). The point at issue mainly hinges on the attribution of the unfossiliferous Banxi Group. Recent research shows that the Banxi Group is not a tectonic melange, an interpretation which previously had been used as evidence of subduction, but rather a successive sediment sequence developed in the Proterozoic Era. As a result, the existence of the so-called "Indo-China Banxi Ocean" is becoming more and more questionable (Chen et al., 1995; Liu and Zhu, 1994). It is now more generally accepted that the south China area was apparently influenced by the ancient-Tethys system. During the period from Late Paleozoic to Triassic, this region went through significant extension, resulting in the development of small scale ocean basins in certain areas. The Yangtse block was surrounded by many continents of varying sizes and was separated by oceanic basins of different types in the Hercynian to Indo-China periods. Thus, this region can be treated as part of the multi-island ocean of the Palaeo-Tethys Era (Feng et al., 1996).

Southwestern Guizhou Province is located on the contiguous area of the Yangtse Block and the Youjiang-Nanpanjiang basin (also referred to as the Youjiang-Nanpanjiang rift, or Youjiang orogenic belt). The basement of the Yangtse block consists of three layers. The basal part is composed of Archean and Early Proterozoic amphibolite-granulite facies. The middle part consists of Middle Proterozoic volcanicclastic metasediments of green schist to amphibolite facies. The upper part is made up of Late Proterozoic low grade

metamorphic rocks. All of the layers form the so called "three layered" fundamental structure. Ever since the Sinian Period, the capping formation was dominated by passive margin shallow water sediments, and volcanic activity was rare despite the emplacement of Permian Emeishan continental flood basalt and sill-like diabases. The basal and middle layers of the Guizhou Province basement are similar to those of the Yangtse block. The capping sedimental formation consists of Devonian to Early Triassic passive marginal sediments and Middle Triassic terrigenous detrital turbidite deposits. During the middle to late Carnian stage of the Triassic Period, the Youjiang area, south of the Yangtse (passive marginal carbonate sediment) evolved into foreland basin facies and accumulated huge terrigenous clastic turbidite. As the nappe structures push intensively northward in the Late Triassic, the turbidite wedge developed northward and overlapped the carbonate on the margin of the craton. After the Carnian stage, the sediment changed to molasse.

The Youjiang-Nanpanjiang Basin straddles a vast area including northeast Yunnan Province, northwest Guangxi Province and southwest Guizhou Province (Fig. 2-3). During the Early Paleozoic Period, the basin was part of the fringe of the Yangtse block. During the late Paleozoic Period, it evolved into the relatively active South China Platform within which some basins underwent sedimentation from the Silurian to the Devonian. During these Periods, a series of deep sea sequences accumulated on the platform, sequences consisting of siliceous pelitic sequence, plus volcanic and terrestrial detrital turbidites (Zeng et al., 1992). Volcanic sedimentation started in the Early Devonian Period and persisted

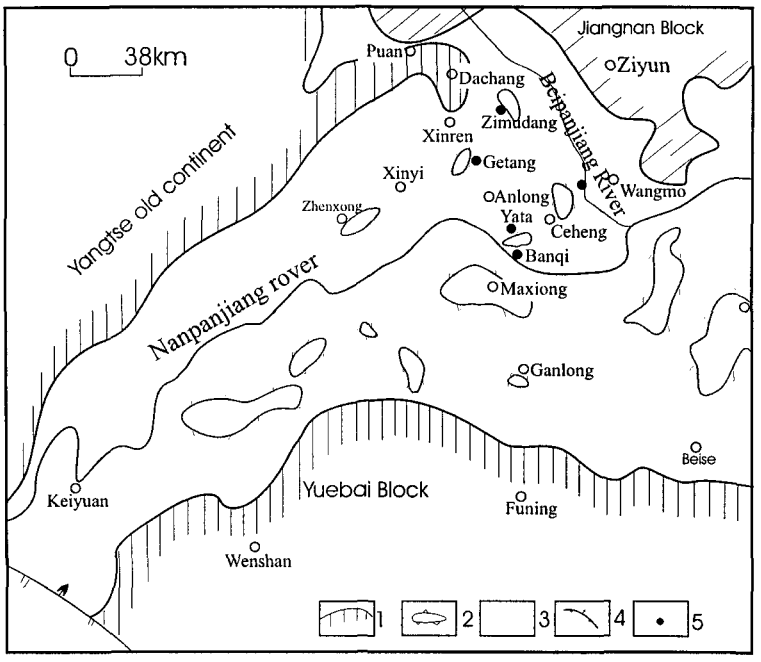

Fig.2-3. Sketch map of the Yunnan-Guizhou-Guangxi Basin (after Xiao et al., 1998).

1.Old continent; 2.Basement uplift; 3.Basin; 4.Fault; 5.Gold deposit

until mid-Triassic Period. In many parts, as a result, the basalt layers are more than 100 m thick and often include intercalated siliceous exhalite (Wu and Li, 1993). The Youjiang-Nanpanjiang basin is also referred to as the Youjiang-Nanpanjiang rift, Youjiang rift, or Dian-Qian-Gui rift. Its rifting activities began during the Devonian Period and ended during the Triassic Period. In the rift system, sediments over 10 000 m thick were accumulated. These include bimodal rift volcanic rocks, and sedimentary sequences of rift type which consist of platform carbonate sediments, and pelitic and siliceous sediments showing characteristics of sedimentary differentiation of trough-basin type. During the early and middle stages of the rift evolution, the clastic sediments were derived from the east and west sides of the rift shoulders. The sediments were first accumulated near the rift axis and then extended southward. During the late stage of the rift, the clastic sediments were derived from its southern and southeastern areas, and the sediment front migrated northwards or northwestwards. Therefore, this rift opens southward and can appropriately be called a rifted-trough (Xia et al., 1992).

The development of the Youjiang-Nanpanjiang rift can be divided into three stages. (1) The early stage of rifting is characterized by the Early Devonian to the beginning of Middle Devonian rift-type molasse-type sediments. The sediments of this stage are a series of clastic rocks including conglomerate rock, sandstone, siltstone, etc., and the bottom of the sequence is characterized by its purplish red color. The thickness can be up to 1 800 m (as was observed in Nandan area), with an estimated accumulation rate of about 64 m/Ma.

(2) The middle stage of the rifting is characterized by a huge accumulation of carbonate and argillaceous rocks from the Middle Devonian to the beginning of the Middle Triassic Period. The total accumulation is as thick as 5 000 m, at an estimated accumulation rate of ~ 35 m/Ma. (3) The late stage rifting is characterized by the huge turbidite accumulation of the Middle Triassic Period and late Triassic molasse. The turbidite sediments are up to 3 000 m thick with an estimated accumulation rate of ~ 240 m/Ma, and the accumulation of the molasse exceeds 1 000 m in thickness at an estimated accumulation rate of ~ 60 m/Ma (Gou, 1985). In the late stage, the clastic material forming the turbidite and molasse sediment was mainly derived from the uplift of the orogenic belt southeast of the region.

2.2. Evolution of the sedimentary environment

Most of the known SHDG deposits in southwest Guizhou are located near the southern edge of the Precambrian Yangtse Craton and the adjoining accretionary fold belts. The major part of Guizhou Province is overlain by the Yangtse Craton, which is composed of Proterozoic crystalline rocks overlain by Paleozoic and Lower to Middle Triassic marine deposits and Upper Triassic terrestrial deposits (Xiong and Coney, 1985; Bureau of Geology and Mineral Resources of Guizhou Province, 1987). The SHDG deposits discovered in the Yunnan-Guizhou-Guangxi area occur mainly in Triassic turbidites (Fig. 2-4). Research shows that the Yunnan-Guizhou-Guangxi area was a triangular rift from the Late Permian to the Late Triassic Period, which was located in the converging region of the Yangtse Old Continent, the Jiangnan and Yuebai Block (Fig. 2-3). The Old Continents

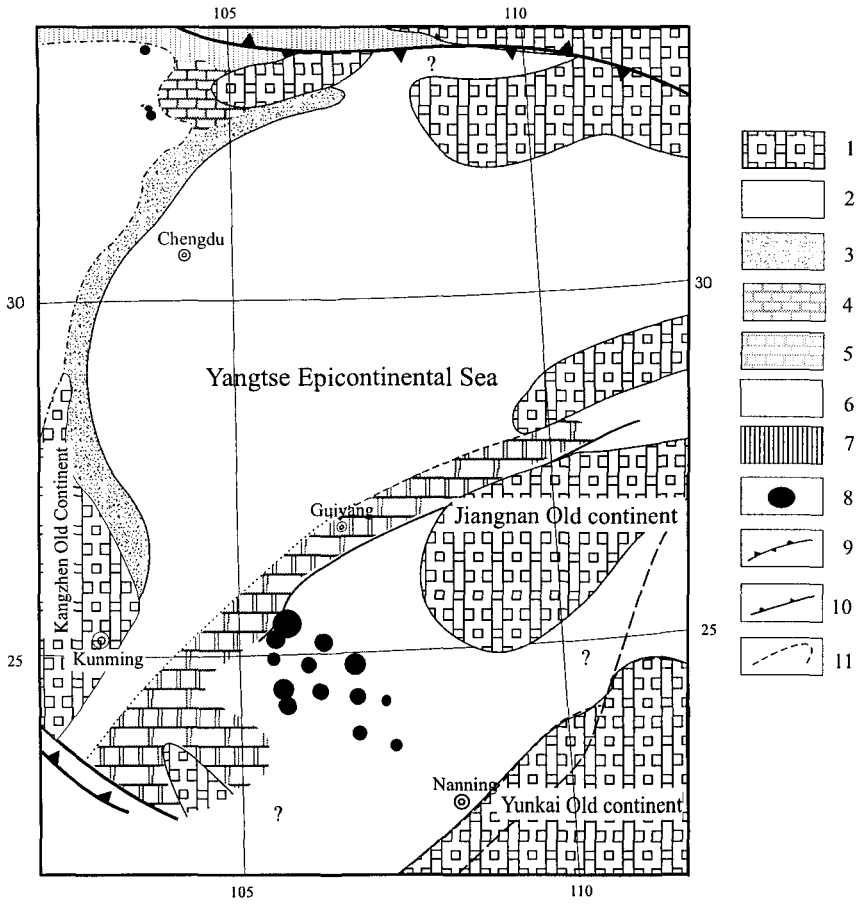

Fig. 2-4. Paleogeography of the Upper Yangtse area during the Middle Triassic Period and distribution of the gold deposits hosted by the Middle Triassic Formation.
1. Old continent 2. Epicontinental clastic and carbonaceous rocks 3. Littoral and neritic clastic rocks
4. Neritic carbonaceous rocks 5. Neritic carbonaceous rocks and reefs
6. Marginal sea and semi-abyssal turbidite faces 7. Island arc turbidite faces 8. Gold deposit
9. Collision zone 10. Subduction zone 11. Synsedimentary fault

(After Yie et al., 1994)

consists of Paleozoic clastic and carbonate sedimentary supercrustal formations and Proterozoic metamorphic basement. The converging of the three blocks during the late Variscan orogeny resulted in a series of complex folds and faults, which can be divided into three structural regions: the Nanpanjiang, Beipanjiang and Pu'an-Anlong terrain (Xiao et al., 1998).

In the Later Permian Period, the Youjiang-Nanpanjiang rift was characterized by large-scale basaltic eruptions extending into the Early Triassic Period. Due to the regional tectonic depression, there was an accumulation of a series of very thick clastic and carbonate sediments. The sediment formation of the Early Triassic Period consists mainly of clastic and carbonate sedimentary rock with pyroclastic rock interlayers, hydrothermal sediment silicalite and localized basaltic rocks, all of which form the lower part of the basin. After the Middle Triassic Period, the basin evolved into a stable depression containing mainly clastic and carbonate sediment rocks. The southern part of the basin is composed of medium to thickly layered pelite, siltstone and fine sandstone cyclothem, and it has a maximum thickness of over 3 000 m. In contrast, the sedimentation in the northwestern part of the basin is dominated by thickly layered carbonate sediment.

The Triassic sediments are the main SHDG host rocks in the Yunnan-Guizhou-Guangxi area. The turbidite rocks of the Middle Triassic Period are widely distributed in the Nanpanjiang River area, the contiguous area of Yunnan, Guizhou, and Guangxi Province, and in the Youjiang River area of western Guangxi. The turbidite rocks consist of dark gray

colored, medium and thin-bedded cyclothem and clastic greywacke with thicknesses ranging from 3 000 to 5 000 m, covering an area of around 80 000 km^2. The distribution of marine and terrestrial interdigitating coal-bearing deposits in the Upper Triassic rock is limited to the marginal zone of the platform. The Early Carnian turbidite deposit within the area was mainly sourced from the external platform regions neighbouring the basin and the adjacent Old Continent (Gou, 1985). So, the Middle Triassic turbidite of the Nanpanjiang and Youjiang River area is likely to be multi-material sourced and multi-centered deposition.

In the Early Permian Period, the Dian-Qian-Gui triangle area was a rather stable platform and accepted a succession of carbonate sediment of platform type. During the Late Permian Period, the area evolved into two distinctive tectonic units. The Dian-Qian-Gui Sea in the Early Triassic was part of the marine basin of southern China. It was a platform area extending from Kaiyuan-Qiubei, Yunnan Province to the northwest part of Zhenfeng-Anshun-Guiyang, Guizhou Province. The Nanpanjiang River-Youjiang River area in the southwest part of Guizhou Province was a subsiding tectonic unit. The lithofacies and palaeogeography of the Early Triassic Period in the Dian-Qian-Gui area (Fig. 2-5) changed gradually eastwards of the Kang-Dian Old Continent from coastal terrigenous clastic sediment to plateau carbonate with sand-pelite, siliceous exhalite and pyroclastic rock interlayers. The off-shelf sediment is distributed to the east of Guiyang, Zhenfeng and Qiubei. In Yunnan Province, the sedimentation is represented by the Louluo group (100 m

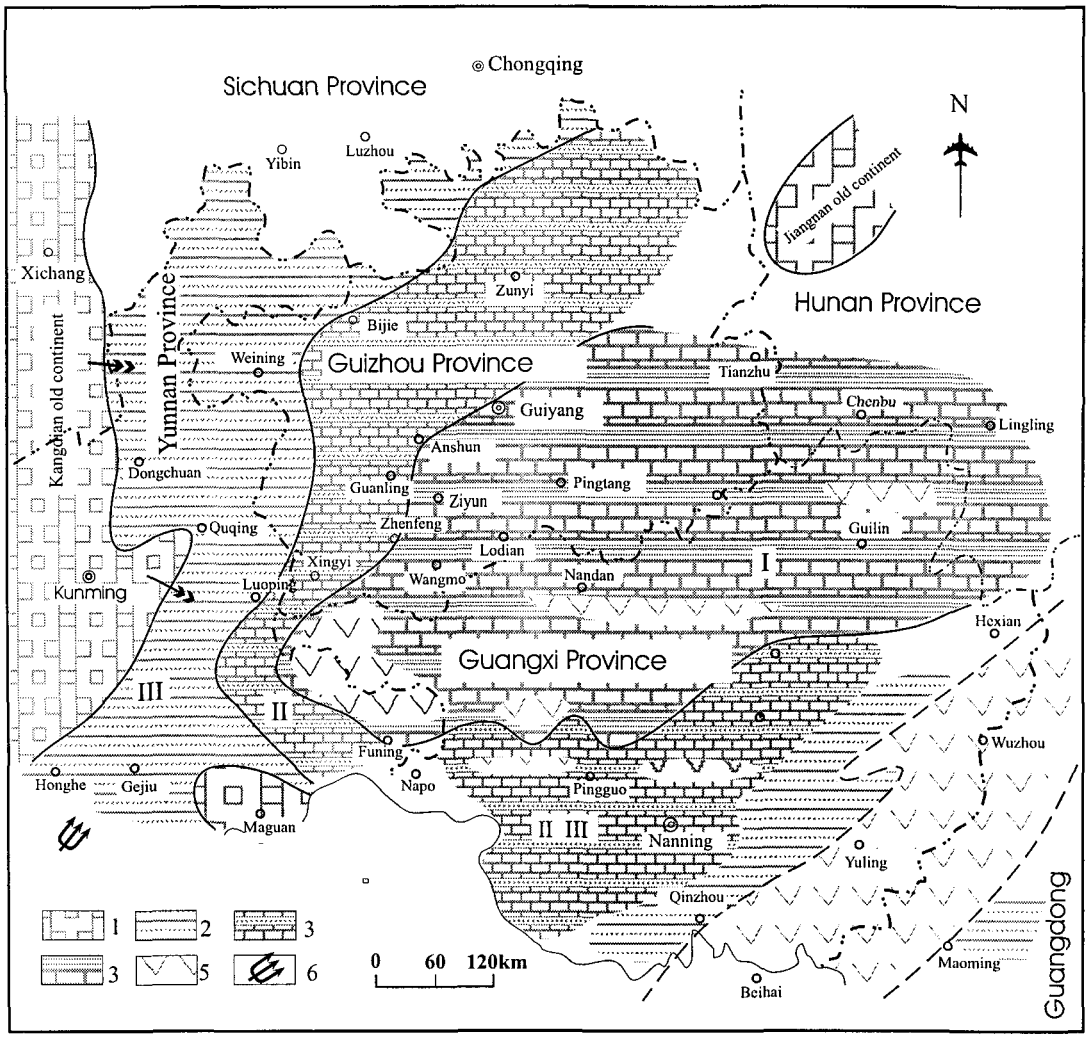

Fig. 2-5. Early Triassic lithofacies and paleogeography in the Yunnan-Guizhou-Guangxi Area
1. Old continent2. Argillaceous sandstone 3. Argillaceous limestone.
4. Thinly layered limestone with shale interlayers 5. Volcanic rock 6. Direction of marine incursion
I.Offshore shelf sediment area; II. Platform sediment area; III.Perezone
(After Gou, 1985)

to 200 m), which consists of dark gray, thinly laminated marls with abundant Ammonoidea, mud shales with thin siliceous intercalated layers and pyroclastic rocks. Volcanic debris in the Louluo group derived from volcanic island arcs in eastern and southwestern Guangxi Province (Gou, 1985).

In the early Middle Triassic Period, after large scale volcanic eruptions and the intrusion of magma, southwest Hunan, east and southeast Guangxi and the west Guangdong areas rose and formed a new Hunan-Guangxi-Guangdong tectonic system (Fig. 2-6) extending north and connecting with the Jiangnan Old Continent. On the other side, the Nanpanjiang and Youjiang River areas subsided, and accumulated several thousands meters thick turbidites. The sedimentation of the turbidites were concomitant with orogenic movement, and the sedimentary material mainly derived from the rising orogenic system.

Based on abundant well-developed trench model structures of the turbidites, it is estimated that the direction of the water current was 260° to 320°, with an average of ~300°, showing a westward turbidite flow. In the Qiubei, Guangnan of Yunnan, and Xilin areas of Northwest Guangxi, located in the western part of the turbidite basin, the proportion of mudstone to sandstone is 1:1, but moving eastward to Gonglan and Guangxi the proportion gradually changes to 1:2. This change suggests that the turbidite source was in the east side of the region as the sandstone proportion is higher there and decreases westwards (Gou, 1985). The chemical constituents of turbidite and the type of heavy minerals it contains indicate turbidite provenance from a granitic source region. The

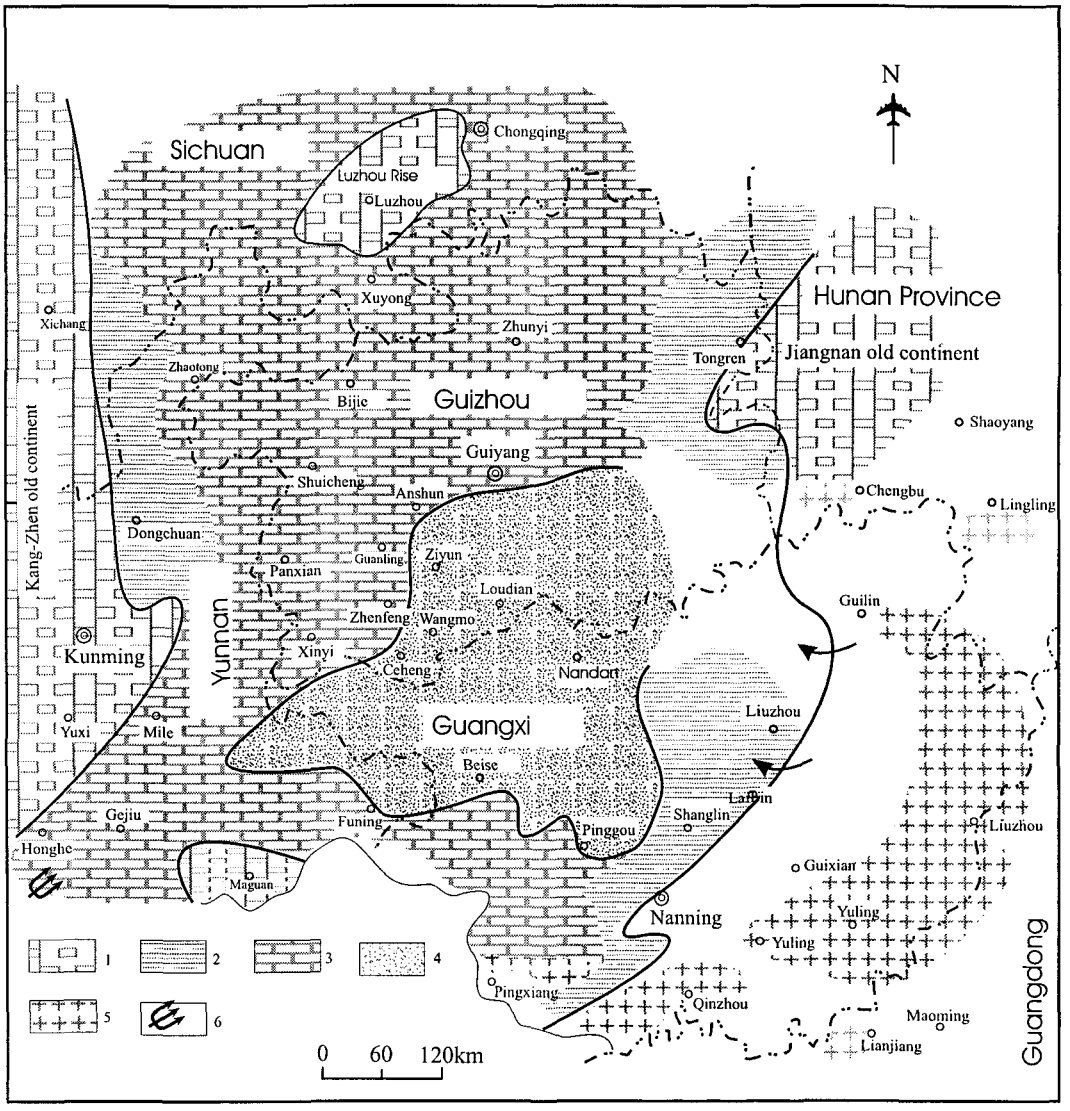

Fig.2-6 Middle Triassic lithofacies and palaegeography in the Yunnan-Guizhou-Guangxi Area.
1. Old continent 2. Sandstone and siltstone 3. Limestone 4. Turbidite
5. Granitoid rocks 6. Direction of marine invasion
(After Gou, 1985)

constitutional type of debris in the turbidite suggests extensive activities of magmatic intrusion and a high relief in the source area. In the platform of the external turbidite basin and at the edge zone of Maguan Old Continent, the Middle Triassic Series consists of limestone and dolomite coexisting with turbidite deposits of the Nanpanjiang and Youjiang River areas.

The westward extension of the Hunan-Guangxi-Guangdong tectonic system raised all the Nanpanjiang River-Youjiang River area into land in the early stage of the Later Triassic Period (Fig.2-7). The Carnian stage turbidite only occurs in the Nanpanjiang area, i.e., at the western rim of the basin. The molasse coal-bearing deposit followed the turbidite sedimentation on a large scale in the Upper Triassic System. The molasse deposits came from a newly-risen, uplifted fold range in the Nanpanjiang River and Youjiang River areas, and consisted of coarse, clastic rocks that were produced by rapid erosion following the deformation and uplifting of the turbidite deposits.

Several lines of geological evidence suggest that large scale activity of the Indo-China orogeny in the area began no later than the Middle Triassic Period and was due to the subduction and compression of the Pacific block towards the South China (Huanan) Platform. In the Early Middle Triassic Period, the Yunkai volcanic arc east of Guangxi rose rapidly after a phase of extensive volcanic eruption and magmatic intrusion, and it extended northward to merge with the Jiangnan Old Continent, thus forming the Hunan-Guangxi-Guangdong orogenic system.

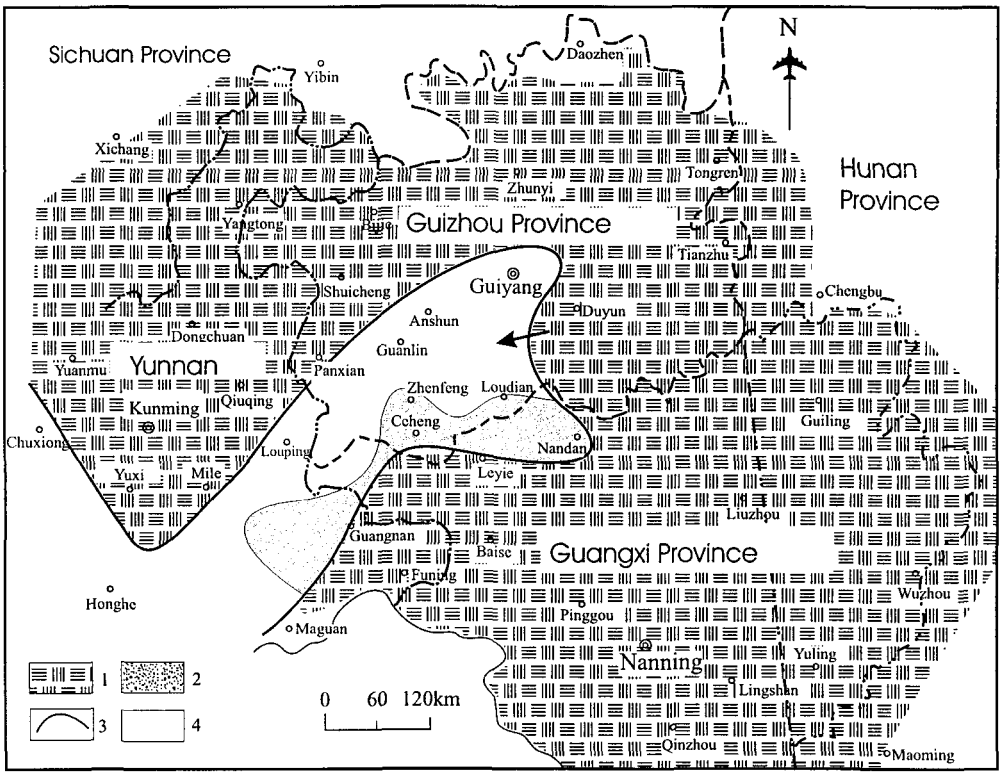

Fig.2-7. Carnian stage of Late Triassic lithofacies of palaeogeography in the Yunnan-Guizhou-Guangxi Area.
1. Continent 2. Early Carnian stage turbidite 3.Boundary of continent and sea
4. Shallow water sedimentary area
(After Gou, 1985)

The uplift of the Hunan-Guangxi-Guangdong orogenic system provided the prerequisites, including sufficient water depth, essential slope and ample material, for the broad turbidite deposition of the Middle Triassic System in the Nanpanjiang River-Youjiang River area. The Middle Triassic incursion was the second large scale invasion of the sea following the Early Triassic incursion. The turbidite deposition in the Nanpanjiang River- Youjiang River area was sustained until the Carnian stage of Late Triassic Period. The Carnian stage turbidite occurs in the Kaiyuan, Qiubei, and Louping district of Yunnan Province, and in the Xingyi, Zhenfeng and Langdai counties to the Guiyang region of Guizhou Province. In southwest Guizhou, turbidite is limited to the early Carnian stage; the thickness of the strata overlying the platform carbonate ranges from 1 000 m to 2 000 m (Gou, 1985).

2.3. Stratigraphy of the southwestern Guizhou area

Southwest Guizhou Province, situated along the southwest margin of the Yangtse platform, was part of the Nanpanjiang Mesozoic basin. Devonian to Triassic shallow-marine carbonate rocks were deposited on a broad cratonic platform near the edge of the Yangtse Craton, the edge of which is marked by reef facies. Turbidites intercalated with argillaceous rocks were deposited on the continental slope and in deep water environments. The area was uplifted during the Late Triassic Period and was covered by widespread terrestrial deposits, including coal beds (Li et al., 1989b).

The Caledonian movement was dominated by depression and the accumulation of tremendously thick Devonian to Triassic sediments in the basin. The outcropping strata in the area are dominated of the Devonian, Carboniferous, Permian and Triassic ages. The Cambrian age sedimentary rocks are occasionally observed on the south margin of Guangxi Province. From the Permian to the Triassic Period, this area went through a whole Wilson cycle (Wilson, 1966; Qin et al., 1996), from juvenile rifting ($D\sim P_1$), to late stage rifting and passive margin development ($P_1\sim T_1$), to syncollisional orogenic foreland basin ($T_2\sim T_3$). The Jurassic sedimentary rocks are localized, whereas the upper Jurassic and Cretaceous age sedimentary rocks are totally absent in the southwest Guizhou area.

Due to the heterogeneous development of the basin, especially in the late stage, the sedimentary types are different depending on the regions and the period of time. In general, the northern part of the basin was rather stable while the southern part was relatively active. So, the northern part is often called a platform facies sediment area, while the southern part is called a platform-basin facies area. The area between them is referred to as a transient area which occurs as bioherm facies or submarine rises.

2.3.1 Cambrian

Rocks of the Middle and Lower Cambrian age were observed in outcrop and these occurred sporadically in Longlin County. Dolomite, limestone, argillaceous limestone with interlayers of mudstone, siltstone, silicalite, and oolitic limestone occur in the core parts of domes and anticlines. The thickness of the Cambrian rocks can be over 1 900 m.

2.3.2 Devonian

The Devonian sedimentary rocks were observed in Ziyun, Wangmo, Panxian, Pu'an County. The rocks are mainly of Middle and Upper Devonian age, while the Lower Devonian sedimentary rocks, consisting of mudstone, limestone, and clastic rocks, are only locally distributed. The strata belong to abyssal-bathyal facies, which are a series of blackish, biogenic sediment sequences.

2.3.3 Carboniferous

The Carboniferous sedimentary rocks can roughly be divided into two parts along the line of Luodian, Ceheng, and Longlin. The Carboniferous rocks in the north of the basin (excluding the Qinglong, Zhenfeng and Ziyun districts) consist of shallow platform facies carbonate rocks, sandstone and shale. The southern part consists of platform-basin facies limestone and silicalite.

2.3.4 Permian

The Lower Permian rocks are composed of four formations; they are, from bottom to top, the Longyin, Liangshan, Qixia, and Maokou Formations. The Longyin Formation consists of three sedimentary types: a platform-depression detrital rock with limestone interlayers, a platform-basin facies carbonate, and a platform facies limestone and argillaceous limestone. The total thickness of the Longyin Formation ranges from several hundred to one thousand meters. The Liangshan Formation consists of paralic facies

sandstone and shale with limestone interlayers, occasionally with coal streaks. The Qixia Formation mainly consists of shallow sea carbonate sediment and it occurs as medium to thick-layered limestone and intercalated carbonaceous and calcareous shale around 100 to 200 m thick. The Maokou Formation was sedimented during the subsequent incursion within which the northern part, often referred to as the "white Maokou", belongs to a shallow sea platform facies composed of thick-layered limestone. The southern part, on the other hand, belongs to platform-basin facies consisting mainly of dark gray medium to thick-layered limestone with dolorudite or siliceous limestone intercalations, and is often referred to as the "black Maokou". In-between the two sediment facies, there exists a transient belt of beach biogenic limestone. The thickness of the Maokou Formation ranges from 60 to 420 m. The upper part of the Maokou Formation is made up of Emeishan Basalt, which started erupting near the end of the Early Permian Period in the northeastern part of the area.

It is noteworthy that in some areas, such as Qinglong, Pu'an, Puding, and Zhijin County, at the top of the Maokou Formation below the Emeishan Basalt, there is a layer of silicalite, siliceous limestone, and siliceous shale with basaltic pebbles, and pyroclastic rocks (0 to 20 m thick). This layer is often referred to as the Dachang bed, and is host to many Sb, Au, Cu, fluorite and pyrite mineralization occurrences. The Dachang bed conformably overlies limestone. Field observation and fossil investigation show that the

Maokou limestone and the Dachang bed were derived from successive sedimentation of the Early Permian Period.

The Upper Permian sedimentary facies change gradually from continental facies (Xuanwei Group), to paralic facies (Longtan Formation), and to marine facies (Wujiaping and Shaiwa Formation) from NW to SE due to the uplift in the northwest part of the region. The Xuanwei Formation consists mainly of sandstone and shale with intercalated coal and siderite beds. The Longtan Formation (50 to 450 m) consists of sandstone, siltstone and shale, and also layers of coal bed, oolitic siderite lenses or bends. It overlies conformably the Emeishan Basalt, and unconformably overlies the Maokou limestone. The Wujiaping Formation (0 ~ 280 m thick), dominated by chert-bearing limestone, unconformably overlies the Maokou Formation, with the proportion of clastic rocks increasing in the direction towards where the Longtan Formation accumulated. The Shaiwa Formation represents the total accumulation of the Later Permian. It consists mainly of sandstone and argillaceous rocks, with intercalated siliceous exhalites, limestone and argillaceous limestone, and has a thickness ranging from 800 to 980 m.

The Changxing and Dalong Formations overlie the Longtan and Wujiaping Formation. The Changxing Formation (0~240 m) consists of limestone and localized intercalated argillaceous limestone and clastic rocks. Extensive gold mineralization was observed in the thin-layered argillaceous limestone near the Zhenfeng area. The Dalong

Formation (~20 m) consists of siliceous shale, siliceous exhalites, commonly with intercalated montmorillonite clay rocks with tuff relics.

2.3.5 Triassic

The Triassic sedimentary rocks are widespread in the area and can be divided into two parts according to sedimentary environments. The northwest part consists of a stable platform facies and the southeast part consists of an active platform-basin facies separated by a bioherm facies. In general, the early Triassic of southwest Guizhou is characterized by passive continental marginal sedimentation. Pyroclastic sediments are only observed at Lekang and Beiceng, respectively of Mowang and Zhenfeng County. From the Middle Triassic Period to the Carnian stage of the Late Triassic Period, in the Youjiang area south of the Yangtse passive marginal carbonate sediments, a foreland basin developed with very thick turbidite accumulations. As nappe development increased northwards, the turbidite migrated and superimposed the carbonate. After the Late Triassic (Carnian stage), the sediments changed to molasse (Fig. 2-8) and formed the sedimentary pattern peculiar to the region (Fig. 2-9).

(1) Early Triassic sedimentary rocks: The lower part of the Early Triassic (Indian stage) can be divided into four different facies distributed from NW to SE. There is the plateau-littoral facies (Feixianguan Formation), the plateau-neritic facies (Yelang Formation), the plateau margin facies (Dayie Formation) and the basin margin facies (Luolou Formation). The Feixianguan Formation (250~850 m) consists mainly of siltstone,

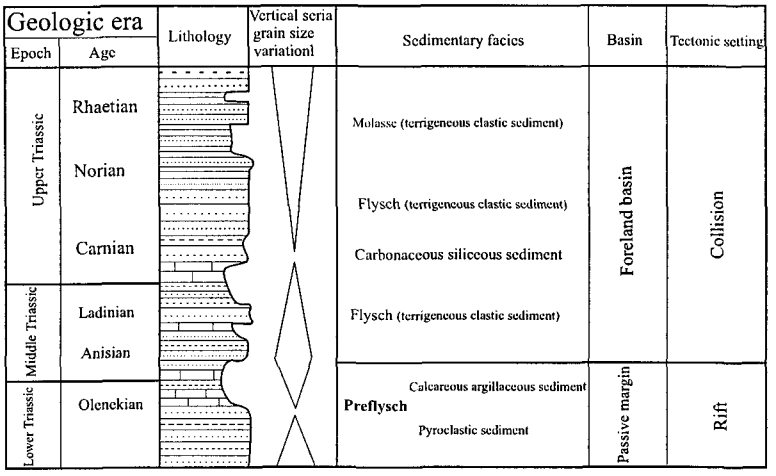

Fig. 2-8. The sedimentary series in the foreland basin in the Nanpanjang River area.
(After Wang et al., 1994a)

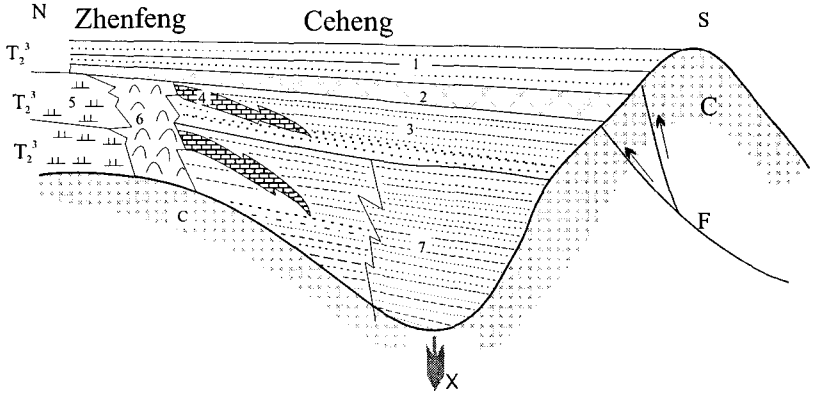

Fig.2-9. Sketch map showing the sedimentary facies in the foreland basin in the Nanpanjang River area.
1. Sandstone 2. Calcareous shale 3. Argillaceous rock 4. Limestone 5. Dolomite 6. Algal limestone
7. Sandstone C. Continental crust F. Thrust fault X. Subsidence direction
(After Wang et al., 1994a)

fine-grained sandstone, and sandy shale, occasionally with limestone and Cu-bearing sandstone intercalations. The Yelang Formation (350~400 m) consists of limestone, argillaceous limestone and mudstone and shale. Gold mineralization was observed around the Zhenfeng area in the thin-layered argillaceous limestone of the Yelang Formation. The Dayie Formation (200~550 m) is dominated by micritic limestone, commonly accompanied by shale, argillaceous limestone, and oil shale intercalations at the bottom of the sequence. The Luolou Formation (30~300 m) consists of limestone and argillaceous limestone with shale intercalations.

The upper part of the Early Triassic sedimentary rocks (Olenekian stage) are also made up of three synchronized formations NW to SE, namely the Yongningzhen, the Anshun and the Ziyun Formations. The Yongningzhen Formation (~600 m) consists of limestone, argillaceous limestone with intercalated sandy shale, and a dolomite and gypsum layer at the top of the sequence. The Anshun Formation (500~600 m) occurs as a narrow belt with varied lithology and is dominated by dolomite near the Zhenfeng area. The Ziyun Formation mainly consists of limestone with intercalated mudstone and argillaceous limestone; the percentage of limestone decreases southwards and gradually clastic and mud rock predominate.

(2) Middle Triassic sedimentary rocks: Laterally, the lower part of the Middle Triassic System (Anisian stage) can be subdivided into a platform facies (Guanling Formation), a reef facies (Xiaomitang Formation), a platform margin facies (Qinyan

Formation), and an open sea platform-basin facies (Xinyuan Formation). The Guanling Formation, ranging from hundreds to more than one thousand meters in thickness, consists of limestone, dolomite, dolomite-marl, and clay rock. The Xiaomitang Formation (200~500 m) consists of reef limestone or bioclastic limestone, which generally contains a large proportion of algae and other bioclastic material. The Qinyan Formation (870 ~ 1 120 m) consists of limestone, argillaceous limestone, clay rock and sandstone. The Xinyuan Formation (100 ~ 1 500 m) is the most widespread sequence in the region and consists of clay rock, siltstone, sandstone with limestone, siliceous mudstone, siliceous exhalites and tuff. It conformably overlies the Ziyun Formation, and locally overlies the Permian System. This formation is characterized by its high Au background and is host to some gold mineralization.

The upper part of the the Middle Triassic sedimentary rocks (Ladinian stage) consist of the Falang, Liangshuijing and Bianyang Formation, extending NW to SE. The Falang Formation (> 1 000 m) consists of limestone, argillaceous limestone, and dolomite with intercalated clay rock, siltstone and fine-grained sandstone. The Liangshuijing Formation (~ 1 600 m) consists of massive algae-bearing sparry limestone with dolomite intercalations. The Bianyang Formation is a huge open sea basinal clastic sequence, and consists of sandstone, siltstone, clay rock and a small proportion of limestone. It is about 3 000 m thick.

(3) Upper Triassic sedimentary rocks: The southern part of the region, due to the Indo-China movement, rose up and accumulated only insignificant sediments in limited areas. The northern part of the region, on the other hand, has four recognizable formations: the Laishike, Banan, Houbachong and Xiujiahe Formation, as they appear bottom to top. They are the products of environmental shifts from marine to continental facies. The Laishike Formation (~ 100 m) consists of mudstone with siltstone, fine-grained sandstone and small proportions of argillaceous limestone intercalations. The Banan Formation (357 ~ 483 m) consists of sandy clay rock, interbedded with siltstone and sandstone, with localized argillaceous limestone, carbonaceous shale and coal beds at the top. The Houbachong Formation (0 ~ 700 m) consists of a sequence of paralic facies rocks, including sandstone, sandy clay rock, and carbonaceous mudstone, with intercalated coal beds. The Xiujiahe Formation (150 ~ 432 m) consists of limnc facies sandstone with sandy shale and carbonaceous shales.

2.3.6 Jurassic

The sedimentary rocks of Jurassic age can only be observed in the mountainous area in the north part of the region, and are present mainly as limnic and alluvial facies.

Following the Jurassic Period, sedimentation became insignificant in the region. Some terrigenous clastic sediments of Late Cretaceous to Early Tertiary agewere observed in sporadic small sized taphrogenic basins. The sedimentary rocks of the Quaternary period,

usually less than 10 m thick, are rare and are only locally distributed as alluvial, lacustrine, and glaciofluvial facies, especially in the karst area (Li et al., 1989b).

2.4. Gold concentration of the sedimentary rocks in the research area

Many researchers have noted that, besides tectonic control, there tends to be lithological control on the distribution of gold mineralization. Indeed, some researchers have even proposed that both gold and hydrothermal fluid derived from the same source bed (Knight, 1957; He et al., 1993; He, 1996). In the research area, gold deposits are mainly located in the Upper Permian and Middle to Lower Triassic sedimentary rocks. The gold mineralization occuring in the Upper Permian sequences is limited to carbonaceous mudstone, shale and breccia, located in the lower part of the Longtan Formation, e.g., the Getang gold deposit. The Zimudang gold deposit mainly occurs in argillaceous, silty limestone and pelite in the upper part of the Lower Triassic Yelang Formation. The gold deposits occur in different horizons from one area to another; however, in the specific mining areas mineralization is commonly limited to one or two lithological horizons.

Geochemical exploration in the area shows that the average gold concentration of drainage sediments is only of 2.1 ppb (Zhang et al., 1989). The average gold contents of the Maokou, Longtan and Changxing Formations of Permian age are 1.3, 4.2, and 1.1 ppb respectively. The average gold content of the Yelang Formation of the Lower Triassic Series is 4.4 ppb. The Longtan and Yelang Formations, which host some of the gold ores in the area, are more enriched than other strata. In the Xuman area, the average gold content of

the middle Triassic Series is as high as 13.4 ppb (Zhang et al., 1992). The fact that SHDG host rocks generally bear high gold concentrations was quoted as evidence for the host rocks being the source beds for the SHDG mineralization in the area (He et al., 1993). The gold anomalies detected in the area mainly occur around anticlines and domes, as is the case for the Laizishan anticline. The slope facies sedimentary rocks, the turbidites, especially the siltstone and pelite within them, are the main host rocks for SHDG deposits in the region, and are often considered to be source beds for Au, As, Tl, etc. (He et al., 1993; Zhang et al., 1992).

2.5. Regional palaeo-geothermal background and magmatic activities

Several studies suggest that southwest Guizhou Province has a high geothermal gradient. Petroleum exploitation in the area shows that the thickness of the Lower and Middle Triassic Series is greater than 1 500 m, and as thick as 3 000 to 5 000 m in certain locations. The average geothermal gradient in the area is 4.75°C/100m, and the organic matter in the Upper Permian sedimentary rocks of the area has reached the dry gas stage (Zhuang, 1995). The vitrinite reflectance of the Upper Permian (Fig.2-10, 11) show that the ancient geothermal temperature of the area was quite high. The color index of the conodont of the Lower Triassic rocks (Fig.2-12; Wu and Li, 1993) shows a similar paleo-geothermal gradient in the area. Listed in Table 2-1 are the relationships between vitrinite reflectance, conodont color index and ancient geothermal temperature, as suggested by Zhuang (1995) on the basis of research on ancient geothermal gradients in the area. Regarding the variation

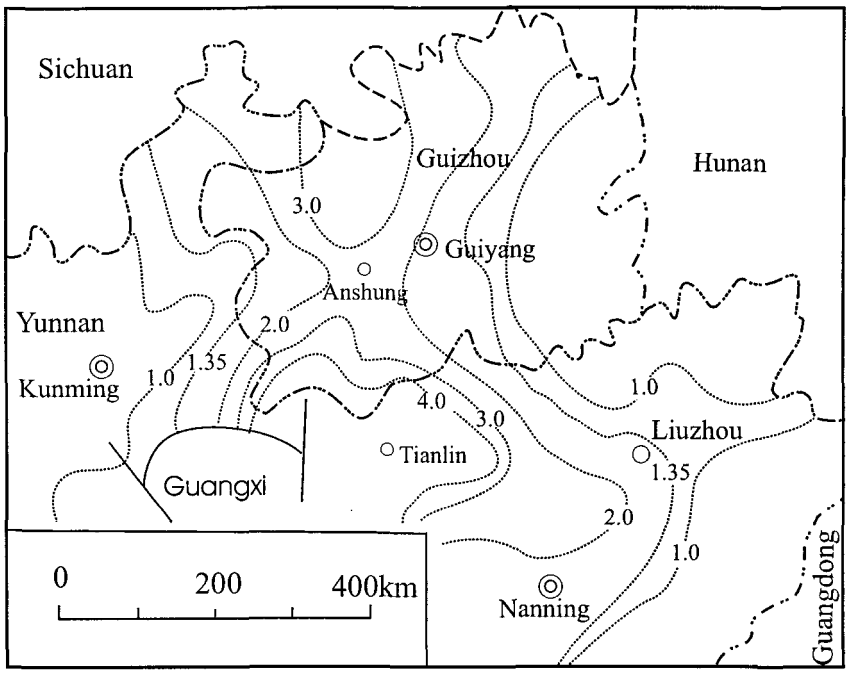

Fig.2-10. Contours of reflectances of Upper Permian vitrain in Yunnan- Guizhou-Guangxi area (after Zhuang, 1995).

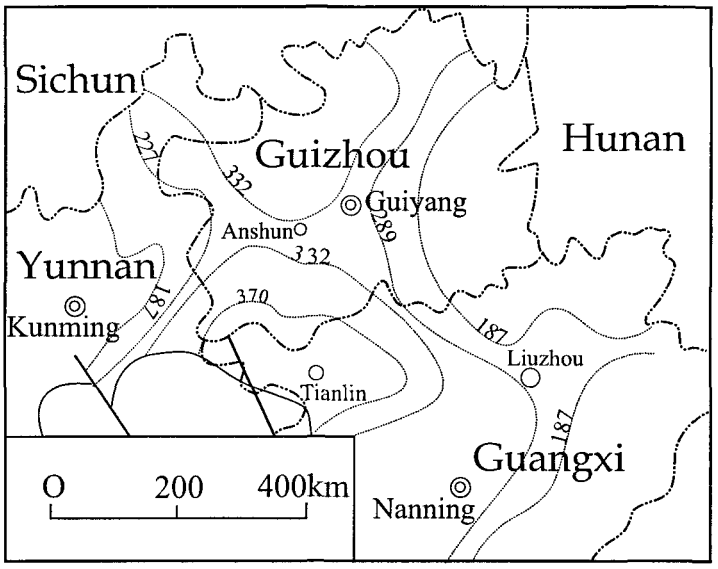

Fig.2-11. Estimated maximum geothermal isopleth (°C) for the Upper Permian succession inYunnan,Guizhou, and Guangxi Provinces (Modified from Zhuang, 1995).

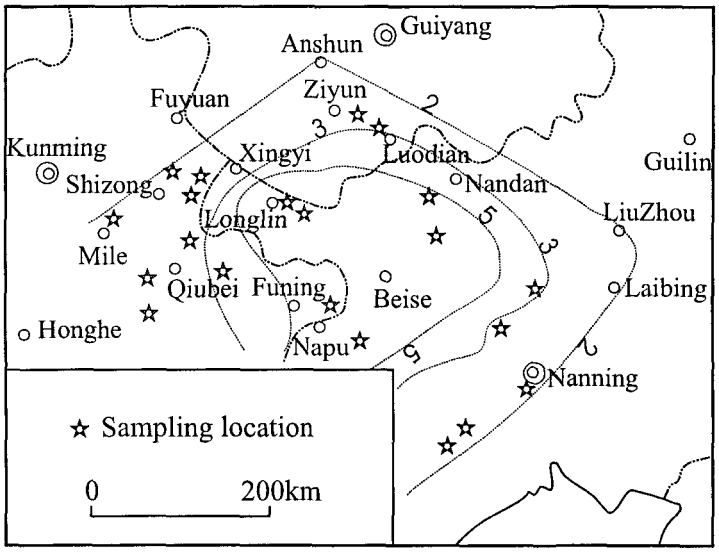

Fig.2-12. Isopleths of the color index of the conodont in the Lower Triassic succession of Yunnan, Guizhou and Guangxi Provinces. (After Wu and Li, 1993).

of the vitrinite reflectance in the strata, it is estimated that in the Upper Permian, the ancient geothermal gradient was about 23°C/100m. In the Lower Triassic to the lower part of the Middle Triassic, the ancient geothermal gradient was estimated at approximately 18.5°C, and in the upper part of the Middle Triassic to the surface, the geothermal gradient was around 4.8°C/100m. Exploratory drilling for petroleum at Anlong County, near the Getang gold deposit, indicates that the average modern geothermal gradient in the upper 2 000 m from the surface is 5°C/100m, which is higher than the average crustal geothermal gradient (3°C/100m).

Table 2-1. The relationships of vitrinite reflectance, conodont color index and the maximum ancient geothermal temperature (Zhuang, 1995)

Conodont color index (CAI)	1	2	3	4	5	
Vitrinite reflectance (R°m)	1.0	1.5	2.0	3.0	4.0	5.0
Maximum ancient geothermal temperature (°C)	100	130	160	200	250	300

Unlike the SHDG mineralization in the Carlin Trend, U.S.A., no igneous rocks are exposed in the immediate vicinity of the gold deposits in the research area. Only Permian Emeishan Basalt and sparsely distributed Yanshannian alkaline ultramafic veins or dikes crop out in the region.

The Emeishan Basalt is one of the best known continental flood basalts (~ 258 Ma) related to hotspot activity (Courtillot et al., 1999). The basalt contains high concentrations of gold (~ 40 ppb) and other trace elements, and consequently has been invoked as the main

source rock responsible for the massive Au-Hg-Sb-As mineralization in the region (Li et al., 1989b; Zhang et al., 1989; He, 1992; Chen et al., 1996). Emeishan basalt covers an area of about 300 000 km^2, while the area spanned by the known volcanic outcrops is only 24 000 km^2 (Fig.2-13). The average thickness of the basalts is about 470 m. The basalt can be divided into three main cycles. The lower cycle is represented by alkali-basalt, which consists of tephrite, nepheline tephrite, analcime tephrite, nosean tephrite, and so on. The middle cycle is considered the main part of the Emeishan basalt with its columnar joints and a few pillow bodies. The upper cycle consists of rhyolite, rhyodacite and dacite. In southwest Guizhou Province, the Emeishan Basalt is mainly located in the southwest part, to the west of the SHDG mineralization area (Fig.2-14). The basalt in the area mainly consists of basaltic lava and basaltic volcanic breccia; its thickness decreases eastwards.

The sub-alkaline ultramafic rocks in southwest Guizhou Province mainly occur in the contiguous area of Zhenfeng, Zhenning and Mowang counties, as veins and dikes. These rocks consist of pyroxenite (porphyritic olivine biotite pyroxenite, porphyritic biotite olivine pyroxenite) and biotitite (porphyritic pyroxene olivine biotite and porphyritic olivine pyroxene biotite). They intruded into the Permian to Triassic strata, and formed a few ultramafic rock belts. The individual intrusions are rather small and range from several meters to about 1 000 m in length and several centimeters to 8 m in thickness. The ultramafic wall rocks are often altered to various degrees; they are commonly extensively

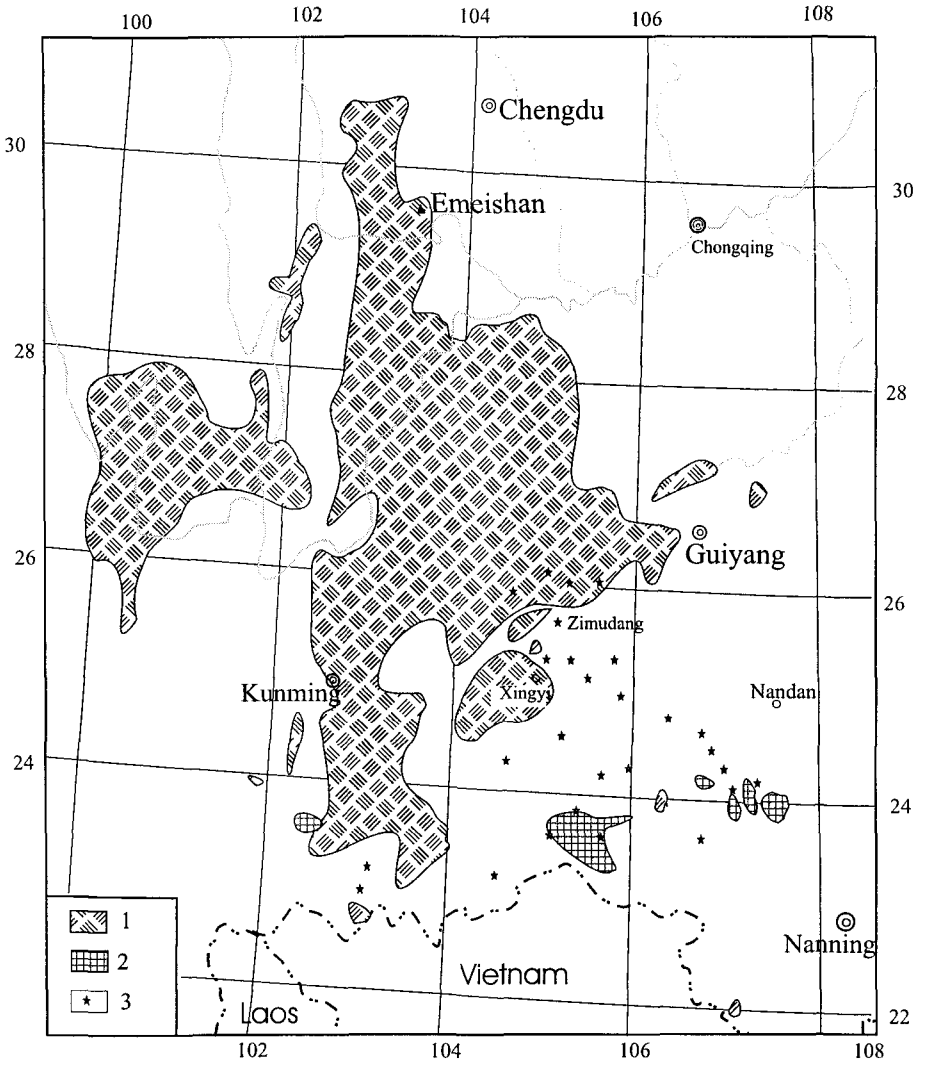

Fig.2-13. Sketch map showing the distribution of Permian and Indo-China-Yanshanian mafic volcanic rocks. 1.Permian Emeishan basaltic rock; 2.Indosinian-Yanshanian mafic volcanic rocks; 3.Gold deposit (After Yang and Dong, 1994)

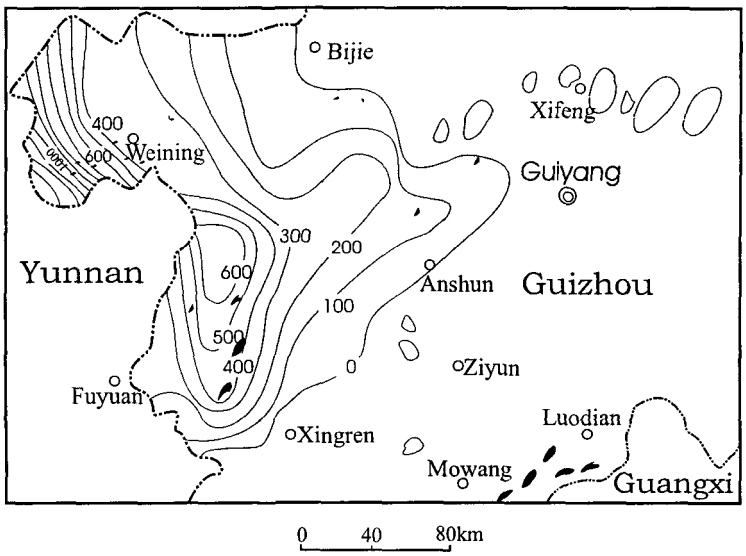

Fig.2-14. Map showing isopachs of the Emeishan Basalt and outcrops of diabase in Guizhou Province. (After Bureau of Geology and Mineral Resources of Guizhou Province , 1987.)

Isopach of Emeishan Basalt Diabase

carbonatized, and discoloration and localized serpentinization and sideritization are not uncommon. Alteration of the host sandstone and argillite is rather weak.

The pyroxenite and biotitite are dark green, massive, brecciated and porphyritic. The brecciated ultramafic rocks usually contain enclaves of wall rock at shallow depths. These ultramafic intrusives are mainly composed of diopside, augite, biotite, and olivine with minor spinel, apatite and rutile. Some of the intrusives contain aegirine, augite and chrome pyrope. All these ultramafic rocks are extensively altered, the alteration including carbonatization, serpentinization, etc. This series of ultramafic rocks was emplaced in the late Yanshanian period, and has been dated at 77.5 to 97 Ma using the whole-rock K-Ar method (Bureau of Geology and Mineral Resources of Guizhou Province, 1987).

2.6. Distribution of the SHDG deposits

The sediment-hosted disseminated gold deposits in southwest China are spatially located near the buried edge of the Yangtse Craton. On a worldwide basis, there is an association of SHDG deposits with rocks of the Early Paleozoic to Jurassic and Cretaceous age (Yang and Dong, 1994; Arehart, 1996). Deposition in deep water during times of high sea level and widespread sub-marine volcanic activity and hydrothermal activity typify these clastic sequences. Most of the SHDG deposits in the area are hosted by rocks formed in deep-sea environments (Tan, 1994).

SHDG deposits are structurally restricted in a significant way. Geochemical reconnaissance and gold exploration in Southwest Guizhou Province show that the distribution of gold anomalies and mineralizations are clearly controlled by similar tectonic settings. The gold anomalies mainly occur around or within the anticlines or domes (Fig. 2-15). The SHDG deposits are often spatially associated or hosted by the same anticlines or domes which host hydrocarbons (Fig. 2-16; Shi et al., 1995, 1998). The association of SHDG deposits and ancient or productive petroleum reservoirs has led some researchers to suggest that petroleum played an important role in gold leaching, transportation, and precipitation (Lin et al., 1993a; Zhang and Zhang, 1998; Zhuang et al., 1998). The relationship between organic matter and SHDG deposits is a major objective of this study.

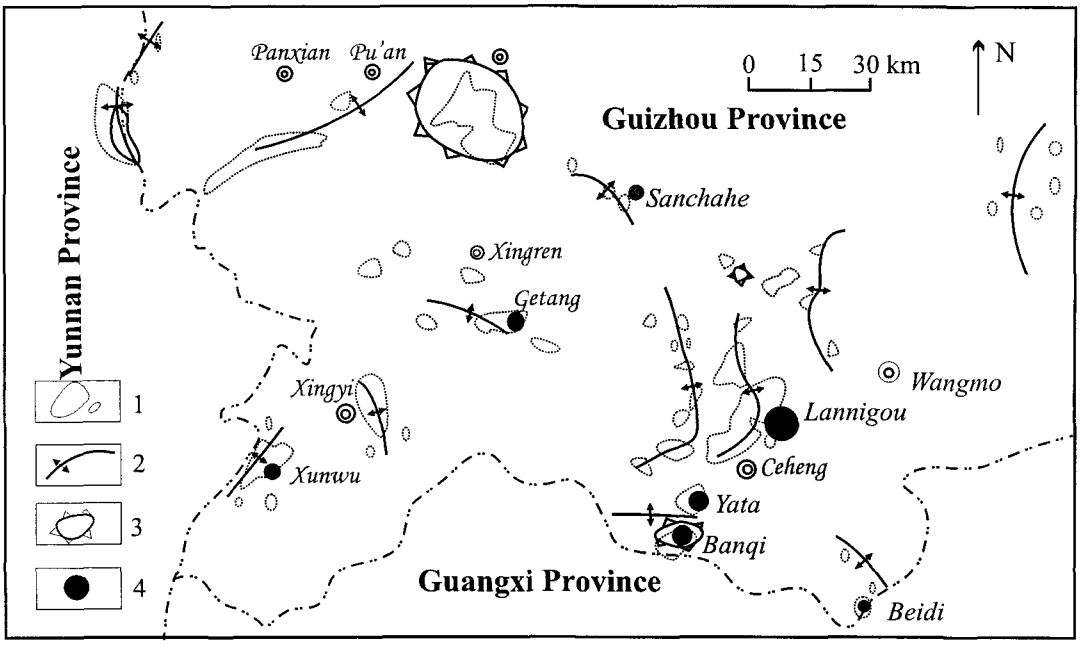

Fig. 2-15. Distribution of Au anomalies and deposits in relation to tectonic setting.
1-Au anomaly; 2- Anticline; 3- Dome; 4. Gold deposit
(After He et al., 1993)

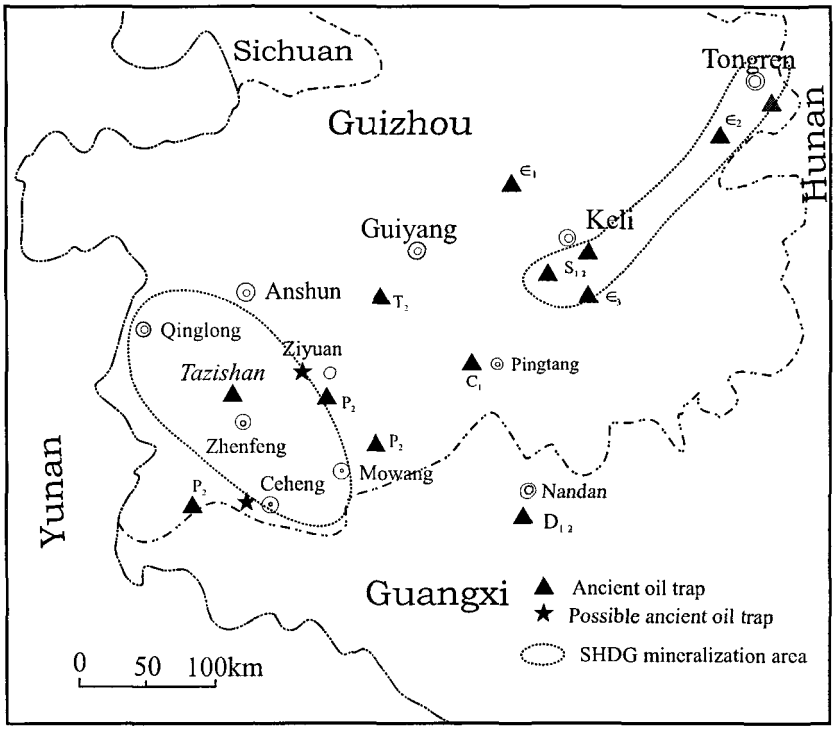

Fig.2-16. The distribution of ancient oil traps in the study area.
(After Shi et al., 1998)

3

GEOLOGY OF TYPICAL SHDG DEPOSITS IN THE RESEARCH AREA

The SHDG gold deposits in southwest Guizhou Province can roughly be classified into three types on the basis of tectonic setting, lithology of the host rocks, mineral assemblage, and the association of metallogenic elements of the ores, etc. (Tan, 1994). The three types are the Au-Sb, the Au-Hg- (Tl), and the Au-As- (Sb) type, and are respectively represented by the Getang, Zimudang, and Lannigou gold deposits. The different geological and geochemical characteristics of the three types of deposits may partly result from their host rocks (possible source beds), which were formed in different geological settings and sedimentary environments. The Au-Sb type gold deposits, represented by the Getang deposit, are hosted by littoral facies deposited at the initial rift-faulting stage. The Au-Hg-(Tl) type gold deposits, represented by the Zimudang deposit, are hosted by carbonate-shale sequences accumulated in the restricted to semi-restricted platform neritic facies at the initial subsidence stage. Finally, the Au-As- (Sb) type gold deposits, represented by the Lannigou deposit, are hosted by turbidites developed along the marginal slope facies of the open-sea basin during the intense subsidence stage of the rift evolution.

3.1. Lannigou gold deposit

The Lannigou gold deposit was first discovered in 1986 around a former realgar deposit. It is located in the contiguous area of three counties; Ceheng and Wangmo County, and for the most part, in Zhenfeng County. It is the largest SHDG deposit in southwest Guizhou Province, and even in the whole Dain-Qian-Gui "gold triangle" area. Tectonically, the Lannigou gold deposit occurs on the southwest fringe of the Yangtze platform which is the northern part of the Youjiang-Nanpanjiang basin (or rift). The sedimentary environment evolved from that of a passive continental margin to a foreland basin during the Early to Middle Triassic period. The magmatic activity in the area is insignificant. Only some small Yanshannian sub-alkali ultramafic intrusives were observed in Beiceng and Zhenfeng County, about 27 km NW of the gold deposit.

3.1.1. Structures in the mining area

The Lannigou gold deposit is situated in a small triangular area limited by the NW trending Banchang thrust fault, near the N-S trending Luofan thrust fault, and the Ceheng E-W trending fault zone to the south (Fig.3-1). The mining area is located SW of the Banchang thrust fault and the eastern limb of the Laizishan anticline. The main folds in the area are the NW trending Yanjia syncline and the nearby S-N trending Laizishan anticline. Second-order folds include the Lintang anticline, the Lannigou syncline, and some nearby S-N trending small synclines and anticlines in the fourth section of the Xuman Formation to

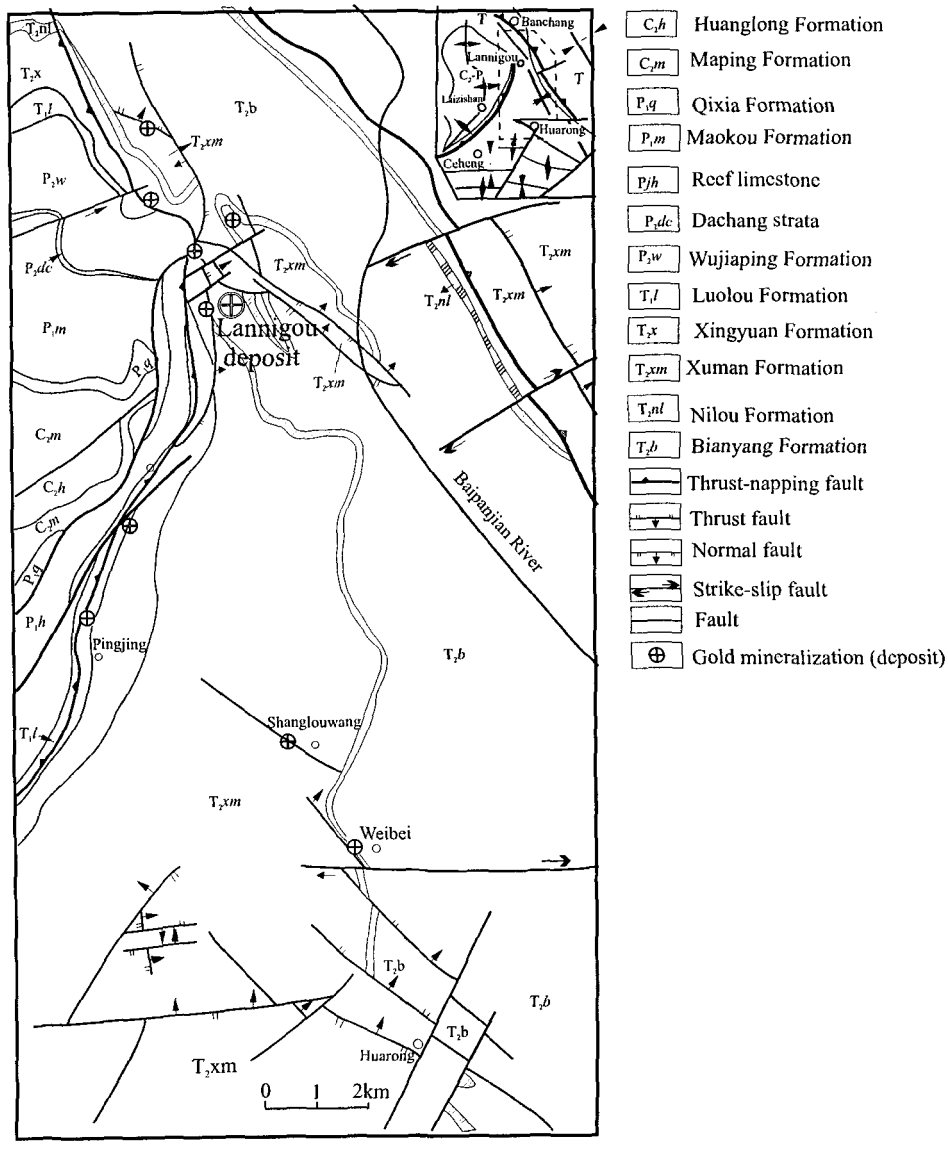

Fig.3-1. Regional geological sketch map of the Lannigou ore field..
(After Wang et al., 1994a)

the east of Luofan. NW trending folds superimposed on N-S trending folds were observed near the Lannigou area (Fig.3-2).

The NNE trending Laizishan anticline (brachydome) is about 25 km long and 12 km wide. The core of the anticline consists of Middle Carboniferous to Permian limestone, bioclastic limestone, and reef limestone. Inbetween the middle and upper Permian strata, there is a so-called "Dachang layer" consisting of mudstone and shales. The sequences of the Carboniferous to Permian are about 1 300 m thick. The Triassic strata occurs on either limb of the anticline, with the west limb mainly consisting of platform carbonate rocks, and the east limb consisting of a foreslope to furrow-like basin clastic rocks, both limbs approximately 1 000 m thick. The two wings of the anticline are asymmetrical, with a rather precipitous east limb (20°~40°) and a less inclined west limb (5°~20°). In the past two decades, a few SHDG deposits have been discovered around the anticline, such as the Lannigou, the Bannian, and the Yangyou gold deposits which are accompanied by various combinations of mercury, arsenic and antimony mineralization.

The Banchang thrust fault occurs along Beiceng, Banchang to Pingpo, about 5 km northeast of the Lannigou gold deposit. The fault is about 60 km long, dipping northeast. The width of the tectonic belt ranges from 1 km to 13 km, and consists of a foreland fold, a lower imbricated structure, an upper imbricated structure and a thrust fault (Luo, 1994). The fault brecciated belt, 30 to 100 m wide, is extensively silicified with no reported Au mineralization. The minimum movement of this structure is 1.5 km horizontally and about

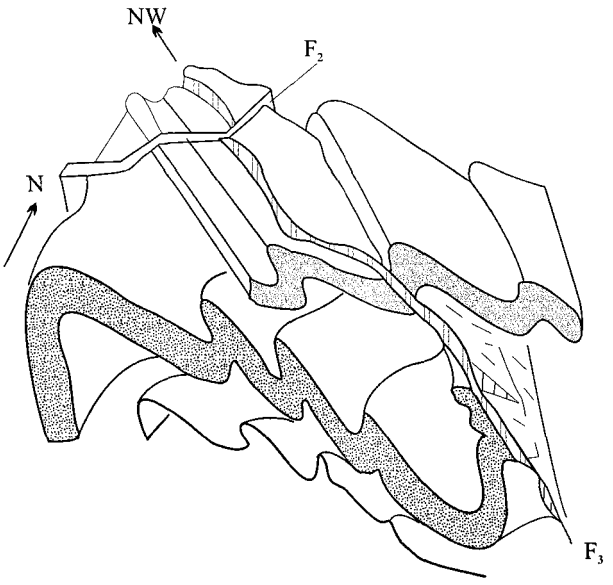

Fig.3-2 Sketch map showing the structural control of the Lannigou gold deposit. The early NS trending close reversed folds were overprinted by the later stage gold mineralization related NW trending folding and thrust fault. (Modified from Wang et al.,1994a)

800 m vertically. The direction of thrusting was southeast to southwest with a sinistral shear component.

The Lannigou gold deposit is located southwest of the Banchang thrust fault (nappe structure) and on the east limb of the Laizishan anticline. There, three groups of faults can be distinguished: the NS trending faults in the western part, the NW trending faults in the eastern part, and the WNW and NE conjugate faults in the central part of the area (Fig.3-3). The major faults include the NW trending F_5 and F_3 faults and the SN trending F_{10} fault. The F_5 fault is a high angle thrust fault occurring in the eastern part of the mining area. Dipping NE, it is over 4 km long with an extremely silicified but weakly mineralized fractured zone up to 30 m wide. The WNW trending F_3 fault is the most important ore controlling structure hosting the major gold resource of the deposit (Fig. 3-4). Both the F_3 fault and the NE trending F_2 fault contain the main ore bodies of the Lannigou deposit and both are confined to the Bianyang Formation. The NNW trending F_{11} and NW trending F_{14} faults are also ore-hosting fractures.

1) S-N trending structures

The S-N trending structures include the F_1, F_7, F_9 compressional thrust faults in the western part of the mining area. The F_1 fault, the largest of the three, is over 8 000 m long dipping west with low to medium obliquity. It is filled with well-developed breccia and is locally associated with gold mineralization. This fault is believed to be part of the Poping thrust structure. Klippen of Permian carbonate were observed overlapping the Triassic

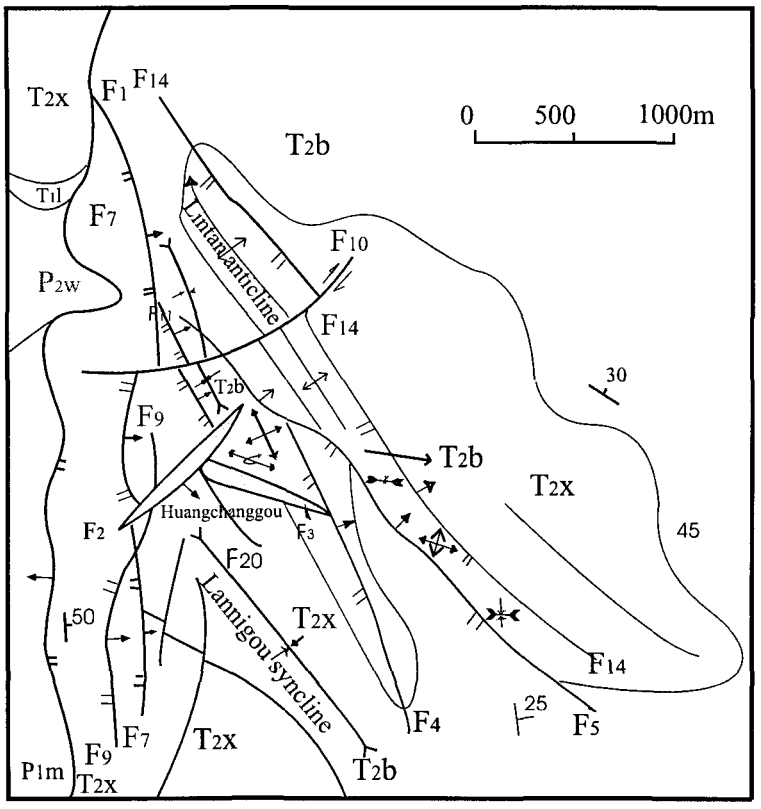

Fig.3-3. Geological map of the Lannigou gold deposit.

T2b Bianyang group sandstone, siltstone and shale T2x Xinyuan group siltstone and shale

T_{1l} Louluo group clay-limestone P2w Wujiaping group bioherm limestone

P1m Maokou group sandstone

F3 Compressive-shear fault

Anticline axis

Anticline dome

Ore-bearing fault

Shear fault

Syncline axis

25 Dip angle and direction

(After Luo, 1994)

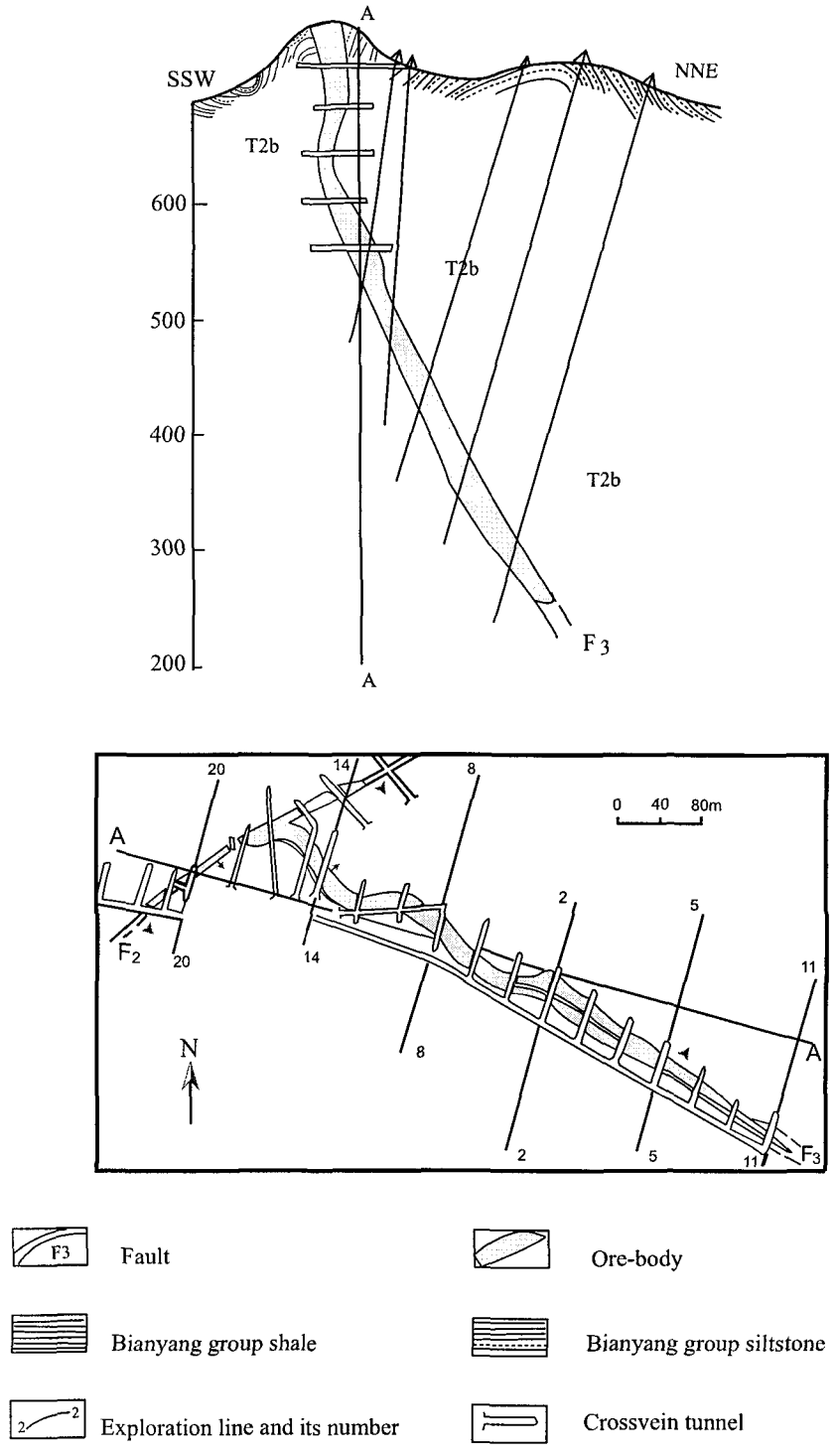

Fig. 3-4. Sketch map showing the fault control of gold mineralization at the Huangchanggou section of the Lannigou deposit. (After Luo, 1994)

clastic rocks near Luofan. The fractured zone is generally about 5 m wide, and gold mineralization is only observed near Rongban where hydrothermal alteration is extensive. The F_7 fault, more than 3 000 m long, is located east of the F_1 fault, dipping eastward with medium pitch angle. Alteration along its fracture zone is rather strong and gold mineralization is observed near Huangchanggou. The F_9 fault is rather minor and alteration within its zone is rather weak, and only weak gold anomalies were observed.

2) NW trending structures

The NW trending structures include the Lannigou syncline, the Lintan anticline and NW trending faults, F_{14}, F_5, F_4, and F_{11} being the major ones. These structures were formed by northeast-southwest directed lateral compression. The folds are 200 to 3 500 m long axially and 400 to 1 000 m wide, and all show flat pitches on the southwestern limbs with steeper dips on the NE limbs. The core parts of the anticlines consist of the third section of the Xinyuan Formation, while the core parts of the synclines consist of the Bianyang Formation. The F_{14} fault occurs approximately along the Lintan anticline axis and is about 4 000 m long, tilting NE with a pitch angle of around 60°. Gold mineralization was discovered near the NW end of fault F_{14} where it cuts through the inflection of the Lintan anticline. The ore zone is more than 200 m long and 2 to 3 m wide, and its highest gold concentration is 30 ppm. Fault F_5 occurs SW of F_{14} and approximately parallels it. No gold mineralization has been found in this fault yet.

3) NE trending structures

The northeast trending structures, consisting of a group of shear faults, include the F_2 fault in Huangchanggou and the F_{10} fault in the northern end of the mining area. Fault F_2 is located on the west slope of the Huangchanggou trench. It is about 500 m long and from 5 m up to 10 m wide at its intersection with the F_3 fault. It dips 45° to 80° southwest, but dips to NW on the surface. The F_2 fault contains the second largest orebody, orebody No.2, which is 270 m along the fault and at the intersection of the F_2 and F_3 faults is large and of high grade. The WNW trending (290°) F_3 fault dips to NNE (55° ~ 85°); it controls the main ore body, the No.1 orebody in the mining area. This fault is about 8 ~ 20 m wide with extensive silicification and pyritization, and the orebody is 8 ~ 15 m with an average grade of 7.5 ppm.

3.1.2. Stratigraphy

The Lannigou deposit is hosted by two distinct sedimentary rocks. Upper Triassic rocks are exposed at the western limb of the Laizishan anticline and are shallow marine carbonate rocks formed in a continental shelf environment. Early to Middle Triassic rocks are exposed at the eastern limb and host the main ore bodies of the deposit. Stratigraphic units in the area include the Triassic Bianyang Formation, and the Xinyuan, the Luolou, the Xuman, the Niluo, and the Permian Wujiaping Formations. In general, the strata are S-N trending, east dipping, with 25° to 40° angles of inclination. The strata are reversed near Lannigou and Huarong due to extensive compression, forming overturned or recumbent

folds. The ores are mainly hosted by the Bianyang Formation and by the fourth and second sections of the Xuman Formation of the Middle Triassic age.

3.1.2.1. Middle Triassic

The Bianyang Formation (T_{2b}) in this area consists mainly of thinly to thickly layered, fine-grained sandstone and siltstone that are interbedded with argillite or alternating beds of sandstone and argillite (Fig.3-5). The clastic components, including moderately sorted and rounded quartz, siliceous rock fragments, minor feldspar, rutile and anatase, etc., make up about 80% of the sandstone; whereas the cementing material, consisting of hydromica, calcite and silica, makes up 10-20% of the whole rock. Bouma turbidite sequences (c-d-e, c-d, and d-e) are common. Sedimentary features, such as flute and groove casts, load structures, and even, oblique and convoluted bedding are also observed in the sequence (Li and Liu, 1995). Bivalve fossils and fossil fragements are commonly present in the argillite and silty argillite. The Bianyang Formation is about 270 m thick and is conformable with the underlying strata. All the orebodies of the Lannigou deposit occur in this formation, the bottom part being the most favorable host.

The Xinyuan Formation (T_{2x}) is divided into four sections based on lithology. From top to bottom, these sections are as follows:

(1) The uppermost section (the fourth section, T_2x^4, 10 to 46.56 m.) consists of gray to dark gray, thinly to moderately thickly layered argillite with 0~10m thick limestone with tubercle texture or marl interbedding containing bivalve fossils and plant fragments.

(A). The Bianyang Formation (T_{2} b) thinly to thickly layered sandstone and siltstone

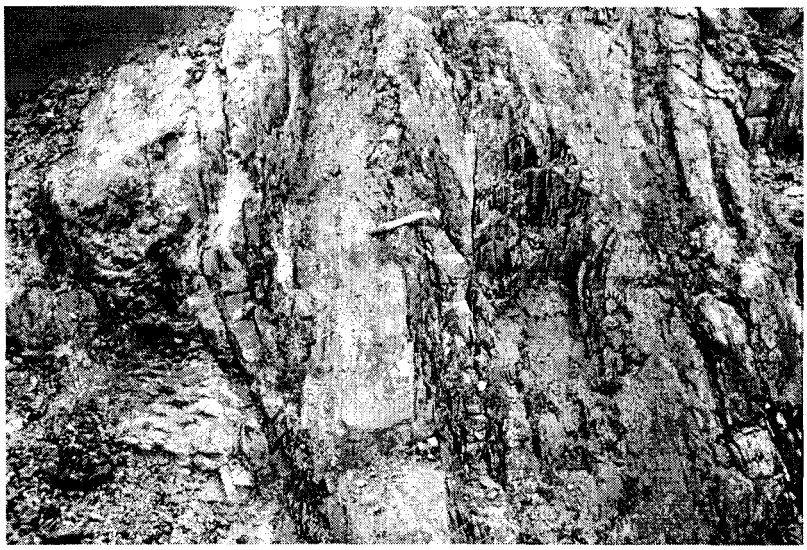

(B). Mineralized Bianyang Formation within F_3 fault

Fig.3-5. Photographs showing the lithology and deformation of the Bianyang Formation in the Lannigou deposit

(2) The third section (T_{2x}^{3}) can be divided into three sub-sections (top to bottom).

1) The third sub-section (T_{2x}^{3-3} , 30 to 109.78 m) consists of light gray thickly layered or massive fine-grained sandstone and muddy siltstone, and is commonly interbedded with thinly laminated argillite. The sandstone generally contains disseminated coarse-grained cubic and nodular pyrite crystals. This sequence is highly mineralized locally where the main ore-controlling fault F_3 cuts through this stratigraphic unit.

2) The second sub-section (T_{2x}^{3-2}, 50 to 209.99 m thick) consists of argillite and interbedded lenses of siltstone.

3) The first sub-section (T_{2x}^{3-1}, 20 to 67.44 m thick) consists of sandstone in the upper part and alternating beds of argillite and sandstone in the lower and middle parts.

(3) The second section of the Xinyuan Formation (T_{2x}^{2} , 0 to 121.78 m) consists of sandstone and muddy siltstone interbedded with fine-grained sandstone. Abundant bivalve fossils were observed in this section.

(4) The first section (T_{2x}^{1}, 0 to 147.46 m) consists mainly of thinly to moderately thick layered argillite with thin micrite. Mud-striped limestone and fine-grained sandstone interbeds occur in the upper and lower part of this sequence.

3.1.2.2. Lower Triassic

(1) The Luolou Formation (T_{1l}, 0 to 76.25 m thick) is distributed in the northern part of the deposit and consists of gray to dark gray limestone with interbedded mudstone and tuffaceous rock. Many ammonite fossils are found in this unit.

(2) The Lixue Formation (L_x) is located in the southern part of the mining area, and is composed of calcirudite, limestone conglomerate, micrite, and bioclastic limestone discordantly overlaying the Permian limestone.

3.1.2.3. Permian

The Wujiaping Formation (P_{2w}) consists of reefal limestone or reefal rudstone.

In the mining area, the Xinyuan Formation and the overlain Bianyang Formation occur in a NW-SE trending widely spaced complicated fold. Despite modifications in the formation due to faults and fractures, on the whole, an anticline and a syncline, respectively, occur to the north and south of the mining area; in addition, a secondary closed anticline can be recognized inbetween the anticline and syncline.

3.1.3. Alteration

Wall rock alteration in the mining area commonly occurs along the fractures and includes silicification, pyritization and accompanying arsenopyritization, carbonatization, and argillization. The alteration zones are distributed along and within the fault zones and

their widths are large. Also, locally concentrated and mineralized in the mining area are cinnabar, realgar and orpiment.

Silicification: Three stages of silicification can be distinguished. Early silicification is presented as fine-grained quartz together with chalcedony generally occuring as irregular fine veins within the fractures. Also, hydrothermal pyrite, arsenopyrite, carbonate, and illite were formed during the early stage of silification. Mid-stage silicification occurs as approximately 1mm wide quartz veinlets accompanied by abundant pyrite, arsenopyrite, carbonate, and illite. Late silicification consists of large clear quartz and quartz-carbonate veins, accompanied by pyrite, realgar, orpiment, stibnite, cinnabar and minor sphalerite.

Pyritization: The pyrite in the ores is unevenly distributed, and commonly concentrated in and near the fracture zones. The estimated volume proportions of pyrite usually varies from 1% to 3% in poor ores and 8% to 10% in richer ores. Argillaceous siltstone contains an average of 3.2% pyrite but up to 20% locally. Pyrite, the most important host mineral to gold, is disseminated in the ores ocurring as small crystals with diameters of 0.01 to 0.50 mm, and occurs as veins locally. Three phases of pyritization were distinguished in the deposit. The first phase comprises diagenetic, framboidal and cubic pyrite which occurs along bedding or as aggregates in unaltered host rocks. The second phase pyrite shows enhedral to subhedral cubic, pyritohedral, and octahedral crystal forms commonly containing framboidal or cubic diagenetic pyrite cores. Pyrite overgrowth textures are common and enriched in As and Au. They also contain significant amounts of trace elements, such as Ag, Cu, Pb, Zn, etc., disseminated within or near quartz veinlets,

and closely associated with acicular arsenopyrite, zoned pyritohedral or octahedral pyrite (He et al., 1993). The third phase pyrite mainly occurs as large cubes. Arsenopyritization has been observed to occur during the last two phases of pyritization intergrowth with pyrite or as fine euhedral, subhedral needles or columnar crystals.

A tentative investigation on the thermoelectricity of pyrite of the Lannigou deposit was carried out in attempt to investigate its possibility as an exploitation method (Su, 1994*, unpublished). It showed that all pyrites in the ores and altered host rocks are of p-type, while some of the pyrites in the unaltered host rocks are of n-p type from the Lannigou deposit. Coefficients of thermoelectricity (â=ΔE/ΔT; ΔE is the thermoelectricity potential, ΔT temperature gap between the two poles) of the pyrites in the ores have a narrow range of variation (+160~180mv/°C), while the coefficients of the pyrites in the host rocks are scattered in a rather large range (-80 ~ 240mv/°C). Most of the pyrite in the mining area are p-type which is consistent with the high As background in the region, and which might have contributed to gold mineralization.

Carbonatization comprises calcitization and (ferroan) dolomitization. Early stage carbonate occurs as ankerite, whereas late stage carbonate occurs as calcite. Late stage carbonatization is closely associated with cinnabar, realgar, orpiment, and stibnite.

---

* Su Wenchao. 1994. Study of the thermoelectricity of the pyrite in the gold deposits of the southwestern Guizhou and evaluation of the ore potential at depth. Institute of Geochemistry, Chinese Academy of Sciences. Report QJ-3115. 52p. In Chinese.

Argillization is represented by neo-formed illite. The illite or illite-quartz veins are spatially associated with pyrite and arsenopyrite.

3.1.4. Ore geology

The Lannigou ore bodies and gold anomalies are restricted by the faults occurring along the fracture zones. The gold ore bodies are mainly hosted by the WNW trending faults and partly by the NE trending faults. For example, the WNW trending F_3 fault zone hosts the major part of the deposit. The No.1 ore body in the F_3 measures up to 650 m long, 600 m wide and 4 to 19 m in thickness. The lenticular ore bodies are hosted by fracture zones, and commonly occur as clusters of small ore bodies in adjacent subsidiary faults (Fig.3-6). The ores are preferentially hosted by fine-grained sandstone and siltstone with mudstone intercalations.

Ores primarily show disseminated, minor veinlets, banded, and brecciated structures. For instance, pyrite and arsenopyrite occur as specks or nebula scattered in the ores forming disseminated structures. Pyrite, realgar, and cinnabar either fill in the joint fissures, fractures, and bedding planes forming veinlets or banding structures, or less commonly, they form dynamically brecciated structures. The ore consists of about 4% sulfide, predominately pyrite, (accompanied by, arsenopyrite, stibnite, sphalerite, galena, realgar, orpiment, cinnabar, etc), and gangue minerals consisting of quartz, clay minerals and carbonates (Fig.3-7). Pyrite, cinnabar, realgar and orpiment usually occur as euhedral and subeuhedral grains disseminated in the ores. Pyrite also occurs as anhedral grains or as

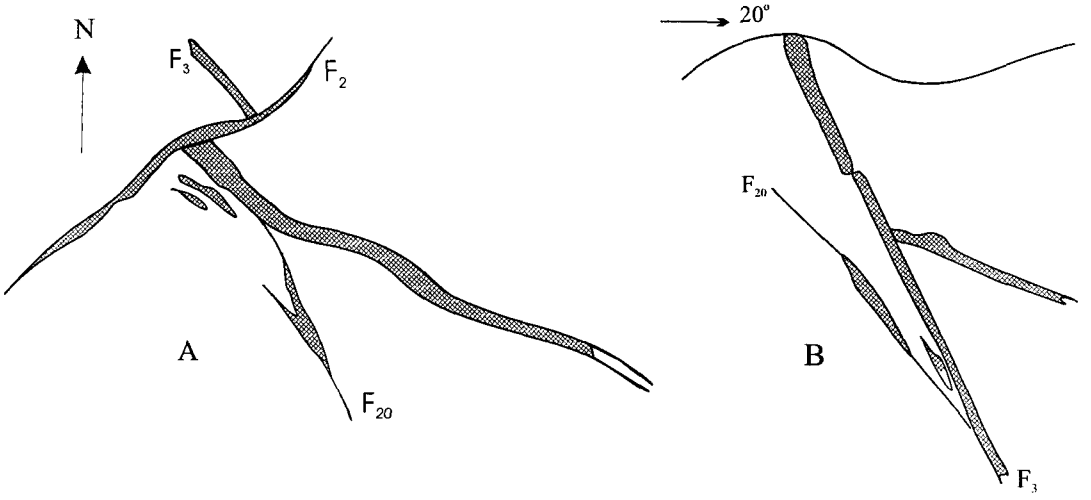

Fig.3-6 Sketch map showing the spatial distribution of the ore bodies in the Lannigou gold deposit.
A. Horizontal B. Vertical
(After Wang et al., 1994a)

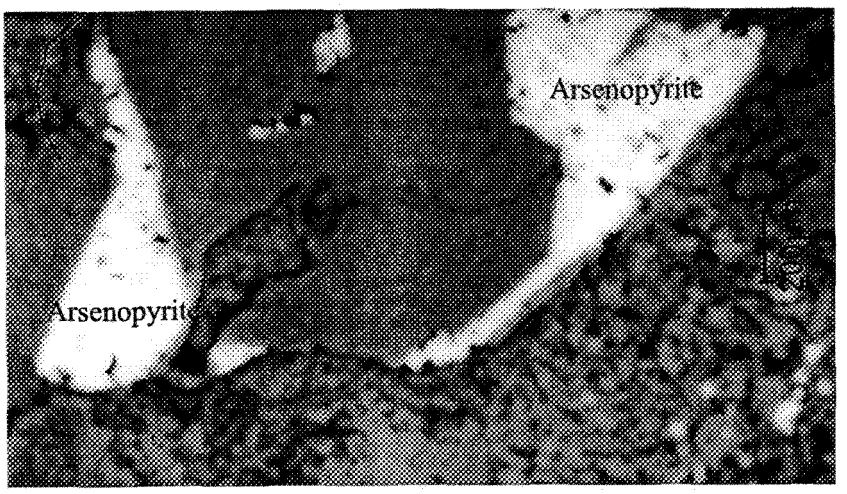

(A). Arsenopyrite in the ore from the Lannigou deposit

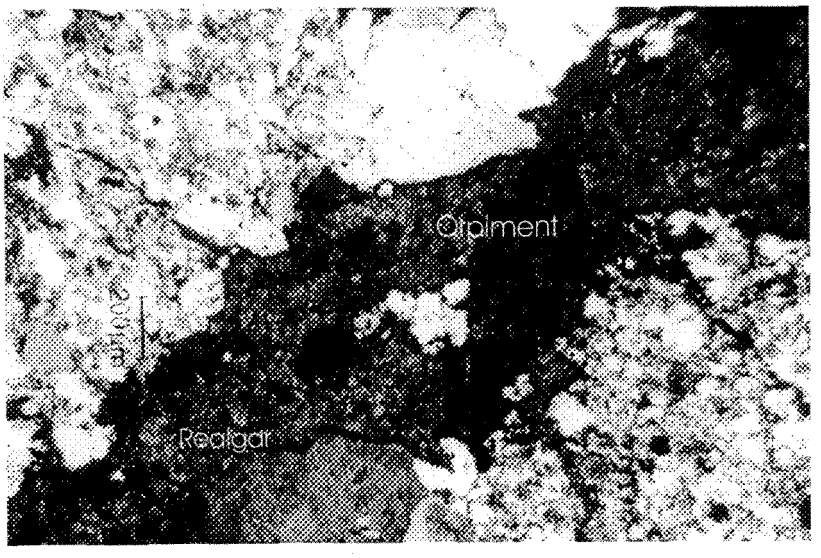

(B). Orpiment and realgar in the late stage calcite vein from the Lannigou deposit

Fig.3-7. Arsenopyrite, orpiment and realgar in the ores from the Lannigou deposit

aggregates. Overgrowths of arsenian pyrite and diagenetic pyrite are common in the ores (Luo, 1994). Arsenopyrite occurs as euhedral and subhedral needles or prismatic crystals.

As, Sb, Hg, and Tl, which are enriched in the ores and generally form the primary geochemical halo around the ore bodies, can be used as fingerprints for geochemical prospecting. The average concentrations of Au, As, Hg in the ores are 8 ppm, 0.53%, and 108 ppm respectively. Arsenian pyrite is the main gold bearing mineral and is host to about 68% of the total gold in the ores. Au concentration is correlated with As in the pyrite, but no separate gold phase has been distinguished under scanning electronic microscopy (Wu, 1992). Most of the gold in the ores resides as submicron "invisible" gold (< 200 nm) in sulfides, such as pyrite, arsenian pyrite, and arsenopyrite. Due to the extensive leaching, the FeO, Fe_2O_3, CaO, MgO, K_2O and Na_2O were removed, and the grade of the oxidized ores are relatively enriched (Table 3-1), In the oxidized ores, "visible" micron size gold (2~6 μm) was observed under SEM in hematite and interstices of quartz (He et al., 1993).

3.2. Getang gold deposit

The Getang gold deposit is located in Anlong and Xingyi County, 27 km northwest of Anlong town. The gold deposit occurs on the eastern limb of the Getang dome that is a northwest-trending anticline about 50 km long. The Permian rocks are exposed in the tectonic inlier at the center of the dome. The core of the dome is the Maokou Formation of the Lower Permian Period, while the limb consists of the Longtan, the Changxing, and the Dalong Formation of the upper Permian System and the Yelang Formation of the Lower

Table 3-1 Chemical compositions of the primary and oxidized ores of the Lannigou, Getang and Zimudang deposit

Deposit	Component ($_{wt}$%)	Primary ore	Oxidized ore	Component ($_{wt}$%)	Primary ore	Oxidized ore	Data source
Lannigou deposit	SiO_2	68.80	86.08	CaO	2.78	0.25	Ni et al., 1997. *
	TiO_2	0.24	0.27	Na_2O	0.38	0.02	
	Al_2O_3	6.40	5.69	K_2O	1.70	1.07	
	Fe_2O_3	2.46	2.01	As	1.43	2.27	
	FeO	5.24	1.28	Au (ppm)	7.47	29.0	
	MgO	1.46	0.49	Sb (ppm)	71	19	
	U (ppm)	1.9	2.5	Th (ppm)	8.3	14	
Getang deposit	SiO_2	66.07	89.59	CaO	3.45	0.15	
	TiO_2	1.19	0.50	Na_2O	0.50	0.20	
	Al_2O_3	10.49	7.34	K_2O	1.32	0.53	
	Fe_2O_3	7.55	2.53	As (ppm)	273	190	
	FeO			Au (ppm)	0.02	8.78	
	MgO	0.29	0.09	Sb (ppm)	35000	200	
	U (ppm)	10.5	1.3	Th (ppm)	3.7	0.2	
Zimudang deposit	SiO_2	13.90~44.66	52.36~70.13	CaO	10.16~40.84	0.04~0.13	Wang et al., 1994a
	TiO_2	0.71~1.20	1.84~3.26	Na_2O	0.01~0.14	0.39~0.40	
	Al_2O_3	2.93~10.33	9.05~16.67	K_2O	0.76~2.64	1.97~3.55	
	Fe_2O_3	3.13~13.41	10.25~15.54	H_2O^+	0.73~2.64	3.40~4.85	
	FeO	1.68~4.43	0.02~1.20	H_2O^-	0.26~0.70	1.61~2.29	
	MnO	0.03~0.15	0.24~0.32	As	0.14~3.30	0.23~0.44	
	MgO	1.40~4.19	0.32~0.33	Au (ppm)	1.71~8.82	6.60~8.90	

* Trace element contents were analyzed by INAA method.

Triassic System (Fig.3-8). Within the mining area, the strata dips about 10° towards SE, forming a monocline structure cut by high-angle reverse faults. In the strata, flat warping and folding are common. Gold mineralization is mainly confined to the inter-stratal faults and related fracture zones, and occurs within the silicified clay breccia and limestone breccia developed within the unconformity between the Upper Permian Longtan Formation and the Lower Permian Maokou Formation. Besides the Getang gold deposit, there are a few other known occurrences of gold, mercury and antimony mineralization around the dome.

3.2.1. Stratigraphy

Sedimentary rocks exposed in the area are of the Permian to Early Triassic age, and include the Lower Permian Maokou Formation, the Upper Permian Longtan, Changxing, and Dalong Formation, and the Lower Triassic Yelang Formation. The Permian Maokou Formation is a massive gray limestone with a karst unconformity at the top. The Maokou Formation is overlain by the Upper Permian Longtan Formation, which consists of argillaceous limestone that contains coal beds, silicified shale, and clastic rocks near the top. The main characteristics of the strata are as follows:

The Yelang Formation (T_{1y}): the upper section consists of dark brown thin to thick layers of silty clay rock and shale, intercalated with light to pale gray moderately layered limestone. The lower part of the formation consists of dark green, yellowish-green

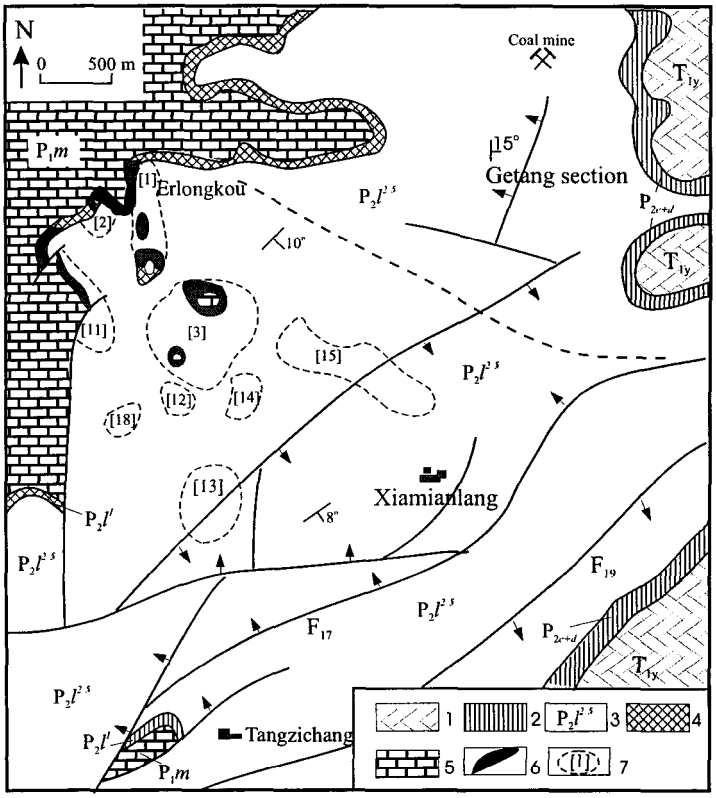

Fig.3-8.Sketch map of the Erlongkou mining section of the Getang gold deposit.
(after He et al., 1993)

1-T_{1y}shale with carbonate intercalations of the Yelang Formation; 2-P_{2c+d} chert lim stone of the Changxing and the Dalong Formation; 3-$P_2l^{2\text{-}5}$ sandstone, pelite and coal bed; 4- P_2l^1 carbonaceous rocks of the Longtang Formation; 5- P_1mlimestone of the Maokou Formation; 6- Outcrop of the gold ore body;7-Number of the ore body and the boundary of the mineralization

moderately layered argillaceous siltstone, clay rock, shale, siliceous rocks and carbonaceous shale. The formation is more than 100 m thick.

The Changxing and ***Dalong Formations*** (P_{2c+d}): both formations consist of dark gray moderately to thickly layered chert-bearing limestone, and gray thinly to moderately layered siliceous exhalite and siliceous shale. The total accumulation of the two formations is about 11 m.

The Longtan Formation (P_{2l}): ranges from 150 to 230 m in thickness and can be subdivided into five sections:

(1) The top subsection (P_{2l}^{5}) is about 63 m thick, consisting of gray thinly layered fine-grained sandstone, siltstone with intercalated carbonaceous clay rock and several layers of anthracite.

(2) The fourth subsection (P_{2l}^{4}) is about 25 to 40 m thick, consisting of silicified limestone, silty shale with intercalated coal bed, and silicified limestone breccia.

(3) The third subsection (P_{2l}^{3}) is about 40 to 66 m and consists of thinly layered gray silty clay rock with intercalated carbonaceous clay rock and coal beds. Argillaceous limestone lenses are common in the lower part.

(4) The second subsection (P_{2l}^{2}) is about 2 to 20 m thick occuring as dark carbonaceous clay rock with a thinly layered coal bed; nodular and disseminated pyrite is common.

(5) The bottom section (P_{2l}^{1}) is about 0.5 to 77.5 m thick. Lithological facies of this section vary extensively laterally. The main rock types consist of three types of breccia: limestone, gray clay rock, and thin-layered clayey siltstone.

The Maokou Formation of the Lower Permian (P_{1m}): occurs as thickly layered to massive limestone over 100 m thick., with a karst unconformity on the top of this formation.

3.2.2. Ore geology

Gold is concentrated along a 3 to 15m-thick breccia horizon at the base of the Longtan Formation (P_{2l}^{1}). The breccia lies over the erosional unconformity between the Longtang and Maokou Formation, which was controlled by the topography of palaeo-base level erosion (Fig.3-9, 10). Regionally, this horizon is characterized by karst development, but in the Getang deposit, it may be a superimposed bedding-plane thrust fault (Cunningham et al., 1988). Lenticular ore-bodies crop out discontinuously along the breccia horizon over a distance of 1 000 m and consist of silicified, argillaceous, carbonate breccia having a chalcedonic matrix.

Controlled by hydrodynamic and palaeo-erosion surface conditions, the lithology and thickness of the breccia layer vary considerably. As such, the local breccia horizon can be divided into four lithological sections as listed below:

The top portion: light gray tephrosious rock with disseminated fine-grained pyrite. Its thickness ranges from 1 to 3 m. It occurs locally in the breccia layer.

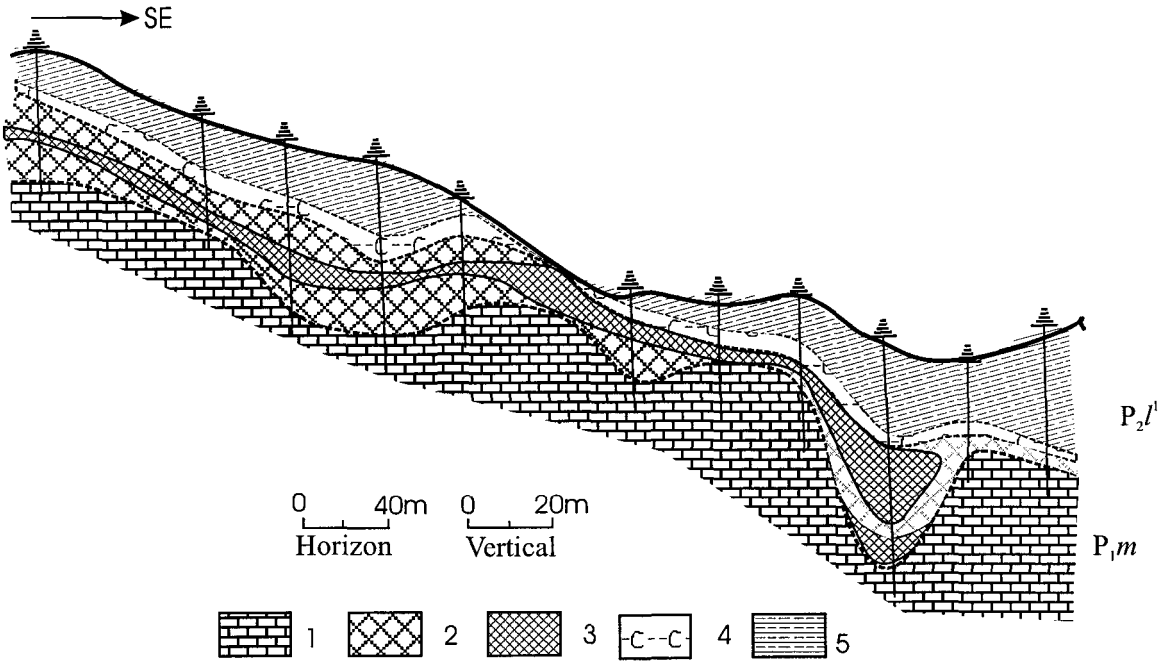

Fig.3-9. Profile section of 3-3' prospecting line at Erlongkou ore block of the Getang gold deposit. (After Wang et al., 1994a.)

1. Maokou Formation limestone 2. Silicified brecciated limestone (mineralized) 3. Ore body
4.The Longtan Formation carbonacious shale 5.Claystone

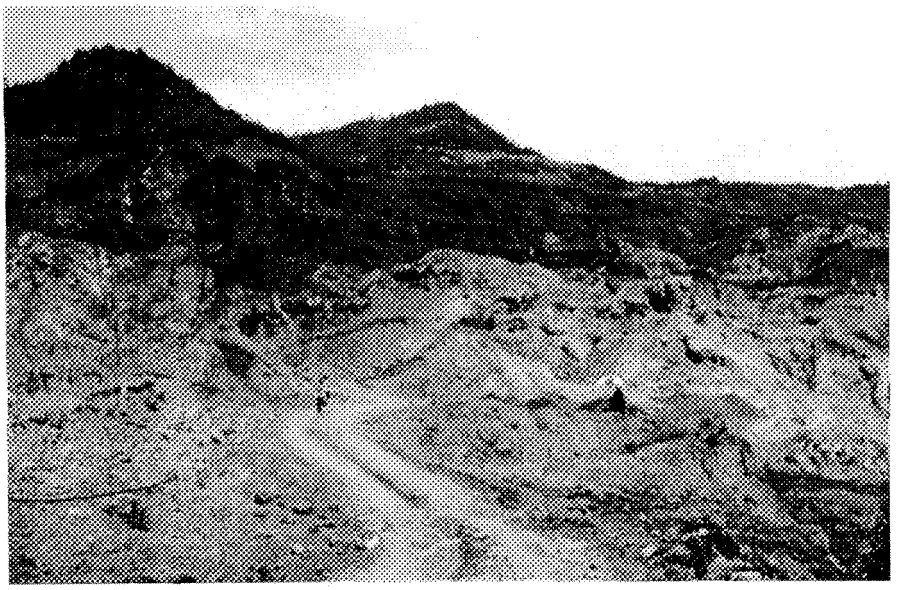

(A) The ore body is covered by a layer of silicified carbonaceous shale

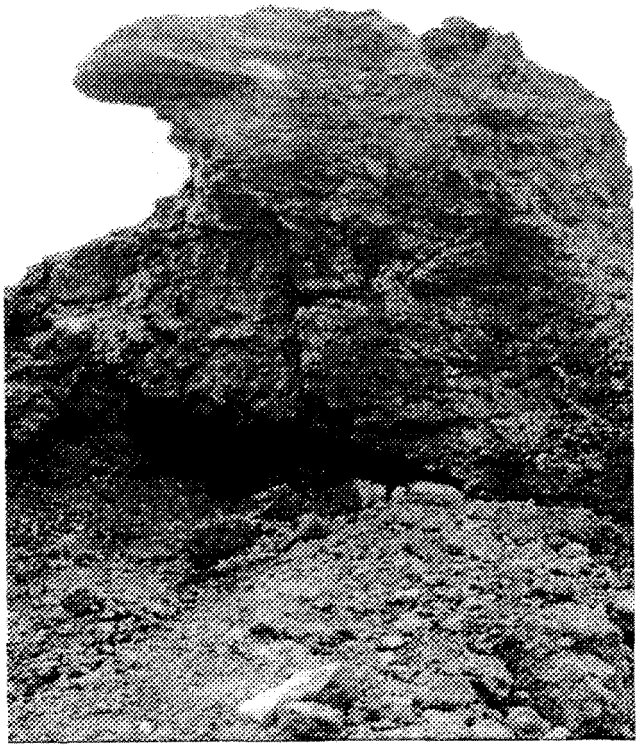

(B). The silicified mineralized breccia in the open-pit mining

Fig. 3-10. The open-pit mining of the Getang deposit

The second portion: light gray clay rock breccia, commonly silicified with localized gold mineralization. Its thickness ranges from 1 to 10 m; locally absent.

The third portion: it is the main gold hosting section and consists of massive gray silicified limestone breccia. It usually ranges from 1 to 10 m in thickness, but it can be up to 40 m, usually wedging out.

The fourth portion: consists of gray clay rock breccia, usually silicified with localized gold mineralization. Limestone or silicified limestone debris of 50×50 cm and larger size were observed locally in the section. This section is 1 to 5 m thick, but is commonly absent or thins out.

The bottom portion: consists usually of 0 to 2 m mottled kaolin conglomerate bearing clay rocks. Occasional 1 to 2 m snuff-colored ferricrete crusts were observed inbetween the Longtan and Maokou Formations.

The gold ore bodies often occur in karst bays, eroded depressions, and solution depressions within the breccia layers listed above. The ores include primary and oxidized varieties, and the former is comprised of pyritized, silicified breccia while the latter occurs as oxidized zones overlying the primary orebody. The breccia consists of rock debris and small quantities of biodetritus in sizes of 0.2~20 cm. The rock debris includes mudstone, carbonate and silicolites.

The ore mineral assemblages consist of sulfides (pyrite, pyrrhotite, chalcopyrite, arsenopyrite, stibnite, cinnabar, galena, sphalerite, realgar and orpiment), oxides (goethite,

magnetite, rutile, etc.), silicates (hydromica, kaolinite, etc.), carbonates (calcite, siderite), and native elements (gold, copper, iron, Zn.). Covellite, arsenolite, valentinite, jarosite, scorodite and other secondary minerals are often observed in the oxidized ores. The minerals were identified using microscopy combining X-ray diffraction. In the oxidized ores, limonite is common. Pyrite is the main sulfide in the primary ore; it occurs as yellow to bright yellow cubic, pyritohedral, octahedral crystals and framboids. Marcasite replaces pyrite along rims and fractures, and often shows pyrite pseudomorph. Goethite (Fig.3-11), the main gold host mineral in the oxidized ore, usually shows colloidal or spheroidal forms, kidney, radial, and acicular structures, and pseudomorphs after pyrite (Liu et al., 1989). Gangue minerals include chalcedonic quartz, illite, calcite, dolomite, jarosite, fluorite and barite. Jasperoid and silicified limestone, containing pyrite and stibnite, overlie the gold deposit.

The gold ore bodies are confined to the silicified breccia, and the gold content increases as the degree of silicification increases. Native gold occurs principally as grains less than 0.5 μm in diameter; locally, grains up to 3 μm were observed. The ore grades from 2 to 5 g of gold per metric ton to as much as 50 g per metric ton locally. Because of extensive leaching, the Au concentration in the oxidised ores are relatively enriched (Table 3-1). The grade of the ore commonly increases from 2 to 3 g of gold per metric ton in primary ore to 4 to 5 g per metric ton in limonite-bearing oxidized ore. Geochemical anomalies of arsenic and mercury are present.

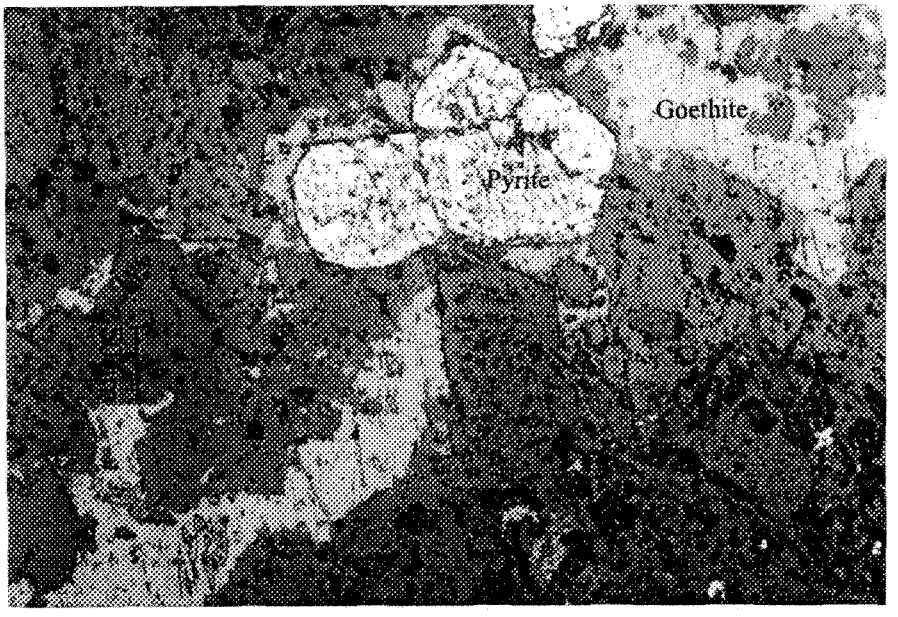

Fig. 3-11. Pyrite and goethite in the oxidized ore from the Getang deposit

3.3. Zimudang deposit

The Zimudang gold deposit, discovered in 1984, occurs in the west part of a NW trending anticline, the Huijiabao anticline, which is a symmetrical fold about 20 km long and 7 km wide (Fig.3-12). Cutting through the Huijiabao anticline at its core, is the Dashan-Zhexiang thrust fault. It is about 30 km long, dipping south or SSW at angles ranging from 15 to 35° and its fault displacement is about 100 m. This fault zone is characterized by breccia and cataclasite. It controls the distribution and occurrences of ores; more than 10 gold showings with accompanying Hg, As, Tl and Sb mineralization have been discovered in the anticline.

3.3.1. Stratigraphy

The sedimentary rocks outcropping in the Huijiabao anticline are composed of sediments from the Upper Jurassic Longtan, Changxing, and Dalong Formations and the Lower Triassic Yelang and the Yongningzhen Formations. The lithological characteristics of the formations are listed chronologically from oldest to youngest:

The Longtan Formation (P_{2l}): consists of yellowish-brown thinly layered clayey siltstone and carbonaceous shale at the base; gray-brown thinly layered silty mudstone with intercalated quartz sandstone and quartzite in its middle and upper parts; and an approximately 30 cm coal bed at the top of the formation. Also, *Brachiopoda*, *lamellibranchiata* and *flora* fragments were observed in the formation. The formation's total exposed thickness is about 100 m.

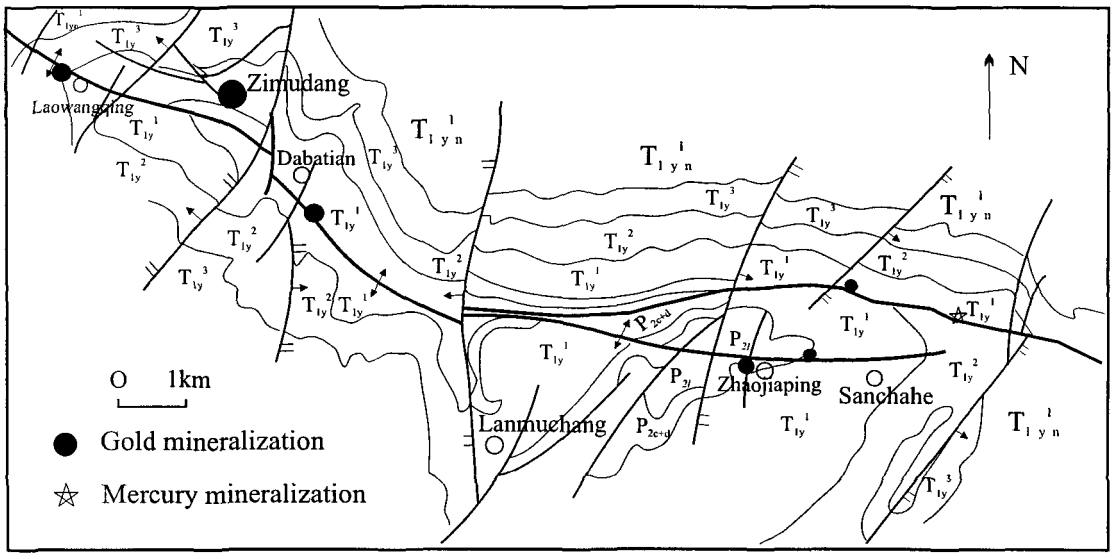

Fig. 3-12. Sketch map of the Huijiabao anticline (after Guo, 1988).

T_{1y}^{1} The first section of the Yongningzhen Formation; T_{1y}^{3} The third section of the Yelang Formation; T_{1y}^{2} The second section of the Yelang Formation; T_{1y}^{1} The first section of the Yelang Formation; P_{2c+d} The Changxing Formation and the Dalong formation; P_{2l} The Longtan Formation.

The Changxing Formation (P_{2c}): consists of thinly layered gray chert nodule-bearing bioclastic limestone in the lower part, pale to light gray thinly layered marlite, calcareous clay rock with thickly layered chert nodule-bearing bioclastic limestone intercalations in the middle and of gray to dark gray medium-layered bioclastic limestone in the upper part. Also, *Ortnotetina yuber* and other fossils were observed. The formation is 50~56 m thick.

The Dalong Formation (P_{2d}): is made up of gray to dark gray thinly layered calcareous mudstone containing fossils such as *Spiriferina sp., Multiplicata.* This formation is 7 to 13 m thick.

The Yelang Formation (T_{1y}) is subdivided into three sections.

1) The first section of the formation (T_{1y}^{1}) consists of dark gray thin-layered mudstone, silty mudstone with dolomitic limestone and calcareous siltstone interbeds in the lower part, medium bedded gray limestone, marlite, with dolomite and calcareous siltstone interbeds in the middle part, and gray thinly to moderately layered silty mudstone, dolomitic limestone, marlite intercalations in the upper part. The thickness of the section varies from 203 to 233 m.

2) The second section of the Yelang Formation (T_{1y}^{2}) consists of gray moderately layered oolitic limestone, purple and dark gray thickly layered argillaceous banded limestone with interbedded dolomitic limestone and clayey siltstone in lower part, gray thickly layered oolitic limestone with argillaceous dolomite intercalations in the upper part. This section is 100 ~ 120 m thick.

3) The third section of the Yelang Formation (T_{1y}^{3}): consists of purple, yellowish-green thinly to moderately layered silty mudstone, calcareous siltstone with gray medium-layered oolite limestone. Marlite intercalations occur at the top and bottom of the sequence. The section is 140~165 m thick.

The Yongningzhen Formation (T_{1yn}): consists of gray thickly layered limestone with thinly layered calcareous siltstone interbeds, and is more than 100 m thick.

All the strata listed above, except for the Yongningzhen Formation, host gold mineralization. The Yelang Formation, which was deposited in restricted to semi-restricted littoral tidal flat environment (Guo, 1988), contains the most favorable strata in the mining area.

3.3.2. Ore geology

The Zimudang gold deposit occurs in the south part of the Huijiabao anticline. There, the ore bodies are hosted by fracture zones which cut through impure carbonate and siltstone of the Yelang to the Changxing Formations.

The ore bodies are mainly confined to faults F_1 and F_2, and to the bedding fault which are characterized by fracture zones along with wider alteration zones (Fig.3-13, 3-14). Fault F_1 , about 2 000 m long, is a low angle thrust fault that cuts across the anticline, dipping south at an angle of about 25 to 30°. F_1 hosts the major part of the known gold reserve of the Zimudang deposit. Therein, ore bodies occur as plates or lenses in the center of the altered zones of fractures, and there are no clear boundaries between the ores and the host

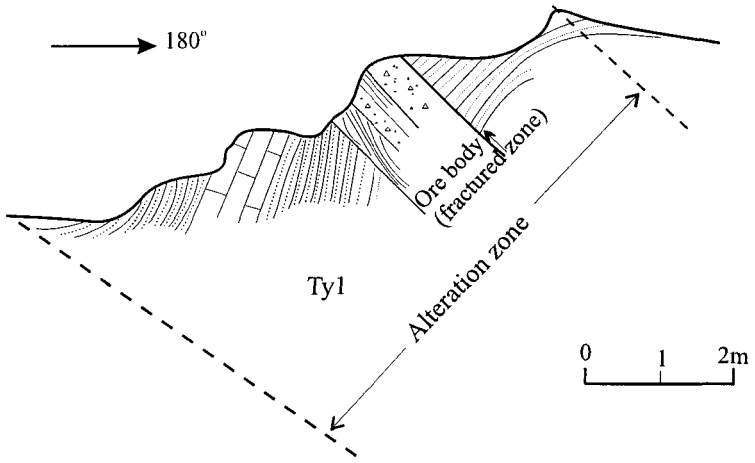

Fig.3-13. Sketch map of profile section showing the occurrence of the ore body in the Zimudang gold deposit. (Modified from Wang et al., 1994a)

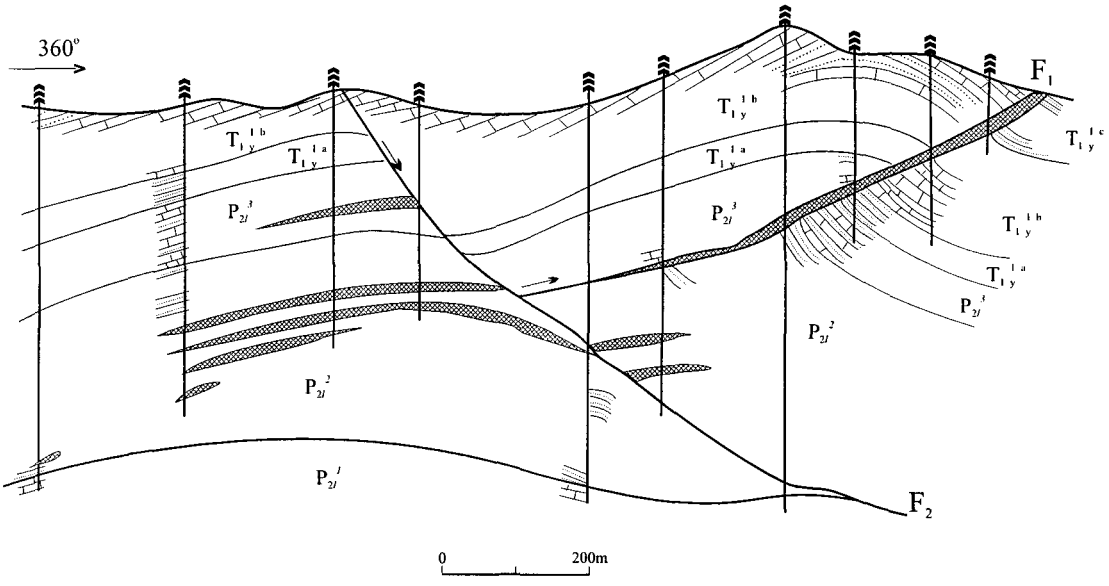

Fig.3-14. Sketch map of the 32-32' exploration section of the Zimudang gold deposit (after Wang et al., 1994a).

1. First section of the Longtang Formation 2. Second section of the Longtang Formation 3. Third section of the Longtang Formation 4. Lower part of the first section of the Yelang Formation 5. Middle part of the first section of the Yelang Formation 6. Upper part of the first section of the Yelang Formation 7. Lime stone 8. Siltstone 9. Ore body

rocks. The F_2 fault, which hosts some irregular lenticular ore bodies, is a steep normal fault oriented sub-parallels to the axis of the anticline. Some bedding faults also host some small lenticular gold ore bodies. The ores are richer in gold in the inner part than in the outer part of the ore bodies.

Sulfidation, silicification and carbonatization are the three major types of alteration in the fracture zones. At locations where alteration is extensive, multiphase alteration is superimposed and symmetrically zoned.

The primary ores are gray to dark gray, composed of pyrite, chalcopyrite, bornite, realgar, arsenopyrite, sphalerite, tennantite and other gangue minerals like calcite, dolomite, barite, chlorite, magnetite, goethite, hematite, and basaltic debris. The oxidized ores are developed on top of the primary ore bodies and consist of fine-grained gold (1~4 μm), ferrihydrite, hydromica, calcite, dolomite, quartz, kaolinite, jarosite, anatase, clay which makes up 80~90%, and trace relics of pyrite and marcasite.

Pyrite is the main sulfide mineral in the ores. Diagenetic pyrite (<0.01 mm) commonly occurs along the bedding plane in framboidal and cubic forms. Hydrothermal pyrite, which is closely associated with gold mineralization, can be divided into two stages: stage I pyrite occurs as large euhedral to subhedral cubic crystals (0.01~0.5 mm) disseminated or conentrated along the bedding surfaces, comprises up to 10~15% of the rocks locally. Stage II pyrite can occur as finely disseminated grains (<0.005 mm) with pyritohedral, cubic and xenomorphic forms, as fine veinlets, or as overgrowths on stage I and diagenetic pyrite. The

gold concentrations of the ores is positively correlated to the content of the stage II pyrite. The stage II pyrite is also richer in arsenic than stage I and diagenetic pyrite. All the hydrothermal pyrite is P-type semiconductor (Guo, 1988).

Based on the alteration, mineral assemblages, ore texture and structural studies, the ore-forming process can be divided into two periods: the hydrothermal and the secondary enrichment periods. Furthermore, the hydrothermal period can be subdivided into three stages: (1) Pyrite-marcasite-arsenopyrite stage, which is the first stage of gold mineralization; (2) Gold (submicron)-pyrite-arsenian pyrite-marcasite stage, which is the main stage of gold mineralization; and (3) Realgar-quartz-calcite stage. In the secondary enrichment stage, the gold that was primarily hosted by sulfides was released, migrated and redeposited onto the surface of ferrihydrite and hydromica and formed as visible gold. The grain sizes of the native gold vary from 290 nm to 31 900 nm in the oxidized ores; however, a 5 nm gold grain was observed in kaolinite by AEM method (Sun et al., 1993).

Au concentration in primary ores (1.71~8.82 ppm) is lower than that in the oxidized ores (6.6~8.95 ppm) due to the leaching of the ores and secondary gold enrichment (Table 3-1). The oxidized ore zone usually measures up to 30 m thick. The oxidized ores become quite porous because of the leaching of sulfides and carbonate. Gold in the oxidized ores mainly (~90%) adheres to ferrihydrite and hydromica (Gao, 1989).

In conclusion, the Getang, Zimudang, and Lannigou gold deposits, which represent the Au-Sb, the Au-Hg- (Tl), and the Au-As- (Sb) SHDG types in southwestern Guizhou

Province are, respectively, different in tectonic setting, in the lithology of the host rocks, in mineral assemblage, and metallogenic elemenst associations of the ores. However, the three deposits have many geological and geochemical characteristics in common. The distribution of gold mineralization in the three deposits is controlled by faults around and/or that cut the anticlines. Orebodies are larger in the horizons with high permeability, high Au background and carbonaceous matter. Silicification and pyritization are two significant alteration types associated with gold mineralization in the three deposit areas. Furthermore, the Au mineralization in all cases is associated with As, Hg, Tl anomalies or mineralization. In the ores, Au mainly occurs in the hydrothermal pyrite as submicron-sized grains. Oxidized ores only represent a small portion of the known Au reserves in the three deposits.

4

GEOCHEMISTRY OF THE SHDG DEPOSITS

4.1. Trace element geochemistry

4.1.1. Rare earth elements and high field strength elements

Trace elements, especially rare earth elements (REE), are widely used to model the petrogenesis and evolution of igneous, sedimentary and metamorphic rocks (e.g., Haskin, 1984; Fleet, 1984). REE are generally regarded as insensitive to hydrothermal alteration. However, literature supporting REE mobility during hydrothermal processes has been rapidly expanding in the last two decades (Nesbitt, 1979; Alderton et al., 1980; Humpheris, 1984; Marsh, 1991; Bao, 1992; Williams-Jones and Wood, 1992; Gouveia et al., 1993; Mongelli, 1993; Prudencio et al., 1993 Van der Weijden and Van der Weijden, 1995). Recently, the potential of REE to provide information about ore forming processes through REE mobility or immobility during ore formation processes has widely been recognized, and detailed REE investigations have been performed on many metallic deposits (Taylor and Fryer, 1980, 1982; Campbell et. al., 1984; Giere, 1986; Whitford et al., 1988; Lottermoser, 1992; Parr, 1992; Wood and Williams-Jones, 1994; Bierlein, 1995; Bierlein et al., 1999). The mobility of trace elements in altered host-rocks, and their distribution in

host rocks and ores may provide constraints regarding the physico-chemical characteristics of the ore-bearing fluids, and may contribute to understanding the ore-forming processes (Lottermoser, 1992).

Wall rock alterations of SHDG deposits, especially pyritization and decarbonatization, have been investigated extensively. Studies have examined stable isotope composition variation and the degree of pyritization around deposits, and have proposed potential applications to geochemical exploration (Hofstra et al., 1991; Stenger et al., 1998a,b; Woitsekhowskaya and Peters, 1998). However, studies on trace elements, including high field strength and rare earth elements in the ores and the altered host rocks, are rare. So, samples from the underground and surface of the Lannigou, Getang and Zimudang deposit were collected, in order to assess their behavior during hydrothermal alteration associated with SHDG mineralization, and their potential as geochemical exploration tools.

4.1.1.1. Analytical procedure

Samples, about 200 g each, were carefully crushed and pulverized to less than 200 mesh. One hundred milligrams of each powdered sample was then placed in a separate PTFE bomb, to which, 1 ml of HF (38%) and 0.5 ml of HNO_3 (68%) were added. The bombs were then placed on a hot plate, and the solutions evaporated to dryness to remove most of the silica. Afterwards, extra HF (38%) and HNO_3 were added to the samples, and the bombs were reheated at 190 °C for 12 hours to remove the remaining silica. After cooling, the bombs were opened, and 1ml of 1μg/ml Rh solution was added as an internal

standard. Once again, the bombs were reheated on the hot plate at about 150 °C until the solutions evaporated to dryness. The final residue was re-dissolved by adding 8ml of 40% HNO_3, re-sealing the bombs and returning them to the electric oven at 110 °C for a period of 3 hours. After cooling, the final solution was increased up to 100 ml in volume by adding distilled de-ionized water. The reagent blanks were treated exactly the same way, as were the samples. The solutions were then analyzed using the Finnigan MAT ICP-MS at the State Key Laboratory of Ore Geochemistry, Guiyang Institute of Geochemistry, Chinese Academy of Sciences. The detection limits for Sc, Cr, Co, Ni, Cu, Zn, Sr, Zr, Mo, Cs, Ba, Pb range from 0.01-0.2 μg/*l*; for Y, Nb, Hf, Ta, W, Th, U and REE, the detection limits range from 0.001-0.005 μg/*l*. The analytical precision is about 5% for all the trace elements listed in Table 4-1.

4.1.1.2. Results and discussion

Unlike magmatic rock, trace element concentrations in sedimentary rocks are rather heterogeneous and generally difficult to compare directly. During the sedimentation process, one of the most significant factors controlling both the suspended- and bottom-sediment capacity for concentrating and retaining trace elements is the grain size. Surface area, grain size, hydraulic behaviors of heavy minerals and geochemical substrate are interrelated with sediment-trace element concentrations. Due to the efficient mixing of source lithologies during sedimentary processes, the REE distributions in terrigenous sedimentary rocks (of same lithological unit) are quite homogeneous (McLennan, 1989). The sedimentary rocks derived from regions sharing the same source, also share similar

Table 4-1. Trace element compositions of the ores and host rocks from the SHDG deposits in SW Guizhou Province (ppm)

	Sample	Mo	Sb	Cs	Sc	Cr	Co	Ni	Cu	Zn	Sr	Y	Zr	Nb	Ba	W	Pb
LN-4	Argillaceous sandstone	0.750	2.24	7.31	17.9	91.5	8.99	22.7	24.8	32.9	91.0	25.0	142	16.2	475	2.89	17.8
LN-8	Bioclastic limestone	0.163	3.28	0.043	1.20	7.73	1.19	6.98	2.96	8.01	99.4	7.04	0.799	0.162	6.93	0.722	3.19
LN-12	Argillaceous siltstone	0.560	2.14	5.90	15.6	81.7	14.3	32.2	21.3	65.8	111	30.4	192	17.6	353	2.78	20.9
LN-13	Oxidized ore	0.370	42.7	3.76	14.2	75.4	12.4	36.1	21.3	70.6	134	27.0	220	16.5	291	4.29	21.8
LN-14	Semi-oxidized ore (altered siltstone)	0.600	42.5	4.87	14.3	79.9	10.4	29.4	20.4	47.7	132	30.2	187	15.6	295	5.53	22.0
LN-15	Primary ore (silicified siltstone)	0.620	33.2	8.90	17.9	103	29.5	44.0	48.5	31.4	406	47.8	287	22.5	260	8.84	28.2
LN-45	Reef limestone (P)	0.220	0.902	0.143	1.40	15.1	2.25	8.01	2.98	3.73	170	6.22	1.10	0.169	10.3	0.627	3.13
LN-46	Primary ore (altered sandstone)	0.480	854	1.12	7.43	30.4	7.65	18.2	21.3	47.8	79.4	19.9	129	6.73	69.8	4.46	13.0
ZMD-1	Oxidized ore (mudstone)	29.0	37.1	4.30	24.6	145	41.8	122	82.8	141	962	48.8	412	46.9	252	18.1	17.9
ZMD-3	Primary ore (siltstone)	0.700	10.8	5.04	24.0	119	43.6	70.7	101	131	419	44.3	446	51.8	74.8	8.65	7.86
ZMD-4	Carbonaceous bed in the ore	1.49	250	8.95	20.0	191	52.1	94.4	177	105	6431	45.3	522	67.2	85.3	228	22.1
ZMD-8	Argillaceous limestone	0.211	0.957	0.410	4.28	23.5	6.78	15.6	13.5	18.3	1885	6.14	53.6	7.11	55.7	1.19	2.71
GT-1	Limestone	0.439	0.910	0.035	1.28	5.53	1.15	7.11	2.78	3.38	178	0.319	0.337	0.086	5.09	0.999	1.86
GT-2	Primary ore (silicified breccia)	12.9	115	1.25	6.45	97.6	14.3	29.8	35.5	15.2	420	27.2	347	46.9	66.3	26.5	10.4
GT-4	Oxidized ore	8.38	114	1.46	1.65	67.3	1.37	11.6	9.69	16.7	203	8.82	139	18.6	24.7	8.29	4.45
GT-5	Silicified carbonaceous shale	61.8	31.5	0.790	3.65	21.9	15.8	27.1	146	9.14	71.5	14.9	137	13.6	39.0	2.00	24.6
GT-6	Coal bed overlain the ore body	197	49.9	1.37	6.95	172	16.8	73.1	29.2	34.5	158	34.4	204	28.7	69.9	9.46	20.2

(Table 4-1. continued)

	Hf	Ta	Th	U	La	Ce	Pr	Nd	Sm	Eu	Gd	Tb	Dy	Ho	Er	Tm	Yb	Lu	ΣREE	$(La/Yb)_N$	δEu
LN-4	3.95	1.27	20.6	3.94	52.5	105	11.5	37.5	6.62	1.20	4.58	0.696	4.32	0.884	2.56	0.389	2.45	0.366	230	14.4	0.67
LN-8	0.025	0.041	0.143	0.707	2.83	2.23	0.524	2.14	0.506	0.112	0.528	0.098	0.569	0.118	0.349	0.041	0.266	0.034	10.3	7.2	0.66
LN-12	5.18	1.39	18.7	4.47	45.6	90.5	9.91	32.8	6.34	1.09	4.93	0.852	5.20	1.09	3.18	0.468	2.92	0.432	205	10.5	0.60
LN-13	5.53	1.25	19.0	4.14	46.4	91.2	10.1	33.3	6.75	1.18	5.12	0.798	4.92	0.951	2.83	0.397	2.59	0.393	207	12.1	0.61
LN-14	4.87	1.20	18.5	4.01	44.7	88.2	9.98	34.3	7.12	1.20	5.60	0.896	5.38	1.06	3.13	0.453	2.93	0.421	205	10.3	0.58
LN-15	7.57	1.68	24.8	8.08	61.6	123	13.9	47.9	10.5	1.89	8.76	1.49	8.81	1.77	5.15	0.722	4.68	0.659	291	8.9	0.61
LN-45	0.026	0.015	0.110	1.04	3.53	1.92	0.556	2.29	0.372	0.089	0.626	0.081	0.683	0.126	0.338	0.05	0.296	0.042	11.0	8.0	0.56
LN-46	3.26	0.547	8.14	1.78	18.6	36.4	3.93	13.8	3.59	0.686	3.77	0.622	3.49	0.664	1.89	0.271	1.67	0.229	89.5	7.5	0.57
ZMD-1	10.1	2.96	12.5	4.65	74.6	152	18.1	64.6	14.3	3.55	12.1	1.76	9.88	1.78	4.90	0.685	3.96	0.585	363	12.7	0.83
ZMD-3	10.6	3.02	11.2	2.12	62.1	141	16.1	57.3	12.7	3.05	10.1	1.60	8.74	1.63	4.35	0.538	3.65	0.511	323	11.5	0.82
ZMD-4	13.0	4.02	13.3	2.59	86.1	183	22.6	83.8	20.3	5.16	15.1	1.77	8.75	1.69	4.95	0.673	4.29	0.638	439	13.5	0.90
ZMD-8	1.38	0.495	1.62	0.819	8.99	19.1	2.26	8.07	1.74	0.424	1.39	0.217	1.20	0.240	0.590	0.073	0.535	0.079	44.9	11.3	0.83
GT-1	0.025	0.018	0.039	1.21	0.155	0.308	0.029	0.143	0.101	0.009	0.039	0.006	0.024	0.006	0.016	0.003	0.010	0.003	0.852	10.5	0.44
GT-2	8.36	2.50	7.93	9.90	42.6	86.4	10.2	36.8	7.78	1.51	5.65	0.752	4.87	0.980	2.87	0.378	2.54	0.364	204	11.3	0.70
GT-4	3.22	1.09	3.01	8.51	17.30	33.9	4.05	13.6	2.95	0.481	1.80	0.254	1.47	0.289	0.851	0.135	0.760	0.100	77.9	15.3	0.64
GT-5	2.80	0.822	4.16	5.45	35.8	63.3	7.28	24.3	3.77	0.883	2.25	0.375	2.33	0.486	1.51	0.244	1.63	0.263	144	14.8	0.93
GT-6	4.84	2.18	6.69	65.5	39.7	73.5	8.28	27.9	4.36	0.515	3.59	0.645	4.60	0.958	2.86	0.416	2.62	0.386	170	10.2	0.40

trace element patterns that make it possible to investigate trace element variations due to alteration.

A common practice in the analysis of element loss or gain is to compare it with an "immobile" element. An inherent problem in the use of "immobile" elements had been the difficulty in finding a convincing way to establish their degree of immobility. If a trace element is immobile during alteration, the addition of other materials (as in silicification) dilutes its concentration, whereas extraction of material (as by dissolution) concentrates it. So, a pair of such immobile element plots on a common regression line through original point, that is, the elements retain constant inter-element ratios. As the mineral constituents of the sedimentary rocks vary, the trace element contents in the unaltered rocks are heterogeneous. However, since the sedimentary rocks were deposited from the same source material for a certain sedimentary formation, especially within certain lithological horizon, the trace components are homogenous enough for geochemical comparison. Total immobile element contents, however, can probably only be approximated (e.g., MacLean and Kranidiotis, 1987). Even Al_2O_3, the least mobile of the components, may show petrographic, but no chemical evidence of short-range movement.

The correlation coefficients for regression lines that pass through bulk composition and origin can be used to select the most immobile element pair (MacLean and Kranidiotis, 1987). As presented in Table 4-2, the widely accepted immobile high field strength elements like Nb, Ta, Zr, and Hf highly correlate with each other in the Lannigou deposit, and similarly the high correlation exists also in the three deposits under study as a whole (Table 4-3). The correlations are consistent with the similar sedimentary environments and

Table 4-2. Trace elements correlations in the ores and the host rocks from the Lannigou deposit

	Sc	Cr	Co	Ni	Cu	Zn	Sr	Y	Zr	Nb	Mo	Sb	Cs	Ba	La	Ce	Pr	Nd	Sm	Eu	Gd	Tb	Dy	Ho	Er	Tm	Yb	Lu	Hf	Ta	W	Pb	Th	U
Sc	1																																	
Cr	0.99	1																																
Co	0.83	0.88																																
Ni	0.79	0.84	0.93	1																														
Cu	0.84	0.88	0.98	0.95	1																													
Zn	0.77	0.77	0.78	0.91	0.82	1																												
Sr	0.62	0.70	0.91	0.95	0.92	0.75	1																											
Y	0.92	0.93	0.93	0.80	0.89	0.71	0.70	1																										
Zr	0.92	0.94	0.94	0.90	0.93	0.86	0.77	0.96	1																									
Nb	0.92	0.95	0.95	0.96	0.96	0.89	0.86	0.90	0.96	1																								
Mo	0.58	0.64	0.79	0.94	0.85	0.84	0.94	0.56	0.70	0.84	1																							
Sb	-0.22	-0.30	-0.15	-0.15	-0.06	0.02	-0.18	-0.13	-0.08	-0.20	-0.10	1																						
Cs	0.80	0.77	0.54	0.33	0.49	0.25	0.21	0.77	0.63	0.55	0.05	-0.33	1																					
Ba	0.80	0.74	0.35	0.30	0.36	0.38	0.07	0.59	0.54	0.53	0.08	-0.34	0.85	1																				
La	0.99	0.99	0.85	0.77	0.84	0.73	0.62	0.94	0.93	0.91	0.55	-0.26	0.83	0.79	1																			
Ce	0.99	0.99	0.85	0.78	0.84	0.74	0.63	0.95	0.94	0.91	0.55	-0.25	0.82	0.78	1.00	1																		
Pr	0.99	1.00	0.88	0.82	0.87	0.76	0.68	0.95	0.95	0.94	0.60	-0.26	0.79	0.75	1.00	1.00	1																	
Nd	0.98	1.00	0.90	0.85	0.90	0.78	0.72	0.96	0.96	0.95	0.64	-0.25	0.76	0.71	0.99	0.99	1.00	1																
Sm	0.96	0.98	0.94	0.89	0.94	0.80	0.78	0.97	0.98	0.97	0.69	-0.18	0.70	0.61	0.97	0.97	0.98	0.99	1															
Eu	0.90	0.93	0.96	0.97	0.98	0.87	0.89	0.91	0.96	0.99	0.85	-0.15	0.53	0.47	0.89	0.90	0.92	0.94	0.97	1														
Gd	0.92	0.94	0.97	0.91	0.97	0.82	0.82	0.97	0.99	0.97	0.73	-0.09	0.63	0.50	0.93	0.93	0.95	0.96	0.99	0.98	1													
Tb	0.91	0.93	0.96	0.86	0.94	0.77	0.77	0.99	0.98	0.93	0.65	-0.08	0.69	0.52	0.93	0.93	0.94	0.96	0.98	0.95	0.99	1												
Dy	0.92	0.94	0.95	0.84	0.92	0.75	0.74	1.00	0.98	0.92	0.62	-0.11	0.73	0.56	0.94	0.95	0.95	0.96	0.98	0.93	0.99	1.00	1											
Ho	0.92	0.94	0.92	0.78	0.88	0.70	0.68	1.00	0.96	0.89	0.54	-0.13	0.78	0.60	0.95	0.95	0.95	0.96	0.97	0.90	0.96	0.99	0.99	1										
Er	0.92	0.93	0.90	0.75	0.86	0.67	0.65	1.00	0.95	0.87	0.50	-0.14	0.80	0.62	0.95	0.95	0.95	0.95	0.96	0.88	0.95	0.98	0.99	1.00	1									
Tm	0.93	0.93	0.88	0.74	0.84	0.67	0.62	0.99	0.94	0.87	0.48	-0.14	0.83	0.65	0.95	0.96	0.95	0.95	0.96	0.87	0.94	0.97	0.98	1.00	1.00	1								
Yb	0.91	0.91	0.85	0.68	0.80	0.61	0.56	0.98	0.92	0.82	0.40	-0.15	0.86	0.67	0.94	0.94	0.93	0.93	0.93	0.82	0.91	0.95	0.97	0.99	0.99	1.00	1							
Lu	0.93	0.93	0.85	0.69	0.80	0.64	0.57	0.98	0.93	0.84	0.42	-0.17	0.86	0.69	0.96	0.96	0.95	0.94	0.94	0.83	0.92	0.95	0.97	0.99	0.99	1.00	1.00	1						
Hf	0.94	0.95	0.94	0.87	0.92	0.84	0.74	0.98	1.00	0.95	0.66	-0.10	0.67	0.58	0.95	0.95	0.96	0.97	0.99	0.95	0.98	0.99	0.99	0.97	0.97	0.96	0.94	0.95	1					
Ta	0.96	0.98	0.93	0.93	0.94	0.87	0.80	0.93	0.97	0.99	0.76	-0.21	0.64	0.62	0.95	0.96	0.97	0.98	0.98	0.98	0.97	0.95	0.95	0.93	0.91	0.91	0.87	0.89	0.97	1				
W	0.76	0.81	0.95	0.97	0.98	0.84	0.94	0.84	0.90	0.93	0.89	-0.02	0.35	0.23	0.76	0.77	0.80	0.84	0.90	0.96	0.94	0.90	0.88	0.83	0.80	0.78	0.73	0.73	0.88	0.90	1			
Pb	0.81	0.77	0.59	0.41	0.53	0.44	0.22	0.85	0.76	0.60	0.08	-0.11	0.88	0.76	0.85	0.84	0.81	0.79	0.77	0.59	0.72	0.78	0.81	0.86	0.88	0.89	0.92	0.93	0.80	0.69	0.45	1		
Th	0.79	0.74	0.47	0.29	0.42	0.32	0.10	0.75	0.65	0.52	-0.03	-0.20	0.94	0.87	0.82	0.82	0.78	0.74	0.69	0.49	0.61	0.67	0.71	0.77	0.80	0.82	0.85	0.86	0.69	0.62	0.31	0.97	1	
U	0.80	0.80	0.73	0.49	0.64	0.37	0.41	0.90	0.77	0.65	0.18	-0.28	0.92	0.66	0.85	0.85	0.83	0.82	0.81	0.66	0.77	0.83	0.86	0.90	0.92	0.92	0.95	0.94	0.81	0.72	0.54	0.92	0.89	1

Table 4-3. Trace elements correlations in the ores and the host rocks of SHDG deposits in Southwest Guizhou Province

	Sc	Cr	Co	Ni	Cu	Zn	Sr	Y	Zr	Nb	Mo	Sb	Cs	Ba	La	Ce	Pr	Nd	Sm	Eu	Gd	Tb	Dy	Ho	Er	Tm	Yb	Lu	Hf	Ta	W	Pb	Th	U
Sc	1																																	
Cr	0.71	1																																
Co	0.81	0.78	1																															
Ni	0.75	0.86	0.89	1																														
Cu	0.48	0.51	0.81	0.64	1																													
Zn	0.87	0.67	0.84	0.84	0.53	1																												
Sr	0.30	0.50	0.61	0.48	0.64	0.39	1																											
Y	0.89	0.86	0.87	0.84	0.54	0.78	0.32	1																										
Zr	0.80	0.85	0.92	0.84	0.70	0.80	0.53	0.89	1																									
Nb	0.68	0.86	0.88	0.82	0.71	0.73	0.60	0.79	0.97	1																								
Mo	-0.14	0.39	0.05	0.32	0.10	-0.07	-0.12	0.15	0.04	0.12	1																							
Sb	-0.05	-0.03	0.01	-0.02	0.06	0.09	0.14	0.03	0.08	0.02	-0.08	1																						
Cs	0.84	0.65	0.67	0.51	0.44	0.56	0.43	0.78	0.66	0.54	-0.22	-0.07	1																					
Ba	0.65	0.31	0.15	0.19	-0.07	0.32	-0.13	0.47	0.22	0.08	-0.17	-0.18	0.69	1																				
La	0.90	0.86	0.88	0.83	0.68	0.77	0.46	0.94	0.91	0.84	0.06	-0.04	0.84	0.53	1																			
Ce	0.91	0.86	0.90	0.83	0.69	0.80	0.49	0.94	0.93	0.86	0.02	-0.03	0.84	0.50	1.00	1																		
Pr	0.90	0.86	0.92	0.84	0.72	0.80	0.54	0.93	0.94	0.88	0.02	-0.02	0.83	0.45	0.99	1.00	1																	
Nd	0.88	0.86	0.93	0.85	0.73	0.81	0.58	0.92	0.95	0.90	0.00	-0.01	0.81	0.40	0.98	0.99	1.00	1																
Sm	0.86	0.83	0.94	0.84	0.74	0.82	0.65	0.88	0.95	0.91	-0.08	0.06	0.79	0.33	0.95	0.96	0.98	0.99	1															
Eu	0.80	0.77	0.95	0.84	0.79	0.82	0.72	0.81	0.93	0.90	-0.12	0.07	0.71	0.21	0.89	0.91	0.93	0.95	0.98	1														
Gd	0.88	0.82	0.95	0.86	0.70	0.85	0.62	0.91	0.95	0.88	-0.08	0.10	0.78	0.33	0.94	0.95	0.97	0.98	0.99	0.97	1													
Tb	0.93	0.81	0.93	0.85	0.63	0.86	0.46	0.96	0.93	0.83	-0.04	0.07	0.80	0.41	0.94	0.96	0.96	0.96	0.95	0.91	0.98	1												
Dy	0.93	0.82	0.90	0.85	0.57	0.83	0.36	0.99	0.91	0.81	0.02	0.04	0.79	0.46	0.95	0.95	0.95	0.94	0.92	0.86	0.95	0.99	1											
Ho	0.92	0.83	0.88	0.82	0.56	0.80	0.36	0.99	0.91	0.80	0.04	0.03	0.82	0.49	0.95	0.95	0.95	0.94	0.91	0.84	0.94	0.98	1.00	1										
Er	0.91	0.84	0.87	0.81	0.56	0.77	0.36	0.99	0.90	0.79	0.06	0.03	0.83	0.50	0.96	0.96	0.95	0.94	0.91	0.83	0.93	0.97	0.99	1.00	1									
Tm	0.90	0.83	0.84	0.80	0.55	0.74	0.34	0.99	0.87	0.76	0.09	0.03	0.84	0.55	0.96	0.95	0.94	0.92	0.89	0.80	0.91	0.96	0.98	0.99	1.00	1								
Yb	0.89	0.82	0.84	0.77	0.56	0.72	0.34	0.98	0.88	0.76	0.08	0.02	0.85	0.54	0.96	0.95	0.94	0.92	0.89	0.80	0.90	0.95	0.97	0.99	1.00	1.00	1							
Lu	0.89	0.83	0.84	0.78	0.58	0.72	0.36	0.98	0.88	0.76	0.09	0.01	0.85	0.55	0.97	0.96	0.94	0.93	0.89	0.81	0.90	0.95	0.97	0.98	0.99	1.00	1.00	1						
Hf	0.82	0.86	0.92	0.83	0.68	0.81	0.54	0.90	1.00	0.96	0.01	0.08	0.70	0.27	0.93	0.95	0.96	0.96	0.97	0.93	0.96	0.94	0.93	0.93	0.92	0.89	0.90	0.90	1					
Ta	0.75	0.93	0.90	0.87	0.69	0.76	0.58	0.86	0.97	0.99	0.18	0.01	0.62	0.19	0.89	0.91	0.92	0.94	0.93	0.90	0.91	0.88	0.86	0.86	0.85	0.83	0.83	0.83	0.97	1				
W	0.33	0.58	0.63	0.50	0.68	0.39	0.95	0.39	0.60	0.66	-0.07	0.20	0.48	-0.10	0.54	0.56	0.60	0.64	0.71	0.75	0.66	0.50	0.41	0.42	0.43	0.42	0.42	0.43	0.61	0.65	1			
Pb	0.56	0.54	0.47	0.46	0.47	0.33	0.14	0.69	0.48	0.34	0.26	0.04	0.67	0.61	0.72	0.67	0.65	0.61	0.54	0.42	0.53	0.59	0.63	0.67	0.71	0.77	0.77	0.79	0.50	0.44	0.24	1		
Th	0.78	0.51	0.43	0.35	0.16	0.46	0.05	0.73	0.51	0.33	-0.16	-0.03	0.87	0.88	0.74	0.72	0.68	0.64	0.58	0.45	0.59	0.67	0.72	0.75	0.77	0.80	0.81	0.81	0.56	0.43	0.13	0.78	1	
U	-0.10	0.48	0.02	0.29	-0.06	-0.08	-0.12	0.21	0.07	0.14	0.95	-0.07	-0.11	-0.09	0.08	0.05	0.04	0.02	-0.06	-0.13	-0.05	-0.01	0.07	0.10	0.12	0.14	0.14	0.14	0.06	0.22	-0.06	0.24	-0.04	1

source areas of the host rocks, and the similar alterations these rocks have undergone. Within the analytical errors, the above element pairs plot on a regression line through the origin (Fig.4-1). This means that these elements are geochemically coherent and immobile during the ore-forming alterations. The rare earth elements and Y are less well correlated with the above high field strength elements and the regression lines shift from the origin (Table 4-2, 4-3, and Figure 4-1), which indicate that the rare earth elements and Y are mobile during the low temperature ore forming alterations. The intra-element correlation among the rare earth elements is significant (generally larger than 0.8) which is consistent with their coherent geochemical behaviors. However, the intra-element correlation between the LREE and HREE are more significant (larger than 0.97), which indicates the fractionation between the two groups. W, Th, U, Mo, Sr, Ba and Zn are much mobile relative to HFSE during hydrothermal alterations as shown by the poor correlation with the latter.

The PAAS (Post-Archean Average Shale), NASC- (North American Shale Composite) and chondrite-normalized REE patterns of the ores and host rocks are shown in Fig.4-2, Fig.4-3, and Fig. 4-4, respectively. Samples from the deposits show similar REE patterns, except for the limestone. The limestone samples from the Lannigou deposit, which are quite pure and extremely low in REE, show negative Ce anomalies (0.33~0.44). Most notably, although the REE patterns of the ores (the most altered host rocks) and the unaltered sedimentary host rocks are quite similar, minor but consistent differences are still discernable. The $(La/Yb)_N$ ratios of the ores (7.5 ~ 8.9) are apparently lower than those of the unaltered host rocks (10.5 ~ 14.4), indicating a fractionation of REE during the

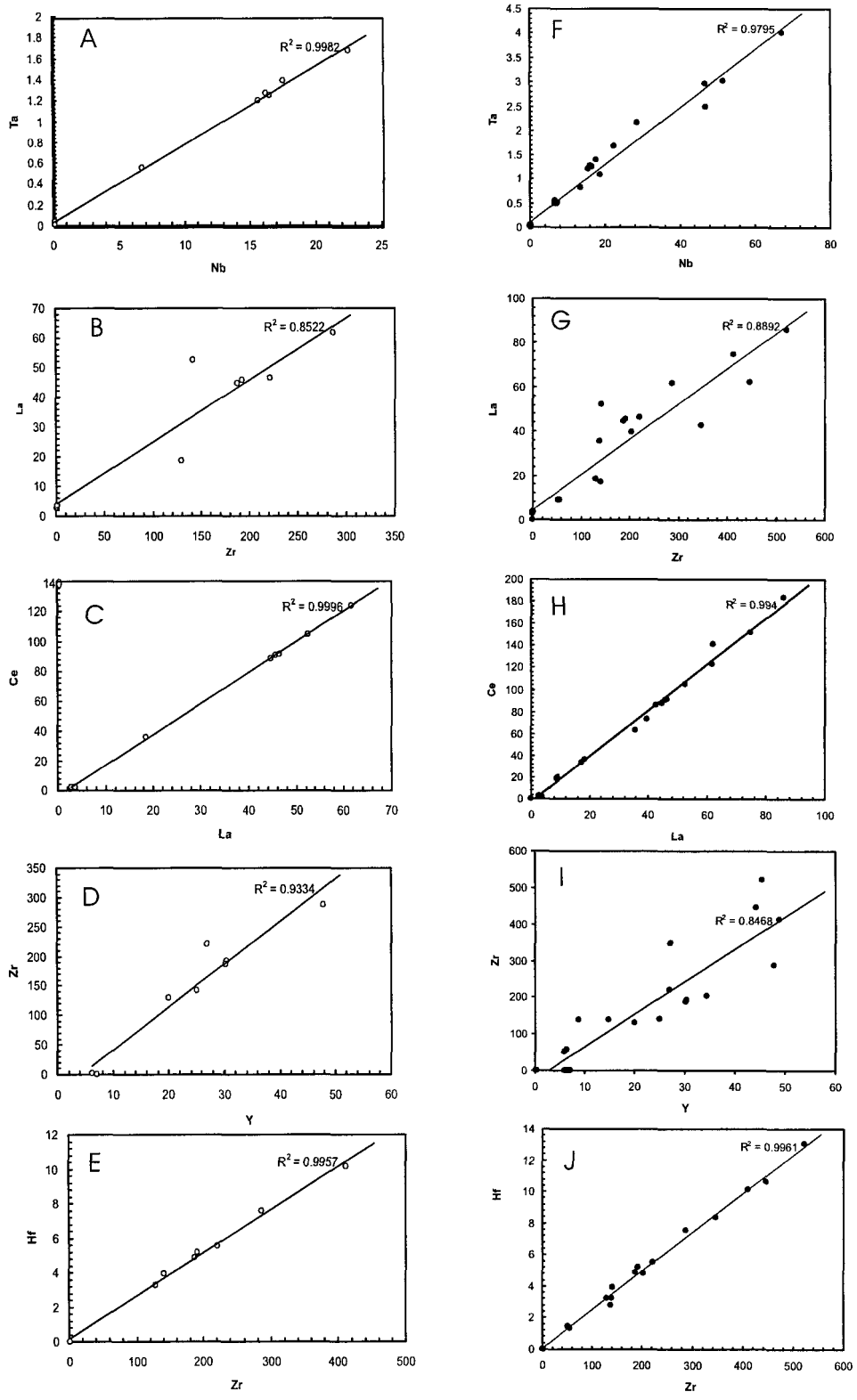

Fig.4-1. Trace element pair plots of the samples from the SHDG deposits of southwest Guizhou.
A, B, C, D, E -samples from the Lannigou deposit;
F, G, H, I, J- samples from the three investigated SHDG deposits of southwest Guizhou

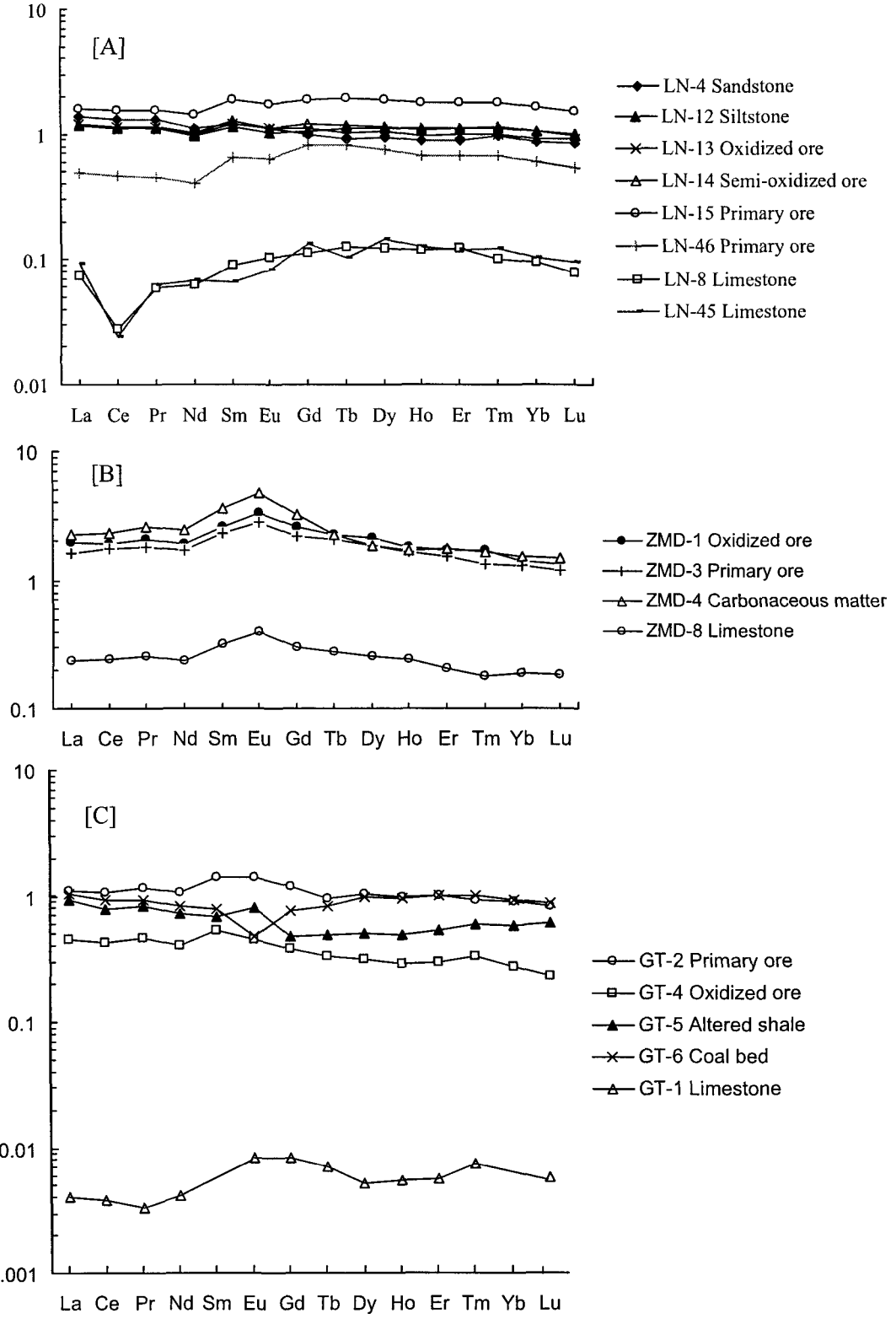

Fig.4-2. PAAS normalized REE patterns of the ores and host rocks of the SHDG deposits in southwest Guizhou.
[A] The Lannigou deposit; [B] The Zimudang deposit; [C] The Getang deposit
Post-Archean Average Shale (PAAS) from McLennan (1989)

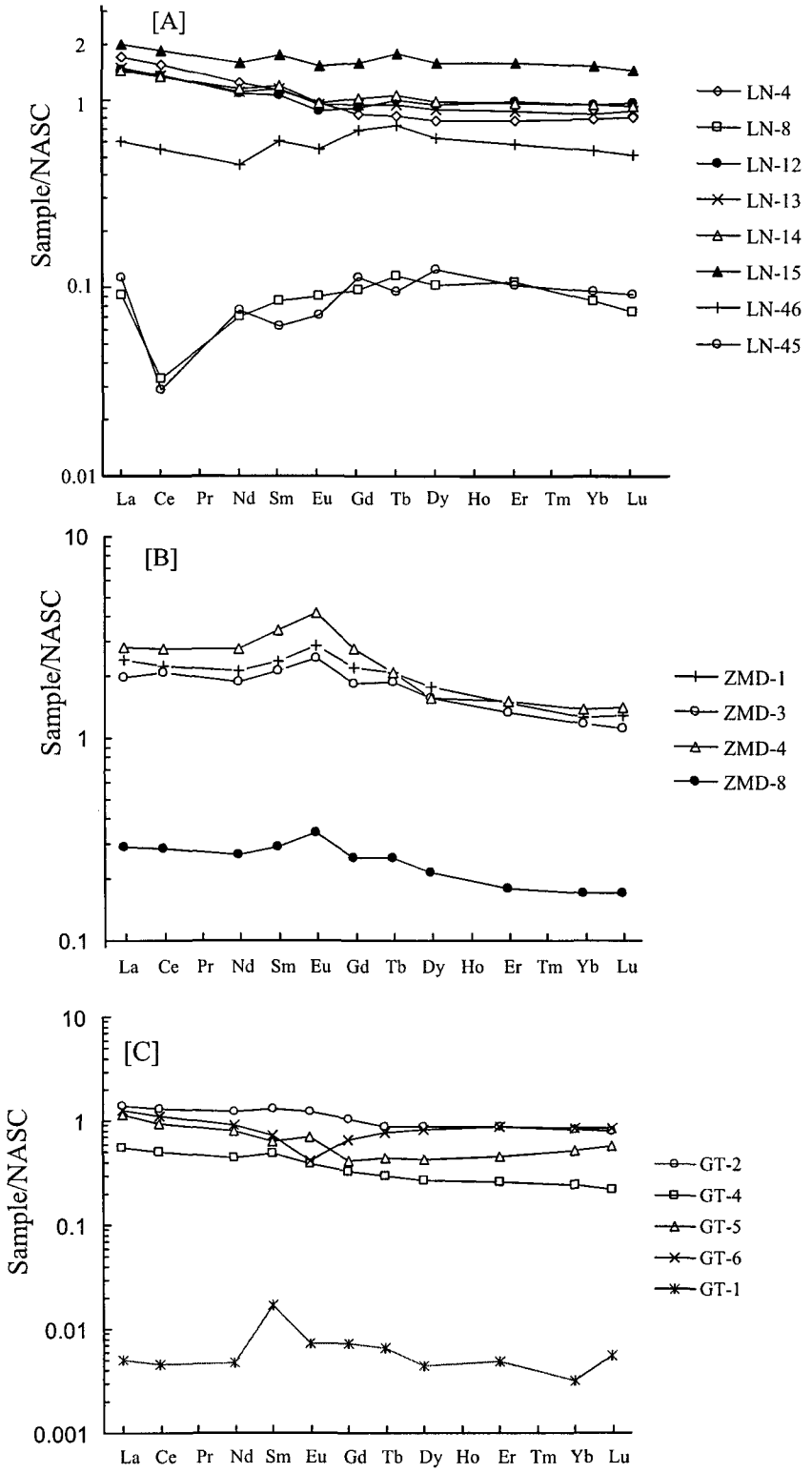

Fig.4-3. NASC normalized REE patterns of ores and host rocks from the SHDG deposits in southwest Guizhou.
[A] The Lannigou deposit; [B] The Zimudang deposit; [C] The Getang deposit
(NASC- North American shale composite by Gromet et al., 1984, recommended)

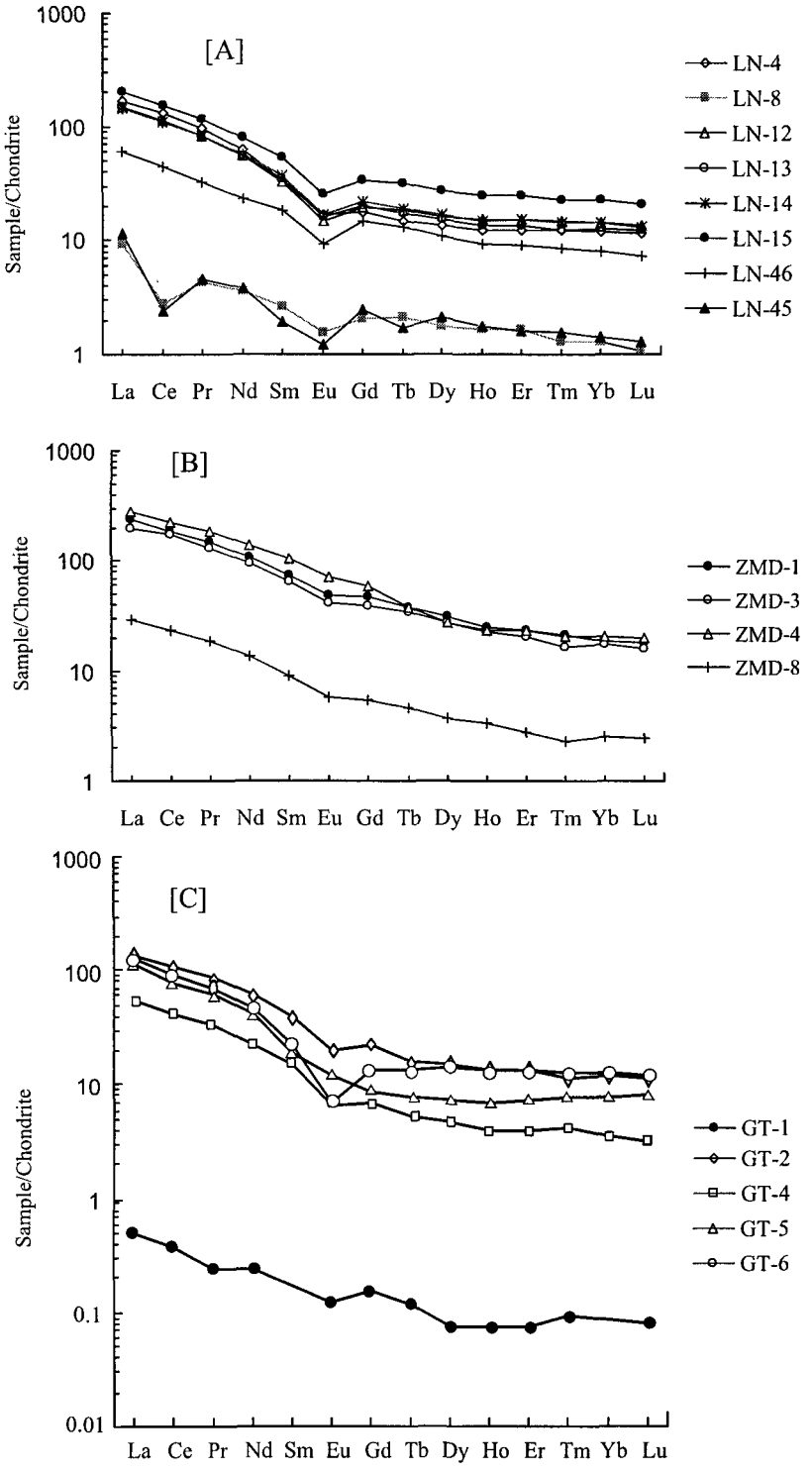

Fig.4-4. The chondrite normalized REE patterns of the ore and host rocks of the SHDG deposits from southwest Guizhou.
[A] The Lannigou deposit; [B] The Zimudang deposit; [C] The Getang deposit
Values for chondrite normalization from Boynton(1984)

hydrothermal alteration. Relative to PAAS (post-Archean average shale), the samples from the Zimudang deposit are relatively enriched in LREE and Eu, which most probably results from the contribution of the volcanic components in the rocks. The oxidized ores are relatively depleted in HREE because of preferential leaching by meteoric water.

An isocon approach (Grant, 1986) on the two samples from the Lannigou deposit, the LN-12 and LN-15 representing the unaltered siltstone and altered siltstone (the primary ore) sampling form the Xiuman Formation turbidite, shows that the REE and Y are mobile during the alteration (Figure 4-5). The slope of the best-fit isocon yield $(M^o/M^A)=1.49$, which is equivalent to $(M^A/ M^o) = 0.67$ and thus a mass decrease of 33%, where the M^A and M^o represent the mass of the altered and original rock respectively. The isocon diagram (Figure 4-5) shows that the LREE are depleted while the HREE are enriched during the alteration. Accordingly, the mass gain and loss estimation for the REE also indicates a differentiation among the rare earth elements. The estimated gain and loss shows mass loss for most of the LREE, for example, La (-9.5%), Ce (-8.6%), Pr (-5.9%), and Nd (-2.3%); and the mass gain for the HREE, for example, Gd (19%), Tb (17%), Dy (14%), Ho (9.2%), Er (8.5%), Tm (3.4%), Yb (7.4%), and Lu (2.2%).

The mobility or the apparent gains and losses of REE during alteration is controlled largely by: (1) the REE concentrations of the reacting minerals; (2) the relative stability of these reacting minerals toward the fluid; (3) the availability of sites within the secondary minerals for accommodating REE released during alterations; (4) the REE concentrations in the incoming fluid; and (5) the ability of the fluid phase to remove REE from the system. So, a correlation is expected to exist between the precursor rock, alteration assemblage,

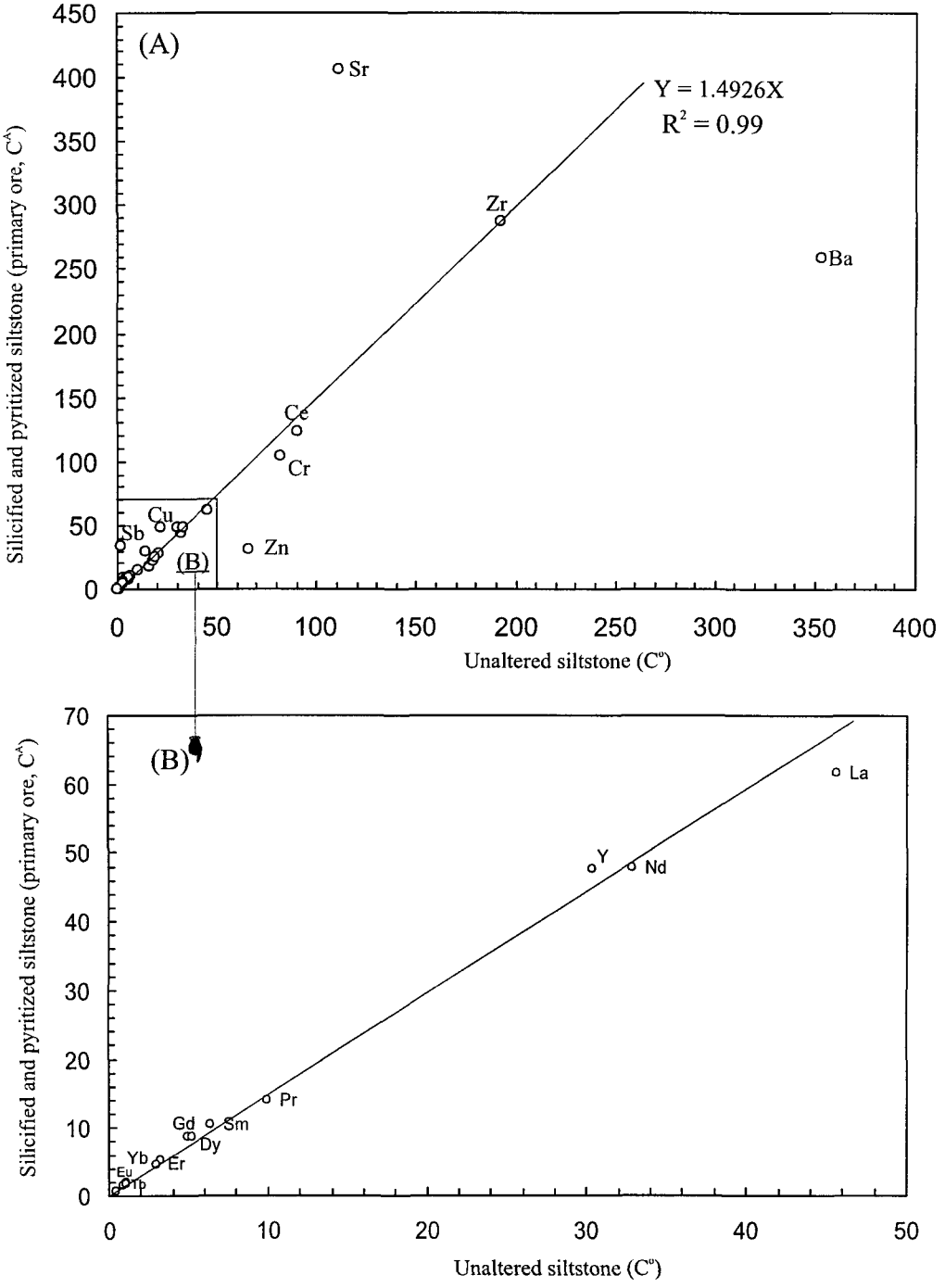

Figure 4 -5. An isocon diagram showing trace elements mobility for samples from the Lannigou deposit.

physico-chemical properties of the ore-forming solution, and fluid/rock ratios. The mineral assemblage of the related alteration includes the formation of clay minerals (illite, kaolinite, and minor smectite), quartz, calcite and sulfides. Silicification may result in dilution, but not in REE fractionation. The minerals that host most of the REE in the sedimentary rocks, such as zircon, apatite, etc., are unlikely to be affected by the alterations associated with SHDG mineralization. Thus no significant changes can be expected, however, minor, but, discernable gain/loss and differentiations of REE do exist. The REE differentiation during the hydrothermal alteration is consistent with the features of the solution phase that are mild acidic to neutral and Cl^- dominated, and the decrease of F^- content in the fluid during argillization resulted in HREE deposition (Wood, 1990; Haas et al., 1995).

The fluid phase is an important factor controlling the mobility of the REE during the alteration. Fluid inclusions, trapped in the ore and gangue minerals, are fossil fluids of ancient mineralized hydrothermal systems. Fluid inclusion data, including temperature, pressure, salinity, density, composition, etc., can be used as a constraint to help understand the hydrothermal alteration and ore forming processes, even though the fluid inclusions in SHDG deposits are small and many are difficult to relate directly to gold mineralization. Our observations on samples from the Lannigou deposit are consistent with results of earlier studies (Yang and Dong, 1994; Zhu and He, 1996; Zhang and Zhang, 1999). The primary fluid inclusions in the SHDG deposits in southwestern Guizhou are usually (5 ~ 15 μm) in size, with relatively large gas to liquid ratios (>10%), and have spherical, rhombic, oval shapes commonly distributed in zones along the growth plane of quartz. On the other hand, the secondary inclusions are rather small (3 ~ 5 μm), with low gas to liquid ratios

(<10%), and show irregular quartz fractures. The primary inclusions can be categorized into four types, liquid inclusion, CO_2 bearing inclusion, gas inclusion and organic bearing inclusion, on the basis of existing phases under ambient conditions (the organic inclusion will be discussed late in chapter 5). The over 90% of the inclusions fluid contain fluid phase only, and only small portion of fluid inclusion contains gas phase within which the gas-liquid ratio generally ranges from 5% to 15%. CO_2 bearing inclusions are rare, and can be distinguished under cooling, generally 3 ~ 8 μm in diameter. The homogenization temperature of CO_2 is commonly in the range of 3.4 to 11.2 °C. Gas inclusions are commonly round, 5 ~ 8 μm in diameter, gas/liquid ratio ranges from 65 to 80%. No daughter mineral bearing inclusion or pure CO_2 phase inclusion has yet been observed. Homogenization temperatures of the fluid inclusions in quartz and calcites from the SHDG deposits in southwestern Guizhou range from 80°C to 320°C (Yang and Dong, 1994; Zhang and Zhang, 1999; Zhu and He, 1996; He et al., 1993; Liu et al., 1999), and the temperature and salinity of the fluid decreases from early to late stage of mineralization (Table 4-4).

The fluid salinities vary in the range of 4%~14% NaCl equivalent. The major components of the fluid inclusions in the Lannigou, Getang and Zimudang deposits determined through decrepitating and gas/liquid chromatography show that the ions are dominated by (Ca^{2+}), Na^+, K^+, while the anions are mainly SO_4^{2-}, Cl^- and F^-. The calculated pH and Eh vary in the range of 5.56~7.33, and -0.41 ~ -0.54 respectively, which suggests that the deposits were formed under rather reducing, neutral to weakly acidic environment (Zhang and Zhang, 1999). In the Lannigou deposit, analysis of static argon in the fluid inclusions shows that the fluid had a low Ar^{40}/Ar^{36} ratio (298~328) and was dominated by

atmospheric argon (Ar^{36} ranging from 90~99%). This may indicate that the hydrothermal solution was mainly derived from meteoric water (Yang and Dong, 1994). The fluid inclusion investigation suggests that the hydrothermal solution was a low salinity, near neutral and rather reducing meteoric water, and it is also supported by the REE data.

Table 4-4. Homogenization temperature, salinity, density and pressure of fluid inclusion from the Lannigou and Getang deposit*

Deposit	Ore stage	Homogenization temperature (°C)	Salinity ($_{wt}$%)	Density (g/cm^3)	Pressure ($\times 10^5$Pa)
Lannigou	Early	251	10.19	0.88	640
	Main	205	7.05	0.89	400
	Late	143	4.67	0.93	120
Getang	Early	220	10.5	0.91	780
	Main	190	5.43	0.90	200
	Late	155	2.78	0.92	90

* All the data listed in the table are average values. From Liu et al., 1999.

The REE composition of hydrothermal fluid can be estimated through fluid inclusion investigation. However, since fluid inclusions are usually very small in size, and REE concentrations are quite low, analysis is difficult, and research is rather rare (Ghazi et al., 1993; Banks et al, 1994). A tentative investigation was carried out by Su et al. (1998a) using the decrepitating-leaching method. Fluid inclusions under 500°C were extracted from quartz vein samples which had been pre-treated with acid washing and heated at 150°C for 10 minutes to remove the water absorbed on the fresh quartz surface. The REE contents of fluid inclusions were analyzed by ICP-MS method, and analysis of inclusions by gas

chromatography during decrepitation was used to estimate the portion of fluid phase in the quartz, and thus to estimate the true concentrations of the REE in the entrapped fluids. Two samples of quartz (N9296 and N9278) associated with the main ore stage, the other (N9419) associated with the later stage were analyzed. The LREE in the solutions are much higher than their detection limits with good reproducibility. However, the HREE are close to the detection limits with rather low reproducibility (Table 4-5). However, their estimation of absolute concentrations is suspicious, because of the heterogeneous distribution of the inclusions in quartz, and since volume varies with the cube of the radius, a few relatively large inclusions may carry far more fluid than thousands of smaller ones. This simple fact alone makes it almost impossible to obtain truly duplicate samples for a test of analytical accuracy. So, it is more reasonable to assume that the patterns of the inclusions are more reliable than their contents; the absolute values are probably meaningless here. The weak negative Ce anomalies and positive or mild negative Eu anomalies (Fig. 4-6) show that the ore-forming environment was rather reducing (Bau, 1991). Relative to the ores and the host rocks, the fluids are HREE depleted, possibly because of the F^- concentration of the fluid solution decreased during the argillization that resulted in the precipitation of the HREE.

4.1.2. Platinum group elements

The platinum group elements consist of Ru (Ruthenium), Rh (Rhodium), Pd (Palladium), Os (Osmium), Ir (Iridium) and Pt (Platinum). The PGE can be divided on the basis of their associations into two sub-groups—the Ir-group (IPGE—Os, Ir, and Ru) and

Table 4-5. REE contents of the fluid inclusions from the Lannigou deposit (ppm)

	Sample	La	Ce	Pr	Nd	Sm	Eu	Gd	Tb	Dy
N9419	Late stage quartz	27.63	37.24	4.96	12.47	0.52	0.16	0.56	0.064	0.25
N9296	Ore stage quartz	4.32	4.96	0.69	1.97	0.27	0.10	0.21	0.019	0.11
N9278	Ore stage quartz	4.14	5.47	0.76	2.14	0.28	0.054	0.18	0.008	0.04
	Sample	Ho	Er	Tm	Yb	Lu	ΣREE	$(La/Yb)_N$	δCe	δEu
N9419	Late stage quartz	0.06	0.15	0.018	0.075	0.014	84.171	248	0.71	0.90
N9296	Ore stage quartz	0.022	0.069	0.009	0.003	0.012	12.764	971	0.63	1.24
N9278	Ore stage quartz	0.007	0.018	0.004	0.008	0.007	13.116	349	0.69	0.69

From Su et al., 1998a.

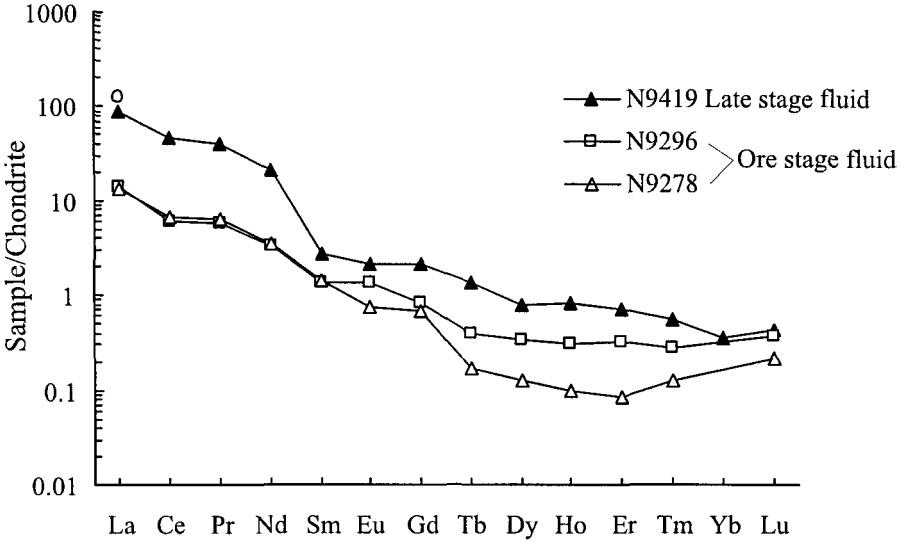

Fig. 4-6. Chondrite normalized REE patterns of hydrothermal fluid in fluid inclusions of the Lannigou deposit (data from Su et al., 1998a).
Values for chondrite normalization from Boynton(1984)

the Pd-group (PPGE—Rh, Pt and Pd). Gold is associated with the latter group. The two groups of PGE behave differently, the Ir-group elements tend to be compatible during mantle melting, whereas, the Pd-group elements are incompatible. PGE were considered to be refractory inert elements and were often used as fingerprints in investigating magmatic system evolution (Campbell et al., 1983). In the last two decades, more and more studies have shown that PGE are mobile during alteration even at low temperature in supergene environments (Barnes et al., 1985; Crocket and Kabir, 1987; Bowles et al., 1994; Hannigan and Peucker-Ehrenbrink, 1998; Hattori and Hulbert, 1998). Platinum group element minerals, such as platinum-gold, as separate mineral inclusions in pyrite or arsenopyrite, have been observed in the SHDG deposits in southwestern Guizhou Province (Wang et al., 1994b) and elsewhere (Mazdab et al., 1999). In some SHDG deposits the PGE concentrations are so high that their economic value is significant for comprehensive utilization[1)].

The significance of PGE is that PGE and Au can be transported together in aqueous solutions as bisulfides, chlorides, and organic complexes (McKibben and Williams, 1990; Pan and Wood, 1994; Wood, 1996), and have been observed associated with each other in many geological circumstances. Since basalt and alkali ultramafic rocks near gold mineralization areas have been considered to be the main source of Au (Liu et al., 1999), the PGE contents of these rocks were analyzed to investigate their possible contribution to gold mineralization in the area.

[1)] Hou et al.1991. Metallogeny and expectation of the fine grain disseminated gold deposits in southeastern Yunnan Province. Tianjin geological academy of the ministry of metallurgic industry, Tianjin. Unpublished report: I-88-92-01-4-1.

4.1.2.1. Analytical Procedure

The PGE were analyzed in the ICP-MS laboratory of the Institute of Geochemistry, Chinese Academy of Sciences using the Finnigan MAT ICP-MS following Qi and Hu's (1999) method. Samples, 5g each, were decomposed with Na_2O_2 in corundum crucibles. After dissolving the fused disc with aqua regia and evaporating the solution to dryness to remove SiO_2, the PGE were concentrated by the Te co-precipitation method. The contents of Ru, Pd, Ir and Pt were determined by ID-ICP-MS. The Rh and Au contents were determined by internal standard-ICP-MS. The detection limits for these elements are less than 0.3ng/g. The precisions of the PGE analyses are about 1.5% to 6.5% RSD.

4.1.2.2. Results and discussion

The analyzed PGE and gold concentrations in the ores and rocks are listed in Table 4-6. The PGE contents of the ores are usually higher than those of the unaltered host rocks as shown by the chondrite normalized PGE patterns (Fig.4-7, 8, 9). Moreover, pyrite hosts much higher concentrations of the PGE than the bulk ores, especially Pd and Pt. In the Lannigou deposit, the Pd/Ir and Pt/Ir ratios of the pyrite vary in the range of 4.90 ~ 175 and 4.1 ~827 respectively, which are higher than those of 1.88 ~8.61 and 1.14 ~7.43 for the altered host rock and the primary ores. And the latter are still higher than those of 0.73 ~ 1.05 and 0.64 ~ 0.86 for the unaltered host rocks. However, Pd/Ir ratios of most pyrite samples are less than 20 except for a few pyrite samples with exceptional high Pd/Ir ratios. The relative enrichment of Pt and Pd in the altered rocks and the ores, which are themselves altered sedimentary rocks, suggest that the reacting hydrothermal solution was enriched in

Table 4-6. The PGE and Au concentrations of the ores, host rocks, pyrite in the ores, basalt and alkali ultramafic rocks in southwest Guizhou (ppb)

	Sample	Ir	Ru	Rh	Pd	Pt	Au	Pd/Ir	Pt/Ir	Pd/Pt
LN-4	Argillaceous sandstone	2	0.26	0.16	1.46	1.71	16.22	0.73	0.86	0.85
LN-8	Bioclastic limestone	1.13	0.13	0.1	1.62	2.21	20.44	1.43	1.96	0.74
LN-12	Argillaceous siltstone	2.23	0.5	0.11	2.34	1.42	22.74	1.05	0.64	1.64
LN-13	Oxidized ore	0.81	0.19	0.14	1.85	2.32	1053	2.28	2.86	0.80
LN-14	Semi-oxidized ore	1.82	0.23	0.2	1.46	5.81	3308	0.80	3.19	0.25
LN-15	Primary ore	0.83	0.26	0.16	2.51	2.58	17070	3.02	3.11	0.97
LN-45	Reef limestone	0.76	0.25	0.11	0.81	5.72	75.37	1.07	7.53	0.14
ZMD-1	Oxidized ore	0.64	0.49	0.22	0.99	4.59	846.7	1.55	7.17	0.22
ZMD-3	Primary ore	0.63	0.48	0.24	4.12	6.42	80.44	6.54	10.2	0.64
ZMD-4	Carbonaceous bed in primary ore	0.72	0.42	0.29	8.03	7.9	16856	11.2	11.0	1.02
ZMD-8	Argillaceous limestone	0.75	0.29	0.12	3.67	2.54	75.8	4.89	3.39	1.45
GT-1	Limestone	0.5	0.26	0.12	1.04	4.34	30.33	2.08	8.68	0.24
GT-2	Primary ore	0.8	0.23	0.12	0.64	4.08	150.6	0.80	5.10	0.16
GT-4	Oxidized ore	0.52	0.17	0.1	2.47	3.47	146.4	4.75	6.67	0.71
GT-6	Coal bed overlain the ore body	0.54	0.54	0.84	1.56	3.55	8.840	2.89	6.57	0.44
LN2002*	Primary ore	0.423	0.705	0.201	3.64	3.142	2275	8.61	7.43	1.16
N9279*	Silicified sandstone	0.888	2.11	0.325	4.365	6.065	142.7	4.92	6.83	0.72
N9244*	Silicified sandstone	0.49	0.376	0.144	2.238	1.261	568.6	4.57	2.57	1.79
LN9808*	Primary ore	0.636	0.512	0.122	2.959	5.192	3432	4.65	8.16	0.57
LN1032*	Pyritized silicified sandstone	0.821	0.297	0.264	4.006	1.67	51.34	4.88	2.03	2.38
N9297*	Pyritized silicified sandstone	0.562	0.395	0.188	1.057	1.004	510.8	1.88	1.79	1.05
N9298*	Pyritized silicified sandstone	0.732	0.359	0.746	2.427	3.175	33.91	3.32	4.34	0.76
N9296*	Pyritized silicified sandstone	0.544	0.71	0.161	2.563	2.418	135.4	4.71	4.44	1.06
N9281*	Pyritized silicified sandstone	0.84	0.679	0.138	2.698	0.954	119.6	3.21	1.14	2.86
N9209*	Pyritized silicified sandstone	0.625	4.446	0.237	2.5	11.16	56.54	4.00	17.9	0.22
LN9809*	Pyritized silicified sandstone	0.794	0.165	0.103	3.39	2.171	2697	4.27	2.73	1.56
N9244*	Pyrite in ore	0.82	0.438		35.05	7.88	18.67	42.7	9.61	4.55
N9224*	Pyrite in ore	1.494	1.637		7.314	8.084	1.77	4.90	5.41	0.90
N9229*	Pyrite in ore	1.267	1.473		15.194	58.99	3.59	12.0	46.6	0.26
N9247*	Pyrite in ore	0.23	0.84		51.58	2.763	0.900	224	12.0	20.00
N9248*	Pyrite in ore	1.229	0.894		27.715	1016	1.440	22.6	827	0.03
N9250*	Pyrite in ore	1.237	1.943		3.59	8.655	3.730	2.90	7.00	0.41
N9273*	Pyrite in ore	0.451	0.332		78.7	20.184	208.0	175	44.8	3.85
N9274*	Pyrite in ore	0.99	1.563		5.737	4.061	4.910	5.79	4.10	1.41
CJ-05*	Alkali-ultramafic rock	1.027	1.003	0.331	41.165	4.907	25.04	40.1	4.78	8.33
CJ-01*	Alkali-ultramafic rock	1.122	1.216	0.295	46.288	5.078	10.26	41.3	4.53	9.09
Ermeishan**	Basalt	0.0698	0.49	0.25	5.48	7.71	1.620	78.5	110	0.71

* Su et al., 1999, unpublished; ** average value of the 14 Ermeishan basalt samples (Zhang and Li, 1998)

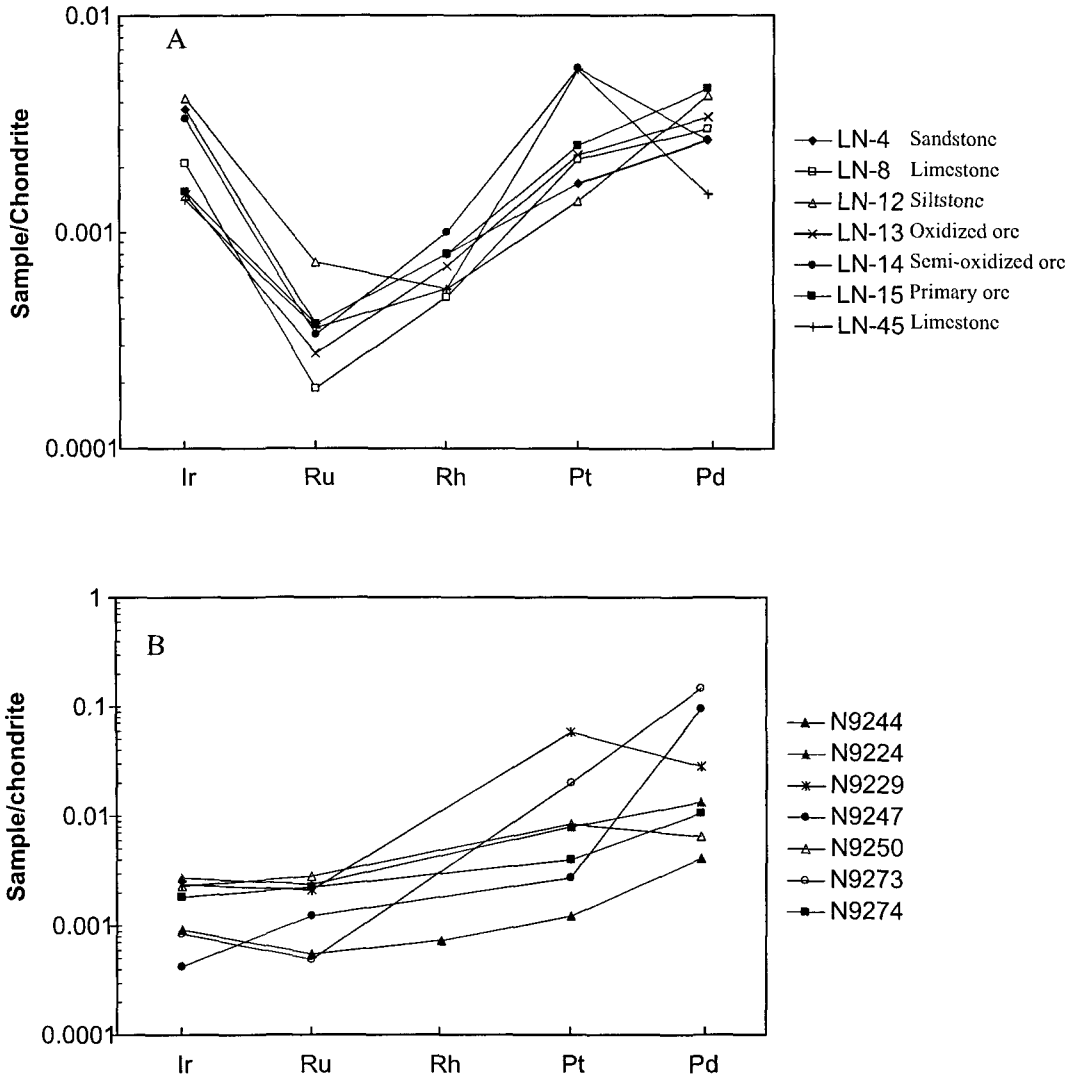

Fig.4-7. Chondrite normalized PGE profiles for the host rocks, ores, and pyrite from the Lannigou deposit.
[A] The host rocks and the ores; [B] The pyrite in the ores
The values for chondrite normalization are from Naldrett and Duke (1980).

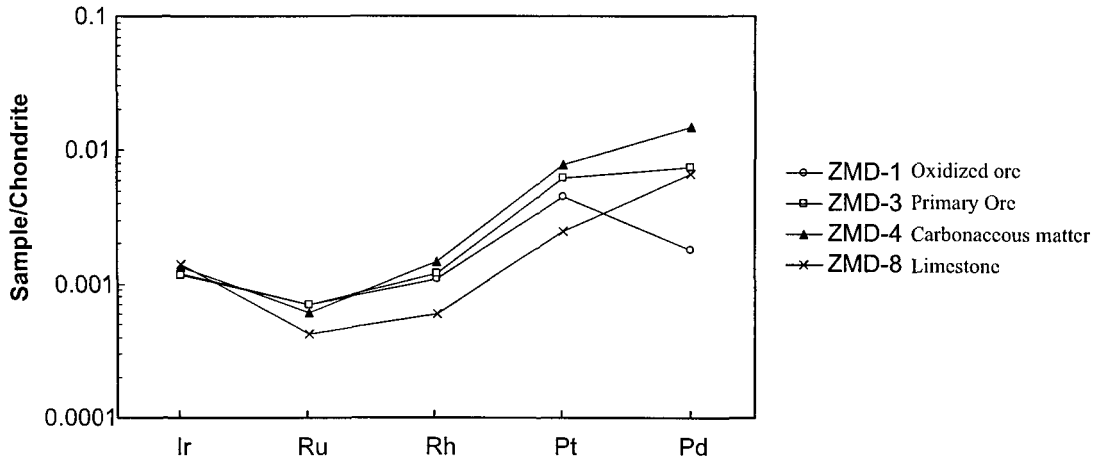

Fig.4-8. Chondrite normalized PGE plot of ores and host rock from the Zimudang deposit

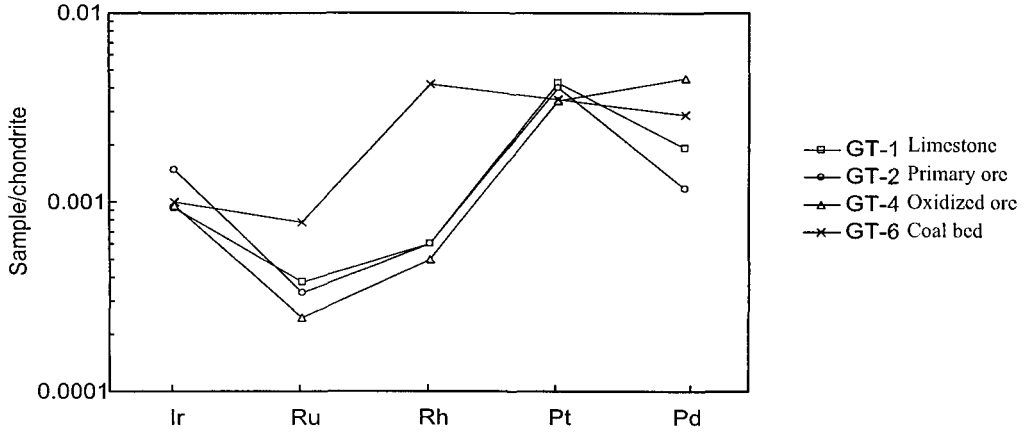

Fig.4-9 Chondrite normalized PGE profiles for ores and host rocks from the Getang deposit.

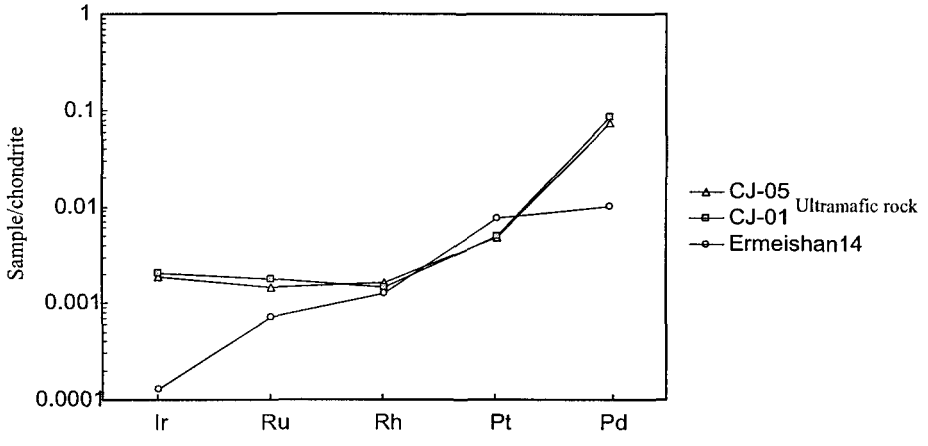

Fig.4-10. Chondrite normalized PGE profiles for the Emeishan basalt and alkali ultra-mafic rock. (C1 chondrite normalizing values for PGE compiled by Naldrett and Duke (1980))

Pt and Pd. The enrichment of Pd and Pt is consistent with their higher solubilities and mobility in hydrothermal systems (Barnes et al., 1985; Mountain and Wood, 1988; Gammons et al., 1992; Farrow and Watkinson, 1997). It is interesting to note here that the carbonaceous bed of the Zimudang deposit is significantly enriched in Pd. The Pd/Ir ratio of the carbonaceous bed is 11.2, it is apparently higher than that of the primary ore (Pd/Ir = 6.54). The PGE distribution pattern of the carbonaceous matter may reflect that of the hydrothermal solution, as PGE are easily removed by a process of catalytic oxidation and desulfidation of organic matter during fluid-organic interaction (Kucha and Przybylowicz, 1999).

As shown in Figure 4-10, the basaltic rocks and the alkali ultramafic rocks outside of the mining area are significantly Pt and Pd enriched. The Pd/Ir ratio of the alkali ultramafic rocks is quite high (40.1~41.3) and the average Pd/Ir ratio of the Emeishan basaltic rocks is as high as 78.5, so if they are the main source of the SHDG deposits, the Pd/Ir ratios of the ores and the pyrite would be higher. It is clear that the PGE patterns of the ores and pyrites are similar to those of the host rocks, rather than those of the basaltic and ultramafic rocks. Therefore, the hypothesis that the ore-forming material (including gold and fluid solutions) was mainly derived from the ultramafic rocks (Liu et al., 1999) is unlikely to be true from the point view of PGE characteristics; moreover, ultramafic rocks are small sized dikes and veins that are far away from gold mineralization.

4.2. Stable isotopes

Stable isotopic geochemical data is important for the understanding of the hydrothermal ore-forming process. The available S, C, O and Pb data on the SHDG deposits in southwest Guizhou is examined and reinterpreted within the framework of this study.

4.2.1. Sulfur isotope

Sulfur isotopic compositions of sulfides of different ore forming stages from the Lannigou, Getang and Zimudang deposits in southwestern Guizhou have been analyzed (Table 4-7, 8, 9). The sulfur isotopic composition ($\delta^{34}S$) of the sulfide in the deposits varies in range of –29.2 ~ +17.9 per mil. The $\delta^{34}S$ values of pyrite in the ores from the Getang and the Zimudang deposit are higher than that of the diagenetic pyrite in the host rocks, but the $\delta^{34}S$ values of sulfides from the Lannigou deposit are quite similar. All the reported sulfur isotopic compositions available are based on pyrite mixtures of different origins because of technique difficulty (Guo, 1988; Li et al., 1989b; Yang and Dong, 1994). It is difficult, and sometimes even impossible to separate the pyrites of different stages, it seems reasonable to assume that the pyrites from the main ore-forming stage usually have high $\delta^{34}S$ values. Yang and Dong (1994) reported that hydrothermal pyrites in the Lannigou deposit, with small diagenetic cores show higher $\delta^{34}S$ values, as in samples LZ1023, LZ1026, and LZ1036 (Table 4-7).

More than one source of sulfur might have contributed to the sulfide in the ores, but the host rocks may have played an important role including the dissolution of the sulfides (mainly pyrite) and sulfates (such as gypsum). Part of the sulfur might also be derived from the decomposition of the organic matter in the host rocks. Sulfur derived from dissolution of diagenetic sulfides will maintain the $\delta^{34}S$ value or even diminish it due to the fact that lighter isotope is more active in chemical reactions, while $\delta^{34}S$ value of the organic sulfur is typically negative. This higher $\delta^{34}S$ values in ore stage pyrites (the hydrothermal pyrite overgrowth) are most likely derived from non-bacterial reduction of sulfate leached from the sedimentary host rocks (Toland, 1960; Kiyosu and Krouse, 1990; Ohmoto and Goldhaber, 1997). The organic matter commonly associated with the SHDG deposits especially the ancient oil traps, supply the necessary light hydrocarbons for the thermal reductions. As shown in Table 4-7, 8, 9, the sulfur isotopic compositions vary from deposit to deposit, so the mechanism may vary. For instance, dissolution of diagenetic pyrite in the host rocks may be dominant in the Lannigou deposit, while in the Zimudang deposit where $\delta^{34}S$ of the hydrothermal pyrite are higher than that of the diagenetic pyrite; sulfate reduction may have had a role to play.

Wide range sulfur isotope values (-31 to +20‰) have been reported from SHDG deposits in the U.S.A. (Arehart, 1996). Similar large range sulfur isotopic composition was reported in a granite-related copper deposit in Quebec, and a sedimentary origin was inferred (Williams-Jones and Samson, 1989). Recent studies have recognized that many sulfides in SHDG deposits are chemically and isotopically zoned as well (Arehart et al.,

Table 4-7. Sulfur isotopic composition of the sulfides from the Lannigou deposit

Stage	Sample No.	Mineral	Morphology	$\delta^{34}S$	Range	Mean Value
Hydrothermal stage	LZ1005	Pyrite	Framboidal, spherical	12.1	9.1-12.6	11.34
	LZ1016	Pyrite	Spherical	11.5		
	LZ1026	Pyrite	Spherical, framboidal	12.6		
	LZ1029	Pyrite	pyritohedral, framboidal	12.4		
	LZ1033	Pyrite	pyritohedral, spherical	9.1		
	LZ1033B	Pyrite	Cubic -100 — -200mesh	11.3		
	LZ1036	Pyrite	Octahedron	12.5		
	LZ1030	Pyrite	pyritohedral, spherical	12.4		
	LZ1039	Pyrite	Cubic, spherical	10.5		
	LZ1043	Pyrite	Octahedron	12.3		
	LZ1047	Pyrite	Octahedron, pyritohedral	11.3		
	LZ1048	Pyrite	pyritohedral, spherical	11.4		
	LZ1061	Pyrite	Cubic, pyritohedral	10.1		
	LZ1061B	Pyrite	Cubic, pyritohedral	10.5		
	LZ1063	Pyrite	Cubic, octahedron	10.1		
	LZ1023	Pyrite	Irregular, spherical assemblage	13.6	13.0-13.6	13.3
	LZ1031	Pyrite	Irregular, spherical assemblage	13.0		
	L92-1	Realgar		11.8	11.4-11.9	11.67
	L92-2	Realgar		11.7		
	L92-4	Realgar		11.6		
	L92-24	Realgar		11.4		
	LZ1037	Realgar		11.9		
	LZ1039	Realgar		11.4		
	LZ1063	Realgar		11.9		
	L92-11	Cinnabar		10.2	10.2-11.9	10.73
	L92-23	Cinnabar		11.3		
	LZ1063	Cinnabar		10.9		
	N9253	Cinnabar		10.5		
	L92-8	Stibnite	Acicular assemblage	9.4	8.4-9.8	9.17
	LZ1037	Stibnite		9.3		
	N9259	Stibnite		9.3		
Diagenesis Stage	N9292	Pyrite	Irregular, fragmental -30 — -60mesh	13.2	11.7-13.2	12.45
	LZ1068	Pyrite	-60 — -80mesh	11.7		

From Yang and Dong, 1994.

Table 4-8 Sulfur isotopic compositions of sulfides from the Zimudang gold deposit

Period		Sample no.	Mineral	$\delta^{34}S$ (‰)	Average (‰)
Diagenetic period		Z-2	Pyrite	+0.31	+1.14
		Z-4	Pyrite	+1.97	
Hydrothermal stage	Pyrite-marcasite-arsenopyrite	Z-7	Pyrite	+3.85	+2.88
		Z-19	Pyrite	+1.64	
		Z-8	Marcasite	+4.26	
		Z-9	Marcasite	+2.46	
		Z-10	Marcasite	+2.50	
		Z-11	Marcasite	+2.83	
	Gold-(arsenian) pyrite-marcasite	Z-5	Pyrite	+2.18	+1.71
		Z-6	Pyrite	+0.16	
		Z-12	Pyrite	+2.60	
		Z-13-1	Pyrite	+2.02	
		Z-14-1	Pyrite	+1.58	
		Z-1	Marcasite	+12.66	+15.28
		Z-3	Marcasite	+17.91	
	Realgar-quartz-calcite	Z-15	Realgar	+2.42	+2.47
		Z-16	Realgar	+2.27	
		Z-17	Realgar	2.73	

From Guo, 1988.

Table 4-9. Sulfur isotopic composition of sulfides from the Getang deposits

Period	Stage	Sample no.	Mineral	$\delta^{34}S$ (per mil)
Hydrothermal period	Pyrite-quartz	G-2	Pyrite	-1.3
		G-14	Pyrite	+2
		G-73	Pyrite	+5
	Stibnite-pyrite-fluorite	G-32	Pyrite	-18.3
		G-64	Pyrite	-23.9
		G-147	Pyrite	-29.2
		G-142	Pyrite	-9.6
	Realgar - gypsum - calcite	G-22	Stibnite	-3.6
		G-3	Stibnite	-1.9
Diagenetic period	Diagenesis	G-1	Pyrite	-18.1
		G-5	Pyrite	-21.2
		G-151	Pyrite	-13.3
		G-154	Pyrite	-13.9

From Li et al., 1989b.

1993a; McKibben and Eldridge, 1995). SHRIMP (super high resolution ion microprobe) analysis of pyrite revealed that the sulfur isotope zoning correlates with Au and As zoning. The pyrite with the highest $\delta^{34}S$ values also contains the highest concentrations of gold. $\delta^{34}S$ values of gold-bearing pyrite overgrowths are around +20‰. In contrast to the gold-rich zones, pre-ore pyrite has $\delta^{34}S$ values ranging from -5 to +10‰ (Arehart et al., 1993a). Such small-scale isotopic measurements have not been made for the deposits in southwestern Guizhou Province.

4.2.2. Pb isotopes

Pb isotopic compositions of ore minerals can be useful in constraining Pb sources in many types of hydrothermal systems. Pb isotopes could serve as a proxy for constraining the source of associated metals, including Au. Since Pb can be transported and deposited as part of the same hydrothermal fluid, the usually low Pb concentration of hydrothermal fluids allow the Pb isotopic compositions to be easily changed through water-rock interactions, hence the source(s) of mineral deposits can be traced (Powell et al., 1991).

The available Pb isotope data of the three SHDG deposits, the Lannigou, Getang and Zimudang deposit, in southwest Guizhou shows that the Pb isotopic compositions of sulfides vary in a wide range (Table 4-10, Fig. 4-11). The host rock (siltstone from the Lannigou deposit) and two pyrite samples separated from unaltered sedimentary host rocks of SHDG deposits from the neighboring region have higher radiogenic isotopic ratios than most of the sulfides in the ores as shown in the $^{206}Pb/^{204}Pb$ ~ $^{207}Pb/^{204}Pb$ diagram. The lower Pb isotopic ratios of the sulfides in the ores maybe caused by input of Pb from lower

Table 4-10. Lead isotopic compositions of SHDG deposits

Deposit	Sample	$^{206}Pb/^{204}Pb$	$^{207}Pb/^{204}Pb$	$^{208}Pb/^{204}Pb$	$^{207}Pb/^{206}Pb$	$^{208}Pb/^{206}Pb$
Getang	Stibnite*	19.65	15.66	37.76	0.7969	1.922
	Orpiment*	19.20	15.69	38.03	0.8172	1.981
	Pyrite	18.601	15.695	38.632	0.8438	2.077
	Stibnite	18.881	15.992	39.144	0.8470	2.073
	Stibnite	18.541	15.327	37.479	0.8267	2.021
	Pyrite	17.715	15.285	37.342	0.8628	2.108
	Stibnite	18.824	15.594	38.580	0.8284	2.050
Lannigou	Siltstone	18.720	15.793	39.217	0.8436	2.095
	Stibnite	17.852	15.478	37.720	0.8670	2.113
Zimudang	Cinnabar	18.578	15.502	38.737	0.8344	2.085
	Quartz	18.389	15.641	38.360	0.8506	2.086
Gedang	Pyrite**	18.465	15.747	38.945	0.8528	2.109
Gaolong	Pyrite**	18.68	15.76	39.02	0.8436	2.089

From: * cited from Li et al., 1989b; ** The two pyrite samples separated from host rocks of the SHDG deposits in the neighboring region, Ni et al., 1997; the remainder from Zhu et al., 1998a;

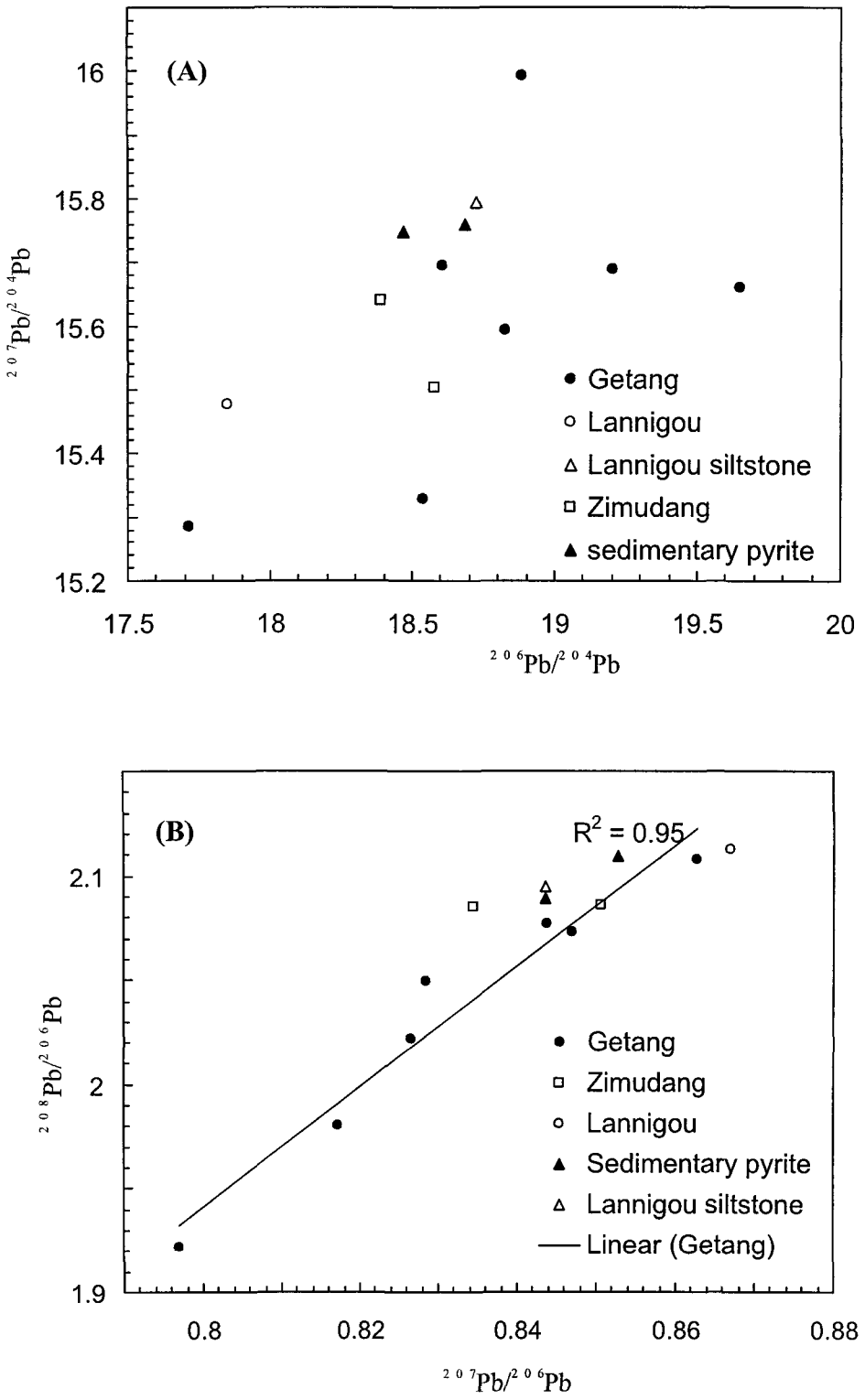

Fig. 4-11. Pb isotope distribution of the sulfides in the ores and host rocks and unaltered host rock of SHDG deposits in southwest Guizhou
(data from Li et al., 1989b; Ni et al., 1997; and Zhu et al., 1998a)
(A) $^{206}Pb/^{204}Pb \sim ^{207}Pb/^{204}Pb$ diagram; (B) $^{207}Pb/^{206}Pb \sim ^{208}Pb/^{206}Pb$ diagram

crustal rocks or igneous rocks, which was brought in by hydrothermal solutions. The wide variation of Pb isotopic compositions of sulfides from the Getang deposit, and the linear distribution of the radiogenic isotope ratios as showing in $^{208}Pb/^{206}Pb \sim ^{207}Pb/^{206}Pb$ diagram (Fig.4-11), indicate that multiple sources may have contributed to the mineralization. A mixed source for the SHDG deposit in southwestern Guizhou Province is perhaps a reasonable hypothesis. However, detailed investigation of the Pb isotopic composition of the ores, upper crustal rocks (including host rocks), magmatic rocks in the area, especially the in situ analysis of the Pb isotopic signatures of the auriferous zoning pyrite, would be necessary to contribute to the understanding of the ore forming processes.

The mixing of Pb sources in hydrothermal systems is a common phenomenon (Heyl et al., 1974; Richards et al., 1991; Foley and Ayuso, 1994; Kesler et al., 1994a). Pb isotopic heterogeneous and overall linear trends have been recognized not only in individual deposits but also in single crystals in the Mississippi Valley deposits (e.g., Cannon et al., 1963; Heyl et al., 1974; Hart et al., 1981; Vaasjoki and Gulson, 1986). The SHDG and MVT deposits are similar in that they are both hosted mainly in sedimentary rocks, and, in many cases, igneous rocks (contemporaneous with ore deposition) are absent. Data from SHDG deposits of Nevada suggests that the Pb in the ores was derived from the mixing of isotopically distinct sources (Arehart et al., 1993a; Arehart, 1996; Groff and others, 1997; Ilchik and Barton, 1997; Tosdal et al., 1998). Similar Pb isotopic variation may exist in the SHDG deposits in the study area; however, because of the paucity of Pb data it is not possible to make this kind of universal correlation.

4.2.3. Carbon, oxygen and hydrogen isotope

It is difficult to document fluid sources owing to the fine-grained nature of the ore and the to alteration assemblages, and to a typical lack of fluid inclusions of sufficient size related to mineralization. The reported O and C isotope data of fluid calculated from that of minerals for the SHDG deposits in southwest Guizhou varies considerably within and between individual deposits. The scattered isotopic composition of the fluids probably derived from evolved meteoric water that equilibrated with the host rocks or through the mixing of meteoric water with formation water or brine (Fig. 4-12). This is supported by the low degree of the metamorphism in the host rocks of the region, as shown by the vitrinite reflectance which is usually less than 3.0 corresponding to anchimetamorphism (Rantitsch, 1995), and the absence of magmatic activity in the vicinity.

Isotopic data from carbonate minerals may provide some insights into the sources of fluid components and water-rock interaction. The $\delta^{18}O$ and $\delta^{13}C$ compositions of calcites from SHDG deposits in the region show that they shift towards the carbonate on the $\delta^{18}O$ vs. $\delta^{13}C$ diagram (Fig.4-13). This indicates that decalcification and decarboxylation of the carbonate and organic matter may have contributed to fluid evolution. Wide variations of hydrogen and oxygen isotopic composition are also present in the SHDG deposits from the U.S.A. (O'Neil and Bailey, 1979; Holland et al., 1988; Ilchik, 1990; Cline and Hofstra, 2000). The C, H, and O isotopic compositions of the SHDG deposits suggest that the ore forming fluid was mainly recycled meteoric water that reacted and equilibrated with the host rocks.

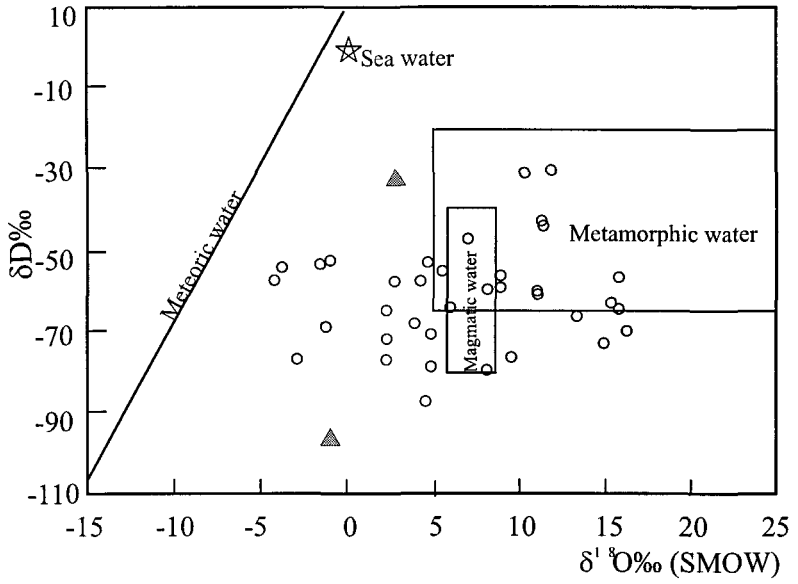

Fig. 4-12. δD‰~δ^{18}O‰ diagram of the ore-forming fluids in the study area (After Liu et al., 1998, ▲ Getang data from Zhu et al., 1998a)

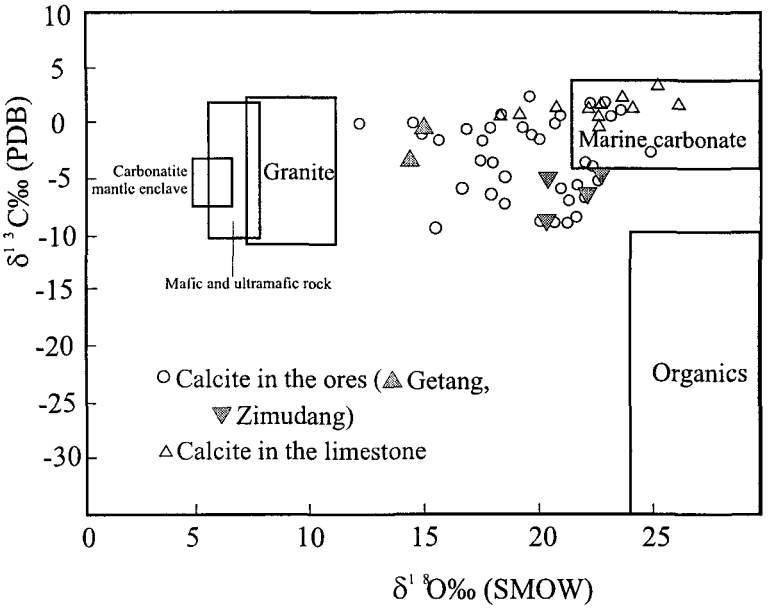

Fig.4-13. δ^{13}C‰ ~δ^{18}O‰ diagram of the calcite in the ores and limestones of the study area. (After Liu et al., 1998; data Getang and Zimudang from Guo, 1988; Li et al., 1989b)

4.3. Age of the mineralization

The dating of the SHDG deposits is difficult because of the paucity of alteration mineral veins clearly related to gold mineralization and the lack of suitable minerals for radiometric dating. However, it is known that Yanshanian orogeny was an important tectonic movement in south China, active from 190 to 65 Ma, and marked by a compressive phase that was followed by an extensional phase. Most of the gold deposits in southwest Guizhou Province are hosted by anticlines and reverse faults that were formed during the compressive phase of this time period; therefore, gold mineralization probably took place during the late extension stage (Casaceli and Gemuts, 1985).

Some studies have proposed that the SHDG deposits in southwest Guizhou were formed around 80~105 Ma. Fission track analysis of quartz samples taken from pyrite-quartz veinlets of the Lannigou and the Beidi deposits dated at 82~83Ma and 85~91Ma respectively for the two deposits (Zhang and Yang, 1992). Su et al. (1998b) dated the Lannigou deposit at 105.6Ma based on Rb-Sr isochron dating of fluid inclusions in quartz. Finally, even though the dates above are not consistent, both correlate with the extensional phase of the Yanshanian movement.

In brief, evidence suggests that mineralization probably took place during the later stages of Yanshanian orogeny around 80~105 Ma.

5

ORGANIC GEOCHEMISTRY OF THE SHDG DEPOSITS

The term "organic matter" or "carbonaceous material" refers to material composed of organic molecules in monomeric or polymeric forms derived from the organic part of organisms. Organic carbon compounds are ubiquitous, abundant components of the oceans, lakes, and sedimentary rocks. Directly or indirectly, they fuel all biogeochemical processes (Summons, 1993). The physiochemical transformation of organic matter, as a common constituent during the geological history of sedimentary basins, is controlled by the same major factors which determine the compositional variation of the inorganic solid phases and of the interstitial water of the sediments, e.g., biological activity at an early stage, then temperature and pressure during diagenesis and metamorphism (Tissot and Welte, 1984). The conversion of organic matter to petroleum products by burial and/or hydrothermal activity is an easy process, occurring in nature in many types of geological environments (Simoneit, 1990).

The association of organic matter in various forms (e.g., petroleum, gas, and coal) with a wide variety of ore deposits types, and its possible role in mineralization has long been an interesting and controversial subject in geology and geochemistry. The origin of sedimentary organic matter coupled with the ability of living organisms to concentrate

metals had first led researchers to emphasize biological accumulation processes. Next, the assessment of the sorptive and ligand properties of humic and marine substances led researchers to stress metal sequestration mechanisms. Finally the recognition of the limited cation-exchange ability of organic substrates, and of the competition of major and trace elements for chelating sites, has now lead researchers to examine reduction mechanisms (Disnar and Sureau, 1990). Petrographic, isotopic and fluid inclusion data, often supported by organic geochemical studies, have now produced clear evidence that most "sedimentary" or strata-bound ore deposits are in fact epigenetic, formed with the participation of hydrothermal fluids, and that the organic-rich layers frequently act as reducing and/or hydrodynamic barriers.

The association of organic matter with ore mineralization is common. As indicated by Gize and Manning (1993): "*It should not be surprising that organic matter is associated with metalliferous ore deposits. Carbon is a relatively common element in the Earth's crust, with an average concentration of approximately 200 ppm. It has been estimated that 82% of the total carbon in sedimentary rocks is present as carbonates, the remaining 18% being organic carbon. Given such a relatively large reservoir of organic carbon, it would be more surprising to find geochemical processes which eliminated organic carbon during ore deposition.*" In some cases, the association may be casual, but in others the hydrocarbon-bearing fluids may have influenced ore deposition.

The association of organic matter and metallic mineralization was investigated extensively in the last century. It is well known that many metalliferous ore deposits are associated with organic constituents. Of particular interest is the ubiquitous occurrence of

organic matter in the Mississippi Valley type (MVT) Pb-Zn mineralization, in disseminated sandstone hosted uranium mineralization, and in the sediment hosted disseminated gold (or the Carlin-type) deposits. The roles of organic matter in metal transportation and deposition have been extensively reviewed by Disnar and Sureau (1990), Manning and Gize (1993), Landis and Gize (1997). Yang (1996) and Tu (1996) demonstrated the consistent temporal and spatial distribution of organic-rich strata and strata-bound deposits, and discussed the similarities and differences between oil-gas accumulations and reworked deposits of active elements. They advocated that the differences have traditionally been overemphasized, while the genetic links were almost completely neglected.

In spite of many studies on the reactions and mechanisms that may affect the Au transportation and deposition, it is very difficult to assess the role actually played by organic material in specific ore forming processes. Krauskopt (1955) commented that "*organic matter is often the principal stumbling block to reconstructing the environment of metal deposition*", and today, a half century later, the role of organic matter in ore genesis is still not well documented, especially with regards to hydrothermal processes. The potential contribution of organic matter to SHDG mineralization in southwest Guizhou was the main objective of this study. However, the result and discussion also have some universal applications to the role of organic matter in other hydrothermal ore-forming processes.

5.1. Organic geochemistry of the SHDG deposits in the research area

5.1.1. Organic matter in the host rocks and ores

Organic matter is a common constituent of sedimentary rocks and the conversion of organic matter to petroleum by burial and/or hydrothermal activity is an easy and universal process (Simoneit, 1990). The SHDG deposits, and also many Au, As, Hg, Sb strata-bound deposits, are preferentially located within anticlines and domes. These same fold crests typically contain significant amounts of mature hydrocarbon material. However, it is very difficult to assess the role actually played by organic materials in gold concentration and accumulation. The role of organic matter in ore genesis is still not well documented, especially in hydrothermal processes.

The solid organic material (kerogen) in the ores and host rocks consists of primarily coal ingredients ("macerals") and secondary ingredients ("migrabitumens"). The "macerals" (International Committee for Coal Petrology, 1971) occur in the interstitial portions of the debris, and mainly consists of vitrinite and inertinite. The term "migrabitumen" signifies secondary organic products generated from fossil organic material in rock during diagenesis and catagenesis. The length of the migration route may range from a fraction of a millimeter to several kilometers. The migrabitumens are amorphous; their shape is adapted to the form of the pores they occupy, e.g., interstices, fissures, and cavities in microfossils and diffuse distributions.

In the Lannigou deposit the macerals are the main constituents of the kerogen, within which vitrinite makes up about 60%. The macerals in ore and host rocks were formed in

diagenetic stage as irregular fragments occurring in interstices of minerals or along the bedding plane. The vitrinite can be divided into telinite and collinite, and the latter can be further subdivided into telocollinite and desmocollinite. Telocollinite often occurs as homogenous, regular shapes like lenses (Fig.5-1a, b). Telinite has high reflectance and commonly with discernable fibrous structure (Fig.5-1c, d). Desmocollinite occurs as irregular shaped grains, bends or veins parallel to the beddings of the rocks, and occasionally telocollinite enclaved by desmocollinite can be observed. The inertinite consists mainly of fusinite and semifusinite. The fusinite still retains the structure of the cells that were filled by clay minerals and pyrite, occurring parallel to the bedding of the rocks (Fig.5-1e). The semifusinite is rare, showing fibrous structure of the plant. Migrabitumen, mainly in form of pyrobitumen often occurs as veins along the fractures or as fragments. Pyrobitumen occurs as a film covering the pyrite and also as enclaves inside pyrite. Pyrobitumen veins cut by late stage quartz veins were observed (Fig.5-1f-h). The reflectances of the vitrinites and pyrobitumens in the samples were not determined for this study; however, former work shows that the vitrinite reflectances range from 1.19% to 2.93% with an average value of 2.32%, while the reflectances of the pyrobitumen range from 2.84% to 3.90% with an average value of 3.24% (Zhuang et al., 1997). The reflectances of the pyrobitumens (R_B^o) are always higher than the corresponding vitrinite (R_V^o). The reflectance of the vitrinite corresponds to a maximum paleo-temperature of 210~329°C (Price, 1983). The paleo-geothermal temperatures indicated by the reflectance of vitrinite are similar or a little bit higher than the results of the homogenization temperature of the fluid inclusions in quartz (163~294°C, Zhang and Zhang, 1999). Bi-

reflection is observed in desmocollinite and pyrobitumen; the optical anisotropy reflects some degree of molecular ordering showing that the vitrinite and pyrobitumen all underwent high degree of thermal maturation. In the Getang deposit, the ores occur in the lower part of the Longtan Formation that consists of a few layers of anthracite, so the silicified breccia contains mainly inertinite (Fig.5-1i-k). Telinite and pyrobitumen were also observed in the ores. The vitrinite reflectance in samples from the Getang deposit range from 2.907% to 3.553% (Lin and Yie, 1997, unpublished data), the estimated maximum paleo-temperature ranges from 328°C to 354°C. In the ores and host rocks of the Zimudang deposit, organic matter in the limestone is dominated by pyrobitumen, while vitrinite and inertinite are dominant in the siltstone. The vitrinite reflectance of the Zimudang deposit varies from 1.925% to 2.975% (Lin and Yie, 1997, unpublished data) which corresponds to an estimated maximum paleo-temperature of 274°C to 331°C. The estimated burial temperature from the vitrinite reflectance in the Getang and Zimudang deposit are higher than those of the homogenization temperatures of fluid inclusions (84~179°C and 123~222°C, respectively, Zhang and Zhang, 1999). The higher estimated paleo-geothermal temperature of the vitrinite in the Getang and Zimudang deposit implies that the hydrothermal processes could not have impacted the organic matter in the host rocks. Actually, the hydrothermal impact on the vitrinite reflectance was observed in the Lannigou deposit.

Organic inclusions are common in quartz and calcite veins. They are usually black to yellowish, <5μ in diameters, and account for about 5% of the total inclusions. The

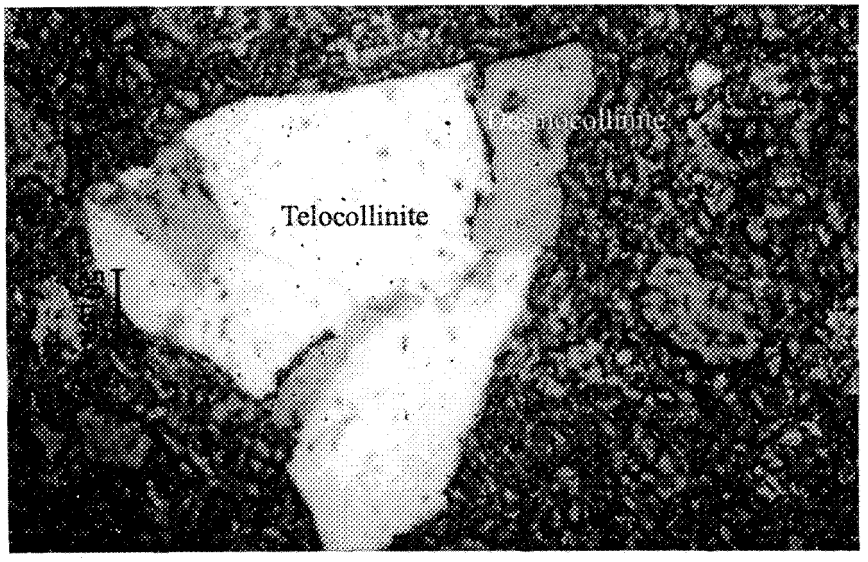

Fig. 5-1a Vitrinite in siltstone from the Lannigou deposit.

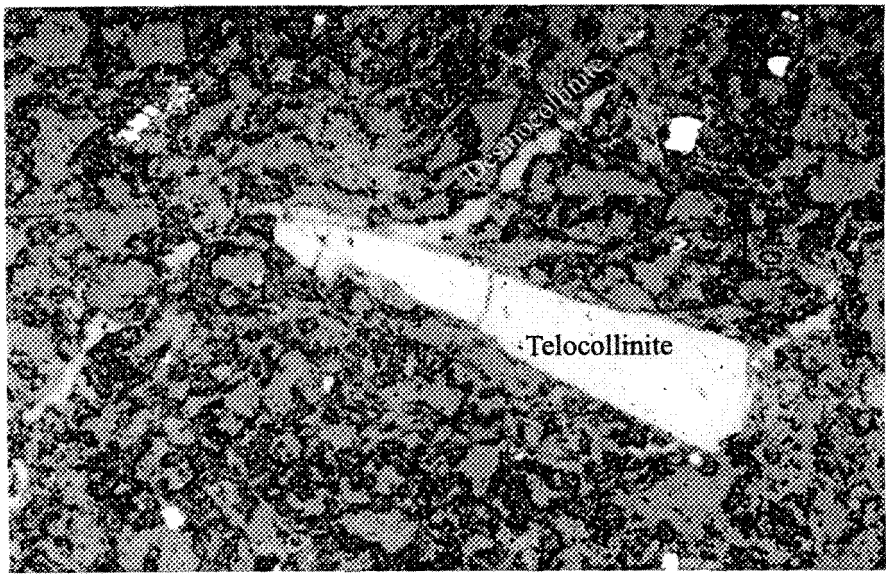

Fig.5-1b. Vitrinite in siltstone from the Lannigou deposit
Desmocollinite generally occurs along the bedding plane.

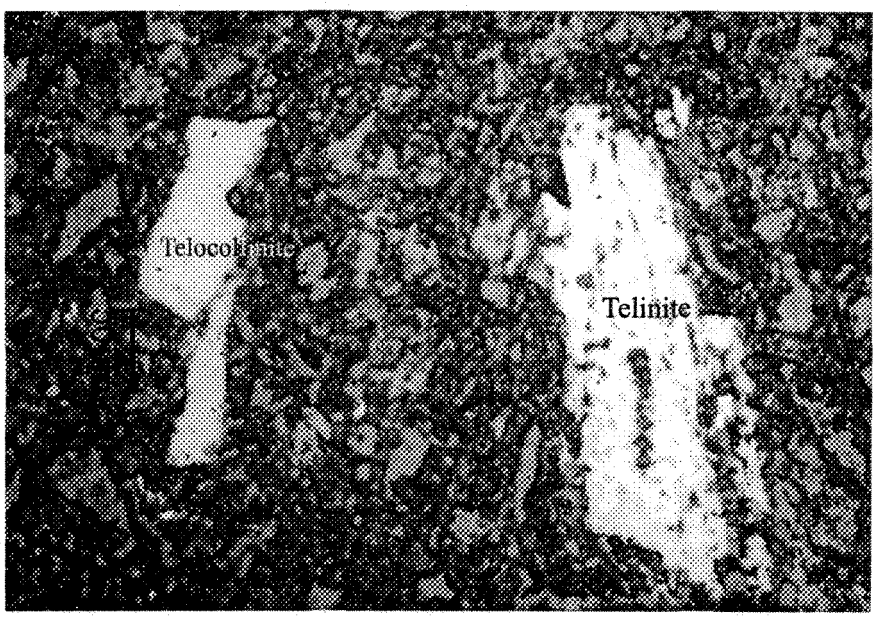

Fig.5-1c. Telinite and telocollinite in the siltstone of the Lannigou deposit.

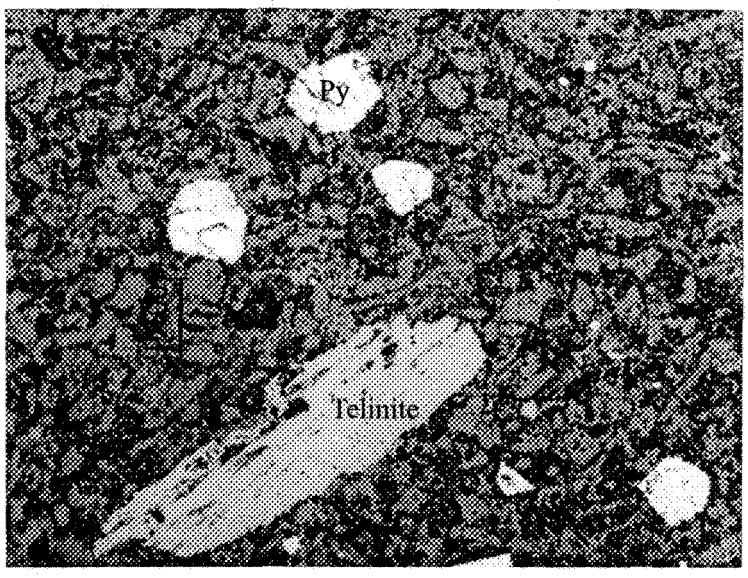

Fig.5-1d. Telinite in pyritized and silicified siltstone.

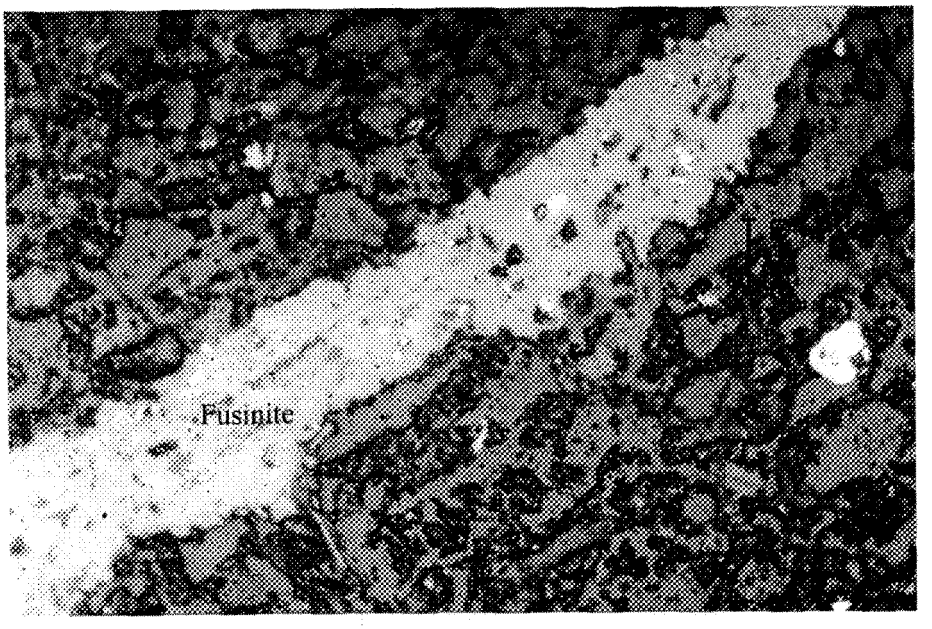

Fig.5-1e. Inertinite in silicified siltstone from the Lannigou deposit.

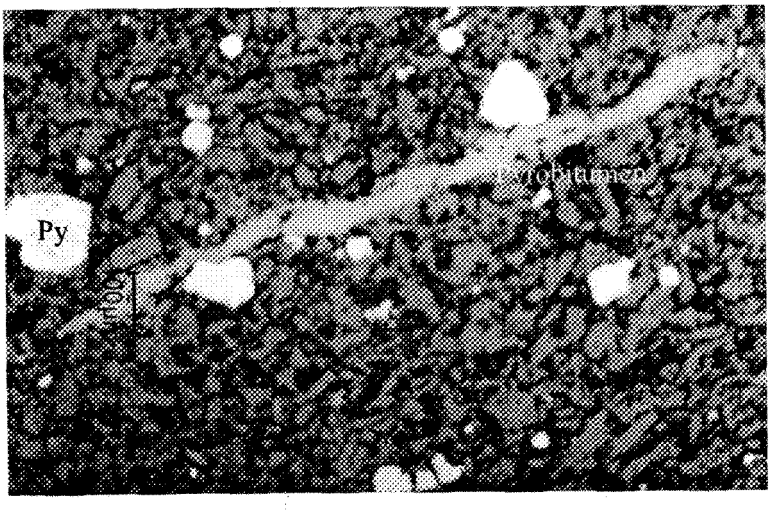

Fig.5-1(f). Pyrobitumen in the ore from the Lannigou deposit.

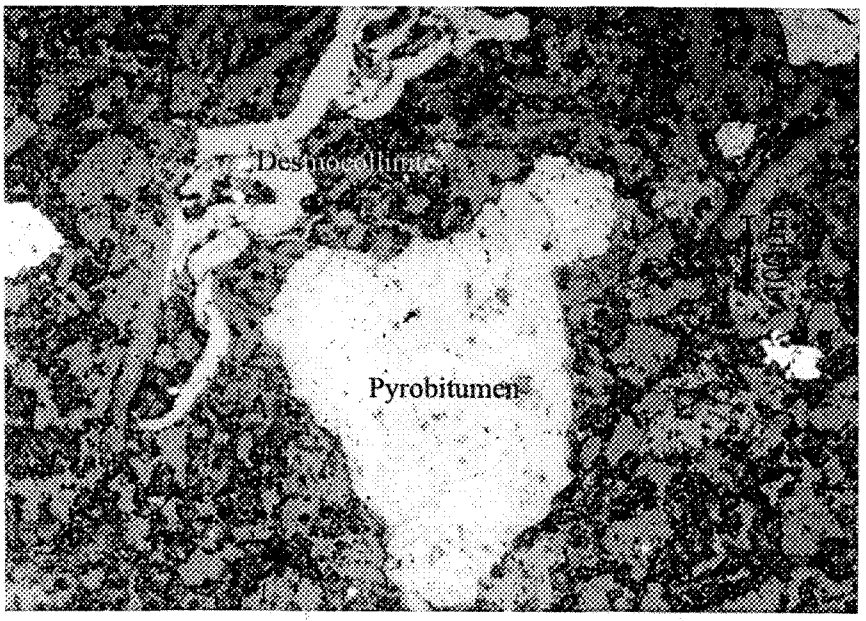

Fig.5-1g. Pyrobitumen and desmocollinite in the ore from the Lannigou deposit.

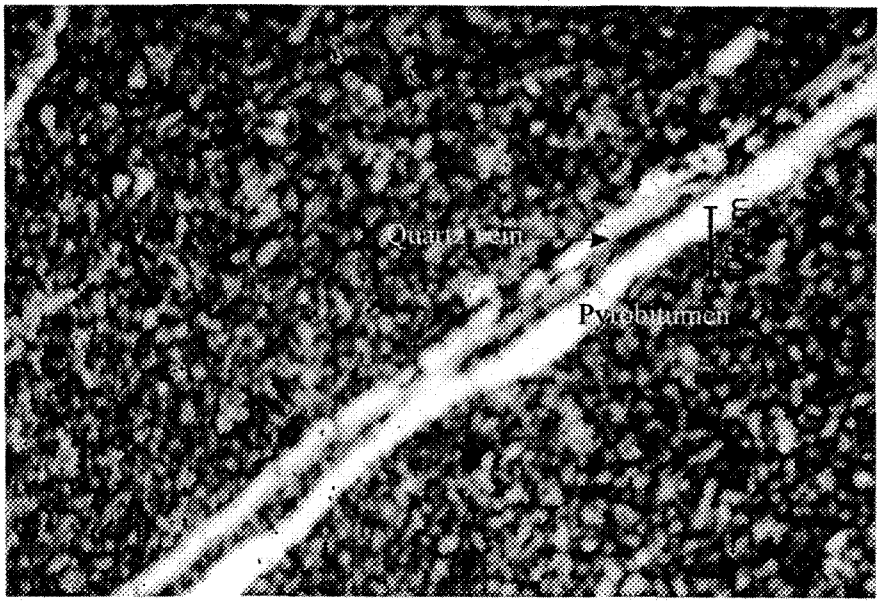

Fig.5-1h. Pyrobitumen vein in silicified siltstone from the Lannigou deposit
The quartz vein lies adjacent and parallel to the pyrobitumen vein and locally cuts the latter.

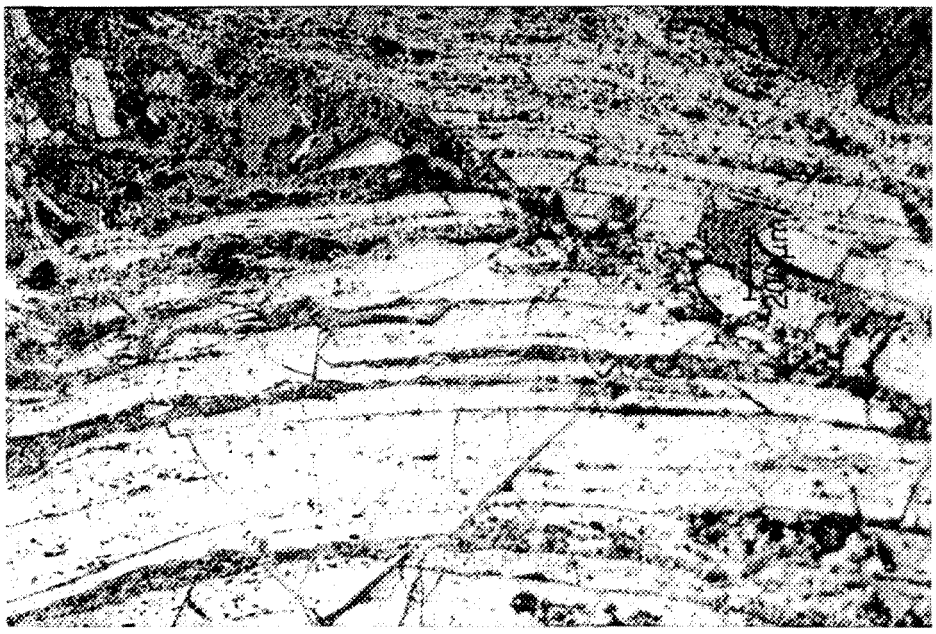

Fig.5-1(i) Inertinite in the ore from the Getang deposit

Fig.5-1(j). Brecciated inertinite in ore from the Getang deposit.

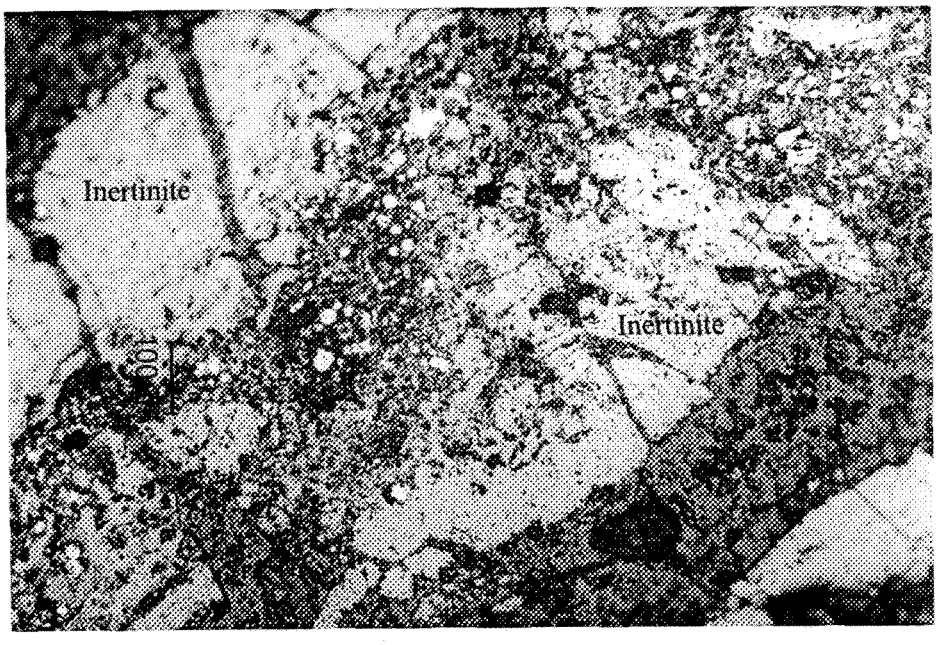

Fig.5-1(k). Inertinite in the ore from the Getang deposit.
Enclaved in the inertinite are fine-grained pyrite.

Fig. 5-1. The organic matter in the ores and host rocks of the Lannigou and Getang deposits.

inclusions from the Lannigou, Getang, and Zimudang gold deposit usually contain fluorescent material. Fluorescent spectral analysis and laser Raman spectroscopy investigations show that the organic matter in the fluid phase is composed mostly of complex aromatics, while the gaseous inclusions mainly consist of light hydrocarbons (C number less than 6) (Bertrand et al., 1986; Khorasani, 1987; Zhang and Zhang, 1999). Gas chromatographic study of the inclusions in quartz veins from the Lannigou gold deposit shows that the gaseous phase is composed mainly of light hydrocarbons, out of which methane, ethane and propane constitute 87.5%, 6.2%, and 2.5% of the total respectively (Zhuang et al., 1997). This suggests that the organic matter in the fluid is over matured, which is consistent with the homogenization temperature determination of the fluid inclusions.

5.1.2. Rock-Eval and GC-MS analysis of the organic matter in the SHDG deposits

The modern pyrolysis procedures generally measure the total hydrocarbons and other gases evolved during pyrolysis via a gas chromatographic (GC) detector as the sample is heated at a fixed rate in a stream of inert gas. The total evolved pyrolyzed gases are measured using a flame ionization detector (FID) for hydrocarbons and a thermal conductivity detector (TCD) for total pyrolyzable gases (Espitalié et al., 1977, 1984). The kerogen or whole-rock sample is gradually heated in a helium stream (rate about 30°C/min), and pyrolyzed hydrocarbons and carbon dioxide are measured as a function of temperature, where S_1 represent free hydrocarbons in the kerogen; S_2 represents

pyrolyzable hydrocarbons generated by pyrolysis, related to the petroleum-generating potential of the sediment. S_2 is normalized to total organic carbon (TOC) to give the hydrogen index, which is proportional to the kerogen elemental H/C ratio. In a similar way, the pyrolyzable CO_2 is measured and normalized to TOC to give the oxygen index, which is sometimes proportional to the kerogen elemental O/C ratio. T_{max} is the temperature at which the S_2 peak reaches the maximum evolution. Rock-Eval pyrolysis of organic matter at the Alligator Ridge gold deposits, Nevada, showed that the ore bodies were located in a "bulls eye" in which indigenous organic matter had been more thermally stressed than in the same strata outside the deposits (Ilchik et al., 1986). However, there is no correlation between gold content and T_{max} value of the ores in the Lannigou deposit.

The total organic carbons and Au contents are listed in table 5-1, and 5-2. The high T_{max} values show that the kerogen in the ores and the host rocks are over matured. The Rock-Eval analysis (table 5-1) shows that there is no correlation between gold content and the total organic carbon (Fig. 5-2). As shown in Fig. 5-3, the samples with low TOC content usually have high HI, which indicates that the organic matter in the rocks migrated (migrabitumen) from TOC rich to the TOC low parts. However, it is very interesting to note that there is a positive correlation between Au, As and S_2 (table 5-3). This might have resulted from the input of allochthonous organic matter before or during the ore forming processes, and the organics might have been brought in by hydrothermal solutions from outside the system or from the adjacent host rocks. The high reflectance of the vitrinite in the host rocks suggests that they were over matured before Au mineralization; that is to say,

Table 5-1. Rock-Eval analysis and the Au, As, Hg contents of the host rocks and ores of the Lannigou, Zimudang and Getang gold deposit

Location	Sample	Rock	Au (ppb)	Hg (ppm)	As (ppm)	TOC (%)	T_{MAX} (°C)	S_1 (mg/g)	S_2 (mg/g)	HI (mg/g.TOC)
Lannigou gold deposit	LN-4	Sandstone	4.0	0.29	51.54	0.55	400	0.09	0.03	5
	LN-8	Limestone	n.d.	0.26	0.97	0.02	401	0.22	0.05	250
	LN-12	Mudstone	4.1	0.21	4.23	0.54	558	0.58	0.1	19
	LN-13	Weathering crust	760	3.03	1457	0.07	378	0.35	0.06	86
	LN-14	Oxidized ore	3550	4.55	4884	0.32	573	0.26	0.07	22
	LN-15	Ore	6650	5.41	2438	0.58	537	0.47	0.15	26
	LN-18	Siltstone	4.4	2.46	746	0.14	462	0.39	0.05	36
	LN-19	Siltstone	22.1	1.4	87.04	0.16	576	0.5	0.06	38
	LN-20	Ore	6090	18.37	3512	0.16	477	0.62	0.15	94
	LN-21	Silty mudstone	460	73	1016	0.1	448	0.52	0.05	50
	LN-22	Ore	3930	46.15	3389	0.14	495	0.44	0.11	79
	LN-23	Ore	4620	2200	5597	0.4	486	0.07	0.15	38
	LN-24	Siltstone	82.91	21.95	1847	0.16	n.d.	0.33	0	n.d.
	LN-25	Ore	1910	17.52	1411	0.08	342	0.49	0.06	75
	LN-26	Siltstone	80	14.15	236.5	0.09	324	0.63	0.06	67
	LN-27	Sandstone	1.8	8.57	1250	1.5	577	0.59	0.08	5
	LN-28	Sandstone	9.6	7.08	1175	0.17	363	0.55	0.06	35
	LN-29	Siltstone	56.8	16.8	315.2	0.06	310	0.3	0.04	67
	LN-30	Siltstone	400	13.99	468.5	0.07	319	0.43	0.05	71
	LN-31	Siltstone	n.d.	5.01	229.7	0.08	329	0.83	0.06	75
	LN-32	Siltstone	6	3.98	31.66	0.37	565	0.82	0.11	30
	LN-33	Ore	6510	1700	485.4	0.1	438	0.6	0.05	50
	LN-34	Pelite	39.7	19.24	485.4	0.72	580	0.48	0.08	11
	LN-35	Mudstone	101.7	16.76	1517	0.19	n.d.	0.24	0	n.d.
	LN-36	Mudstone	760	21.46	1753	0.2	450	0.36	0.07	35

Table 5-1. Rock-Eval analysis and the Au, As, Hg contents of the host rocks and the ores of the Lannigou, Zimudang and Getang gold deposit (continued)

Location	Sample	Rock	Au (ppb)	Hg (ppm)	As (ppm)	TOC (%)	T_{MAX} (°C)	S_1 (mg/g)	S_2 (mg/g)	HI (mg/g.TOC)
Lannigou gold deposit	LN-37	Siltstone	2000	36.75	2309	0.32	523	0.39	0.1	31
	LN-38	Siltstone	1320	5.07	2382	0.13	486	0.43	0.12	92
	LN-39	Mudstone	2240	95.83	1898	0.34	523	0.46	0.07	21
	LN-40	Sandstone	1040	79.81	2446	0.1	495	0.5	0.06	60
	LN-41	Ore	6360	23.6	3201	0.39	483	0.58	0.14	36
	LN-42	Ore	1480	83.62	3211	0.94	476	0.47	0.13	14
	LN-43	Ore	800	16.83	1140	0.27	465	0.17	0.08	30
	LN-44	Siltstone	80	6.11	897	0.31	581	0.25	0.08	26
	LN-45	Limestone	200	7.09	6.28	0.02	448	0.24	0.07	350
	LN-46	Ore	9690	91.16	5832	0.18	412	0.42	0.55	306
Zimudang gold deposit	ZMD-1	Oxidized ore	800	3.22	919	0.03	540	0.24	0.08	267
	ZMD-3	Ore	240	1.75	593	0.17	578	0.32	0.09	53
	ZMD-4	Carbonaceous bed	9530	39.4	42647	0.56	544	0.72	0.74	132
	ZMD-5	Semi-oxidized ore	18.1	2.21	3044	0.04	451	0.36	0.07	175
	ZMD-8	Limestone	149	0.200	1.38	0.05	448	0.59	0.07	140
Getang gold deposit	GT-1	Limestone	6.60	2.47	7.69	0.04	442	0.43	0.07	175
	GT-2	Ore	1000	4.30	351	2.3	589	0.66	0.08	3
	GT-3	Ore	10360	2.40	231	1.14	593	0.6	0.08	7
	GT-4	Oxidized ore	109.2	3.64	72.0	0.05	445	0.4	0.06	120
	GT-5	Silicified carbonaceous shale	13.0	2.00	53.5	12.1	594	3.44	0.65	5

Note: n.d. = not detected.

Table 5-2. Organic carbon and gold concentrations of the Lannigou, Getang and Zimudang deposit

Sample no.	Deposit	TOC (%)	Au (ppm)	Sample no.	Deposit	TOC (%)	Au (ppm)	Reference
L1	Lannigou	0.220	7.495	G7	Getang	0.384	0.025	Tu et al., 1998
L2-1	Lannigou	0.897	1.181	Zs2	Zimudang	0.558	1.667	
L4	Lannigou	2.086	0.622	Zs3	Zimudang	0.740	0.009	
L5	Lannigou	0.622	8.333	Zs6	Zimudang	1.379	0.189	
L8	Lannigou	0.003	0.003	Zs7	Zimudang	4.245	0.006	
L11	Lannigou	0.259	0.006	Zs8	Zimudang	0.695	0.102	
G1	Getang	2.734	0.009	Zs9	Zimudang	3.436	0.005	
G6	Getang	0.727	0.203	ZS10	Zimudang	14.569	0.055	
LN-10	Lannigou	0.47	0.006	LN-16	Lannigou	0.44	2.77	Li et al., 1996
LN-11	Lannigou	0.77	0.012	LN-17	Lannigou	0.54	7.82	
LN-12	Lannigou	0.73	7.01	LN-18	Lannigou	1.42	0.066	
LN-13	Lannigou	0.48	4.31	LN-19	Lannigou	0.71	0.015	
LN-14	Lannigou	0.55	4.66	LN-27	Lannigou	0.45	0.18	
LN-15	Lannigou	0.23	1.86	LN-29	Lannigou	0.64	0.012	
LN-15-A	Lannigou	0.71	1.65					

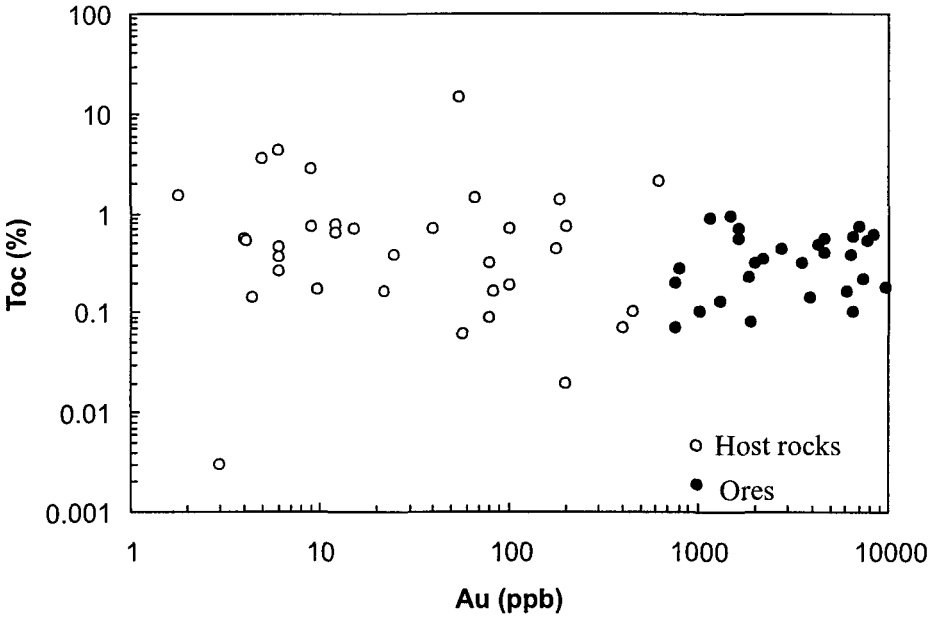

Fig. 5-2. Diagram showing the relation between the Au contents of the ores and host rocks and TOC for the SHDG deposits in SW Guizhou.

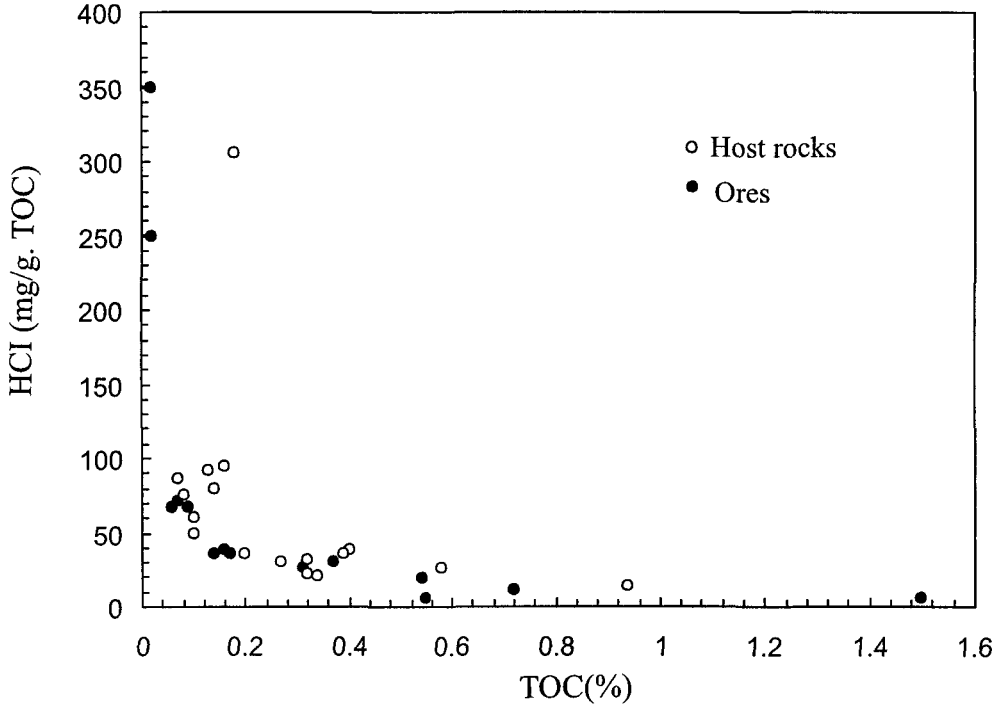

Fig. 5-3. The TOC vs HCI(mg/gTOC) diagram of the Lannigou deposit.

migrabitumens were emplaced during the hydrothermal processes from the adjacent host rocks or outside of the system.

Table 5- 3. Correlation between Au, As, Hg and the parameter of the Rock-Eval analysis

	Au	Hg	As	TOC	T_{MAX} (℃)	S_1	S_2	HI
Au	1							
Hg	0.38	1						
As	0.62	0.03	1					
TOC	-0.01	-0.01	-0.04	1				
T_{MAX}	0.09	0.01	-0.07	0.52	1			
S_1	0.07	-0.18	-0.04	0.09	0.02	1		
S_2	0.71	0.07	0.93	0.09	0.07	0.08	1	
HI	0.21	-0.07	0.50	-0.43	-0.31	-0.18	0.45	1

The compositions of the chloroform extractable organic matter and GC-MS analysis of the samples reflect their degree of maturation (table 5-4, 5-5). Component analysis of the samples from the Lannigou deposit shows that the degree of maturation of the ores is lower than those of siltstone, but higher than those of mudstone. GC-MS analysis of the Lannigou deposit sample shows that the hydrocarbon composition and the biomarkers of the organic matter in the ores and host rocks are extremely similar (Fig. 5-4, 5, 6), which implies that no significant amount of hydrocarbons were brought in by the hydrothermal solution. An exception here is that the oxidized ore sample LN-14 was sampled near surface, and apparently bears an input from the surface vegetation, resulting in an enrichment of high C number hydrocarbons (Fig.5-4). The Pr/Ph (Pristane/phytane) ratios, the ratio of the relative abundance of isoprenoids pristane and phytane, are around 1.0, which show that the kerogen in the samples are mainly marine and partly of terrigenous in origin.

Table 5-4. Component analysis of soluble organic material in ores and the host rocks of the Lannigou deposit

Location	Sample no.	Sample description	Chloroform "A" (ppm)	Saturated alkanes (%)	Aromatic + non-alkanes (%)	Bitumen (%)
Rongban	LN-4	Sandstone	28	26	62	12
Huangchanggou	LN-14	Oxidized ore	48	42	49	9
Huangchanggou	LN-15	Primary ore	53	44	44	13
516 elevation tunnel	LN-20	Primary ore	35	26	52	21
	LN-27	Siltstone	43	19	62	19
	LN-32	Silty mudstone	47	25	57	18
560 elevation tunnel*	L-11	Mudstone	35	13	76	11
	L21	Siltstone	28	15	74	11
	L16	Ore	40	8	79	13
	L17	Ore	31	13	73	14
720 elevation tunnel*	L348	Mudstone	55	13	67	20
	L39	Ore	38	13	71	16
	L40	Ore	33	10	70	19

*Li and Liu, 1998.

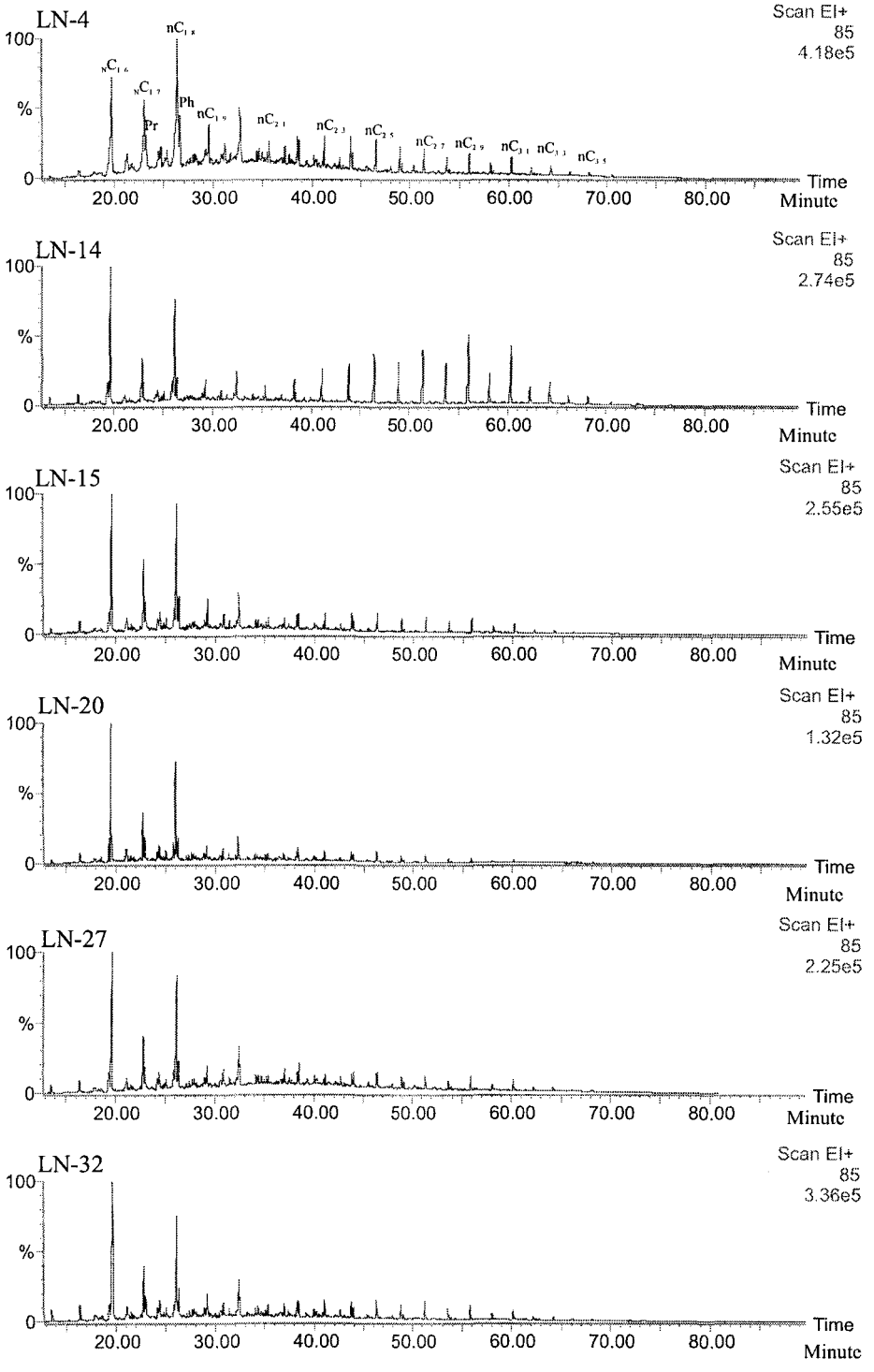

Fig.5-4. Mass spectrogram of alkanes of the samples from the Lannigou deposit. LN-4 Sandstone; LN-14 Oxidized ore; LN-15 Primary ore; LN-20 Primary ore; LN-27 Siltstone; LN-32 Silty mudstone

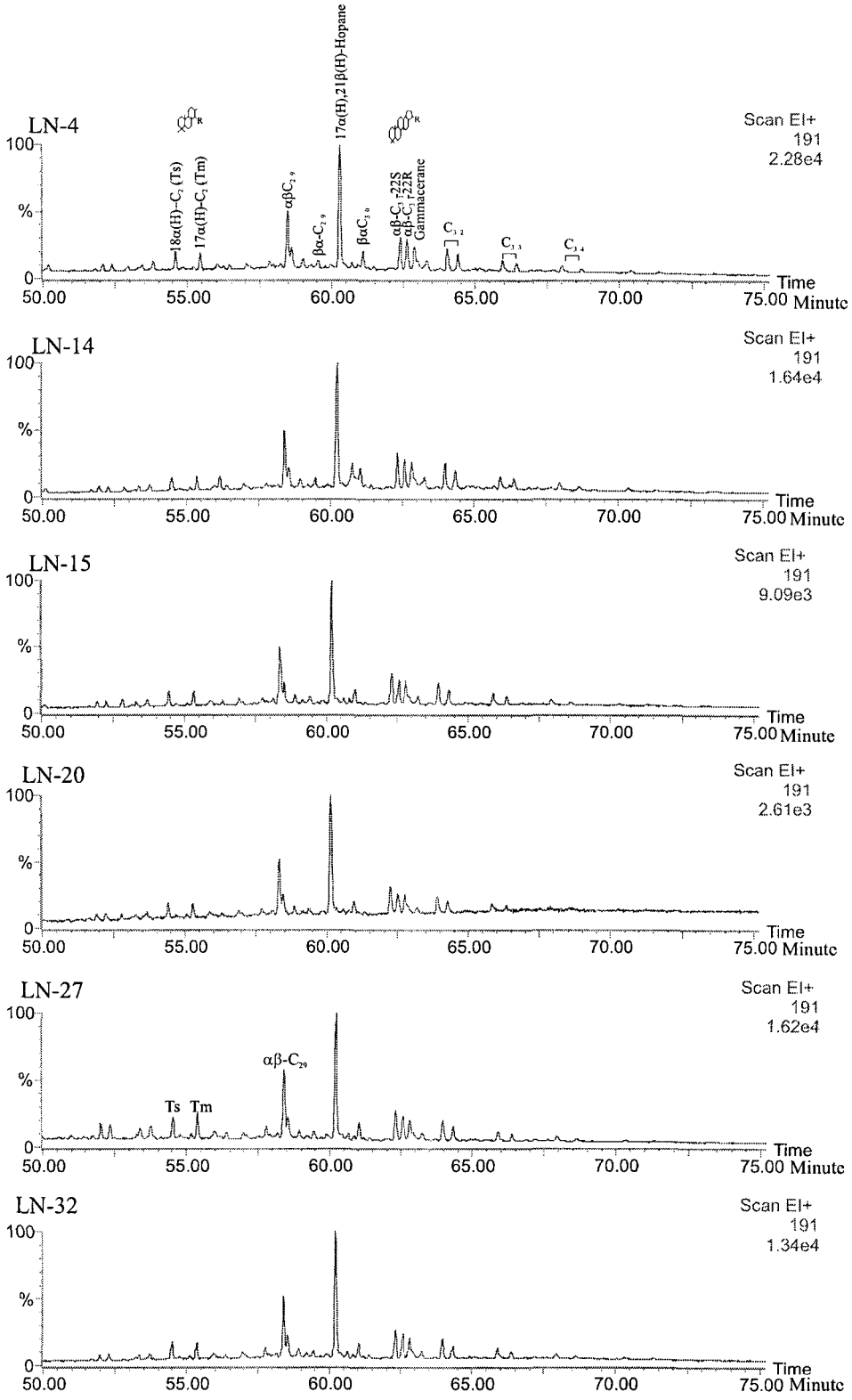

Fig.5-5. m/z191 Mass spectrogram of terpanes of the samples from the Lannigou deposit. LN-4 Sandstone; LN-14 Oxidized ore; LN-15 Primary ore; LN-20 Primary ore; LN-27 Siltstone; LN-32 Silty mudstone

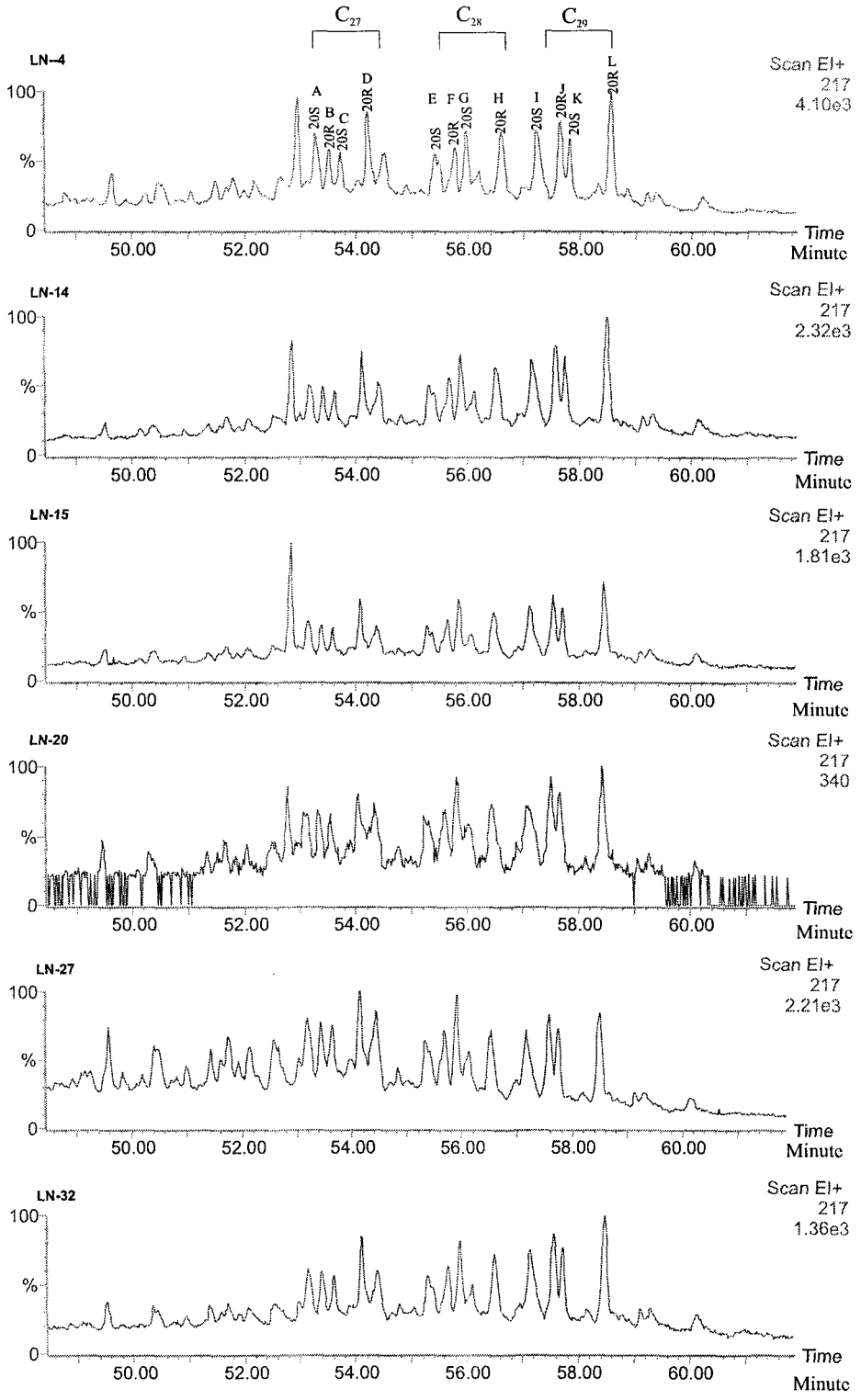

Fig.5-6. m/z217 Mass spectrogram of steranes of the samples from the Lannigou deposit. LN-4 Sandstone; LN-14 Oxidized ore; LN-15 Primary ore; LN-20 Primary ore; LN-27 Siltstone; LN-32 Silty mudstone

A. 5α(H)-Cholestane (20S); B. 5α(H),14β(H),17β(H)-Cholestane (R); C.5α(H),14β(H),17β(H)-Cholestane (20S) ;D. 5α(H)-Cholestane (20R) E. 5α(H)-Ergostane (20S); F. 5α(H),14β(H),17β(H)-Ergostane (20R); G.5α(H),14β(H),17β(H)-Ergostane (20S); H. 5α(H)-Ergostane (20R); I. 5α(H)-Stigmastane (20S); J.5α(H),14β(H),17β(H)-Stigmastane (20R); K. 5α(H),14β(H),17β(H)-Stigmastane (20S); L. 5α(H)-Stigmastane (20R)

Table 5-5. The parameters of the biomarkers in the host rocks and ores of the Lannigou deposit

	Au	Pr/n-C_{17}	Ph/n-C_{18}	Pr/Ph	T_m/T_s	$\frac{\alpha\alpha\alpha - S - C_{29}}{\alpha\alpha\alpha - (R+S) - C_{29}}$	$\frac{\alpha\beta C_{31} - 22S}{\alpha\beta C_{31} - 22R}$
LN-4	4ppb	0.70	0.47	0.85	0.98	0.39	1.09
LN-14	3.55ppm	0.58	0.27	1.02	1.03	0.37	1.23
LN-15	6.65ppm	0.58	0.32	1.10	0.99	0.40	1.29
LN-20	6.09ppm	0.65	0.25	1.37	0.89	0.42	1.44
LN-27	2ppb	0.57	0.30	1.02	1.23	0.39	1.30
LN-32	6ppb	0.61	0.36	0.93	0.97	0.40	1.21

Pr/n-C_{17} is the ratio of pristane and normal-alkane with 17 carbon in its molecule; Ph/n-C_{18} is ratio of phytane and normal-alkane with 18 carbon in its molecule; both Pr/ n-C_{17} and Ph/n-C_{18} are decreasing with increase degree of organic maturation. Pr/Ph (pristane/phytane): The ratio of the relative abundance of the isoprenoids pristane and phytane. The ratio is characteristic of organic facies and depositional environment; values less than 1.0 are often associated with carbonate source rocks and oils while values greater than 4.0 are typical of terrigenous organic matter. Tm/Ts is the ratio of 17α(H)-22,29,30-Trisnorhopane and 18α(H)-22,29,30-Trisnorhopane, the ratio decreases with the progress of organic maturation, the ration is less than 1.0 beginning from "oil-window". $\frac{\alpha\alpha\alpha - S - C_{29}}{\alpha\alpha\alpha - (R+S) - C_{29}}$ is the ratio of 5α(H)-Stigmastane(20S) and 5α(H)-Stigmastane; $\frac{\alpha\beta C_{31} - 22S}{\alpha\beta C_{31} - 22R}$ is ratio of 17α(H),21β(H)–30–Homohopane (22S) and 17α(H),21β(H)–30–Homohopane (22R), both ratios increase as the maturation of organic matter progresses.

Table 5-6. Gold concentrations of kerogen from the Lannigou deposit

Sample no.	Rock	TOC (%)	Au (ppm)	Kerogen type	Ro (%)	Au in kerogen (ppm)	Proportion of total Au in kerogen (%)
LG10	S	0.41	0.09	II_2	2.61	0.84	3.83
LG16	O	1.13	8.24	II_2	2.79	24.80	3.40
LG18	O	0.69	3.09	II_2	2.84	13.46	3.01
LG21	MO	0.60	0.14	II_2	2.60	6.15	1.95
LG40	O	0.99	3.12	II_2	2.74	6.15	1.95
LG45	S	0.09	0.09	II_2	2.76	1.36	1.36
LG61	M	0.56	0.09	II_2	2.77	0.69	4.26

Note: S-siltstone; M-mudstone; MO-weak mineralized rock; O-ore; Ro=Vitrinite reflectance

From: Li and Liu, 1998.

Organic matter in the ores and host rocks contains only a very small part of the gold in the samples (Table 5-6). Gold contents were analyzed by graphite furnace atomic absorption analysis method. The kerogens contain 1.1 to 2.4% sulfides (Li and Liu, 1998), that is to say, part of the gold resides in the fine-grained sulfides. Thus, the organic matter may account for even less gold in the ores. Vitrinite reflectances of the ores are somewhat higher than those of the host rocks, which indicate the effects of hydrothermal fluid on the sedimentary rocks (Table 5-7). On the other hand, T_{max} of bulk organic matter of the ores are lower than the host rocks in the profile traversing the ore vein (the fault zone), which may be due to the uncertainty of the determination and partly to the input of migrated hydrocarbons from host rocks or possibly, partly from outside of the system.

An organic geochemical investigation carried out in the neighboring area, in the Larma gold deposit in the Qinling area, also supports the possibility that the organic matter in the ores and host rocks have a common source (Zeng and Yen, 1994). Biomarkers and REE patterns of the kerogen and pyrobitumens are very similar and suggest that the pyrobitumens were the product of the in situ maturation of kerogen in the host rocks.

Organic investigations on the SHDG deposits in the Carlin Trend, U.S.A., also support that the organic matter in the ores is indigenous. The organic matter in the host rocks was over matured when the gold mineralization took place; a hydrocarbon stage (HC) was recognized in the Carlin Trend as a pre-ore alteration (Kuehn and Rose, 1995). All veinlet types of the early hydrocarbon stage contain high bulk density CH_4 fluid inclusions. Production of CH_4 by thermal maturation of organic matter occurred before ore deposition, and interestingly reservoir conditions of 0.4 to 1.4 kbars at 155±20°C are recorded in the

Table 5-7. Gold and organic matter contents, maturation of the ores and host rocks from the Lannigou deposit

Location	Sample no.	Description	Au (ppm)	TOC (%)	T_{max} (°C)	Ro (%)	
						Average	σ
560 elevation tunnel A	L10	Gray siltstone	0.99	0.41		2.61	0.08
	L11	Dark gray mudstone		0.67	586	2.67	0.07
	L14	Dark gray mudstone	0.01	0.61	578		
	L16	Mineralized mudstone	8.24	1.13	545	2.79	0.07
	L18	Mineralized siltstone	3.09	0.69		2.48	0.08
	L19	Dark gray mudstone		1.04	585		
	L20	Gray silty mudstone	0.14	0.60		2.77	0.09
	L22	Dark gray mudstone	0.01	0.64	580		
560 elevation tunnel B	L23	Dark gray silty mudstone		0.76	589		
	L25	Mineralized siltstone	8.07	0.32		2.74	0.09
	L26	Mineralized mudstone		0.67	572		
	L27	Dark gray silty mudstone		0.31	582		
	L31	Dark gray mudstone		0.59	585		
720 elevation tunnel	L37	Gray siltstone	0.09	0.56			
	L38	Dark gray mudstone	0.02	0.57	594		
	L40	Mineralized sandstone	3.12	0.99	515	2.74	0.09
	L41	Mineralized sandstone	10.7	0.25			
	L42	Dark gray mudstone	0.04	0.99	588		
	L44	Dark gray mudstone		0.70	589		
	L45	Gray siltstone	0.09	0.09		2.76	0.12
	L46	Dark gray mudstone	0.04	0.69	585		

From: Li and Liu, 1998.

countless crosscutting planes of secondary CH_4-rich fluid inclusions. HC stage veinlets are cut by all other veinlet types and contain secondary inclusions of fluids typical of later veinlets of the paragenesis. Hausen and Park (1985) proposed that the bituminous matter in the ores at Carlin, Getchell, and Alligator Ridge was mostly petroleum residues emplaced in the host rocks prior to gold mineralization. However, Ilchik at al. (1986) found no fundamental differences between the type and abundance of organic matter in background samples and those samples spatially associated with mineralization in the Alligator Ridge gold deposits. Moreover, the pyrobitumens were indigenous — derived locally from the organic matter, not introduced from outside of the system. The hydrothermal system, which operated in the vicinity area of the deposits, increased the maturity of the organic matter significantly. The hydrocarbon maturation of the host rocks took place significantly prior to SHDG mineralization (Kuehn, 1989; Kuehn and Rose, 1995).

5.2. Discussion--Contribution of organic matter to SHDG mineralization

The organic geochemical data on the SHDG deposits in southwest Guizhou and those from the Carlin Trend in the U.S.A. all suggest that the organic matter in the ores was indigenous. However, contribution of hydrocarbon from host rocks and adjacent traps cannot be ignored as was indicated by the Rock-Eval analyses that hydrocarbon migration in the ores and host rocks do exist. The role of organic matter in processes of SHDG and other hydrothermal ore genesis can be subdivided into a number of contributing phenomena. First, organic materials may be relatively rich in metals of interest and act as sources of ore-forming components in their own right. Second, organic liquids may act as

transporting agents for ore components, enabling them to be transported to sites where concentration may take place. Third, the evolution of organic matter as a diagenetic process may result in the modification of aqueous pore fluids and affect their efficiency as transporting agents. Finally, organic materials may influence the precipitation of ore minerals from aqueous fluid phase.

5.2.1. Extraction of the organisms and the formation of the source rocks

Anomalously high amounts of metallic elements in black shale, peat, coal and petroleum and the non-fortuitous association of organic compounds with mineralization are now widely accepted as resulting from a few basic phenomena more or less directly related to the development and activity of living organisms. Living organisms are capable of actively concentrating various elements in their cells and producing very reactive compounds such as H_2S that exert a strong control on the redox potential of sedimentary environments. Biological organic remains, more or less altered by chemical, microbial and thermal diagenetic processes, can also interact with metals through their intrinsic reducing, acidic and chelating properties (Disnar and Sureau, 1990).

5.2.1.1. Biological processes

In the early nineteen thirties, Goldschmidt (1930) and Goldschmidt and Peters (1933) discovered unexpectedly high concentrations, first of Ge, and later of numerous other trace elements in coals. In 1937, Goldschmidt (1937) proposed the following explanations for this metal enrichment: (1) co-precipitation with Fe and Mn hydroxides; (2) precipitation of metal sulfides; and (3) accumulation with decaying plant remains of micronutrients and

ballast elements concentrated by living organisms. The latter mechanism is now known as the Goldschmidt enrichment principle (Brooks, 1972).

Marine plants are capable of concentrating some trace elements from the seawater to such an extent that the contents of these elements can be n to $n\times10^5$ times higher than the normal levels (Table 5-8). However, except for a few elements such as I, K, P, S, etc., the majority of the trace elements in plants are in lower concentration than in sedimentary rocks (on average), only a few reaching the average levels. Actually, "biosorption" includes the concentration of metals in biological membranes of living and dead organisms. In the cells, heavy metals are tightly bound to biological molecules through several N-, S- or O-containing ligands arranged in more or less specific chelating sites. The various proteinic and other reactive heteroatomic functional groups of humic substances endow them with the acidic and ligand properties susceptible to promote mineral dissolution, as well as metal binding and transport. Carboxylic groups play an important role in metal-organic complexation. The loss of carboxylic and other groups in the course of diagenesis may provoke the release of the metals to the medium. But the situation is quite complex as metal sulfides are formed in the presence of H_2S derived from the direct reduction of inorganic sulfate impurities by the organics. A small part of the initially complexed metals remained associated with the NSO radicals produced by thermal maturation. Sequestration by organic materials certainly plays only a minor role in metal accumulation, unless the aqueous medium is highly mineralized (e.g. as a result of weathering of a preexisting ore-body).

The concentration coefficient (marine plant/sea water) of gold in marine plants is up to 1200, and is about 12 times that of the average shale and clay (Disnar and Sureau, 1990).

Table 5-8. Typical enrichment of elements in marine plants

(A) Essential elements		(B) Non-essential elements	
Element	Enrichment factor (relative to seawater)	Element	Enrichment factor (relative to seawater)
Al	6000	*Ag*	*830*
B	24	*As*	*10000*
C	12300	*Au*	*1200*
Ca	25-750	Ba	1000
Co	2300	Be	1700
Cu	3700	Bi	3530
Fe	70000	Cd	4000
I	500-25000	Cr	20000
K	140	Cs	1400
Mg	4	F	3500
Mn	26500	Ga	17000
Mo	45	*Hg*	*1000*
Na	3	Li	170
P	50000	Ni	600
Rb	70	Pb	267000
S	14	Sn	330
Se	8900	Ti	12000-80000
Si	500-6700	W	35
Sr	33-175		
V	1000		
Zn	15000		

From: Trudinger et al. (1979), Bowen (1966).

Because of the high degree of enrichment of gold in marine plant, the gold contents of three series of sedimentary rocks, which were commonly accepted as Au source beds in south China, usually show positive correlation with their organic carbon contents (e.g., Hu et al., 2000). Trace elements may be associated with these groups such as carboxylic acid (-COOH), phenolic hydroxyl (-OH), mercapto (-SH) and imino (=NH) in organic matter. The degree of organic complexing decreases with increase in coal rank, and carboxylic acid groups do not persist much beyond the brown coal/lignite stage. For example, metal-cystine complexes would not survive mild diagenesis, but mercapto (-SH) groups may be expected to persist to the bituminous stage (Swaine, 1990).

Humic acids are probably the main complexing agents in some geological systems and, together with fulvic acids, they could have complexed with several trace elements significantly during the early stages of coalification. Pyrite is common in coal, and several other sulfides have been reported, albeit at trace levels. In coals, gold is most likely to exist as a colloid in the organic matter or precipitated on the surface or within pyrite or other sulfides. The gold contents of coals from different places vary considerably. Generally up to 10 ppb gold could be expected in most coals, except for special coals, such as those from Wyoming, Germany and Russian, where more than 100ppb Au was reported (Swaine, 1990). Data reported for gold concentrations in coal ashes are at the ppm level, 1ppm gold was found in some coals from Utah and Wyoming, U.S.A., and up to 3ppm gold in coal from Cambrian, Wyoming-North Dakota, the U.S.A. Some of the high gold concentrations found in the coals might result from late stage hydrothermal fluid enrichment or special detrital sources (Swaine, 1990).

Although biological process do play a role in gold concentration, the extent of enrichment of gold by marine and terrestrial plants during their life and in the subsequent sedimentation and diagenesis could not have been sufficiently high to be of metallogenic significance.

5.2.1.2. Gold and organic matter interaction in supergene environments

The role of organic matter in gold transport and precipitation of Carlin-type Au mineralization is still unclear and controversial. In spite of several experimental studies of the interaction of Au with humic substances, there is little agreement as to the role natural organic matter play in Au transport and deposition (Wood, 1996). Moreover, no thermodynamic data for these interactions have been derived. The weight of experimental evidence seems to be equally divided between, on the one hand, that which supports the formation of soluble Au-humate complexes and, on the other hand, that which supports the predominant reduction and precipitation of Au by humic substances.

Humic substances represent the largest fraction of organic matter in aquatic and sedimentary environments. Owing to the presence of functional groups containing oxygen, and to a lesser extent, nitrogen and sulfur, these substances are capable of interacting with gold in solution in a number of ways. Humic substances may (1) form soluble complexes with metal ions; (2) cause precipitation of metal ions via reduction; (3) cause precipitation of metal ions via adsorption, ion exchange or other sorption processes (when humic substances themselves are insoluble); (4) modify the sorption behavior of colloidal particles of metals; and (5) affect the rates of geological processes (Wood, 1996). From calculated

stability constants based on ideal stoichiometric formulae, the order of stability of organo-gold complexes has been shown to be S-donors >> N-donors > OH-donors >>COOH-donors (Varshal et al., 1990). Varshal et al. (1990) suggest that up to 91% of the total dissolved gold present in surface waters occurs as fulvate complexes with a molecular weight greater than 600. On the other hand, Bergeron and Harrison (1989) demonstrated that humic acid could reduce $AuCl_4^-$ to a colloidal sol of the metal under very acidic conditions, whereas at higher pH a protective organic film apparently coated the colloid particles produced. Au sol formation by humic substances depends on the stability of the Au-complexes in solution (Vlassopoulos et al., 1990). From dissolution and infrared experiments, Bowell et al. (1993) demonstrated that gold-fulvic acid reactions are dominant in acidic pH environments and involve colloidal adsorption in which gold forms hydromorphically stable colloid-sized particles with fulvic acid. At higher pH, gold-fulvate complexes form and increase in importance with pH increase. Some reduction may still be important at higher pH with gold (III) species being reduced by fulvic acid to Au^+ species and then chelated. Lower molecular weight organic acids are normally present in very low concentrations in surface and subsurface waters, and are easily degraded thermally and biologically (Reuter and Perdue, 1977).

Au-organic matter interaction in natural systems probably includes a wide variety of processes from elemental gold-organic matter associations to true dissolved gold-organic matter complexes (Baker, 1978; Fedoseyeva et al., 1986; Machesky et al., 1992). The complexing, adsorption and uptake of Au by organic matter might be important processes in hypergene zones that control supergenic gold mineralization (such as laterite-type gold

deposit, e.g., Porto and Hale, 1996) and enrichment of gold in host rocks during sedimentation and diagenesis. The organic matter in the host rocks in southwest Guizhou may have contributed to the primary accumulation of Au in rocks that become the main source of the SHDG mineralization.

5.2.2. Possible contribution of oil generation and migration

It is well known that thermal maturation of organic matter due to deep burial and thermal events is universal in natural environments. The conversion of organic matter to petroleum produced by hydrothermal activity is an easy process, occurring in nature in many types of environments. Petroleum generation and migration is a ubiquitous process associated with hydrothermal activity and metallic mineral formation.

According to Lewan (1983) and Schimmelmann et al. (1999), the generation of petroleum occurs in four stages: (1) pre-oil (a thermal immature stage) found in close association with the source rock; (2) incipient-oil; (3) primary-oil and (4) post-oil, following distant transport from source rock, and during which thermal decomposition of the oil sets in. Hydrous pyrolysis operates efficiently in natural settings, like the Guyamas basin (Simoneit and Lonsdale, 1982) and in hot spring deposits (Clifton et al., 1990; De Ronde and Ebbesses, 1996), environments known to generate huge metallic ore deposits.

If the stability limit is exceeded, thermal cracking of old oil accumulations can occur with or without aqueous hydrothermal solutions. The cracking, or thermal degradation of the already generated oil is both time and temperature dependent, like the generation of oil from precursor organic matter (kerogen); however, temperature is by far the more dominant

variable (Hunt, 1979; Tissot and Welte, 1984). There is a broad (but not complete) consensus that, under all but the most exceptional natural deep burial or hydrothermal conditions, oil is fully cracked to methane and pyrobitumen at some point within the approximate temperature range of 150°C to 200°C (e.g., Blanc and Connan, 1994). However, numerous petroleum-geochemical analyses of deeply buried, high-rank, fine-grained rocks from ultra-deep well-bores demonstrate that C_{15+} hydrocarbons persist in moderate to high concentrations at vitrinite reflectance (R_o) values of 2.0~5.0%, and persist in measurable concentrations up to R_o=7.0~8.0%, at which point the thermal deadline for C_{15+} hydrocarbons is finally approached (Price and Wenger, 1992; Price, 1993). High temperature (300~350°C) petroleum in the hydrothermal vent water of the Guaymas basin spreading center is well known (Simoneit, 1990). However, the extent to which these findings can be applied to the full range of natural settings and/or longer duration is a matter of considerable controversy (e.g., Price, 1994; Seewald, 1994). Anyhow, petroleum is stable in the whole temperature range of the SHDG mineralization.

Reservoir maturation appears to crack the hydrocarbons containing more than 20 carbon atoms into smaller molecules that become part of the gasoline range. The maturation of crude oil in the reservoir is believed to involve several hydrogen disproportion reactions. The cracking reactions with large molecules give up hydrogen to permit increased formation of low-molecular-weight paraffin. The large molecules condense to polycyclic aromatic hydrocarbons, which eventually form asphalts or pyrobitumens in the reservoir. Bacterial degradation of oil can occur if reservoir temperatures do not exceed about 82°C and if oxygen, inorganic trace nutrients, and water

are present (Tissot and Welte, 1984). Anaerobic sulfate-reducing bacteria also can degrade oils in a manner similar to aerobic strains but require more time. Laboratory experiments indicate that both sulfate and elemental sulfur in the presence of H_2S are capable of oxidizing hydrocarbons, including methane.

Petroleum represents a complex mixture of organic compounds, mixed with "impurities" such as included water or salts. The organic constituents can be subdivided into several fractions, including saturated and aromatic hydrocarbons, resins and asphaltenes (Tissot and Welte, 1984). Resins and asphaltenes are composed of relatively high molecular weight species, with complex structures that include the heteroatoms N, S, and O and host to numerous nonhydrocarbon fractional groups.

The significant metal contents in some samples of oils and oilfield brines (Sverjensky, 1984; Manning, 1986) suggest that petroleum may play an important role in ore metal transport. For example, high concentrations of mercury (up to 21 ppm) in petroleum associated with mercury depositing geothermal systems have been reported. Extrapolation of mercury solubilities in organic phases suggest that extremely high concentrations of mercury can dissolve in the organic phase, and that organic phase transport may control mercury mobilities in many mercury ore-forming hydrothermal systems (Fein and Williams-Jones, 1997, and the references therein). Similarly, SHDG deposits and petroleum accumulations are often hosted in the same tectonic traps and produced in a similar temperature window (70~240°C). Thus, a genetic relationship is not a unreasonable suspicion. The potential importance of hydrocarbons (petroleum) as

transporting agents for Au and Hg may be a plausible explanation for the intimate relation between Au and Hg in Carlin-type deposits.

Experimental results which are seemingly supportive to the hypothesis that crude oil is able to leach and transport gold, and may play an important role in the formation of some Carlin-type deposits by promoting leaching, migration, reduction and precipitation have been reported by Liu et al. (1994b) and Lu and Zhuang (1996). A preliminary experimental study shows that during primary migration, crude oil can remove Au from source beds, and that Au is concentrated in the migrated oil rather than the remnant oil and kerogen. Under low temperature conditions, crude oil and oilfield water can dissolve relatively high concentrations of Au from auriferous pyrite (Lu and Zhuang, 1996). In laboratory experiment, gold solubility in crude oil can be very high, and even a small portion of oil in water solution will greatly increase its gold solubility (Lin et al., 1993b; Liu et al., 1994b; Lu and Zhuang, 1996). At 70°C, crude oil can dissolve up to 880 ppb gold (Lin et al., 1993b). If the amount of Au extracted by and transported in the crude oil during secondary migration is significant, then oil migration can significantly affect Au distribution; migration of hundreds of miles is common in some environments. However, Au concentrations of crude oils all over the world are usually quite low, less than 3.0 ppb (Shah et al., 1970; Hitchon and Filby, 1983), except in a few cases where the oil may have interacted with nearby hydrothermal systems or been enriched in gold by other geological processes (Table 5-9). Therefore, despite the fact that Au solubility in crude oil can be very high (ppm grade) in laboratory experiments, the potential of crude oil to remove Au from

Table 5- 9. Gold concentration in Crude oil

Location	Sample No.	Au (ppb)			Source
		Content	Average	Sample number	
Shengli oil field, China	G32-24 G15-S-5 C6-8	106 132 108			Lin et al., 1993a
Jianghan oil field, China	Q26 Lu-0	2 4			This study
Kelamayi	F-3	6			Lin et al., 1993a
Western Canada			0.44 (< 1.32)	88	Hitchon et al., 1975
World wide		< 3	1 (0~3)		Jones, 1975 Barwise and Whitehead, 1983

the source beds and transport the Au within the sequences it traverse during oil generation and migration may be quite limited.

The occurrence of oil and bitumen in mercury ore deposits has been reported from many localities. Petrographic studies of Californian material by Bailey (1959) and of Russian material by Shabo et al. (1983) suggested that cinnabar and bitumen were in each case deposited from a common fluid. The association of bitumens with mercury ore led to an assumption that organic matter caused the precipitation of the mercury. It may be significant, however, that in many cases the mercury occurs with oil rather than solid bitumens. The trace element concentrations in petroleum fractions (Chakhmakchev et al., 1981) shows that mercury is enriched within lighter fractions, while many other metals are enriched within heavier oils. Russian researchers have suggested the use of hydrocarbon analyses in prospecting for mercury. In a study of the Plamennoya mercury-antimony deposit, Vershkovskaya et al. (1972) found that the maximum bitumen concentrations in organic matter were associated with ores containing the highest mercury contents. Mercury is so abundant in some oil and gas fields that mercury anomalies are also used in prospecting for hydrocarbons. It is important to recognize that Au and Hg behave differently during petroleum evolution. Hg can be removed from petroleum and made available for precipitation from the aqueous phase. However, Au is unlikely to be removed from porphyrin complexes under conditions of pH achieved under natural conditions (Manning and Gize, 1993).

Some researchers have proposed that the destruction of oil accumulations is the main cause of gold mineralization (e.g., Lin, 1993; Lin et al., 1993a, b). Theoretically, oilfield

brine, which contains dissolved hydrocarbons and soluble organic acids, could be very important for Au leaching and transportation. However, the partition coefficient of Au between crude oil and oil field brine is very high; almost all of the gold is concentrated in the crude oil (Lu and Zhuang, 1996). The high partition coefficient between oil and brine will make the brine less potential for Au transportation. Gold dissolved in crude oil is mainly concentrated in the bituminous fractions that are easily retarded during oil migration. Experiments on the interaction between crude oil and gold-bearing aqueous solution show that under neutral to acidic conditions, most of the gold was extracted by the oil phase, and more than 90% of the Au partitions into bituminous constituents (Lin et al., 1993b; Liu et al., 1993; Lu and Zhunag, 1996). Natural asphalt samples from Italy contain up to 1 ppm gold (Colombo et al., 1964). Gold contents of the bulk bitumen from the hot-spring deposit at Cherry Hill, California, range from 0.28 ppm to 37 ppm (Pearcy and Burruss, 1993). Therefore, the Cherry Hill bitumen is enriched some 10^2~10^4 times relative to maximum values in crude oils and asphalt.

Chakhmakhchev et al. (1985) analyzed 50 specimens of chloroform bitumoid extracted from rocks of the Triassic and Jurassic age, and also 16 specimens of oils from productive strata of the same ages in the East Caucasus foothills. The oils from the productive strata in the Prikum-Sukhokum zone of the East Caucasus foothills show almost the same geochemical signature as bitumens from the rocks of the Jurassic and Triassic Periods, suggesting that the oils are syngenetic with the rocks. This means that the oil had not traveled large distances either vertically or laterally. The bitumoid, both syngenetic (high in Corg and having low bitumoid yields) or epigenetic (low in Corg but with fairly

high bitumoid yields, light, oily and mobile, and considered to be migrated or para-autochtonous), are enriched in Au (190 ~370 ppm and 30~50 ppm for the bitumoid in Jurassic and Triassic strata, respectively) more than 10^2 times that of the crude oils (Chakhmakhchev et al., 1985, table 5-10).

Table 5-10 Gold contents of bitumoid and oils from productive strata of Caucasus foothills

	Bitumoid				Petroleum	
	Syngenetic		Para-autochthonous			
Average	Jurassic	Triassic	Jurassic	Triassic	Jurassic	Triassic
Au (ppm)	370	30	190	50	0.34	0.08

From: Chakhmakhchev et al., 1985.

Bitumens have diverse origins. They may be diagenetic products that are generated pre-oil window, residues of migrating petroleum, and distillates around igneous intrusions or organic precipitates from hydrothermal fluids. The distinction between these types is important because bitumens of different origins have different opportunities to interact with and take up metals. The mere occurrence of bitumens within an ore deposit is not a guarantee that they have a hydrothermal origin. They could represent petroleum migration into the fracture porosity of a pre-existing hydrothermal system. On the other hand, in most cases of SHDG deposits, the hydrothermal fluid tends to follow the pre-existing bitumen veins. The bitumen samples not associated with ore minerals are possibly of diagenetic origin, deposited at lower temperatures than those in hydrothermal deposits, often with a lower degree of thermal maturation.

The origin of the metal enrichments in bitumen is a consideration if the metal were transported with the migrating hydrocarbons or adsorbed by the hydrocarbon/bitumen in situ. Many different factors, besides source rock, may contribute to metal concentrations in

bitumens. Enhanced metal concentration may occur when metals are leached from minerals along brine-petroleum migration pathways, and new minerals may be produced as small crystals, chemically reduced by bitumen from aqueous solutions and then carried along suspended in the oil, to become entrapped in organic matter. Conversely, loss of organometallic components during migration will also affect metal concentrations (Parnell, 1992; Mossman et al., 1993). Hydrothermal solutions encountering migrating hydrocarbons may contribute to the genesis of various metals. Clearly, bitumen plays a significant role in metallogeny, although the specific processes of concentration are not well understood.

While bitumen may serve as a convenient reductant for metals, migrating bitumens are accompanied in many instances by aqueous fluids, which govern to a large extent the type and amount of minerals that develops. The role of bitumen in mineralization goes far beyond the passive provision of a convenient reductant. Highly anomalous concentrations of elements (e.g., V, Pt, Au, U and Ni) occur in solid bitumens, and numerous minerals develop authigenically in association with bitumens.

Metal enrichments in solid bitumens from different occurrences have been reviewed by Parnell (1988). Metals which occur as an intrinsic component of bitumens could have been either (a) inherited from the hydrocarbon source rock as organometallic complexes (Poplavko et al., 1978), (b) scavenged by migrating hydrocarbon-bearing fluids or (c) deposited in the bitumens at the site of mixing of metal-bearing and hydrocarbon-bearing fluids. Ore mineral inclusions within solid bitumens have been observed by many researchers. The metal enrichments in solid bitumen can clearly be much higher than in petroleum or oilfield brines, especially if the bitumens contain mineral inclusions.

Crude oils do contain mineral matter, which could be transported within the oil where the mineral inclusions are smaller than the pore spaces through which the oils pass, which is the case in fractured rocks. Oils passed through 5μm filters leave a residue (Curiale, 1987), indicating the presence of particles above this size. Au contents in bitumen samples from Carlin-type deposits vary within a wide range, and this may be due to the micro mineral inclusions either in the forms of fine-grained auriferous pyrite or submicron or colloidal metal gold. In addition, metals that are normally transported under oxidizing conditions and do not reach high levels in petroleum, such as uranium, may be highly enriched within bitumens. Some elements, such as lead and antimony, may be almost entirely restricted to mineral inclusions as opposed to organometallic complexes. Unlike other metals (Ti, V, Cr, Mn, Fe, Co, Ni, Zn, Se, Rb, Sr, Ag, Sb, Cs, Ba, Hf, Ta, W, Hg, Th and U), As, Pt, Pd and Au, were found to be more concentrated in the derived bitumen matter than in stratiform kerogens in Elliot Lake organic matter (Mossman et al., 1993). This may hint that during the maturation of kerogens in the sedimentary rocks the noble metals are prone to concentrate in movable phases produced by kerogen hydrous pyrolysis, and thus contribute to the remobilization and migration of the metals within the source beds. Thus, bitumen may play an important role in noble metals (Au, Pt, Pd) transportation under low temperature environments. However, Parnell (1992) reported that the bitumens obtained from ore deposits contain significant proportions of ore mineral inclusions, whereas the bitumens unassociated with mineral inclusions, bear no metallic signature at all. The migration of noble metals along with the bitumens perhaps is limited to an insignificant distance due to filtration effects.

The metal contents of bitumens are, therefore, not a guide to the role of petroleum as a transporting agent for the metals. On the contrary, the metal enrichments are in some cases due to the reductive properties of organic materials, which would make transport in petroleum impossible. The interception of migrating hydrocarbons by metal-rich groundwater, rather than hydrocarbon/metal co-transport, is probably responsible for a substantial number of metalliferous hydrocarbon occurrences.

To clarify the question of the potential of petroleum to act as a major Au carrier for SHDG mineralization, we must focus on two factors. Firstly, Au ions or elemental Au will partition differently between different fractions of petroleum during migration and within the reservoir. Secondly, the Au ions or elemental Au that previously was bound into the bituminous fraction will be released into oilfield brines (which are enriched in organic acids) during the maturation of the crude oil. Only if these two factors exist, can the Au be transported and released into the oilfield brine and participate in the ore-forming processes. In light of the observations of authigenic minerals in solid bitumens (e.g., Parnell et al., 1994), it is less likely that metals will be able to be released into the brine and contribute to the mineralization processes directly. It is possible that the Au in oil cannot be removed either during migration or in the reservoir; therefore, SHDG mineralization and oil accumulation may be two separate processes.

5.2.3. Potential contribution of organic acids in oilfield brine

Oil field brines are known to be rich in dissolved organic anions, especially acetate. Several authors have speculated on their potential as complexing agents for the transport of

base metals (Gardner, 1974; Giordano, 1985; Carothers and Kharaka, 1978; Fisher, 1987; Hennet et al., 1988; MacGowan and Surdam, 1988). Although the concentration of organic acids in some oil field waters is low or nil, analytical concentrations of up to ~10 000 ppm acetate have been reported in others, together with as much as ~4 400 ppm propanoate, ~2 500 ppm molonate (propandioate), ~700 ppm butanoate, ~500 ppm oxalate, ~400 ppm pentanoate, and ~100 ppm each of hexanoate and heptanoate, along with lesser concentrations of many other organic anions (Hennet et al., 1988). The presence of carboxylic acid anions in oil field waters is generally attributed to the thermal maturation of kerogen. Alternatively, they may be produced in relatively shallow hydrocarbon reservoirs during water washing and degradation of paraffin by sulfate-reducing and other bacteria that thrive at the oil-water interface. Also, they may be generated at the oil-water interface in deeper reservoirs by the hydrolytic disproportionation of hydrocarbons in petroleum, which generally favors dissolution of carbonate and detrital silicates by lowering the pH of the aqueous phase. Organic species in subsurface waters form strong complexes with dissolved cations, especially Ca, Mg, Fe and Al (Kharaka, 1997). An infrared spectroscopy investigation of organic fractions extracted from the Cheleken brines shows that the extractive and sorptive properties of Au and Hg are determined by their interaction with naphthenic acids (Myakon'kiy and Dmitriyev, 1991).

The solubility of the different petroleum compounds of different molecular weight and of different type varies considerably in water. The solubility decreases with increasing carbon number, but the long-chain hydrocarbon molecules are relatively more soluble than would be expected from an extrapolation of the solubilities of the lower members of the

series. The solubilities measured ranged from about 100 to less than 0.1 ppm in C_4-C_{10} range and below 0.01 ppm in the C_{12}-C_{30} range (McAuliffe, 1980). In the case of the higher n-alkanes, Millipore filtration (50 nm = 500 Å pore size) reduced the n-alkane content of the accommodated n-alkanes as much as 97% (Peake and Hodgson, 1966).

The solubilities of oils are in the range of several up to 100 ppm below 100°C, but increase up to 100 ppm or more between 100 and 200°C. The more insoluble higher boiling point compounds increase their solubility with increasing temperature at a far greater rate than the more soluble lower boiling compounds. The presence of heteroatoms (N, S, O) on a hydrocarbon molecule drastically increases its solubility in water. Salinity increases were found to considerably decrease the solubilities of hydrocarbons (Price, 1976).

Thermodynamic calculations indicate that the oxidative solubilities in the presence of calcite of hydrocarbons are much greater than their stoichiometric counterparts at oxygen fugacities corresponding to those at the depths of sedimentary basins, which are as much as ~60 orders of magnitude lower than they are on the Earth's surface (Helgeson, 1992; Helgeson and Pokrovskii, 1992; Helgeson et al., 1993; Pokrovskii and Helgeson, 1994). In the presence of calcite, the oxidative solubilities resulting from the formation of aqueous CO_2, n-carboxylic acids, and other oxidized organic aqueous species from n-alkanes in crude oil are several orders of magnitude greater than their stoichiometric counterparts. The carbonate and carboxylate species in oilfield waters may be in metastable equilibrium with one another, and that normal alkanes in crude oil with carbon numbers (n) ranging from 1 to ~6-15 cannot be in equilibrium with both higher molecular weight hydrocarbons in the

crude oil and aqueous oxygen-bearing carbon species such as CO_2 and n-carboxylic acids in oilfield waters (Helgeson, 1991; Helgeson et al., 1993). In contrast, such metastable equilibrium states may be achieved for n-alkanes with carbon numbers greater than ~6-15, depending on the activity of aqueous CO_2. These observations have significant implications with respect to the development of secondary porosity during the maturation of crude oil at the oil-water interface in young dynamic basins in which extensive fluid flow occurs and oil and water are in pervasive contact (Helgeson et al., 1993).

Organic matter can influence the transport of ore-forming components by contributing to the transport potential of aqueous pore fluids, and by modifying their composition. Dissolution, transport, and precipitation processes, although poorly understood, hinge on the role of organic acids during hydrothermal disproportionation of petroleum under diagenetic conditions and subsequent fluid migration. One of the problems associated with assessing the role of organic anions in aqueous transport processes is that there may be species generated during catagenesis whose stability is low over periods of time appropriate for geological processes. Studies of natural oil field waters have shown that abundances decrease as aliphatic chain length increases beyond that of ethanoic (acetic) acid, and that the abundance of total acids decreases as a function of temperature (Pokrovskii and Helgeson, 1994).

In terms of transportation processes, which may take place over periods of geological time, there is no doubt that the role of acetic acid anions should be considered in low temperature solution modeling. However, the role of other organic anions is more difficult to assess, as it may involve short time periods prior to their decomposition. Two lines of

indirect evidence suggest that the role of organic anions may be greater than that suggested by the presence of acetic anions alone in present-day brines. First, there is abundant evidence that kerogen loses oxygen-bearing groups as maturity increases, as shown by a Van Krevelen type diagram; at least a proportion of these may contribute to a water soluble population of geologically unstable organic anions (Fig.5-7). Second, studies of the phenomena of secondary porosity in sandstones (Surdam et al., 1984, Surdam and MacGowan, 1987) provide abundant evidence for which organic anions are believed to be responsible. Neither the phenomenon of functional group removal from kerogen nor that of secondary porosity generation can be fully described at present in the absence of pertinent experimental data, but their potential for ore transport processes should not be ignored.

In general, organometallic complexing enhances the transport of metals in hydrocarbon-bearing fluids, and organic reduction enhances ore deposition. Organometallic complexes include compounds in which metallic cations are bonded to heteroatoms (including N, S, O) in a variety of structures, and poly-complexes associated with electrostatically polar functional groups such as carboxyl radicals (Yen, 1975). There are essentially three pathways through which organic matter can contribute to the ore-forming potential of waters and brines. First, dissolution during catagenesis and diagenesis will enable trace components of minerals (such as Pb from feldspars) to enter solution. Organic anions, whether long-lived or transient, may enhance this process, which includes secondary porosity. Second, petroleum liquids may lose base metals originally incorporated during their maturation, as a consequence of exchanges with coexisting aqueous pore fluids (such as Cu). Third, biological or thermal processes of petroleum degradation will

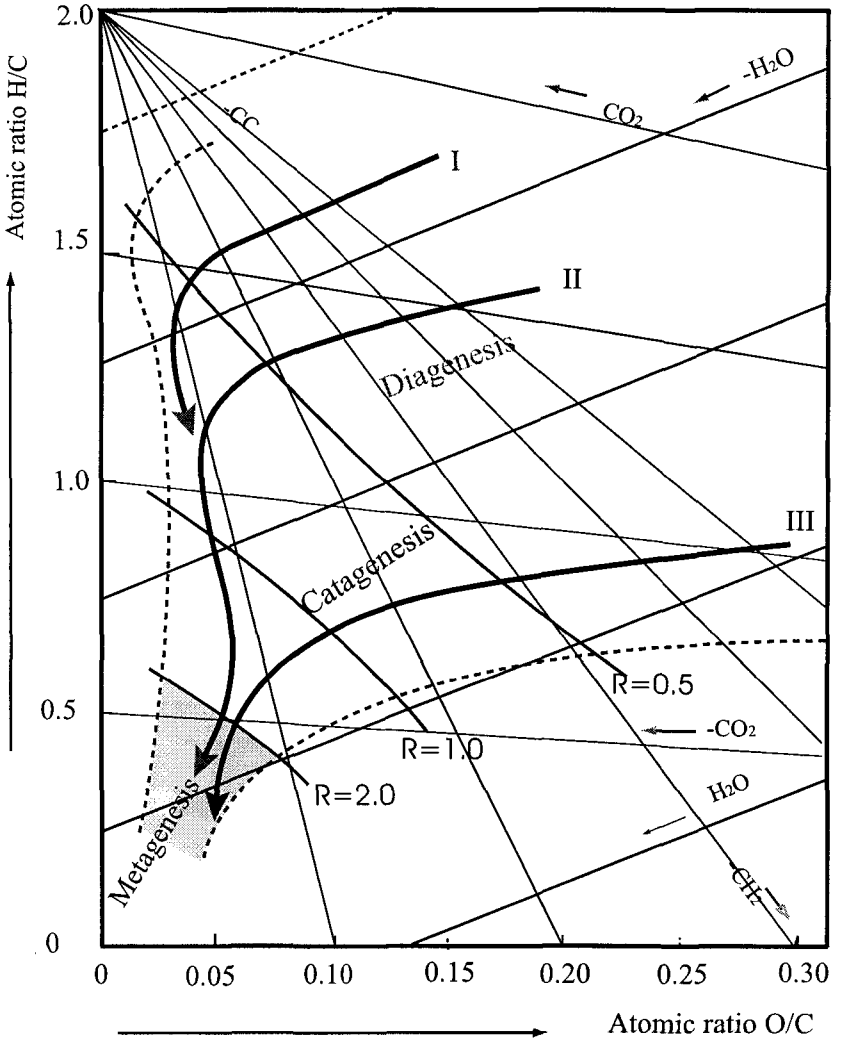

Fig. 5-7. General scheme of kerogen evolution from diagenesis to metagenesis in the Van Krevelen diagram.

R: Approximate iso-values of vitrinite reflectance

→ Evolution paths of the principal types of kerogen

(After Tissot and Welte, 1984.)

ultimately involve the destruction of the porphyrin complex and the release of elements such as V, Ni, and Co, as well as Cu and other constituents.

Despite the high concentration of carboxylic anions in oilfield brines, most of the organic (acidic) ligands form insoluble salts with calcium (or other cations) and thus limit their significance as complexing agents in Na-Ca-Cl rich natural hydrothermal brines. Experimental investigations show that the decarboxylation of acetic acid and acetate anions is catalyzed by a variety of mineral surfaces over a range of temperatures. Acetate can survive moderate hydrothermal temperatures (<300°C) long enough to promote the mobility of metals as acetate complexes (Palmer and Drummond, 1986; Drummond and Palmer, 1986; Bell et al., 1994). Water-soluble organic acids have been suggested as being important migrating ligands in some base metal transportation (Seward and Barnes, 1997), but gold solubility in acetate at 25°C is extremely low (Vlassopoulos et al., 1990), and Au solubility in carboxylic solutions under elevated temperatures is still unknown. It is possible that the soluble carboxylic and dissolved hydrocarbons might have increased Au solubility in the fluid, and this was checked experimentally in this study and will be discussed later.

5.2.4. Contributions of organic matter during hydrothermal processes

Following processes may play important role in hydrothermal ore-forming processes: (1) bio- and abio-degradation (thermal maturation) of organic matter; (2) interaction between the mineralizing hydrothermal solutions, and the pre-existing degraded hydrocarbons and H_2S reservoir; (3) interaction between ore-forming fluids, hydrocarbons

and H_2S produced in the thermal maturation caused by the heating of hydrothermal system; and (4) the biodegradation of organic matters induced by circulating meteoric waters (Bouabdellah et al.,1996; Dixon and Davidson, 1996; McGoldrick et al., 1996; Tritlla and Gardellach, 1997; Zentilli et al., 1997). Geological and geochemical evidence show that the ore deposition of SHDG and other strata-bound base metal deposits occurs under reducing environments. Sulfate reduction, through either biodegradation or abio-degradation, plays an important role in the ore-forming processes (Gize and Barnes, 1987; Leventhal, 1990; Henry et al., 1992; Disnar, 1996; Sicree and Barnes, 1996; Bechtel et al., 1998). Low temperature biological sulfate reduction and thermochemical sulfate reduction by organic matter, such as light hydrocarbon gases and organic acids, may be the immediate source of the reduced sulfur in a number of sedimentary, strata-bound ore deposits (Berner, 1970; Barros and Deming, 1983; Trudinger at al., 1985; Krouse et al., 1988; Dixon and Davidson, 1996).

There is a significant structural control on the localization of ore zones in SHDG deposits, consisting of both folds and faults (Arehart, 1996; Tu, 1996). Most of the SHDG mineralization in southwest Guizhou occurs around anticlines or domes that are also the known ancient oil traps. The Lannigou, Getang and Zimudang deposit all occur around anticlines, and the ore bodies are confined within the faults cutting the anticlines. Fold crests may have trapped or inhibited movement of ore fluids, or acted as a release point for overpressured hydrothermal fluids, all of which could have resulted in ore deposition. These same fold crests (and gold ores) typically contain a significant amount of mature

hydrocarbon material. In a regional sense, SHDG deposits are often associated with organic rich rocks.

The SHDG or Carlin-type gold deposits in southwest of China and northern Nevada, U.S.A., all contain carbonaceous matter, and many of the ore bodies were formed right in fossil oil reservoirs. The structural similarity and the presence of degraded hydrocarbons in SHDG deposits suggest that these fold culminations are paleo-hydrocarbon traps. An anticline-trapping model for gold-bearing hydrothermal fluids akin to hydrocarbon structural trapping can account for the anticline, SHDG deposit, and hydrocarbon association (Presnell, 1993).

Organic material is not a major constituent of most naturally occurring hydrothermal fluids, but the ability of some organic ligands to form strong complexes with metals makes them attractive as transporting agents for ore-forming metals. The association between gold and organic matter has been described in a variety of hydrothermal ore deposits (Wood, 1996). Four factors may restrict the effectiveness of any one organic complex as hydrothermal ore-transporting agent. First, the organic ligand must persist without serious degradation (e.g., decarboxylation) at elevated temperatures during extraction of the metals from source rocks, as well as during hydrothermal transport. Second, the organic ligand must be present at high enough concentrations to provide the minimum solubility necessary for the metal migration. Third, the organic ligand must not form insoluble salts (like oxalic acid) with competing "hard" ions, such as, Ca^{2+}, Mg^{2}+, Fe^{2+}, Al^{3+}, or easily be adsorbed to mineral surfaces. Fourth, the metal-organic complex must be sufficiently stable so that

metal solubility is above the minimum necessary for concentrating the metal into ore bodies.

Oil field brines have been proposed as possible ore-forming fluids for the Mississippi Valley-type mineral deposits by numerous authors (e.g., Billings et al, 1969; Carpenter et al, 1974; Manning, 1986; Sverjensky, 1984, 1987). Similarly, the oil field brine might constitute part of the ore-forming hydrothermal solution of SHDG mineralization; the organic matter in the oil field brine may also contribute to Au transportation.

In order to assess the role of organic matter in the transport of ore metals within the aqueous phase, it is necessary to consider the possible significance of the organic anions that might be present. Some of the organic anions (notably ethanoic, propanoic) are second only to chloride in their potential abundance. These species, at least, should therefore be considered in models for complexing behavior within postulated ore-forming field brines. However, there are some conundrums here: (1) unlike mercury, which mainly occurs in the lighter fractions of crude oil (Chakhmakhchev at al., 1981), about 98% of the ¸petroleum gold exists in the bituminous fraction, and gold solubility in crude oil decreases sharply when temperature increases to about 90°C, the enrichment of gold in bitumen, through adsorption and reduction due to the reductive properties of organic materials, could make transport in petroleum impossible (Parnell, 1988; Liu et al., 1994b); (2) even though as much as 8ppm of gold in petroleum was reported (Chakhmakhchev et al., 1985), the average gold content in petroleum is only 1ppb, with a range of 0 to 3 ppb (Barwise and Whitehead, 1983), and the high concentrations of Au might be due to fertilization through interaction of hydrothermal fluids during the secondary migration or in the reservoirs; (3)

experimental results show that, during the migration of crude oil through a water-wet silt column, the polar sulfur compounds related to the heavy fraction are readily adsorbed during migration (Greibrokk et al., 1994).

During the migration of crude oil, the minerals of the pore walls and their associated bound pore waters present a polar surface, adsorb the more polar constituents and lead to a relative decrease in concentration of polar hydrocarbons, a process often termed geochromatography (Killops and Killops, 1993). This will limit the capability of crude oil as a gold transporting agent during primary and secondary petroleum migration because gold is mainly complexed on S-groups.

Gaseous phase gold organic complexes might also be a possible form of gold migration for low temperature hydrothermal mineralization. Since most of the Au-organic complexes are stable at low temperature, especially lower than 150°C, some of them are stable beyond 200°C. It is worthy to note that a few Au-organic complexes have melting points lower than 200°C, and decomposition points up to 300°C; those complexes are rather volatile and can exist as gases (Cotton and Wilkinson, 1972; Stein et al., 1981; Li et al., 1996).

The possible genetic association between petroleum accumulations and strata-bounded deposits was first advocated by Tu and co-workers, and the major similarities and differences between deposits of the two categories were summarized in the book **Geochemistry of strata-bounded deposits in China** (Tu, 1996). Rasmussen and Buich (2000) reported that pyrobitumen and oil inclusions were discovered in an Early Archean

(ca. 3 235 Ma) deep-sea volcanogenic massive sulfide deposit in the Pilbara Craton of Australia. The oil occurs in fluid inclusions within hydrothermal barite, and pyrobitumen is inter-grown with polymetallic sulfides. Petrographic textures show that oil was emplaced and thermally altered (coked) before late-stage sulfide mineralization. The results demonstrate that sub-seafloor hydrothermal petroleum generation was active during the Early Archean and contributed to the composition of the hydrothermal fluids, and likewise may have acted as a source of metals. It is conceivable that some of the sulfur in the mineralization was derived by thermogenic (hydrothermal) reduction of sulfate using hydrocarbons as a reductant, whereas, some of the sulfur was directly derived from the oil. Whether hydrocarbons were responsible for localizing metal precipitation is, however, unclear. It is possible that some of the sulfur was directly derived from the oil (c.f., Kesler et al. 1994b), because many oils contain several percents sulfur.

Free oil was observed in the Carlin-type gold ore-bodies of Yankee basins, in the Alligator Ridge district of northeastern Nevada (Hulen and Collister, 1999). The liquid hydrocarbons occur as (1) primary and secondary fluid inclusions in calcite ± realgar vein networks encircling the orebodies; (2) vug- and fracture- filling free oil proximal to the orebodies in scattered, residual pods and lenses of unoxidized, basal pilot limestones. The fluid inclusions and free oils are geochemically equivalent and have similar thermal maturities (early to peak oil-generation stage). The timing of entrapment of the fluid-inclusion oils is paragenetically constrained as dominantly pre-mineral and syn-mineral. Associated free oil could have arrived at any time prior to, during, or after mineralization. Oil migration appears to have taken place during both burial diagenesis and later circulation

of the Yankee hydrothermal system. However, it must be admitted that even if the oil-bearing calcite veins are hydrothermal, the oil trapped in them could have been preconcentrated in the Yankee basin rocks during Mesozoic burial diagenesis. The Yankee basin free oil is apparently younger than spatially and genetically associated fluid-inclusion oil; the former coats the calcite containing the inclusions. Since the two types have a similar geochemistry and biomarker, they could have accumulated nearly contemporaneously.

In conclusion, the partition coefficient between crude oil and oilfield brine is very high, almost all of the gold is concentrated in the crude oil rather than brines. Furthermore, Au in oil mainly exists in the bituminous fraction; thus, the thermal degradation will not alter Au distribution in oil significantly. The released Au would preferentially be relocated into the heavier remains of the oil. It is clear that the oil production and accumulation alone will not result in Au migration and deposition that would be meaningful for SHDG mineralization.

Oxidation of organic compounds with aqueous sulfate may contribute to gold deposition processes. Any inorganic-soluble sulfur species of valences below +6 can serve as the initiator of the reaction (Toland, 1960). The ability of sulfates to reduce to polysulfides or free sulfur through initiation by sulfur species of lower valence may well have geological significance, even though the reaction rate can be very slow at lower temperatures. The role of organic acids in the abiogenic reduction of sulfate and the sulfur isotope effect was also investigated by Kiyosu and Krouse (1990). Sulfate becomes progressively enriched in ^{34}S with the decreasing concentration of the sulfate.

5.3. Experiment study of organic matter contributions to gold solubility in hydrothermal solution

Since SHDG deposits in southwest Guizhou were often found to be associated with organic matter, ancient oil traps and hydrocarbon migration were recognized, it is reasonable to infer that the organic matter in the host rocks and in the adjacent reservoir may have contributed to gold leaching and transportation. The available data on gold solubility in crude oil was determined without considering the possible effects of solid organic matter and sulfides in the geological environment (Liu et al., 1993; Lu and Zhuang, 1996). To investigate the possible effects of organic matter in the source rocks on gold solubility in hydrothermal solutions, a simulation experiment was carried out. Pyrite, lignite and siltstone (which is a common host rock for SHDG deposit) and crude oil were included in the experiment for the purpose of getting some general ideas on gold solubility in natural geological system.

In order to avoid masking the organic matter transformation during its reaction with gold, a substrate with a certain degree of evolution in the course of natural diagenesis was chosen, namely lignite from Yushou, Yunnan Province, with ~0.5% vitrinite reflectance. The lignite is low in sulfides and Au content, which is convenient for processing and interpretation of results. The lignite was initially purified by Soxhlet extraction with dichloromethane (CH_2Cl_2) for three days, in order to remove the soluble organic matter. Heavy fractions—essentially pyrite—were separated by decantation in carbon tetrachloride (CCl_4). The lignite was then washed by dichloromethane and ethanol to remove the

remaining carbon tetrachloride, and the 60 to 100-mesh fraction was finally used for the experiment.

Pyrite was hand picked with grain sizes ranging from 80 to 130 mesh, cleaned in an ultrasonic bath with 2 M HCl for five minutes, and finally rinsed with distilled water and dried at ambient temperature. Twenty two long-necked hard glass tubes were cleaned and dried; to each was added 100 mg of pyrite, then 10 ml distilled water, and finally 1 mg Au in the form of $KAuCl_4$. After three days, the color of the solutions changed from golden yellow to colorless. The solutions in the tubes were analyzed by AAS (atomic absorption spectroscopy), and it was found that the gold concentrations were lower than 10 ppb. The clear solutions in the upper part of tubes were then discarded, and air-dried for later use. Observation of the pyrite under scanning electron microscopy showed that spherical gold had precipitated on the surfaces of the pyrite grains, similar to that was observed by Möller and Kersten (1994).

A low maturated and sulfur-rich crude oil from the Jianghan oilfield was chosen for the experiment. Its low maturation might be more representative to the characteristics of oil at secondary migration stage and, thus, make it possible for us to discuss the contribution of oil migration on the leaching of gold from the source rocks, and also to compare the present result with previous ones using the same crude oil (Liu, et al., 1993). Siltstone used in the experiment was sampled from the Lannigou deposit; it was crushed to 150 to 200 Meshes. The gold contents of the crude oil, siltstone, and pyrite used in the experiment are 4.1 ppb, 4 ppb, and 9.1 ppb respectively, while the gold contents in the lignite solutions is under the AAS detection limit (~ 0.1 ppb).

The 0.2 M NaCl+0.01M Na_2S reaction solution was prepared by dissolving spectroscopically pure NaCl and Na_2S reagents in double distilled water that had been boiled and cooled under an Ar atmosphere. Starting materials for A, B, C and D series experiments are 100 mg auriferous pyrite + 10 ml 0.2 M NaCl+0.01 M Na_2S solution; 100 mg auriferous pyrite +100 mg siltstone + 10 ml 0.2 M NaCl+0.01 M Na_2S solution; 100 mg auriferous pyrite +100 mg lignite + 10 ml 0.2 M NaCl+0.01M Na_2S solution; and 100 mg auriferous pyrite +50 mg lignite + 50 mg siltstone + 10 ml 0.2 M NaCl+0.01 M Na_2S solution respectively. These were to evaluate the possible contribution of siltstone and lignite on the gold solubility in sulfide solution. The tubes were then sealed under an argon atmosphere and placed in a thermostat-controlled water bath at 80°C for periods of 3, 6, 9 and 14 days. After the completion of the reactions, the tubes were taken out and opened, where H_2S gas could be smelled. The solutions were filtered and sampled directly, and analyzed for gold concentration by graphite furnace atomic absorption spectroscopy (PE 3100). The analytical sensitivity is higher than 0.1 ppb, and a relative error less than 15%. The pH of the solution was detected by PHS-2 acidometer at ambient temperature (~25°C), the Eh was not determined but based on the fact that H_2S escaped, it was rather reducing.

The experimental results show that gold solubility in bisulfide solution is rather low, usually lower than 10 ppb (Table 5-11). However, in the series D, with lignite and siltstone (clay minerals) in the system, gold solubility apparently increases. As gold solubility in sulfide solution is both pH and oxygen fugacity sensitive (e.g., Benning and Seward, 1996), and these were not well confined in this experiment, so the solubility variation can be the result of pH differences. However, the degradation of the lignite catalyzed by clay

Table 5-11. Gold solubility experiment on the contribution of the lignite and crude oil

Series	Starting material	Time duration			
		3days	6days	9days	14days
A	100mg auriferous pyrite+10ml (0.2M NaCl + 0.01M Na_2S)	6.2ppb	2.4ppb	14.6ppb	12.6ppb pH10.1
B	100mg auriferous pyrite+200mg siltstone +10ml (0.2M NaCl +0.01M Na_2S)	2.2ppb	5.4ppb	2.6ppb	7.2ppb pH11.4
C	100mg auriferous pyrite + 200mg lignite+10ml (0.2M NaCl +0.01M Na_2S)	2.8ppb	8.0ppb	4.8ppb	9.2ppb pH6.35
D	100mg auriferous pyrite + 100mg lignite + 100mg siltstone +10ml (0.2M NaCl + 0.01M Na_2S)	62.4ppb	54.6ppb	89.4ppb	89.6ppb pH7.64
E	100mg auriferous pyrite + 10g crude oil				470ppb
F	100mg auriferous pyrite + 10g crude oil + 100mg lignite				710ppb
G	100mg auriferous pyrite + 1g crude oil + 10ml (0.2M NaCl+0.01M Na_2S)				160ppb
H	100mg auriferous pyrite + 1g crude oil + 100mg lignite +10ml (0.2M NaCl+0.01M Na_2S)				260ppb
I	100mg auriferous pyrite + 1g crude oil + 100mg siltstone+10ml (0.2M NaCl+0.01M Na_2S)				38ppb
J	10ml (0.2M NaCl + 0.01M Na_2S)				pH10.20

minerals probably also has played an important role. The newly formed carboxylic acids and hydrocarbons may increase gold solubility of the solution. However, it is still not known whether the increased gold solubility is due to gold-organic complexation or to a reduction of the gold ions in the solution to form gold sol that was protected by the soluble organics.

The direct involvement of clays as natural catalysts to promote, at low temperatures, the transformation of dispersed organic matter into liquids and gaseous hydrocarbons has been the subject of increasing interest (Johns, 1979). Kerogen is a complex high molecular weight, organic and acid insoluble organic polymer. It has been established that as sediment and its dispersed organic matter are exposed to increasing temperature during burial in a subsiding basin, the organic matter is altered continuously. The idea of clay mineral catalysis is not new. Grim (1947) suggested that the clay minerals in shales concentrate organic constituents by sorption, and later act as catalysts in petroleum conversion. Kinetic studies of clay-organic reactions have demonstrated the effectiveness of clay and transit metals catalysis in organic acid decarboxylation and cracking reactions, and suggest that clays act as acid geocatalysts (Goldstein, 1982, 1983; Johns, 1982; Johns and McKallip, 1989; Li et al., 1998; Schoonen et al., 1998; Seewald et al., 2000).

Experiments with crude oil were also carried out, making it clear that crude oil can dissolve more gold than these inorganic solutions (Table 5-11). Series E, F, G, H, and I were designed to investigate the gold solubility in crude oil, oil-solution system and possible contribution of siltstone and lignite in the system. The fluid phase was filtered, the crude oil was rinsed by ethanol and benzene, while the benzene insoluble part was

discarded on the consideration that they will have difficulty to remove out of the pore system of the source rocks. The solutions were heated under 80°C to near dryness and then mixed with pure silica to decompose the organic matter. Analyses show that crude oil increases gold solubility in the whole liquid fraction (in ion or colloidal form). It is interesting to note that the lignite in the system (series F) also significantly increases Au solubility, but siltstone in the system lowered the gold solubility in the fluid. The gold solubility in crude oil reported by Lu and Zhuang (1996) is 487 ppb in the gold foil + crude oil system, it is similar to the present result of series E which produced a solubility of 470 ppb (at 150°C).

This experiment was a very preliminary one, and it created more questions than answers about organic contribution on gold solubility in organic matter bearing solutions. However, it suggests that organic matter may play an important role in gold leaching and transportation and is worthy of further investigation.

5.4. Conclusion

Organic matter is closely associated with SHDG mineralization. In a supergene environment, the complexing, adsorption and uptake of gold by organic matter might be important processes that control the enrichment of the gold in the host rocks during sedimentation and diagenesis. Also, humic acids may be important transport agents in supergene gold ore mineralization. In hydrothermal processes, crude oil is unlikely to have played an important role in gold transportation. However, organic acids produced by thermal maturation and decomposition of organic matter and colloidal, or molecular

dissolution of crude oil in fluid, might be significant for gold leaching and migration, which is worth further investigation. The high grade maturation of organic matter in the ores and the host rocks, as well as the higher maturation of organic matter in the mineralized host rocks relative to the unaltered rocks, show that oil formation (if it ever took place in the mining area) predates hydrothermal gold mineralization. Organic geochemical investigation of the Lannigou deposit shows that new hydrocarbons were brought in during ore forming hydrothermal processes from the adjacent host rocks or outside of the system. Hydrocarbons in hydrothermal solutions might have promoted Au migration. During the precipitation of gold, the light hydrocarbons that pre-existed in anticlines and domes might have contributed to thermal reduction of sulfate and thus the pyritization and gold precipitation.

6

DISCUSSION AND CONCLUSIONS

The three SHDG deposits, the Lannigou, Zimudang and Getang deposits, in southwest Guizhou Province investigated in this study represent three different mineralization types (Au-As- (Sb), Au-Hg- (Tl), and Au-Sb type, respectively) occurring in different sets of sedimentary rocks. The three deposits have a number of geological and geochemical characteristics in common, such as: similar ore mineral assemblages, alterations, association with organic matter, ore-forming conditions (T, P, pH...), etc. Based on trace element and organic geochemical investigations of the three deposits (with an emphasis on the Lannigou deposit), the source of the gold, the possible mechanism of gold transportation and deposition, and metallogenetic model are discussed as follows.

6.1. The source of the gold

Establishing the source (or sources) of gold in SHDG deposits is critical to understand the ore-forming mechanism and genetic modeling (Christensen, 1993). The SHDG deposits in southwest Guizhou were considered to be typical strata bound gold mineralization (Zhang et al., 1992; Han and Sheng, 1996; He, 1996). The source bed concept adopted to explain the stratigraphic control of the strata-bound deposits (Knight,

1957) proposes that most, if not all, of the ore-forming materials were derived from strata wherein the ore-forming materials had been contemporaneously deposited with other sedimentary components. Subsequently the ore-forming materials migrated an appreciable distance to form the orebodies. The sedimentary rock sequence as a reasonable source of gold is supported indirectly by the association, on a worldwide basis, of SHDG deposits with rocks of the Early Paleozoic to Jurassic and Cretaceous ages (Titley, 1991).

The Permian to Triassic sedimentary rocks host most of the SHDG deposits in southwest Guizhou. In the Permian to Triassic sedimentary rocks, deep water and turbidite sequences of shelf or slope environments commonly contain large amounts of volcanic sediment and the rocks are relatively enriched in gold which may be an important source of Au for the SHDG mineralization in the region. The ores are preferentially hosted by one or two lithological horizons in individual mining areas. The Lannigou deposit, which is hosted by gold rich Triassic turbidite (4~6ppb), is one example. However, the permeability of the strata is also critical for gold mineralization. The siltstone and sandstone in the region with relative high gold concentrations and moderate permeability may serve as source beds for the SHDG deposits. The widespread Permian basalt and basaltic tuff are also enriched in gold (~40ppb) and may have contributed to gold mineralization. The SHDG deposits are tectonically and lithologically controlled. Many orebodies are controlled by faults traversing a few strata of different ages and lithologies. In contrast to the favorable rocks like silty carbonates to calcareous siltstones and calcareous shales, igneous (dike and sill rocks) and clean carbonates or shales are generally less mineralized and can form barriers to fluid flow. For example, the orebodies in the Lannigou deposit are mainly hosted by the

Middle Triassic turbidite. In the Zimudang deposit, orebodies occur mainly in the impure carbonate and siltstone of Permian to Triassic in age. In the Getang deposit, the gold mineralization is limited to the breccia by the underlying pure carbonate and the capping carbonaceous shale over the ore bodies.

Some researchers advocate that the hydrothermal solution and part of the ore-forming material (gold) were derived from hidden and unidentified granitic plutons in southwest Guizhou (e.g., Yang and Dong, 1994), but geophysical reconnaissance and petroleum drilling in the region do not support this hypothesis. The small scale alkali ultramafic dikes and veins outcropping in Yinghe and Beicheng of Ceheng County, outside of the mining area, have been proposed as the main source for the metals in the SHDG deposits by some researchers, and these researchers have further advocated that the hydrothermal solution and the gold were all derived from the mantle (e.g., Liu et al., 1999). However, PGE data on the ores and pyrite from the Lannigou deposit are generally similar to the host rocks, even though the former are relatively enriched in Pd and Pt. The Pd/Ir ratios of the pyrite (which host most of the gold in the ores) are commonly less than 20, which are higher than those of the altered (2~9) and unaltered host rocks (~1). However, the Pd/Ir ratios of the pyrite are apparently lower than those of the ultramafic rocks (40~41) and the Emeishan basalt (~79). If the ultramafic rocks and/or the basaltic rocks were the major source of gold mineralization, much higher Pd/Ir ratios could be expected in the pyrite in response to a relatively higher Pd solubility. This suggests that the mantle rocks could not have been the major source of the gold mineralization; on the contrary, most of the gold was probably derived from the host rocks. A reconsideration of the limited lead isotope data of the

previous studies shows that Pb in some of the ores are less radiogenic than the sedimentary rocks, which infers possible lower crustal or mantle input. The linear distribution of the radiogenic isotope ratios as shown in Fig.4-11 also indicates more than one source may have contributed to the gold mineralization.

In conclusion, the gold in the southwest Guizhou SHDG deposits may have been derived from a large variety of sequences including the host rocks, the underlying strata, and volcanic rocks such as the basaltic rocks in the vicinity of gold mineralization. The small ultramafic intrusives emplaced during late Yanshanian extension, which probably contribute to the SHDG mineralization in the region, could not be the major source of hydrothermal solution and gold.

6.2. Possible mechanism of gold transportation

The behavior of gold in hydrothermal solutions is of considerable interest to economic geologists and hydrothermal geochemists. It is widely believed that Au(I) is the most stable oxidation state under most hydrothermal conditions (Seward, 1982). A wide range of anions such as HS^-, Cl^-, Br^-, I^-, $S_2O_3^{2-}$, SCN^-, CN^- and organic complexes can dissolve gold under laboratory conditions (Seward, 1993). Generally speaking, gold is soluble under acid, oxidizing conditions as a chloride complex (Gammons and Williams-Jones, 1995) or under near neutral reducing conditions as bisulfide complexes (Seward, 1973; Shenberger and Barnes, 1989; Benning and Seward, 1996). Chloride and sulfide ligands are abundant in nature and sufficiently stable to account for gold transport and deposition over the temperature range 150~350°C. Indeed, it is widely accepted that gold in

low temperature and mesothermal hydrothermal systems is transported as a bisulfide complex. $AuHS^0$ is the dominant aurous-hydrosulfide complex over a wide range of temperatures and pressures in reduced sulfur-containing hydrothermal solutions of low pH, and is thought to play an important role in the transportation and deposition of gold in ore depositing environments (Benning and Seward, 1996). Gold is highly soluble as $AuCl_2^-$ only in equilibrium with hematite or at high temperature (>300°C) (Shenberger and Barnes, 1989; Gammons and Williams-Jones, 1995). The mineral assemblage present in the SHDG deposits (Kaolinite – sericite – pyrite - organic matter ± arsenopyrite ± arsenic) also supports the conclusion that bisulfide complexes rather than chloride complexes are more likely inorganic agents for gold transport in the fluids ultimately responsible for the formation of SHDG deposits. In addition, the lack of significant base metals (which are transported normally as chloride complexes, e.g., Wood, 1987) and the relatively low salinity of fluid inclusions in SHDG deposits suggest that chloride transport was not operative.

In the SHDG ore-forming systems, organic matter is an ubiquitous component. The organic fluid inclusions were observed in the ores and 0.02 to 2.3% TOC contents were analyzed in the ores and host rocks of the three deposits under study. In the case of the Lannigou deposit where hydrothermal impact on the organic matter maturation is significant, hydrocarbons derived from the thermal maturation of the organic matter in the host rocks might have participated in the fluid system. But for the deposits like the Getang and the Zimudang within which the hydrothermal temperatures are lower than the thermal events recorded by the vitrinite, the hydrocarbons derived from the hydrothermal impact

maybe absent. However, regarding the common association of SHDG mineralization and the ancient oil traps in southwest Guizhou, organic matter can be a universal constituent of the ore-forming solution.

Under the influence of the organic matter, colloidal Au might play an important, even predominant role in gold transportation. The suggestion that colloidal forms are important in the formation of some gold deposits was considered early in the past century. Frondel (1938) conducted experiments showing that colloidal gold was stable up to 350°C when colloidal silica was present. Colloidal gold is ubiquitous in natural water and an important form in epithermal precious-mineral systems (Saunders, 1990; Vilks et al., 1998). Dissolution of gold colloids is to be expected if equilibrium is maintained between colloids and aqueous gold species. Therefore, under the influence of organic matter colloidal gold could have played an important role in the gold transportation.

Experiment on gold solubility carried out in this study shows that organic matter in solution significantly increases Au solubility, within which Au may occur either as gold sol protected by hydrocarbons or Au-organic complexes. The Au solubility of solutions increases dramatically (about 10 times) when organic matter (lignite) was added into the system, most probably due to the catalyzed maturation of the lignite leading to a newly formed organic matter in the solution. The intimate association of SHDG deposits and organic matter, especially the close spatial association with ancient and modern oil traps, are not casual. The brines entrapped in anticline traps rich in hydrocarbons and organic acids and/or organic compounds generated during the thermal process, must have contributed to the gold leaching and transportation during the ore-forming processes.

6.3. Mechanism of gold deposition

It is generally accepted that the deposition of gold could be affected by the destabilization of bisulfide complexes in a number of ways, including oxidation, reduction, and changes in pH and temperature (Arehart, 1996). Usually more than one mechanism is responsible for the formation of all of the observed features of SHDG deposits: the mechanisms involved in a change of the activity of sulfur or other dissolved species in solution, a change in oxygen fugacity, or a decrease in temperature.

Temperature decrease is a method of depositing jasperoid while dissolving calcite (Fournier, 1985, 1986). However, the stability constants for gold bisulfide complexes change very little with temperatures over the range 150~300°C and in fact may retrograde under some conditions (Seward, 1973; Shenberger and Barnes, 1989; Hayashi and Ohmoto, 1991). Therefore, for gold complexed as a bisulfide, temperature decreases alone are not very effective in depositing gold.

Reduction is a possible mechanism. Organic matter, by its reducing properties, may play a major role in the genesis of hydrothermal gold deposits: (1) by direct reduction of Au species in solution; or (2) indirectly through sulfides whose formation it affects (Gatellier and Disnar, 1989). Early studies (Hausen and Kerr, 1968; Raditke and Scheiner, 1970) suggest that organic matter plays an active role in gold deposition on the assumption of Au chloride complexes are the major contributors to gold solubility. Experiments on the interaction between Au bisulfide complexes and organic matter (lignite, sapromyxite) show that gold could be reduced to metallic gold (0.5 ~ 1.5μm) in the temperature range of 40 to

200°C (Hu et al., 1993). Carbon-rich units can cause fluid reduction and contribute to gold precipitation (Gatellier and Disnar, 1989; Phillips and Law, 1997). So, gold deposition can occur when the ore-forming fluids enter rocks containing reactive organic matter, in which the organic matter and the hydrocarbons derived from the thermal maturation of organic matter supply a reducing environment. In addition, mineral zoning in some large ore bodies is from arsenopyrite (more reduced) at the very center of the deposits to pyrite-realgar away from the center (more oxidized), and late stages of mineralization are characterized by the presence of barite (an oxidized phase) suggesting that the fluids increase in oxidation state through the time and space. Fluid inclusion results of the Lannigou, Getang and Zimudang deposits show that the deposits were formed under rather reducing (Eh= -0.41 ~ -0.54) conditions (Zhang and Zhang, 1999).

Oxidations across the sulfide-sulfate boundary (Fig.6-1) results in a sharp decrease in bisulfide concentrations and can be a particularly effective precipitation mechanism (Romberger, 1986). The paucity of gold in or associated with barite and abundant gold in arsenian pyrite indicate that gold deposition took place before the fluids were out of the pyrite stability field. On the other hand, the maximum solubility for gold bisulfide, which is below the sulfide-sulfate boundary, and the close spacing of the gold solubility contours suggest that nearly complete precipitation of dissolved gold can be caused by only slight changes in the oxygen fugacity while the system is still in the pyrite stability field.

Any ***pH change*** away from the H_2S-HS^- boundary should result in deposition of gold from bisulfide complexes because of the dependence of gold solubility on the activities of both H_2S and HS^-. However, gold solubilities below pH~5 may essentially be constant due

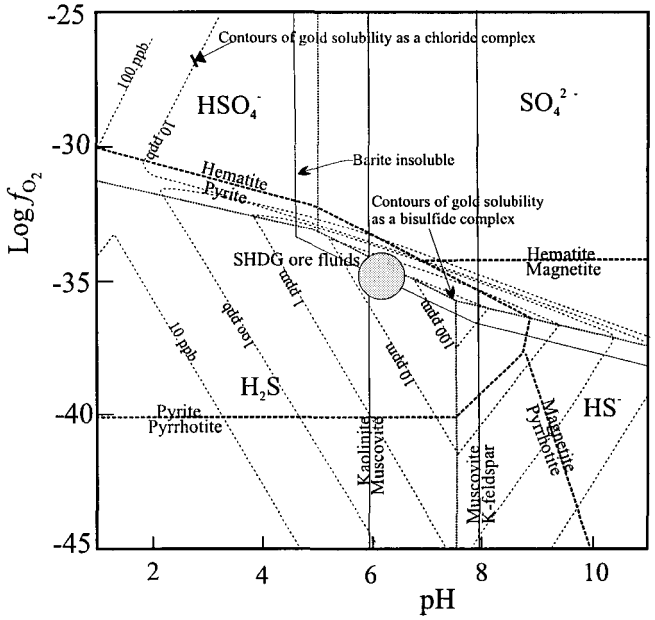

Fig. 6-1. f_{O_2} versus pH diagram showing stability fields of various minerals, aqueous sulfur species and gold solubility contours. T=250°C, ΣS=0.05 m/kg H_2O, $K^+=10^{-5}$ m/kgH_2O, Ba^{2+}=0.02 m/kgH_2O; barite soluble/insoluble assumed at $m_{Ba}m_{SO_4}=10^{-3}$. (After Arehart, 1996)

to the presence of a neutral gold bisulfide complex (Benning and Seward, 1996). If this is the case, little gold deposition will accompany a decrease in pH. Increasing pH, while effective in depositing gold, is incompatible with the observed alteration effects (calcite dissolution). In addition to the above considerations, pH changes are likely to have been buffered at near-neutral values by reactions such as sericite-K feldspar, magnetite-pyrite (at fixed oxygen fugacity) and carbonate equilibria. The pH values of the fluid inclusions in the Lannigou, Getang and Zimudang deposit range from 5.6 to 7.3, which is in the pH range of high Au-hydrosulfide stability (Benning and Seward, 1996). Therefore, changes in pH are unlikely to have been a major cause of ore deposition.

All the mechanisms discussed above are based on the assumption that gold precipitation happened when the hydrothermal fluid equilibrium was disturbed and became over saturated. However, it has also been known for some time that a solution component that is below bulk saturation can "precipitate" in the presence of a "surface". Chemical reactions at the mineral-water interface can influence or directly result in ore deposit formation. In addition, specific sorption and/or oxidation-reduction reactions can concentrate a metal solute as it passes through a host body. Newbury, Skey, and Wilkinson first showed this by plating out precious metals on various metal sulfide surfaces (see Skey, 1871, and Liversidge, 1893, for reviews of this research). Recently, extensive experimentation and spectroscopic measurements (Bancroft and Hyland, 1990) have shown that this phenomenon is driven by adsorption-reduction reactions at the sulfide-aqueous solution interface.

The reduction-adsorption of gold on pyrite surface during pyrite precipitation may be an important process which does not require the ore-forming fluid to have reached saturation with respect to gold (Hochella and White, 1990). Growth of pyrite during gold sorption may explain the common occurrence of invisible gold in pyrite, which is common in SHDG deposits. During pyritization, Au^+ was probably incorporated into pyrite by adsorption onto pyrite surfaces during crystal growth, rather than as a result of superimposition in the earlier stages of generation (Mironov et al., 1981; Simon et al., 1999). Growth of the particle during exposure to a gold solution could lead to a higher gold concentration, due to the substrate which continues to provide a new surface for Au sorption. Pyritization has been proposed to be an effective mechanism of gold precipitation from ore-forming solutions (Hofstra et al., 1991; Stenger et al., 1998a) on account of the decreasing H_2S fugacity of the solution (Kuehn and Rose, 1995). However, the association of SHDG deposits and organic matter, the spatial association of SHDG deposits with ancient and modern oil traps, and also the high $\delta^{34}S$ values of the auriferous pyrite all suggest this would not be the case. On the other hand, the association of gold deposition and pyritization may be due to the reduction-adsorption of gold on pyrite surface rather than the decreasing of H_2S fugacity. Indeed, the contribution of organic matter to Au deposition through thermal sulfate reduction is evidenced by: 1) the hydrothermal maturation of organic matter related to the alteration and gold mineralization (Ilchik et al., 1986), where light hydrocarbons can be powerful sulfate reductants in ore-forming processes; 2) the high content of CH_4 and H_2S in secondary fluid inclusions in the hydrocarbon stage and main gold ore stage (Kuehn and Rose, 1995); and 3) the SHRIMP

measured sulfur isotope composition (around 20 per mil) of the ore depositing fluids (Arehart et al., 1993b), which clearly resulted from thermal sulfate reduction (Ohmoto, 1986; Ohmoto and Goldhaber, 1997). The relationship between Au content S_2 parameter in the Lannigou deposit suggests that the potential of hydrocarbon production of the organic matter in the rocks was a controlling factor for gold deposition. Furthermore, the higher $\delta^{34}S$ values of the hydrothermal pyrite (the samples with small cores and large overgrowths) indicate that hydrocarbon reduction of sulfate may have been an important sulfur source for pyritization.

Surface complexation may be an alternative to the reduction-sorption mechanism, dissolved gold species simply exchanges one ligand for a surface group, without reduction of the gold ion. In solutions where the aqueous gold speciation is dominated by linear Au(I) complexes with soft ligands, such as CN^-, HS^-, and $S_2O_3^{2-}$ (Renders and Seward, 1989; Bancroft and Hyland, 1990), there is not necessarily a redox potential between solution and pyrite surface. Actually, in the absence of a redox potential difference, surface complexation is the only apparent sorption mechanism (Schoonen et al., 1992).

Although either a reductive sorption mechanism or a surface complexation mechanism is consistent with the observed sorption behavior, neither of the two mechanisms alone can explain the rapid removal of Au(0) colloids from solution. The removal of gold colloids may due either to direct uptake of the gold colloids or to dissolution and subsequent adsorption. The adsorption of sulfide minerals are apparent, especially pyrite (Zhu et al., 1998b). Gold colloids are usually negatively charged (Van Olphen, 1977; Enzweiller and Joekes, 1991) and are attracted to positively charged

surfaces. But, in natural circumstances, pyrite and other transition metal sulfides are also negatively charged (pHi.e.p ≈ 0.6 ~ 3.3, Bebie et al., 1998). So, the gold colloids are expected to show little or no interaction with sulfides. However, the electronic charges in the texture of sulfides are not evenly distributed and the interactions are not limited to static electronic, and what is more, chemical adsorption cannot be ignored. Submicroscopic metallic gold could also precipitate onto solid hydrocarbons and form fine-grained mixture (Kucha and Plimer, 1999).

Pyrite is the most important mineral hosting gold in the Lannigou, Getang and Zimudang deposits, and what is more, all the pyrite in the ores from the Lannigou deposit has found to be of p-type semiconductor. The semiconductivity of pyrite might have contributed to Au deposition. The experiment by Möller and Kersten (1994) shows that the amount of Au deposited at the cathodes (p-type part) exceeds that accumulating at the anodes (n-type part) (Fig. 6-2). Adsorption onto the surface of pyrite is apparently facilitated by arsenic, which causes pyrite, normally an n-type semiconductor, to become locally a p-type semiconductor. The p-type sites would have a stronger electrochemical interaction with negatively charged complex anions such as $Au(HS)_2^-$. The coatings of arsenian pyrite on pyrite could act like p-n junctions, which would have a strong electrostatic character and adsorption potential for gold due to different types of conductivity (Mironov et al., 1981; Möller and Kersten, 1994; Möller et al., 1997).

Adsorption of $Au(HS)_2^-$ and $Au(Hs)^0$ onto pyrite probably involves complexation reactions within which S^{2-} acts as donor ligand on the pyrite surface, forming a tri-atomic surface complex such as S_{py}-Au^+-$S_{sb}H$. Here Spy stands for sulfur from the donor ligand on

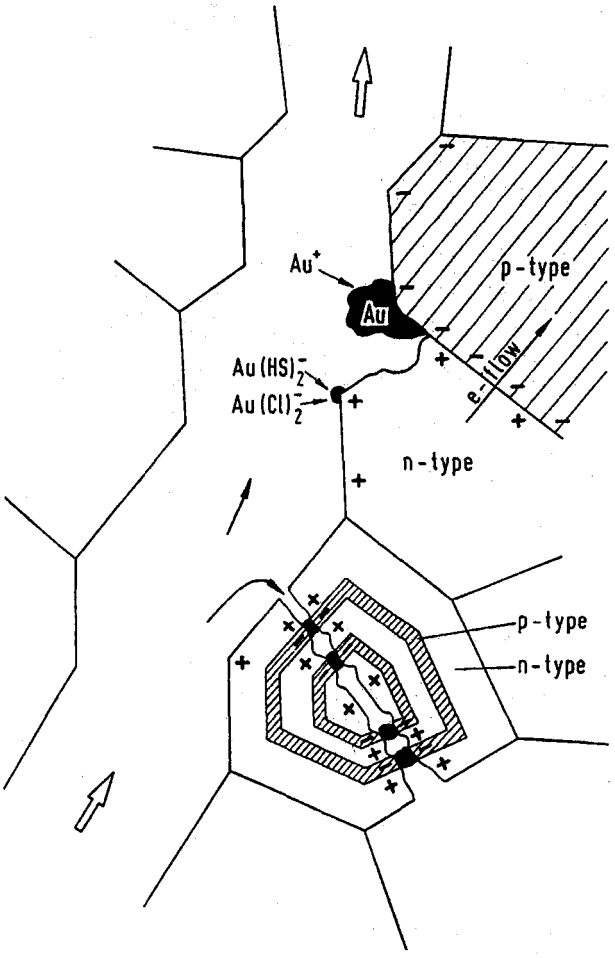

Fig.6-2. Electrochemical reactions of a gold-bearing fluid moving along a pore made up of n-type and p-type sulfides as well as fractured n- and p-type zoned crystals (Möller and Kersten, 1994).

pyrite surface and S_{sb} stands for sulfur form the gold-bisulfide complex in the hydrothermal solution. Chemical reduction of ionic gold to Au^0 usually follows adsorption of aqueous gold complexes on the surfaces of most sulfide minerals (Jean and Bancroft, 1985; Hyland and Bancroft, 1989; Starling et al., 1989; Eggleston and Hochella, 1991; Becker et al., 1997; Scaini et al., 1998).

To sum up, the mechanisms of gold deposition are very complex; these may include changes in oxygen fugacity, pH, Eh, temperature, and the activity of sulfide and other dissolved species in solution. Chemical reactions at the mineral-water interface could have played an important role in the gold precipitation. The reduction-adsorption and surface complexation of gold on (arsenian) pyrite surface during (arsenian) pyrite precipitation may be a predominant process, which does not require the ore-forming fluid to have reached saturation with respect to gold. The semiconductor nature of (arsenian) pyrite may significantly promote the surface reaction processes between Au and (arsenian) pyrite surfaces.

6.4. Metallogenetic model

Any model that purports to explain the ore-forming process for SHDG deposits must account for all of the observed features of these deposits. Primary among these are the paragenetic association of gold with sulfide minerals, major alteration features, including decarbonatization and silicification, fluid inclusions, and stable isotope data. On a large scale, the model must account for the age and tectonic environment of the deposits.

Carlin-type systems have been interpreted in terms of three modes of origin: metamorphic (release of fluid during regional thermal metamorphism), igneous related (circulation of magmatic or external fluids by igneous activity), or amagmatic (circulation of non-magmatic fluids during regional extension).

Models involving a regional metamorphic origin suggest that deep-seated, possibly mantle-derived magmatic activity preceded crustal extension and provided sufficient heat to generate and circulate the fluids required for deposit formation (Seedorf, 1991). This model suggests that H_2O and CO_2 in the hydrothermal fluid were derived from devolatilization reactions of subjacent metasedimentary rocks, with metals and sulfur being scavenged from this source as well. Igneous heat may be involved, but only in a regional sense. Derivation of sufficient H_2O from dehydration reactions to account for the known mineralization and the light δD values of the ore fluids is a major problem for this model.

The magmatic link model proposes that plutons simply provided the thermal energy necessary for focusing a hydrothermal system (Arehart et al., 1993c, Keuhn and Rose, 1995). In this case, gold is derived largely from sedimentary rocks, with little or no contribution from the pluton.

In models appealing to amagmatic origin, gold is thought to have been derived from sedimentary rocks during deep circulation of meteoric water driven by elevated geothermal gradients during extension (Hofstra, 1995, 1997; Ilchik and Barton, 1997). By systematically bringing hotter, more deeply buried rocks toward the surface, crustal thinning raises the geothermal gradient. Brittle faulting in the upper 10 km of the crust

increases secondary permeability. Consequently, by increasing the temperature gradient, the permeability, and possibly, the topographic relief, the likelihood of fluid circulation is greatly enhanced. Deep circulation of meteoric water leads to reactions with the variably reduced sedimentary rocks resulting in dilute silica- and sulfide-bearing solutions capable of scavenging gold but not base metals.

Fluid-inclusion, oxygen and hydrogen stable-isotope studies at the Carlin (Kuehn and Rose, 1995), Jerritt Canyon (Hofstra et al., 1991) and Alligator Ridge (Ilchik and Barton, 1997) deposits indicate that ore fluids were deeply circulating as evolved meteoric fluids. Models for these deposits suggest that fluids scavenged gold from rocks in the deeper parts of the convection cells, and then moved to shallower levels where they mixed with a cooler meteoric fluid, reacted with wall rocks, and precipitated gold. However, the genetic relationships between fluids and magmatism, metamorphism, and extensional tectonism remain enigmatic. Some models relate mineralization to a combination of regional calc-alkaline magmatism and extensional tectonism. Proposed heat sources include an enhanced geothermal gradient associated with extension (Ilchik and Barton, 1997) and igneous activity (Sillitoe an Bonham, 1990). This hypothesis, however, is not compelling for several reasons. Except for a few so-called Carlin-like deposits that show clear magmatic contribution (e.g., Zarshuran deposit in Iran, Asadi et al., 2000), most SHDG deposits lack demonstrable time-space links to intrusive centers. Neither do they show district-scale temperature or geochemical zoning features like those found in many porphyry-related precious metal deposits. The lack of nearby enrichments in base metals or silver makes it different to districts where gold-bearing jasperoids have igneous connections. Furthermore,

isotopic data indicates a predominantly sedimentary source for sulfur and a meteoric one for H_2O. However, nothing precludes igneous-driven circulation of meteoric fluids through the sedimentary section in districts with contemporaneous magmatism, provided that similar fluid composition and alteration are generated (Ilchik and Barton, 1997). Nevertheless, the large quantities of gold occurrences of similar type and age, and the widespread hydrothermal alteration strongly suggests the involvement of a major regional process in their formation, which is inconsistent with a more restricted distribution of known intrusives in north Nevada, U.S.A., and the lack of magmatic intrusives in the vicinity of the SHDG mineralization in southwest Guizhou.

The complete lack of igneous rocks associated with the SHDG deposits in southwest Guizhou suggests that the hydrothermal fluids were not derived from an igneous source. In the time range that can be related to the SHDG mineralization in the region, there is no metamorphism event recorded in the Devonian to Triassic rocks (Ministry of Geology and Mineral Resources, P. R. China, 1987; Wang et al., 1994a; Wang, 1996). The lack of silver and base metal enrichment and the notable association of antimony, mercury and thallium eliminate the potential of connate water or metamorphic water as main sources (Phillips et al., 1983; Mosier et al., 1986; Goldfarb et al., 1988). The geological and geochemical characteristics of the deposits show that only an amagmatic origin can account for the gold mineralization in the region. The SHDG mineralization in the region was initiated by the extension of the late Yanshanian orogeny that caused regional high geothermal gradients. Two different types of fluids, circulating meteoric water and formation water or brine sealed in ancient oil traps, were possibly involved in the mineralization process. The

hydrocarbons and organic acids in the brine would have significantly increased the potential of the fluid to leach and transport gold. Relatively abundant organic matter in the system may have controlled the redox condition of the fluid, leading to the dissolution of sulfates (barite) and thermal- (abio-) reduction of the sulfate as evidenced by the high $\delta^{34}S$ values in the auriferous pyrite. This abundant reduced sulfur made gold dissolution and transport by bisulfide complexes favorable. Metals commonly transported as chloride complexes were not mobilized. The mixing of the two fluids and the interaction with the host rocks resulted in decarbonatization, silicification, argillization and sulfidation, which might have disturbed the system and resulted in the oversaturation of Au and precipitation. However, colloidal gold can be important species in hydrothermal system when organic matter protects it. The mineral-water interface reactions, including surface complexation and reduction-adsorption must have played significant role in Au deposition.

Finally, a descriptive model of the SHDG deposits in the research region (Fig.6-3) can be proposed as follows:

Host rocks: siltstone, fine-grained sandstone, silty mudstone, and argillaceous limestone.

Gold sources: mixed sources ranging from deep crustal rocks, host rocks, to Permian basaltic rock.

Fluids: circulated meteoric water, organic bearing formation water or brine sealed in the traps.

Driving force: high geothermal gradient caused by late Yanshanian extension.

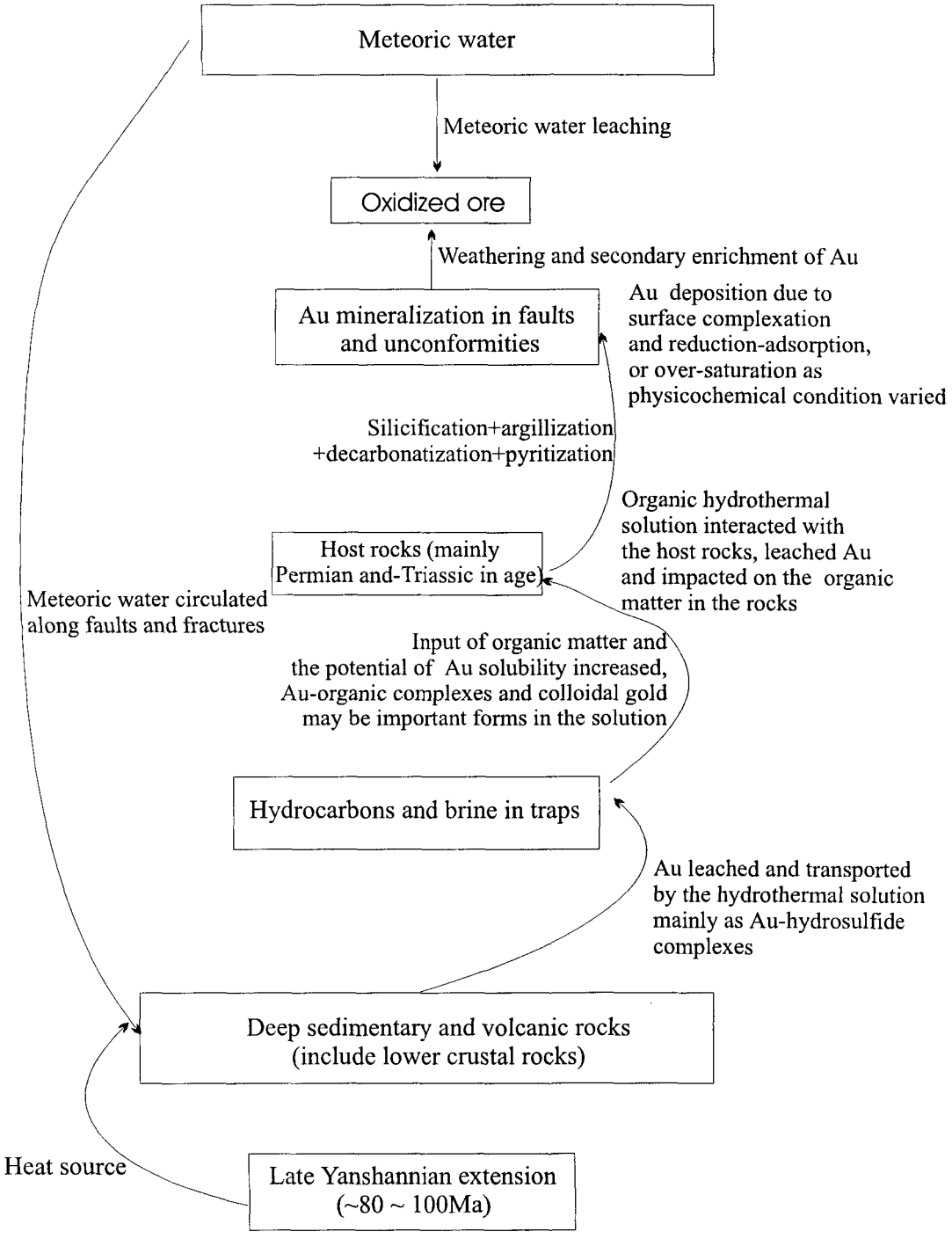

Fig.6-3. A schematic diagram showing the metallogenetic model of the SHDG mineralization in southwest Guizhou.

Age range: mainly ~100 Ma to 80 Ma corresponding to regional extension.

Depositional environment: rocks with higher permeability like turbidites formed in somewhat anoxic environments are preferential.

Tectonic settings: fault zones (including related unconformity and bedding faults) cut across anticlines or domes.

Mineralogy: native gold (submicron-sized) + (arsenian) pyrite + realgar + orpiment ± arsenopyrite ± cinnabar ± stibnite ± lorandite ± (native mercury, native arsenic) ± barite ± fluorite, quartz, calcite, carbonaceous matter.

Texture/structure: silica replacement of carbonate, generally less than 1 percent fine-grained sulfides disseminated in the altered host rocks.

Alteration: unoxidized ore: quartz + jasperoid + illite + kaolinite + calcite; oxidized ore: kaolinite + illite + goethite + jarosite ± scorodite.

Geochemical signature: Au + As + Hg + Sb + Tl.

6.5. CONCLUSIONS

1. High field strength elements, such as Nb, Ta, Zr, and Hf, were immobile during hydrothermal alteration in the Lannigou, Getang and Zimudang deposits. REE were mobile during the alteration, within which the LREE were depleted while HREE were enriched. PGE elements investigation of the ores, host rocks, basalt, and the ultramafic dikes which are roughly contemporaneous with gold

mineralization, show that the late Yanshanian ultramafic dikes were unlikely a major gold source. A mixed source, which may include host rocks, underlying crustal formation and the widespread Au rich basaltic rocks, can be inferred.

2. The SHDG deposits commonly occur around the anticlines or domes which host ancient hydrocarbon reservoirs. The organic matter in the host rock might have contributed to the gold pre-concentration and source bed formation. The generation and migration of crude oil in the study area apparently predated gold mineralization, and crude oil cannot be an important agent of gold transportation for the SHDG mineralization. However, hydrocarbons in the system clearly contributed to gold mineralization through thermal sulfate reduction.

3. The colloidal crude oil, hydrocarbons and organic acids in the solution could have greatly increased gold solubility as organic complexes, or protected gold colloidal solution. Except Au bisulfide complexes, Au colloidal solution likely played an important role in gold leaching and transportation.

4. The SHDG deposits in southwest Guizhou are amagmatic in origin. The Au was leached from host and the underlying rocks by circulated meteoric water heated by the high geothermal gradient caused by Late Yanshanian extension.

POSTSCRIPT

Southwest Guizhou is an undeveloped and poor area in China. The exploitation of the SHDG deposits have greatly improved the local economy. However, since the proportion of the oxidized ore in the SHDG mineral deposits in southwest Guizhou Province is smaller than in the U.S.A., most of this ore is mined by small companies and local farmers lacking funding and employing inefficient techniques. The primary ores are often considered refractory because much of the gold occurs as sub-micron grains in pyrite and marcasite and the ores contain high contents of organic matter. The organic matter makes gold extraction by cyanide solutions inefficient. As a result, it is a common practice for small companies in southwest Guizhou to utilize a roasting method to remove the organic carbon in the ores and thus increase the performance of cyanidation. Dust from open pit mining and effluent from the smelters will certainly deteriorate the down wind soils, waterways and vegetation. Although the acidic drainage could be mitigated by the widespread carbonate nearby, mining activities will increase the danger of poisoning metals exposure to local residents. The exploitation of these gold resources might create serious environmental inpacts to the fragile ecosystem of the karst area.

In conclusion, to ensure sustainable social and economic development, measures should be implemented to ensure environmental protection. Also, local authorities should be made aware and prodded to consider the potential environmental and social impacts of gold mining in the area.

REFERENCES

Alderton, D. H. M., Pearce, J. A., and Potts, P. J., 1980. Rare earth element mobility during granite alteration: evidence from southwest England. Earth and Planetary Science Letters, 49:149-165.

Arehart, G. B. 1996. Characteristic and origin of sediment-hosted disseminated gold deposits: a review. Ore geology reviews, 11:383-403.

Archart, G. B., Chryssoulis, S. L., and Kesler, S. E. 1993a. Gold and arsenic in iron sulfides from sediment-hosted disseminated gold deposits: Implications for depositional processes. Economic Geology, 88: 171-185.

Arehart, G. B., Eldridge, C. S., Chryssoulis, S. L., and Kesler, S. E. 1993b. Ion microprobe determination of sulfur isotope variations in iron sulfides from the Post/Betze sediment-hosted disseminated gold deposit, Nevada, USA. Geochimica et Cosmochimica Acta, 57: 1505~1519.

Arehart, G. B., Foland, K. A., Naeser, C. W., and Kestler, S. E. 1993c. $^{40}Ar/^{39}Ar$, K/Ar, and fission track geochronology of sediment-hosted disseminated gold deposits at Post/Betze, Carlin Trend, northeastern Nevada. Economic Geology, 88: 622~646.

Asadi, H. H., Voncken, J. H. L., Kühnel, R. A., and Hale, M. 2000. Petrography, mineralogy and geochemistry of the Zarshuran Carlin-like gold deposit, northwest Iran. Mineralium Deposita, 35: 656~671.

Bagby, W. C., and Berger, B. R. 1985. Geologic characteristics of sediment-hosted, disseminated precious-metal deposits of the west United States. Reviews in Economic Geology, 2: 169~202.

Bailey, E. H. 1959. Froth veins, formed by immiscible hydrothermal fluids, in mercury deposits, California. Geological Society of America Bulletin, 70(5): 661~663.

Baker, W. E. 1978. The role of humic acid in the transport of gold. Geochimica et Cosmochimica Acta, 42: 645~649.

Bancroft, G. M., and Hyland, M. M. 1990. Spectroscopic studies of adsorption/reduction reactions of aqueous metal complexes on sulphide surfaces. In: Mineral-Water Interface Geochemistry. Chapter 13. Edited by Hochella, M. F., and White, A. F. Mineralogical Society of America. Reviews in Mineralogy, 23: 511~ 558.

Banks, D.A., Yardley B.W.D., Campbell A.R., and Jarvis K.E. 1994. REE composition of an aqueous magmatic fluid: a fluid inclusion study from the Capitan Pluton, New Mexico, USA. Chemical Geology, 113(3-4): 259~272.

Bao Zhiwei, 1992. A geochemical study of the granitoid weathering crust in Southeast China. Geochimica, 2:166-174. (In Chinese).

Barnes, S. J., Naldrett, A. J., and Gorton, M. P. 1985. The origin of the fractionation of platinum-group elements in terrestrial magmas. Chemical Geology, 53: 303~323.

Barros, J. A., and Deming, J. W. 1983. Growth of "black smoker' bacteria at temperatures of at least 250°C. Nature (London), 303:423-426.

Barwise, A. J. G., and Whitchead, E. V. 1983. Fossil Fuel Metals. *In* The significance of trace elements in solving petrogenetic problems and controversies. *Edited by* Augustithis, S. S. , Theophrastus publications S. A. Athens Greece, 599-643.

Bau, M. 1991. Rare-earth element mobility during hydrothermal and metamorphic fluid-rock interation and the significance of the oxidation state of europium. Chemical Geology, 93: 219~230.

Bebié, J., Schoonen, M. A. A., Fuhrmann, M., and Strongin, D. R. 1998. Surface charge development on transition metal sulfides: An electrokinetic study. Geochimica et Cosmochimica Acta, 62(4): 633~642.

Becker, V., Hochella, M. F. Jr., and Vaughan, D. J. 1997. The adsorption of gold to galena surfaces. Calculation of adsorption/reduction energies, reaction mechanisms, XPS spectra, and STM images. Geochimica et Cosmochimica Acta, 61: 3565~3586.

Bechtel, A., Pervaz, M., and Puttmann, W. 1998. Role of organic matter and sulphate-reducing bacteria for metal sulphide precipitation in the Bahloul Formation at the Bou Grine Zn/Pb deposit (Tunisia). Chemical Geology, 144:1-21.

Bell, J. L. S., Palmer, D. A., Barnes, H. L., and Drummond, S. E. 1994. Thermal decomposition of acetate : catalysis by mineral surface. Geochimica et Cosmochimica Acta, 58: 4155~4177.

Benning, L. G., and Seward, T. M. 1996. Hydrosulphide complexing of Au(I) in hydrothermal solutions from 150-400°C and 500-1500bar. Geochimica et Cosmochimica Acta, 60: 1849~1871.

Bergeron, M., and Harrison, Y. 1989. *Le transport chimique de l'or dans les environnements de surface: formation d'un colloïde et complexation organique.* Canadian Journal of Earth Sciences, 26: 2327~2332.

Berner, R. A. 1970. Sedimentary pyrite formation. American Journal of Sciences, 268:1-23.

Bertrand, P., Pittion, J., and Bernaud, C. 1986. Fluorescence of sedimentary organic matter in relation to its chemical composition. Organic Geochemistry, 10: 641~ 647.

Bierlein, F.P., 1995. Rare-earth element geochemistry of clastic and chemical metasedimentary rocks associated with hydrothermal sulphide mineralisation in the Olary Block, South Australia. Chem. Geol., 122: 77-98.

Bierlein, F. P., Waldron, H. M., and Arne, D. C. 1999. Behaviour of rare earth and high strength elements during hydrothermal alteration of meta-turbidities associated with mesothermal gold mineralization in central Victoria, Australia. Journal of Geochemical Exploration, 67: 109~125.

Billings, G. K., Kesler, S. E., Jackson, S. A. 1969. Relation of zinc-rich formation waters, northern Alberta, to the Pine Point ore deposit. Economic Geology, 64(4): 385~391.

Blanc, P., Connan, J. 1994. Preservation, degradation, and destruction of trapped oil. The petroleum system; from source to trap. AAPG Memoir, 60: 237~247.

Bouabdellah, M., Heroux, Y., Brown, A. C. 1996. Pétrographie et altération de la matière organique du gisement de plomb-zinc-cuivre de Bddiane, district de Touissit; Bou Beker, Maroc nord oriental. Canadian Journal of Earth Sciences, 33(10): 1363~1374.

Bowell, R. J., Gize, A. P., and Foster, R. P. 1993. The role of fulvic acid in the supergene migration of gold in tropical rain forest soils. Geochimica et Cosmochimica Acta, 57: 4179~4190.

Bowles, J. F. W., Gize, A. P., Cowden, A. 1994. The mobility of the platinum-group elements in the soils of the Freetown Peninsula, Sierra Leone. The Canadian Mineralogist, 32: 957~967.

Bowen, H. J. M. 1966. Trace Elements in Biochemistry. Academic Press, New York. 241p.

Boynton, W. V. 1984. Geochemistry of the rare earth elements: meteorite studies. In: Henderson, P. (ed), Rare Earth Element Geochemistry. Elsevier, 63~114.

Brooks, R. R. 1972. Geobotany and biogeochemistry in mineral exploration. Harper & Row, New York. 290p.

Bureau of Geology and Mineral Resources of Guizhou Province. 1987. Regional geology of Guizhou Province. Geological Memoirs, series 1- Regional Geology, Ministry of Geology and Mineral Resources, P.R.C. Beijing, Geological Publishing House, 539~542.

Campbell, I.H., Lesher, C.M., Coad, P., Franklin, J.M., Gorton, M.P. and Thurston, P.C., 1984. Rare earth element mobility in alteration pipes below massive Cu-Zn-sulfide deposits. Chem. Geol., 45: 181-202.

Campbell, I. H., Naldrett, A. J., and Barnes, S. J. 1983. A model for the origin of the platinum-rich sulfide horizons in the Bushveld and Stillwater complexes. Journal of Petrology, 24: 133~165.

Cannon, R. S., Pierce, A. P., and Delevaux, M. H. 1963. Lead isotope variation with growth zoning in a galena crystal. Science, 142: 574~576.

Carothers, W. W., Kharaka, Y. K. 1978. Aliphatic acid anions in oil-field waters; implications for origin of natural gas. AAPG Bulletin, 62(12): 2441~2453.

Carpenter, A. B., Trout, M. L., Pickett, E. E. 1974. Preliminary Report on the Origin and Chemical Evolution of Lead-and Zinc-Rich Oil Field Brines in Central Mississippi. Economic Geology, 69(8): 1191~1206.

Casaceli, R. J., and Gemuts, I. 1985. Precious metal deposits related to continental extension. Global Tectonics and Metallogeny, 3(1): 7~8.

Chakhmakhchev, V. A., Kurganskaya, E. V., and Punanova, S. A. 1981. Distribution of trace elements in petroleum fractions. Geochemistry International, 18(1): 177~181.

Chakhmakhchev, V. A., Lositskaya, I. F., Punanova, S. A., and Semenova, R. A. 1985. Trace elements and porphyrins in the geochemical correlation of petroleum and bitumoids. Geochemistry International, 22(9): 1~6.

Chen Daiyan, Wang Hua, Ren Dayin. 1996. Some geochemical problems of ore-forming elements of titanium deposit host strata in southwestern Guizhou. Kuang Wu Xue Bao = Acta Mineralogica Sinica, 16 (3): 307~314. (In Chinese)

Chen Xu, Rong Jiayu, Rowley, D. B. et al. 1995. A comment on the early Mesozoic Banxi Group in south China. Geology Review, 41(5): 389~400. (In Chinese)

Cheng, Q-M, Hattoric, K, Fan, J-Z, Wang, S-C. 1992. Exploration history and geology of disseminated gold deposit at Maoling in Proterozoic sedimentary rocks in North China Platform. J. Geochemical Exploration, 51(1): 93~108.

Christensen, O. D. 1993. Carlin trend geologic overview. *In* Gold deposits of the Carlin Nevada. Edited by Christensen, O. D. Society of Economic Geologists Guidebook Series, 18: 12~26.

Clifton, C. G., Walters, C. C., Simoneit, B. R. T. 1990. Hydrothermal petroleums from Yellowstone National Park, Wyoming, U.S.A. Applied Geochemistry, 5(1-2): 169~191.

Cline, J. S., and Hofstra, A. A. 2000. Ore-fluid evolution at the Getchell Carlin-type gold deposit, Nevada, USA. European Journal of Mineralogy, 12; 195~212.

Cluer, J. K., Enkhtuvshin, K., and Robertshaw, P. 2000. Sedimentary rock-hosted gold mineralization at Zalaa Uul, Khentii Range, northeastern Mongolia. Mineralium Deposits, 35: 587~597.

Colombo, U. P., Sironi, G, Fasolo, G. R., Malvano, R. 1964. Systematic neutron activation tenchnique for the determination of trace metals in petroleum. Anal Chem, 36: 802~807.

Cotton, F. A. and Wilkinson, G. 1972. Advanced inorganic chemistry (3rd edition). New York-London-Sydney-Toronto: Inter-science Publishers, 1044~1055.

Courtillot, V., Jaupart, C., Manighetti, I., Tapponnier, P., Besse, J. 1999. On causal links between flood basalts and continental breakup. Earth and Planetary Science Letters, 166 (3-4): 177~195.

Crocket, J. H., and Kabir, A. 1987. PGE in Hawaiian basalt: implications of hydrothermal alteration on PGE mobility in volcanic fluids. In: Prichard, H. M.; Potts, Philip J.; Bowles, J. F. W.; Cribb, S. J. (eds), Geo-Platinum 87: 256.

Cunningham, C. G., Ashely, R. P., Chou, I-M, Huang, H., Wang, C-Y, and Li, W-K. 1988. Newly discovered sedimentary-hosted disseminated gold deposits in the People's Republic of China. Economic Geology, 83: 1462~ 1467.

Curiale, J. A. 1987. Distribution and occurrence of metals in heavy crude oils and solid bitumens; implications for petroleum exploration. Exploration for heavy crude oil and natural bitumen--AAPG Studies in Geology, American Association of Petroleum Geologists, United States, 25: 207~219

De Ronde, C. E. J., Ebbesen, T. W. 1996. 3.2 b.y. of organic compound formation near sea-floor hot springs. Geology, 24(9): 791~794.

Disnar, J. R. 1996. A comparison of mineralization histories for two MVT deposits, Treves and Les Malines (Causses Basin, France), based on the geochemistry of associated organic matter. *In* Organics and ore deposits. *Edited by* Giordano, T. H. Ore Geology Reviews. 11(1-3): 133~156.

Disnar, J. R., and Sureau, J. F. 1990. Organic matter in ore genesis: Progress and perspectives. Organic geochemistry, 16(1-3):577-599.

Dixon, G., and Davidson, G. J. 1996. Stable isotope evidence for thermochemical sulfate reduction in the Dugald River (Australia) strata-bound shale-hosted zinc-lead deposit. Chemical geology, 129(3-4): 227-246.

Doebrich, J. L., and Theodore, T. G. 1996. Geologic history of the Battle Mountain mining district, Nevada, and regional controls on the distribution of mineral systems. *In* Geology and Ore Deposits of the American Cordillera. *Edited by* Coyner, A. R., and Fahey, P. L. Geological Society of Nevada Symposium Proceedings, Reno/Sparks, Nevada, April 1995, p. 453~483.

Drummond, S. E., and Palmer, D. A. 1986. Thermal decarboxylation of acetate. Part II. Boundary conditions for the role of acetate in the primary migration of natural gas and the transportation of metals in hydrothermal systems. Geochimica et Cosmochimica Acta, 50: 825~833.

Eggleston, C. M., and Hochella, M. F. Jr. 1991. Scanning tunneling microscopy of galena (100) surface oxidation and sorption of aqueous gold. Science, 254: 983~986.

Enzweiller, J., and Joekes, I. 1991. Adsorption of colloidal gold on colloidal iron oxides. J. Geochem Exploration, 40: 133~142.

Espitalié, J., LaPorte, J. L., Madec, M., Marquis, F., Leplat, P., Paulet, J., and Boutefeu. 1977. Méthode rapide de caractériasation des roches méres deleur potential pétrolier at de leur degré d'évolution. Rev. Inst. Fr. Pet., 32: 23~42.

Espitalié, J., Marquis, F., and Barsony, I. 1984. Geochemical logging. In: Analytical Pyrolysis. Edited by Voorhees, K. J. Butterworths, Boston, 276-304.

Evans, J. G. 1980. Geology of the rodeo Creek NE and Welches Canyon quadrangles, Eureka County, Nevada, US geology survey bulletin, 1473, 81p.

Farrow, C. G. and Watkinson, D.H. 1997. Diversity of precious-metal mineralization in footwall Cu-Ni-PGE deposits, Sudbury, Ontario: Implication for hydrothermal model of formation. The Canadian Mineralogist, 35: 817~839.

Fedoseyeva, V.I., Fedoseyev, N. F., and Zvonareva, G. V. 1986. Interaction of some gold complexes with humic and fulvic acids. Geochemistry International, 23(3): 106~110.

Fein, J. B., and Williams-Jones, A. E. 1997. The role of mercury interactions in the hydrothermal transport of mercury. Economic Geology, 92: 20~28.

Feng Qinglai, Liu Benpei, Ye Mei. 1996. Tectono-palaeographic pattern of Palaeotethyan stage in South China. Geological Science and Technology Information, 15(3): 1~6. (In Chinese)

Fisher J.B. 1987. Distribution and occurrence of aliphatic acid anions in deep subsurface waters. Geochimica et Cosmochimica Acta, 51(9) : 2459~2468.

Fleet, A.J., 1984. Aqueous and sedimentary geochemistry of the rare earth elements (Chapter 10). In: Henderson, P. (Eds), Rare Earth Element Geochemistry. (Developments in Geochemistry, 2.) Elsevier, Amsterdam, 343~374

Foley, N. K., and Ayuso, R. A. 1994. Lead isotope compositions as guides to early gold mineralization. The North Amethyst vein system, Creede District, Colorado. Economic Geology, 89: 1842~1859

Fournier, R. M. 1985. Silica minerals as indicators of conditions during gold deposition. US Geological Survey Bulletin, 1646: 15~26.

Fournier, R. M. 1986. Carbonate transport and deposition in the epithermal environment. In: Geology and geochemistry of Epithermal System. Edited by B. R. Berger and P. M. Bethke. Reviews of Economic Geology, 2: 63~72.

Frondel, C. 1938. Stability of colloidal gold under hydrothermal conditions. Economic Geology, 33(1): 1~20.

Gammons, C. H., Bloom, M. S., Yu, Y. 1992. Experimental investigation of the hydrothermal geochemistry of platinum and palladium. I. Solubility of platinum and

palladium sulfide minerals in NaCl/ H2SO4 solutions at 300°C. Geochimca et Cosmochimica Acta, 56: 3881~3894.

Gammons, C. H., and Williams-Jones, A. E. 1995. The solubility of Au-Ag alloy + AgCl in HCl/NaCl solutions at 300°C: New data on the stability of Au(I) chloride complexes in hydrothermal fluids. Geochimica et Cosmochimica Acta, 59: 3453~3468.

Gao Lide. 1989. A primary study on rock and mineral features of Zimudang Au ore and the existing state of Au in Xingren, Guizhou Province. Geology of Guizhou, 6(1): 23~ 29. (In Chinese)

Gardner, L. R. 1974. Organic versus inorganic trace metal complexes in sulfidic marine waters; some speculative calculations based on available stability constants. Geochimica et Cosmochimica Acta, 38(8): 1297~1302.

Gatellier, J. P., Disnar, J. R. 1989. Organic matter and gold-ore association in a hydrothermal deposit, France. Applied Geochemistry, 4(2): 143~149.

Ghazi A.M., Vanko D.A., Roedder E., and Seeley R.C. 1993. Determination of rare earth elements in fluid inclusions by inductively coupled plasma-mass spectrometry (ICP-MS). Geochimica et Cosmochimica Acta. 57(18): 4513~4516.

Giere, R., 1986. Zirconolite, allanite and hoegbomite in a marble skarn from the Bergell contact aureole: implications for mobility of Ti, Zr and REE. Contrib. Mineral. Petrol., 93: 459-470.

Giordano T.H. 1985. A preliminary evaluation of organic ligands and metal-organic complexing in Mississippi Valley-type ore solutions. Economic Geology, 80(1): 96~106.

Gize, A. P., and Barnes, H. L. 1987. The organic geochemistry of two Mississippi Valley type lead-zinc deposits. Economic Geology, 82: 457~470.

Gize , A. P., and Manning, D. A. C. 1993. Aspects of the organic geochemistry and petrology of metalliferous ores. *In* Organic Geochemistry, *Edited by* M. H. Engel and S. A. Macko. Plenum Press, New York. 565~580.

Goldfarb, R. J., Lerach, D. L., Pickthron, W. J., and Paterson, C. J. 1988. Origin of lode-gold deposits of the Juneau gold belt, southeastern Alaska. Geology, 16: 440~443.

Goldschmidt, V. M. 1930. *Über das Vorkommen des Germanium in Steinkohle und steinkohlen-Producten. Nachr. Ges. Wiss. Goettingen, Math, -Phys,* Kl., 1~4.

Goldschmidt, V. M. 1937. The principles of disribution of chemical elements in mineral and rocks. Journal of Chemical Society, 1: 655~673.

Goldschmidt, V. M., Peter, C. l. 1933. *Ueber die Anreicherung seltener Elemente in Steinkohlen.* Ges. Wiss. Goettingen, Nachr., mat.-phys. Kl. 4 : 371~386.

Goldstein, T. P. 1982. Clays as acid geocatalysts in generation and maturation of petroleum. Am. Assoc. Petrol. Geol. Bulletin, 66(9): 1444.

Goldstein, T. P. 1983. Geocatalytic reactions in formation and maturation of petroleum. Geol. Bulletin, 67(1): 152~159.

Gou Hancheng. 1985. Preliminary research on tectonic background and material source area of turbidite deposit formation of Middle-Upper Triassic in Yunnan, Guizhou, and Guangxi Province. Acta Sedimentologica Sinica, 3(4): 95~107.

Gouveia, M.A., Prudencio, M.I., Figtueiredo, M.O., Pereira, L.C.J., Waerrnborgh, J.C., Morgado, I., Pena, T. and Lopes, A., 1993. Behavior of REE and other trace and major elements during weathering of granitic rocks. Evora, Portugal. Chem. Geol., 107: 293~296.

Grant, J. A. 1986. The isocon diagram — A simple solution to Gresens' equation for Metasomatic alteration. Economic Geology, 81: 1976 ~ 1982.

Greibrokk, T., Lundanes, E. L., Norli, H.R., Dyrstad, K., and Olsen, S. D. 1994. Experimental simulation of oil migration — Distribution effects on organic compounds groups and on metal/metal ratios. Chemical Geology, 116: 281~299.

Grim, R. E. 1947. Relation of clay mineralogy to origin and recovery of petroleum. Am. Assoc. Petrol. Geol. Bulletin, 31:1491~1499.

Groff, J. A., Heizler, M. T., McIntosh, W. C., and Norman, D. I. 1997. 40Ar/39Ar dating and mineral paragenesis for Carlin-type gold deposits along the Getchell Trend, Nevada: Evidence for Cretaceous and Tertiary gold mineralization. Economic Geology, 92: 601~622.

Gromet, L. P., Dymek, R. F., Haskin, L. A., and Korotev, R. L. 1984. The "North American Shale Composite": its compilation, major and trace element characteristics. Geochimica et Cosmichimica Acta, 48: 2469~2482.

Guo Zhenchun. 1988. The geological features and origins of the Zimudang gold deposit in Xingren County, Guizhou Province. Geology of Guizhou, 5(3): 201~218. (In Chinese)

Haas, J. R., Shock, E. L., and Sassani, D. C. 1995. Rare earth elements in hydrothermal systems: Estimates of standard partial molar thermodynamic properties of aqueous complexes of the rare earth elements at high pressures and temperatures. Geochimica et Cosmochimica Acta, 59 (21): 4329~4350.

Han Zhijun and Sheng Xueyong. 1996. Gold deposits in southwestern Guizhou and their metallogenetic model. Guizhou Geology, 13(2): 146~153. (In Chinese)

Hannigan, R., and Peucker-Ehrenbrink, B. 1998. Weathering of black shales as sources of radiogenic Os in seawater. Geological Society of America, 1998 annual meetingAbstracts with Programs - Geological Society of America 30(7): 223.

Hart, S. R., Shimizu, N., and Sverjensky, D. A. 1981. Lead isotope zoning in galena: an ion microprobe study of a galena from the Buick mine, southeast Missouri. Economic Geolgoy, 76: 1873~1878.

Haskin, L. A., 1984. Petrogenetic modeling — use of rare earth elements (Chapter 4). In: Henderson, P. (Eds), Rare Earth Element Geochemistry. (Developments in Geochemistry, 2.) Elsevier, Amsterdam, 115~152.

Hattori, K. and Hulbert, L. J. 1998. PGE patterns and osmium isotope compositions of uranium veins in the Nicholson deposit, Athabasca Basin. Geological Society of America, 1998 annual meeting Abstracts with Programs - Geological Society of America 30(7): 371.

Hausen, D. F. and Kerr, P. F. 1968. Fine gold occurrence at Carlin, Nevada. In: J. D. Ridge (editor). Ore deposits of the United States, 1933-1967. Volume 1, New York, AIME, 908~940.

Hausen, D. M. and Park, W. C. 1985. Observation on the association of gold mineralization with organic matter in Carlin-type ores. Denver Region Exploration Geologists Society Symposium, Denver, Colorado, April 25-26, 1985, Proceedings, 119~136.

Hayashi, K. I. and Ohmoto, H. 1991. Solubility of gold in NaCl- and H_2S-bearing aqueous solutions at 250-350°C. Geochimica et Cosmochimica Acta, 55: 2111~2126.

He L-X. 1996. A genetic model for gold deposits in southwestern Guizhou: a co-source of heat, water and ore-materials. Guizhou Geology, 13(2): 154~160. (In Chinese)

He L-X, Zeng R-L, and Lin L-Q. 1993. Gold geology of Guizhou Province. Beijing, Geology Publishing House, 156p. (In Chinese)

He S-L. 1992. A preliminary explanation of Au formation in southwestern Guizhou by using geological and geochemical data. Geology of Guizhou, 9(2): 150~160. (In Chinese)

Helgeson, H. C. 1991. Organic/inorganic reactions in metamorphic processes. Canadian Minealogist, 29: 707~739.

Helgeson, H. C. 1992. Calculation of the thermodynamic properties and relative stabilities of aqueous acetic and chloroacetic acids, acetate and chloroacetates, and acetyl and chloroacetyl chlorides at high and low temperatures and pressures. Applied Geochemistry, 7: 291~308.

Helgeson, H, C., Knox, A. M., Owens, C. E., and Shock, E. L. 1993. Petroleum, oil field brines, and authigenic mineral assemblages: Are they in metastable equilibrium in hydrocarbon reservoirs? Geochimica et Cosmochimica Acta, 57: 3295~3339.

Helgeson, H. C., and Pokrovskii, V. A. 1992. Calcaulation of the oxidative solubilities of hydrocarbon liquids in aqueous electrolyte solutions coexisting with authigenic carbonate minerals in sedimentary basins. Geological Society of America Abstracts with Programs, 24(7): A325.

Hennet, R. J.-C., Crerar, D. A., and Schwartz, J. 1988. Organic complexes in hydrothermal systems. Economic Geology, 83: 742~764.

Henry, A. L., Andrerson, G. M., and Héroux, Y. 1992. Alteration of organic matter in the Viburnum Trend lead-zinc district of southeastern Missouri. Economic Geology, 87: 288~309.

Heyl, A. V., Landis, G. P., and Zartman, R. E. 1974. Isotopic evidence for the origins of Mississippi Valley-type mineral deposits: A review. Economic Geology, 69: 997~1006.

Hitchon, B., Filby, R. H., and Shah, K. R. 1975. Geochemistry of trace elements in crude oils, Alberta, Canada. In: The role of trace metals in Petroleum. Edited by T. F. Yen. Ann Arbor Science Publishers, Ann Arbor, Michigan, 111~122.

Hitchon, B, and Filby, R. H. 1983. Trace element in Alberta crude oils. Open file report 1983-02 Alberta Research Council, Edmonton.

Hochella, M. F. Jr., and White, A. F. 1990. Mineral-water interface geochemistry: an overview. In: Mineral-water interface geochemistry. Edited by M. F. Hochella, Jr. and A. F. White. Reviews in Mineralogy, 23: 1~16.

Hofstra, A. H. 1995. Timing and duration of Carlin-type gold deposits in Nevada and Utah—Relation to back-arc extension and magmatism. Geological Society of America Abstracts with Programs. 27(6): A-329.

Hofstra, A. H. 1997. Isotopic composition of sulfur in Carlin-type gold deposits: implications for genetic models. In: Carlin-type gold deposits field conference. Edited by Vikre, P., Thompson, T. B., Bettles, K., Christensen, O., Parratt, R. Society of Economic Geologists Guidebook Series, 28: 119~130.

Hofstra, A. H., Leventhal, J. S., Northrop, H. R., Landis, G. P., Rye, R. O., Birak, D. J., and Dahl, A. R. 1991. Genesis of sediment-hosted disseminated-gold deposits by fluid mixing and sulfidation: chemical-reaction-path modeling of ore-depositional processes documented in the Jerritt Canyon district, Nevada. Geology, 19: 36~40.

Holland, P. T., Beaty, D. W., and Snow, G. G. 1988. Comparative elemental and oxygen geochemistry of jasperoid in the northern Great Basin: Evidence for distinctive fluid evolution in gold-producing hydrothermal systems. Economic Geology, 83: 1401~1423.

Hu K, Zhai J-P, Liu Y-J, Wang H-N, Zhang J-R, and Jia R-F. 2000. Genesis and organic geochemical characteristics of the carbonaceous rock stratabound gold deposits, south China. Science in China (Series D), 43(5): 507~520.

Hulen, J. B. and Collister, J. W. 1999. The oil-bearing, Carlin-type gold deposits of Yankee Basin, Alligator Ridge District, Nevada. Economic Geology and the Bulletin of the Society of Economic Geologists, 94, (7): 1029~1049.

Humphris, S. E., 1984. The mobility of the rare earth elements in crust. In: P. Henderson (Eds), Rare earth element geochemistry (Developments in Geochemistry, 2). Elsevier, Amsterdam. pp317-342 (Chapter 9). Ilchik, R. P., and Barton, M. D. An amagmatic origin of Carlin-type gold deposits. Economic Geology, 1997, 92: 269~288.

Hunt, J. M. 1979. Petroleum geochemistry and geology. San Francisco, W. H. Freeman Co., 617p.

Hyland, M. M., and Bancroft, G. M. 1989. An XPS study of gold deposition at low temperatures on sulphide minerals: Reducing agents. Geochimica et Cosmochimica Acta, 53: 367~372.

Ilchik, R. P. 1990. Geology and geochemistry of the Vantage gold deposits, Alligator Ridge-Bald Mountain mining district, Nevada. Economic Geology, 85: 50~75.

Ilchik, R. P., and Barton, M. D. 1997. An amagmatic origin of Carlin-type gold deposits. Economic Geology, 92(3): 269~288.

Ilchik, R. P., Brimhall, G. H., and Schull, H. W. 1986. Hydrothermal maturation of indigenous orgainc matter at the Alligator Ridge gold deposits, Nevada. Economic Geology, 81:113-130.

International Committee for Coal petrology. 1971. International handbook of coal petrology. Suppl, end. CNRS, Paris.

Jean, G. E., and Bancroft, G. M. 1985. An XPS and SEM study of gold deposition at low temperatures on sulfide minerals: concentration by adsorption/reduction. Geochimica et Cosmochimica Acta, 49: 979~987.

Jewell, P. W., and Parry, W. T. 1987. Geology and hydrothermal alteration of the mercur gold deposit, Utah. Economic Geology, 82(7): 1958~1966.

Jones, P. 1975. Trace elements and other elements in crude oil—a literature review. Report of British Petroleum Research Centre. Sunbury.

Johns, W. D. 1979. Clay mineral catalysis and petroleum generation. Annual Review Planetary Sciences, 7: 183~198.

Johns, W. D. 1982. Clay mineral catalysis and petroleum generation. Am. Assoc. Petrol. Geol. Bulletin, 66(9): 1445.

Johns, W. D., and McKalliip, T. E. 1989. Burial diagenesis and specific cataclytic activity of illite-smetctite clays from Vienna Basin, Austria. Geol. Bulletin, 73(4): 472~482.

Joralemon, P., 1951. The occurrence of gold at the Getchell mine, Nevada. Economic Geology, 46: 267~310.

Joralemon, P., 1975. Discussion of K-Ar relations of granodiorite emplacement and tungsten and gold mineralization near the Getchell mine, Humboldt County, Nevada. Economic Geology, 70: 405~406.

Kesler, S. E., Cummings, G. L., Kirstic, D., and Appold, M. S. 1994a. Lead isotope geochemistry of Mississippi Valley-type deposits of the southern Appalachians. Economic Geology, 89: 307~321.

Kesler, S. E., Jones, H. D., Furman, F. C., Sassen, R., Anderson, W. H. ; Kyle, J. R. 1994b. Role of crude oil in the genesis of Mississippi valley-type deposits; evidence from the Cincinnati Arch. Geology, 22(7): 609~612.

Kharaka, Y. K. 1997. Organic species in oil-field waters; sources, controls and diagenetic water-rock interactions. American Association of Petroleum Geologists 1997 annual convention Annual Meeting Abstracts - American Association of Petroleum Geologists and Society of Economic Paleontologists and Mineralogists, 6: 60.

Khorasani, G. K. 1987. Novel development in fluorescence microscopy of complex organic mixtures: application in petroleum geochemistry. Organic Geochemistry, 11(3): 157~168.

Killops, S. D., and Killops, V. J. 1993. An Introduction to Organic Geochemistry. John Wiley & Sons, Inc. New York. 265pp.

Kiyosu, Y. and Krouse, H. R. 1990. The role of organic acid in the abiogencic reduction of sulfate and the sulphur isotope effect. Geochemistry Journal, 24: 21~27.

Knesl, J. and Kneslova, A. 1999. Gold mineralizations types in Slovakia and possibilities of their utilization. Mineralia Slovaca, 31(3-4): 171~174.

Knight, C. L. 1957. Ore genesis; the source bed concept. Economic Geology, 52(7): 808~817.

Korpas, L. and Hofstra, A. H. 1999. Potential for Carlin-type gold deposit in Hungary. In: Carlin gold in Hungary. Edited by Korpas, L. and Hofstra, A. H. Geologica Hungarica, Serie Geologica, 24: 133~135.

Krauskopf, K. 1955. Sedimentary deposits of rare metals. Economic Geology, 50: 411~463.

Krouse, H. R., Viau, C., Eliuk, L., Ueda, A., and Halas, S. 1988. Chemical and isotopic evidence of thermochemical sulphate reduction by light hydrocarbon gases in deep carbonated reservoirs. Nature (London), 333: 415~419.

Kucha, H. and Plimer, I. R. 1999. Gold in organic matter, Maldon, Victoria, Australia. Economic Geology, 94: 1173~1180.

Kucha, H. and Pryzybylowicz, W. 1999. Noble metals in organic matter and clay-organic matrices, Kupferschiefer, Poland. Economic Geology, 94: 1137~1162.

Kuehn, C. A. 1989. Studies of disseminated gold deposits near Carlin, Nevada: Evidence for a deep geologic setting of ore formation. Unpublished Ph.D. thesis. Pennsylvania State University. 395p.

Kuehn, C. A., and Rose, A. W. 1995. Carlin gold deposits, Nevada: Origin in a deep zone of mixing between normally pressured and over pressured fluids. Economic Geology, 90: 17~36.

Landis, P., and Gize, A. P. 1997. Organic matter in hydrothermal ore deposits. *In* Geochemistry of Hydrothermal Ore Deposits. Third Edition. *Edited by* H. L. Barnes. John Wiley &Sons, Inc. New York. 613~655.

Lattanzi, P. 1999. Epithermal precious metal deposits of Italy—an overview. Mineralium Deposita, 34: 630~638.

Leventhal, J. S. 1990. Organic matter and thermochemical sulfate reduction in the Viburnum Trend, southeast Missouri. Economic Geology, 85: 622~632.

Lewan, M. D. 1983. Effects of thermal maturation on stable organic carbon isotopes as determined by hydrous pyrolysis of Woodford Shale. Geochimica et Cosmochimica Acta, 47(8): 1471~1479.

Li J-L, Qi F, and Xu Q-S. 1996. The role of carbonaceous and organic materials in the formation of Carlin-type disseminated gold deposits. Mineral Deposits, 15(3): 193~206. (In Chinese)

Li J-L, Sun S, Xu T-H, et al. 1989a. New evidence for the tectonic evolution of south China orogenic belt. Scientia Geologica Sinica, 24(3): 217~225. (In Chinese)

Li, S-Y, Guo, S-H, and Tan X-F. 1998. Characteristics and kinetics of catalytic degradation of immature kerogen in the presence of mineral and salt. Organic Geochemistry, 29(5-7): 1431~1439.

Li W-K, Jiang X-S, Jiu R-H, Meng F-Y, and Zhang S-X. 1989b. Geological characteristics and ore-forming process of the fine-grained gold deposits in the southwestern Guizhou Province. In: Contributions to the project of regional metallogenic conditions of main gold deposit types in China. VI. Southwestern Guizhou Province. Edited by Shenyang institute of geology and mineral resources. Geological Publishing House, Beijing. 1~81. (In Chinese)

Li Z, and Liu T-B. 1995. Ore-forming conditions of the Lannigou gold deposit in southeastern Guizhou; a petrological and geochemical study. Mineral Deposits = Kuangchuang Dizhi, 14(1): 51~58. (In Chinese)

Li Z, and Liu T. 1998. Microbial and organic matter processes in the formation of the Carlin-type gold deposit. (Chapter 13). In: Yie Liangjun edited. Biomineralization and its geological background microbes and their hosting organic sediments. Oceanography Publishing House, Beijing, 311~333. (In Chinese)

Li Z-P, and Peters, S. G. 1998. Comparative geology and geochemistry of sedimentary-rock-hosted (Carlin-type) gold deposits in the People's Republic of China and in Nevada, USA. U.S. Department of the Interior, U.S. Geological Survey. Open-File Report 98-466. 149p.

Lin Q. 1993. Geochemistry and organic geochemistry of gold deposits in southwestern Guizhou Province. Unpublished Ph.D. thesis. Institute of Geochemistry, Chinese Academy of Sciences. Guiyang. pp1-87. (in Chinese)

Lin Q, Fu J-M, Liu D-H, Shen G-Y, and Lu J-L. 1993a. The evolution of oil and gas and the genesis of sedimentary reworked gold ore deposits. Geochemica, No.3, 217~226. (In Chinese)

Lin Q, Fu J-M, Liu D-H, Sheng G-Y, and Lu J-L. 1993b. Genetic relationship between the oil gas evolution and some gold deposits. Geochimica, 22(3): 62~71. (In Chinese)

Liu, D-S, and Geng, W-H. 1985. On the mineral association and mineralization conditions of the Carlin-type gold deposits in China. Geochimica, No.3, 277~282. (In Chinese)

Liu, D-S, Tan, Y-J, Wang, J-Y, and Wei, L-M. 1994a. Carlin-type gold deposits in China. In: Chinese Carlin-type Gold Deposits. Edited by Liu, Dongsheng, Tan, Yunjian, Wang, Jianye, and Jiang Shufang. Nanjing University Press, Nanjing, 1~36.

Liu H-Z. 1994. The mineralization of rift and micro-aulacogen in Yangtse Block. Journal of Guilin College of Geology, 14(1): 10~22. (In Chinese)

Liu H-C and Zhu B-Q. 1994. Geochronology investigation of the Banxi Group in western Hunan Province. Chinese scientific bulletin, 39(2): 148-150. (In Chinese)

Liu J-Z, Fu Jiamo, and Lu Jialan. 1993. Laboratory studies on leaching, extraction and reduction of gold by organic matter. Mineral Deposits, 12(3): 111~118. (In Chinese)

Liu, J-Z, Fu, J-M, and Lu, J-L. 1994b. Experimental research on the role of organic matter in formation of sedimentary-reworked gold ore deposits. Science in China (Series B), 37(7):859-859.

Liu, J-M, Liu, J-J, Zheng, M-H, and Gu X-X. 1998. Stable isotope compositions of micro-disseminated gold and genetic discussion. Geochemica, 27(6): 585~591. (In Chinese)

Liu J-S, Tao C-G, Chen T-J, Cheng J-H, and Chen M-Y. 1989. On geological characteristics of three fine impregnation-type gold deposits in Southwestern Guizhou. In: Collections of metallogenic conditions for the major type gold deposits in China: VI. Southwestern Guizhou Province. Edited by Li Wenkang. Geologic Publishing House, Beijing, 115~154. (In Chinese)

Liu, X-F, Su, W-C, and Zhu, L-M. 1999. An approach on mechanism of juvenile fluid mineralization for Carlin-type gold deposits in Yunnan-Guizhou-Guangxi. Geology and Prospecting, 35(1): 14~19. (In Chinese)

Liversidge, A. 1893. On the origin of gold nuggets. Journal of Royal Society of New South Wales, 27: 303~343.

Lottermoser, B.G., 1992. Rare earth elements and hydrothermal ore formation processes. Ore Geology Review, 7(1): 25~41.

Lu, J-L and Zhuang, H-P. 1996. Experimental studies on the role of organic matter in the mineralization of gold and silver at low temperature. Geochimica, 25(2): 172-180. (In Chinese)

Luo X-H. 1994. Geological characteristics, genesis and exploration of the Lannigou gold deposit, Zhenfeng, Guizhou Province. In Liu Dongsheng edited. Carlin-type gold deposits in China. Published by Nanjing University Press. 100-115. (In Chinese)

Ma C-X, Liu R-G, Lu Guide. 1992. Pre-Sinian geology of the northeast Jiangxi Province. Geological Publishing House, Beijing. 231p. (In Chinese)

MacGowan, D. B., Surdam, R. C. 1988. Difunctional carboxylic acid anions in oilfield waters. Organic Geochemistry, 12(3): 245~259.

Machesky, M. L., Andrade, W. O., and Rose, A. W. 1992. Interaction of gold (III) chloride and elemental gold with peat-derived humic substances. Chemical Geology, 102: 55~71.

MacLean, W. H., and Kranidiotits, P. 1987. Immobile elements as monitors of mass transfer in hydrothermal alteration: Phelps Dodge massive sulfide deposit, Matagami, Quebec. Economic Geology, 82: 951~962.

Manning, D.A.C. 1986. Assessment of the role of organic matter in ore transport processes in low-temperature base-metal systems. Transactions of the Institution of Mining & Metallurgy (Section B: Applied Earth Science) 95: 195~200.

Manning, D. A. C., and Gize, A. P. 1993. The role of organic matter in ore transport processes. *In* Organic Geochemistry. *Edited by* M. H. Engel and S. A. Macko. Plenum Press. New York. 547~563.

Marsh, J.S., 1991. REE fractionation and Ce anomalies in weathered Karoo dolerite. Chem. Geol., 90: 189~194.

Mazdab, F. K., Barton, M. D., Hervig, R. L. 1999. Trace element distributions in iron sulfides and associated oxides, with a focus on Fe-oxide-rich hydrothermal systems. Geological Society of America, 1999 annual meeting Abstracts with Programs - Geological Society of America, 31(7): p32.

McAuliffe, C. D. 1980. Oil and gas migration: Chemical and physical constraints. In: AAPG studies in geology No.10, Problems of Petroleum Migration. Edited by Robert, III. W. H., Cordell, J. R. 89~107.

McGoldrick, P. J., Dunster, J., and Aheimer, M. 1996. Lady Loretta stratiform sediment-hosted Zn-Pb-Ag deposit, NW Queensland; a microbial oasis in a late Paleoproteozoic shallow sea. *In* Geological Society of America, 28th annual meeting. Abstract with Programs - Geological Society of America, 28(7), p473.

McKibben, M. A., Eldridge, C. S. 1995. Microscopic sulfur isotope variations in ore minerals from the Viburnum Trend, Southeast Missouri; a SHRIMP study. Economic Geology, 90(2): 228~245.

McKibben, M. A., and Williams, A. E. 1990. Solubility and transport of platinum-group elements and Au in saline hydrothermal fluids: constraints from geothermal brine data. Economic Geology, 85: 1926~1934.

McLennan, S. M. 1989. Rare earth elements in sedimentary rocks: influence of provenance and sedimentary processes. In: Lipin, B. R. and McKay, G. A. (eds), Geochemistry and mineralogy of rare earth elements. Reviews in Mineralogy, 21, pp.169~200.

Ministry of Geology and Mineral Resources, P. R. China. 1987. Basic characteristics of Geological Evolution (Chapter 3). In: Regional Geology of Guizhou Province. Geological Memoirs, Series 1- Regional Geology. Geological Publishing House, Beijing, 632~635. (In Chinese)

Mironov, A. G., Zhmodik, S. M., and Maksimova, E. A. 1981. An experimental investigation of the sorption of the sorption of gold by pyrites with different thermoelectric properties. Geochemistry International, 18: 153~160.

Mongelli, G. 1993. REE and other trace elements in a granitic weathering profile from "Serre", Southern Italy. Chem. Geol., 103: 17~25.

Mosier, D. L., Singer, D. A., Sato, T., and Page, N. J. 1986. relationship of grade, tonnage, and basement lithology in volcanic-hosted epithermal precious- and base-metal quartz-asularia-type districts. Mining Geology, 36:245~264.

Mossman, D. J., Gooarzi, F., Gentzis, T. 1993. Characterization of insoluble organic matter from the lower Proterozoic Huronian supergroup, Elliot Lake, Ontario. Metalliferous black shales and related ore deposits—Precambrian research, 61(3-4): 279~293.

Mountain, B. W., and Wood, S. A. 1988. Chemical controls on the solubility, transport, and deposition of platinum and palladium in hydrothermal solutions: a thermodynamic approach. Economic Geology, 83: 492~510.

Möller, P., and Kersten, G. 1994. Electrochemical accumulation of visible gold in pyrite and arsenopyrite surfaces. Mineral Deposita, 29: 404~413.

Möller, P., Sastri, C. S., Kluckner, M., Rhede, D., and Ortner, H. M. 1997. Evidence for electrochemical deposition of gold onto arsenopyrite. European Journal of Mineralogy, 9: 1217~1226.

Myakon'kiy, A. G., and Dmitriyev, S. N. 1991. The nature of gold and mercury compounds with organic acids in the thermal brine, Cheleken Peninsula. Geokhimiya, 9: 1353~1358.

Naldrett A J, and Duke J M. 1980. Platinum metals in magmatic sulfide ores. Science, 208: 1417~1424.

Nesbitt, H.W., 1979. Mobility and fractionation of rare earth elements during weathering of a granodiorite. Nature (London), 279: 206~210.

Ni S-J, Liu X-F, Jin J-F, and Lu Q-X. 1997. Ore-forming fluid geochemistry of the fine disseminated gold deposits in the Dian-Qian-Gui triangle area. Publish House of Chengdu University of Science and Technology, Chengdu. 122p.

O'Neil, J. R., and Bailey, G. B. 1979. Stable isotope investigation of gold-bearing jasperoid in the central Drum Mountains, Utah. Economic Geology, 74: 852~859.

Ohmoto, H. 1986. Stable isotope geochemistry of ore deposits. In Stable isotopes in high temperature geological processes. Edited by Valley, J. W., Taylor, H. P. Jr., O'Neil, J. R. Review in Mineralogy, 16: 491~559.

Ohmoto, H., and Goldhaber, M. B. 1997. Sulfur and carbon isotopes. In Geochemistry of Hydrothermal Ore Deposits. Third edition. Edited by Barnes, H. L. John Wiley & Sons, Inc. 517~611.

Palmer, D. A., and Drummond, S. E. 1986. Thermal decarboxylation of acetate. Part I. The kinetics and mechanism of reaction in aqueous solution. Geochimica et Cosmochimica Acta, 50: 813~823.

Pan, P., and Wood, S. A. 1994. Solubility of Pt and Pd sulfides and Au metal in aqueous bisulfide solutions. II. Results at 200 C to 350C and saturated vapor pressure. Mineralium Deposita, 29: 373~390.

Parnell, J. 1988. Metal enrichment in solid bitumen: a review. Mineral Depoista, 23: 191~199.

Parnell, J. 1992. Metal enrichment in bitumens from Carboniferous-hosted ore deposits of the British Isles. Chemical Geology, 99(1-3): 115~124.

Parnell, J., Carey, P. F., and Bottrell, S. H. 1994. The occurrence of authigenic metals in solid bitumens. Journal of Sedimentary Research, A64(1): 95~100.

Parr, J.M., 1992. Rare-earth element distribution in exhalites associated with Broken Hill-type mineralisation at the Pinnacles deposit, New South Wales, Australia. Chem. Geol., 100: 73-91.

Peake, E., and Hodgson, G. W. 1966. Alkanes in aqueous systems. I: Exploratory investigations on the accommodation of C_{20}-C_{33} n-alkanes in distilled water and occurrence in natural water systems. J. Am. Oil Chem. Soc., 43: 215~222.

Pearcy, E. C. and Burruss, R. C. 1993. Hydrocarbons and gold mineralization in the hot-spring deposit at Cherry Hill, California. In: Bitumens in Ore Deposits. Edited by J. Parnell, H. Kucha, and P. Landis. Spring-Verlag. Berlin. 117~137.

Phillips, G. N., Groves, D. I., and Clark, M. E. 1983. The importance of host-rock minerlalogy in the location of Archaean epigenetic gold deposits. In: J. P. R. DeVilliers and P. A. Cawthorn (editors), ICAM 81, Proceedings of the first international congress on applied mineralogy. Geological Society of South Africa, Special Publication, 7:79~86.

Phillips, G. N., and Law, J. D. M. 1997. Hydrothermal origin for Witwatersrand gold. SEG Newsletter, 31:26-33.

Philips, G. N., and Powell, R. 1993. Link between gold provinces. Economic Geology, 88: 1084~1098.

Pokrovskii, V. A. and Helgeson, H. C. 1994. Solubility of petroleum in oil-field waters as a function of the oxidation state of the system. Geology, 22: 851~854.

Poplavko, E. M., Ivanov, V. V., Orekhov, V. S., Tarkhov, Yu. 1978. A Metal content of oil shales and some theories on their genesis. Geochemistry International, 15(5): 90~97.

Porto, C. G., Hale, M. 1996. Mineralogy, morphology and chemistry of gold in the stone line lateritic profile of the Posse Deposit, central Brazil. Journal of Geochemical Exploration, 57(1-3): 115~125.

Powell, R., Will, T. M., and Phillips, G. N. 1991. Metamorphism in Archean greenstone belts: Calculated fluid compositions and implications for gold mineralization. Journal of Metamorphic Geology, 9: 14~150.

Presnell, R. 1993. The association of gold and hydrocarbons in sediment-hosted disseminated gold deposits. AAPG Bulletin, 77(8): 1459.

Price L.C. 1993. Thermal stability of hydrocarbons in nature: limits, evidence, characteristics, and possible controls. Geochimica et Cosmochimica Acta, 57(14): 3261~3280.

Price L.C. 1994. Basin richness and source rock disruption - a fundamental relationship. Journal of Petroleum Geology, 17(1): 5~38.

Price, L. C. 1976. Aqueous solubility of petroleum as applied to its origin and primary migration. AAPG Bulletin, 60: 213~244.

Price, L. C., Wenger, L. M. 1992. The influence of pressure on petroleum generation and maturation as suggested by aqueous pyrolysis. Organic Geochemistry, 19(1-3): 141~159.

Prudencio, M.I., Braga, M.S.A. and Gouveia, M.A. 1993. REE mobilization, fractionation and precipitation during weathering of basalts. Chem. Geol., 107:251-254.

Qi L, and Hu J. 1999. Fast determination of platinum group elements and gold in geological samples by ICP-MS. Rock and Mineral analysis, 18(4): 267-279. (In Chinese)

Qin J-H, Wu Y-L, Yan Y-G, and Zu Z-F. 1996. Hercynian-Indosinian sedimentary-tectonic evolution of the Nanpanjiang basin. Acta Geologica Sinica, 70(2): 99~107. (In Chinese)

Radtke, A. S. 1985. Geology of the Carlin gold deposit, Nevada. U.S. Geological survey Professional Paper, 1267, 124p.

Radtke, A. S., and Scheiner, B. J. 1970. Studies of Hydrothermal gold deposit (I): Carlin gold deposit, Nevada: the role of carbonaceous materials in gold deposition. Economic Geology, 65(2): 87-102.

Rantitsch, G. 1995. Coalification and graphitization of graptolites in the anchizone and low epizone. International Journal of Coal Geology, 27(1): 1~-22.

Rasmussen, B. and Buick, R. 2000. Oily old ores: Evidence for hydrothermal petroleum generation in an Archean volcanogenic massive sulfide deposit. Geology, 28(8): 731~734.

Renders, P. J., and Seward, T. M. 1989. The adsorption of thio gold (I) complexes by amorphous As_2S_3 and Sb_2S_3 at 25° and 90°C. Geochimica et Cosmochimica Acta, 53: 255~268.

Reuter, J. H., and Perdue, E. M. 1977. Importance of heavy metal-organic matter interactions in natural waters. Geochimica et Cosmochimica Acta, 41: 325~334.

Richards, J. P., McCulloch, M. T., Chappel, B. W., and Kerrich, R. 1991. Sources of metals in the Porgera gold deposit, Papua New Guinea: Evidence from alteration, isotope and noble gas geochemistry. Geochimica et Cosmochimica Acta, 55: 565~580.

Romberger, S. B. 1986. Ore deposits: Disseminated gold deposits. Geoscience Canada, 13(1): 23~31.

Rota, J. C., 1988. The gold quarry mine: history and general geology. In Bulk minable precious metal deposits of the Western United States. Edited by Schafer, R. W., Cooper, J. J., and Vire, P. G. Geological Society of Nevada, Reno, NV. 49~56.

Ryan, R. J., and smith, P. K. 1998. A review of the mesothermal gold deposits of the Meguma Group, Nova Scotia, Canada. Ore geology reviews, 13(1-5): 153~183.

Rye, R. O., 1985. A model for the formation of carbonate-hosted disseminated gold deposits based on geologic, fluid-inclusion, geochemical, and stable isotope studies of the Carlin disseminated gold deposits, Nevada. In Geologic characteristics of sediment- and volcanic- hosted disseminated gold deposits—search for an occurrence model. Edited by Tooker, E. W. U.S. Geology Survey Bulletin, 1646: 35~42.

Saunders, J. A. 1990. Colloidal transport of gold and silica in epithermal precious-metal systems; evidence from the Sleeper Deposit, Nevada. Geology, 18(8): 757~760.

Scaini, M. J., Bancroft, G. M., and Knipe, S. W. 1998. Reactions of aqueous Au^{1+} sulfide species with pyrite as a function of pH and temperature. American Mineralogist, 83: 316~322.

Schimmelmann, A., Lewan, M. D., Wintsch, R. P. 1999. D/H isotope ratios of kerogen, bitumen, oil, and water in hydrous pyrolysis of source rocks containing kerogen types I, II, IIS, and III. Geochimica et Cosmochimica Acta, 63: 3751~3766.

Schoonen, M. A. A., Fisher, N. S., and Wente, M. 1992. Gold sorption onto pyrite and goethite: A radiotracer study. Geochimica et Cosmochimica Acta, 56:1801-1814.

Schoonen, M. A. A., Xu, Yong; Strongin, D. R. 1998. An introduction to geocataclysis. Journal of Geochmical Exploration, 62(1-3): 201~215.

Seedorf, E. 1991. Magmatism, extension, and ore deposits of Eocene to Holocene age in the Great Basin; mutual effects and preliminary proposed genetic relationships. In: Geology and ore deposits of the Great Basin. Edited by Raines, G. L., Lisle, R. E., Schafer, R. W., and Wilkinson, W. H. Symposium Proceedings: Geological Society of Nevada, 133~178.

Seewald, J. S. 1994. Evidence for metastable equilibrium between hydrocarbons under hydrothermal conditions. Nature, (London), 370(6487): 285~287.

Seewald, J. S., Eglinton, L. B., and Ong, Y-L. 2000. An experimental study of organic-inorganic interactions during vitrinite maturation. Geochimica et Cosmochimica Acta, 64(9): 1577~1591.

Seward, T. M. 1973. Thio complexes of gold and the transport of gold in hydrothermal ore solutions. Geochimica et Cosmochimica Acta, 37(3): 379~399.

Seward, T. M. 1982. The transport and deposition of gold in hydrothermal systems. In: Gold'82, Geochemistry and Genesis of Gold Deposits. Edited by R. P. Foster. Balkema. 165~181.

Seward, T. M. 1993. The hydrothermal geochemistry of gold. 37~62. In: Gold Metallogeny and Exploration. Edited by Foster, R. P. Chapman & Hall. 432p.

Seward, T. M., and Barnes, H. L. 1997. Metal transport by hydrothermal ore fluids. *In* Geochemistry of hydrothermal ore deposits. *Edited by* Barnes, H. L. Third edition. John Wiley & Sons, Inc. 425-485.

Shabo, Z. V., Alekseyeva, N. I., Mamchur, G. P., Manzhas, N. I. 1983. Organic compounds of the Slavyansk ore shows and the association with endogenic mineral formation. International Geology Review, 25: 299~308.

Shah, K. R., Filby, R. H., Haller, W. A 1970. Determination of trace elements in petroleum by neutron activation analysis; II, Determination of Sc, Cr, Fe, Co, Ni, Zn, As, Se, Sb, Eu, Au, Hg, and U. Journal of Radioanalytical Chemistry, 6(2): 413~422.

Shenberger, D. M., and Barnes, H. L. 1989. Solubility of gold in aqueous sulfide solutions from 150 to 350°C. Geochimica et Cosmochimica Acta, 53:269-278.

Shi J-X, Wang H-Y, and Lin Q. 1998. The relationship between the low temperature Au, Sb and Hg mineralization and organics. In Low Temperature Geochemistry, *Edited by* Tu Guangchi. Science Press, Beijing, 53-76

Shi J-X, Yu X-Y, and Wang H-Y. 1995. The role of ancient oil reservoirs, bitumens and bitumen inclusions in metallogenetic research. Acta Mineralogica Sinica, 15(2): 117~122. (In Chinese)

Shumlyanskiy, V. O., Ivantishina, O. M. 1998. Prerequisites to a search of the Carlin gold deposit type in the Carpatho-Dinar region. Geological Journal, no. 1-2: 258~269.

Sicree, A. A., and Barnes, H. L. 1996. Upper Mississippi Valley district ore fluid model; the role of organic complexes. *In* Organic and ore deposits. *Edited by* Giordano, T. H. Ore Geology Reviews, 11(1-3): 105~131.

Sillitoe, R. H., and Bonham, H. F. 1990. Sediment-hosted gold deposits—Distal products of magmatic-hydrothermal systems. Geology, 18: 157~161.

Simon, G., Huang, H., Penner-Hahn, J. E., Kesler, S. E., and Kao, L-S. 1999. Oxidation state of gold and arsenic in gold bearing arsenic pyrite. American Mineralogist, 84: 1071-1079.

Simoneit, B. R. T. 1990. Petroleum generation, an easy and widespread process in hydrothermal systems: an overview. Applied Geochemistry, 5:3~15.

Simoneit, B. R. T.; Lonsdale, P. F. 1982. Hydrothermal petroleum in mineralized mounds at the seabed of Guaymas Basin. Nature (London), 295(5846): 198~202.

Skey, W. 1871. On the capability of certain sulphides to form the negative pole of a gavanic circuit or battery; also on the electromotive power of metallic sulphides. Trans and Proc. New Zealand Institute, Vol. III. 225~235.

Starling, A., Gilligan, J. M., Carter, J. M., Foster, A. H. C., and Saunder, R. A. 1989. High-temperature hydrothermal precipitation of precious metals on the surface of pyrite. Nature, 340: 298~300.

Stein, J., Fackler, J. P. Jr. et al. 1981. Structure and properties of transition-metal yilide complexes, 2: Organometallic complexes of gold (III). Journal of American Chemistry Society, 103: 2192~2198.

Stenger, D. P., Kesler, S. E., Peltonen, D. R., and Tapper, C. J. 1998a. Deposition of gold in Carlin-type deposits: The role of sulfidation and decarbonation at Twin Creeks, Nevada. Economic Geology, 93: 201~215.

Stenger, D. P., Kelsler, S. E, and Vennemann, T. 1998b. Carbon and oxygen isotope zoning around carlin-type gold deposits; a reconnaissance survey at Twin Creeks, Nevada. Journal of Geochemical Exploration, 63(2): 105~121.

Su W-C, Qi L, Hu R-Z, and Zhang G-P. 1998a. Analysis of rare-earth elements in fluid inclusions by inductivity coupled plasma-mass spectrometry (ICP-MS). Chinese Science Bulletin, 43(22): 1922~1927.

Su W-C, Yang K-Y, Hu R-Z, and Chen F. 1998b. Fluid inclusion chronological study of the Carlen-type gold deposits in southwestern China: as exemplified by the Lannigou gold deposit, Guizhou Province. Acta Mineralogica Sinica, 18(3): 359~362. (In Chinese)

Summons, R. E. 1993. Biogeochemical cycles—A review of fundamental aspects of organic matter formation, preservation, and composition. In: Organic Geochemistry. Edited by Michael, H. Engel and Stephen A. Maacko. Plenum Press, New York. 3~21.

Sun Z-Y, Yie X-X, Liu Y-K, and Wuan G-Q. 1993. Submicron gold analysis by AEM combined EPMA. Chinese Science Bulletin, 38(9): 803~806. (In Chinese)

Surdam, R. C., Boese, S. W., Crossey, L. J. 1984. The chemistry of secondary porosity. In: McDonald, D. A., and Surdam, R. C. (eds), Clastic diagenesis-- AAPG Memoir, 37: 127~149.

Surdam, R. C., MacGowan, D. B. 1987. Oilfield waters and sandstone diagenesis. Applied Geochemistry, 2(5-6): 613~619.

Sverjensky, D.A. 1984 Oil field brines as ore-forming solutions. Economic Geology 79(1) :23~37.

Sverjensky, D. A. 1987. The role of migrating oil field brines in the formation of sediment-hosted Cu-rich deposits. Economic Geology, 82(8): 1130~1141.

Swaine, D. J. 1990. Trace elements in coal. London, Butterworths, United Kingdom. 278p.

Tan Y-J. 1994. Geochemical types of the micro- and fine-grained disseminated gold deposits in Yunnan-Guizhou-Guangxi region. Mineral Deposits, 13(4): 308~321.(In Chinese)

Taylor, R. P. and Fryer, B. J., 1980. Multi-stage hydrothermal alteration in porphyry copper systems in northern Turkey: the temporal interplay of potassic, prophylitic and phyllic fluids. Canadian Journal of Earth Sciences., 17: 901~926.

Taylor, R. P. and Fryer, B. J., 1982. Rare earth element geochemistry as an aid to interpreting hydrothermal ore deposits. In: A. M. Evans (Eds), Metallization associated with acid magmatism. Wiley, New York, N.Y. 357~365.

Teal, L. and Jackson, M. 1997. Geologic overview of the Carlin Trend gold deposits and descriptions of recent deep discoveries. SEG Newsletter, society of Economic Geologists, 31:1~25.

Tissot, B. P., and Welte, D. H. 1984. Petroleum formation and occurrence. Springer-Verlag. 699p.

Titley, S. R. 1991. Phanerozoic ocean cycles and sedimentary-rock-hosted gold ores. Geology, 9: 645~648.

Toland, W.G. 1960. Oxidation of organic compounds with aqueous sulfate. Journal of American Chemistry Society, 82: 1911~1916.

Tooker, E. W. 1985. Geologic Characteristics of sediment- and volcanic-hosted disseminated gold deposits — search for an occurrence model. U. S. Geological Survey Bulletin 1646, 150p.

Tosdal, R. M., Clin, J. S., Hofstra,A. H., Peters, S. G., Wooden, J. L., and Young-Mitchell, M. N. 1998. Mixed sources of Pb in sedimentary-rock-hosted Au deposits, Northern Nevada. *In* Contributions to the gold metallogeny of Northern Nevada. Edited by Tosdal, R. M. U.S.G.S. Open-File Report, 98-338. U.S. Geological Survey, Menlo Park, CA. 223~233.

Tritlla, J., and Gardellach, E. 1997. Fluid inclusions in pre-ore minerals from the carbonate-hosted mercury deposits in the Espadan Ranges (eastern Spain). Chemical Geology, 137(1-2):91-106.

Trudinger, P. A., Swaine, D. J., and Skyring, G. W. 1979. Biogeochemical cycling of elements; general considerations. In: Biogeochemical cycling of mineral-forming elements. Edited by Trudinger, P. A., and Swaine, D. J. Elsevier Sci. Publ. Co., Amsterdam, Netherlands, 1~22.

Trudinger, P. A., Chambers, L. A., and Smith, J. W., 1985. Low-temperature sulphate reduction: biological versus abiological. Canadian Journal of Earth Sciences, 22: 1910~1918.

Tu G-Z. 1996. Comparison between oil-gas accumulations and reworked deposits of active metals. In: Geochemistry of strata-bound deposits in China. Edited by Tu Guangzhi. Science Press, Beijing, China, 165~177.

Turner, S. J., Flindell, P. A., Hendri, D., Hardjana, I., Lauricella, P. F., Lindsay, R. P., Marpaung, B., and White, G. P. 1994. Sediment-hosted gold mineralisation in the Ratatotok District, North Sulawesi, Indonesia. Journal of Geochemical Exploration, 50(1-3): 317~336.

Vaajoki, M. and Gulson, M. 1986. Carbonate-hosted base metal deposits; lead isotope data bearing genesis and exploration. Economic Geology, 81(1): 156~172.

Van der Weijden, C. H. and Van der Weijden, R. D. 1995, Mobility of major, minor and some redox-sensitive trace elements and rare earth elements during weathering of four granitoids in central Portugal. Chem. Geol., 125(3/4): 149~168.

Van Olohen H. 1977. An introduction to clay colloid chemistry (second edition). New York. John Wiley & sons. 318p.

Varshal, G. M., Velyukhanova, T. K., and Baranova, N. N. 1990. Geochemical and analytical aspects of the reactions of gold with humic substances in natural waters, soils, and rocks. Geochemstry International, 27: 10~19.

Vershkovskaya, O. V., Pikovskiy, Yu. I., Solov'yev, A. A. 1972 Carbonaceous matters dispersed in rocks and ores of the antimony-mercury deposit in Plamennoye. Doklady Akademii Nauk SSSR, 205(4): 952~955.

Vilks, P., Caron, F., and Haas, M. K. 1998. Potential for the formation and migration of colloidal material from a near-surface waste disposal site. Applied Geochemistry, 13: 31~42.

Vlassopoulos, D., Wood, S. A., and Mucci, A. 1990. Gold speciation in natural waters: II, The importance of organic complexing — Experiments with some simple model ligands. Geochimica et Cosmochimica Acta, 54: 1575~1586.

Wang, K-R, Zhou, Y-Q, Sun, L-G, and Ren, Z-G. 1994b. Study on the gold occurrence from several typical Carlin-type gold deposits in China. Publish House of the Chinese University of Science and Technology, 103p. (In Chinese)

Wang Y-G. 1996. Major geo-events and regional geological features of Guizhou. Guizhou Geology, 13(2): 99~104. (In Chinese)

Wang, X-Z, Cheng, J-P, and Zhang, B-G. 1992. Geochemistry of the reworked type gold deposits in China. Science Press, Beijing, p176. (In Chinese)

Wang Y-G, Suo S-T, and Zhang M-F. 1994a. Tectonics and Carlin-type gold deposits in Southwestern Guizhou, China. Geological Publishing House, Beijing, 115p. (In Chinese)

Wells, J. D. and Mullens, T. E. 1973. Gold-bearing arsenian pyrite determined by microprobe analysis, Cortez and Carlin gold mines, Nevada. Economic geology, 68: 187~201.

Whitford, Whitford, D. J., Korsch, M. L., Porritt P. M. and Craven S. J. 1988. Rare-earth element mobility around the volcanogenenic polymetallic massive sulfide deposit at Que River, Tasmania, Australia. Chemical Geology, 68: 105~119.

Williams-Jones, A. E. and Samson, I. M. 1989. A sulfur isotope study of the granite-related, Madeleine copper deposit, Gaspé, Quebec: An example of a sedimentary sulfur source. Economic Geology, 84: 1507~1514.

Williams-Jones, A. E., Wood, Scott A. 1992. A preliminary petrogenetic grid for REE fluorocarbonates and associated minerals. Geochimica et Cosmochimica Acta, 56: 725~738.

Wilson, J. T. 1966. Did the Atlantic close and then re-open? Nature, 211: 676~681.

Woitsekhowskaya, M. B., and Peters, S.G. 1998. Geochemical modeling of alteration and gold deposition at the Betze deposit, Eureka County, Nevada. USGS Open-file 98-338, edited by M. Tosdal. 211~222.

Wood, S. A. 1987. Application of a multiphase ore mineral solubility experiment to the separation of base metal and gold mineralization in Archean greenstone terrains. Economic Geology, 82(4): 1044~1048.

Wood, S. A. 1990. The aqueous geochemistry of the rare-earth elements and yttrium. 1. review of available low temperature data for inorganic complexes and the inorganic REE speciation of natural waters. Chemical Geology, 82: 159~186.

Wood, S. A. 1996. The role of humic substances in the transport and fixation of metals of economic interest (Au, Pt, Pd, U, V). *In* Organic and ore deposits. *Edited by* Girodano, T. H. Ore Geology Reviews, 11(1-3): 1~31.

Wood, S.A. and Williams-Jones, A.E., 1994. The aqueous geochemistry of the rare-earth elements and yttrium 4. Monazite solubility and REE mobility in exhalative massive sulfide-depositing environments. Chemical Geology, 115: 47~60.

Wu J and Li S-T. 1993. Application of thermal-process parameters in ore-forming process analysis; a case study of the "gold-triangle area" between Yunnan, Guizhou and Guangxi. Earth Science. Journal of China University of Geosciences, 18(6): 725~734. (In Chinese)

Wu X-Q. 1992. Study on the occurrence of gold and its specific technological property in Lannigou gold mine. Gold, 13(6): 11~16. (In Chinese)

Xia, B-D, Lu H-L, Wu, Y-G, et al. 1992. The Yunnan-Guizhou-Guangxi rift system. Experimental Petroleum Geology, 14 (1): 20-30. (In Chinese)

Xiao R-G, Chen H-Q, and Fan J. 1998. Geological condition controlling Carlin-type gold deposits of Yunnan-Guizhou-Guangxi area. Acta Mineralogica Sinica, 18(3): 344~349. (In Chinese)

Xiong, J., and Coney, P. J. 1985. Accreted terranes of China. In: Howell, D. G. edited, Tectonostratigraphic terranes of the circum-Pacific. Houston, Texas, Council energy Mineral resources, Earth Science Series 1, 349~361.

Xu B, Guo L-Z, and Shi Y-S. 1992. The Proterozoic terrains and multiphase collision orogenesis in Anhui-Zhejiang –Jiangxi province. Geological Publishing House, Beijing. 112 p. (In Chinese)

Xu T-H, Sun S, and Li J-L. 1987. Huanan orogenic belt or Huanan platform. Sciences in China (series B), 10: 1107~1115. (In Chinese)

Yang, K-Y and Dong, Z-S. 1994. Carlin-type gold deposits in Yunnan, Guizhou, Guangxi and northwestern Sichuan Provinces. In: Advances of gold deposit researches in China. Edited by Gold resource section of Chinese Academy of Sciences. Volume I(2), Dizhen Publish House. 284~347. (In Chinese)

Yang W-H. 1996. Role of organic matter in mineralization of strata-bound deposits (Chapter 3). In: Tu Guangzhi (ed), Geochemistry of Strata-Bound Deposits in China. Beijing, Science Press, 48~83.

Yen, T. F. 1975. Vanadium and its bonding in petroleum. In: The role of trace metals in petroleum. T. F. Yen edited. Ann. Arbor. Science 1975. 167~181.

Yie L-J, Li Z, Liu T-B, and Che C-L. 1994. Study of outer continental shelf basinal sedimentary and strata bound gold deposit-A case study of Youjiang basin SW margin of the Yangzi terrain (chapter 2). In: Advance in the gold mineral resources researches in China. Edited by Gao et al. Earthquake Publish House, Beijing.

Zeng Y-F, Liu W-J, and Chen H-D. 1992. Sedimentation characteristics and evolution of the Youjiang complex basin. Guangxi Geology, 5(4): 1~14.

Zeng, Y-F., and Yen, H-S. 1994. The characteristics of organic matter in the carlin-type gold mineralization—a case study of the Larma deposit in Qinling area. In: Liu Dongshen edited, Carlin-type gold deposits in China. Nanjing University Press. 374~382.

Zentilli, M., Munizaga, F., Graves, M. C., Boric, R., Wilson, N. S. F., Mukhopahyay, P. K., and Snowdon, L. R. 1997. Hydrocarbon involvement in the genesis of ore deposits: an example in Cretaceous stratabound (manto-type) copper deposits of central Chile. International Geology Review, 39(1): 1~21.

Zhang, C-J., and Li, X-L. 1998. Geochemical characteristics of platinum group elements in Emeishan basalts. Acta Petrologica Sinica, 14(3): 299~304. (In Chinese)

Zhang F and Yang K-Y. 1992. Fission track chronological study of the fine disseminated gold deposits in southwestern Guizhou. Chinese Science Bulletin, 37(17): 1593~1595. (In Chinese)

Zhang J-R, Lu J-J, Zhou K-J, and Zhang X-H. 1992. Metallogenic characteristics in micro-fine disseminated gold deposit belt of east southern of Yangtse plate. Journal of Nanjiing University (Earth Sciences), 4(3): 76~85. (In Chinese)

Zhang, Y-X, Cun, G., and Liu, L-D. 1996. Gold deposits in China: Advances and considerations. Geological Publishing House. Beijing, 205p. (In Chinese)

Zhang Y-Q, Wei F-L, and Xiao S-Z. 1989. Geochemical characteristics and expectation of the sediment-hosted disseminated gold deposits in southwest Guizhou Province. In: Contributions to the project of regional metallogenic conditions of main gold deposit types in China. VI. Southwestern Guizhou Province. Edited by Shenyang institute of geology and mineral resources. Geological Publishing House, Beijing. 155~174. (In Chinese)

Zhang Z-J and Zhang W-H. 1998. The study of organic ore-forming fluids in the Lannigou gold (mercury, antimony) deposit, Guizhou Province. Mineral Deposits, 17(4): 343~354. (In Chinese)

Zhang Z-J, and Zhang W-H. 1999. Investigation into metallogenic fluid feature in Carlin-type gold deposits and its relation to mineralization in southwest Guizhou Province.

Earth science – Journal of China University of Geosciences, 24(1): 74~78. (In Chinese)

Zhu, L-M, and He, M-Y. 1996. Geochemistry of the fluid inclusions in disseminated gold deposits of southwestern Guizhou Province. Volcanology and Mineral Resources, 17(1/2): 65~75. (In Chinese)

Zhu L-M, Liu X-F, Jin J-F, and He M-Y. 1998a. The study of the time-space distribution and source of ore-forming fluid for the fine-disseminated gold deposits in the Yunnan-Guizhou-Gangxi area. Scientia Geologica Sinica, 33(4): 463~473. (In Chinese)

Zhu X-Q, Zhang Z-G, and Jiang Z-C. 1998b. Experimental study of the metallogeny of the Carlin-type gold deposits in southwestern Guizhou Province. Chinese Science Bulletin, 43(22): 2431~2334. (In Chinese)

Zhuang, H-P, Lu, J-L, Fu, J-M, Liu, J-Z, and Shi, J-X. 1997. Preliminary investigation on the light hydrocarbons in ore-forming fluid of gold and antimony deposits in southwestern Guizhou Province. Chinese Science Bulletin, 42(16): 1752~1755. (In Chinese)

Zhuang H-P, Lu J-L, Fu J-M, Ren Z-G, and Zou D-G. 1998. Crude oil as a potential gold migrant—possible petrological and geochemical evidences. Science in China (Series D), 28(6): 552~558. (In Chinese)

Zhuang X-G. 1995. The paleogeothermal field of northwestern Guangxi; characteristics and its role in the formation of micro-disseminated gold deposits. Mineral Deposits, 14(1): 82-89. (In Chinese)

Appendix

Sample list

Eighty-three samples were collected from the Lannigou, Getang and Zimudang deposit. The samples mentioned in the text are briefly described as follows.

Samples from the Lannigou deposit

Sample No.	Description	Location
LN-4	Argillaceous sandstone (Xiuman Formation)	No. 843 gallery, south of the Huangchanggou section
LN-8	Bioclastic limestone (Wujiaping Formation)	East of Rongban village
LN-9	Siltstone (Bianyang Formation)	Huangchanggou, near F_1 fault
LN-10	Primary ore, silicified, pyritized siltstone, with disseminated pyrite and arsenopyrite	Huangchanggou, near F_1 fault
LN-11	Moderately layered fine-grained sandstone	East of Huangchanggou, near F_3 fault
LN-12	Argillaceous siltstone	East of Huangchanggou, near F_3 fault
LN-13	Oxidized ore from the weathering crust over ore body	Top of the ore body, at the surface of the F_3 fault zone near Huangchanggou
LN-14	Semi-oxidized ore	Huangchanggou, within the F_3 fault zone
LN-15	Primary ore, silicified, pyritized siltstone	Huangchanggou, within the F_3 fault zone
LN-18	Siltstone (Bianyang Formation)	Huangchanggou, YD516 tunnel, 502 cross-drift, LN18 to LN 32 are profile sampling with a interval of 3 m
LN-19	Silicified siltstone	
LN-20	Ore (silicified, pyritized siltstone)	
LN-21	Silty mudstone	
LN-22	Ore (silicified, pyritized siltstone)	
LN-23	Ore (silicified, pyritized siltstone)	
LN-24	Silicified siltstone	
LN-25	Ore (silicified pyritized siltstone)	
LN-26	Siltstone	
LN-27	Sandstone	

LN-28	Sandstone	Huangchanggou, YD516 tunnel, 502 cross-drift, LN18 to LN 32 are profile sampling with a interval of 3 m
LN-29	Silicified siltstone	
LN-30	Silicified and pyritized siltstone	
LN-31	Siltstone	
LN-32	Siltstone	
LN-33	Ore (silicified and pyritized siltstone) with cinnabar and calcite veins	YD516-2 tunnel, No.1 ore body
LN-34	Pelite (occurrence 45°∠65°)	Huangchanggou, LN-34 to LN44 are profile sampling across the F3 fault, interval 5 m
LN-35	Silicified mudstone	
LN-36	Mudstone (occurrence 40°∠50°)	
LN-37	Silicified siltstone (occurrence 20°∠40°)	
LN-38	Silicified and pyritized siltstone (occurrence 30°∠65°)	
LN-39	Ore (silicified and pyritized mudstone)	
LN-40	Silicified and pyritized sandstone	
LN-41	Ore (silicified and pyritized siltstone 10°∠70°)	
LN-42	Ore (silicified and pyritized siltstone)	
LN-43	Ore (silicified and pyritized siltstone)	
LN-44	Siltstone (occurrence 5°∠30°)	
LN-45	Limestone (Permian, Laizishan anticline)	Southwestern of the Lannigou deposit
LN-46	Ore (silicified, pyritized sandstone)	Huangchanggou, 516 tunnel (north branch), contains realgar, orpiment, cinnabar and calcite veins.

Samples from the Zimudang deposit

ZMD-1	Oxidized ore	Open pit mining site
ZMD-3	Primary ore, silicified and carbonatized silty shale, with disseminated fine grain pyrite	Tunnel of the Zimudang deposit
ZMD-4	Carbonaceous bed (pyrobitumen, pyrite, calcite)	Tunnel of the Zimudang, occurs along fracture in the ore
ZMD-5	Semi-oxidized ore (silicified siltstone)	Open pit mining site
ZMD-6	Thick-layered limestone (the second section of the Yielang Formation)	East of Zimudang village
ZMD-8	Argillaceous limestone (the first section of the Yielang Formation)	North of the Huilong town

Samples from the Getang deposit

GT-1	Limestone (Maokou Formation)	Near the Getang deposit
GT-2	Primary ore (silicified breccia)	Production tunnel of the Getang
GT-3	Primary ore (silicified breccia)	Open pit mining site
GT-4	Oxidized ore	Open pit mining site
GT-5	Silicified carbonaceous shale	Hanging wall of the ore body from the open pit mining site
GT-6	Anthracite (Longtan Formation)	Coal mine near the Getang gold deposit

BELL & HOWELL INFORMATION & LEARNING
300 North Zeeb Road
Ann Arbor, Michigan 48106
Telephone 734-761-4700

SHIPPING NOTICE :

To :

DENISE BERNARD
UNIV QUEBEC A CHICOUTIMI
BUR DES ETUDES SUPERIEURES
555 BOUL UNIV CHICOUTIMI
CHICOUTIMI QUEBEC G7H 2B1
CANADA

Date: 2 4 02
By : JV6

School : 0862M QUEBEC-CHIC-M

Total Cartons/packages: 5

We have shipped to you at the address shown above the following :

Seq No.	Pub Number	ISBN	Author
1	MQ62002	0-612-62002-6	Pelletier, Claude
2	MQ62003	0-612-62003-4	Pelletier, Nicole
3	MQ62004	0-612-62004-2	Saoudi, Abdelhamid
4	MQ62005	0-612-62005-0	Tremblay, Christine
5	MQ62006	0-612-62006-9	Turcotte, Sophie

BELL & HOWELL INFORMATION & LEARNING
300 North Zeeb Road
Ann Arbor, Michigan 48106
Telephone 734-761-4700

PPING NOTICE :

O :

DENISE BERNARD
UNIV QUEBEC A CHICOUTIMI
BUR DES ETUDES AVANCEES
555 BOUL UNIVERSITE CHICOUTIMI
CHICOUTIMI QUEBEC G7H 2B1
CANADA

Date: 2 4 02
By : JV6

School : 0862 QUEBEC-CHIC-D

Total Cartons/packages: 2

We have shipped to you at the address shown above the following :

Seq No.	Pub Number	ISBN	Author
1	NQ62007	0-612-62007-7	Bonnay, Marianne
2	NQ62008	0-612-62008-5	Bao, Zhiwei